AN INVESTIGATION OF DISTORTION INDICES FOR PREDICTION OF STALLING BEHAVIOR IN AIRCRAFT GAS TURBINE ENGINES

by

Annette Flanagan Campbell

Thesis submitted to the Graduate Faculty of the
Virginia Polytechnic Institute and State University
in partial fulfillment of the requirements of the degree of

MASTER OF SCIENCE

in

Mechanical Engineering

APPROVED:

W. F. O'Brien, Chairman

R. G. Leonard H. L. Moses

August, 1981

Blacksburg, Virginia

II. ACKNOWLEDGEMENTS

The author wishes to express her sincere appreciation to the members of her advisory committee: Professors R. G. Leonard, H. L. Moses, and W. F. O'Brien, Chairman. She gratefully acknowledges assistance provided by P. S. Batterton of NASA Lewis Research Center and W. G. Steenken of the General Electric Company.

The author is truely indebted to her parents for their unfaltering support in all educational endeavors. She is most grateful to Kevin, her husband, for his generous love, support, and encouragement.

III. TABLE OF CONTENTS

IV. LIST OF FIGURES

Note: The figures in Appendix C are plots of the indices versus loss in stall pressure ratio and engine speed. They are indexed at the beginning of Appendix C.

V. LIST OF TABLES

VI. LIST OF SYMBOLS

c	chord length of rotor blade
CC	correlation coefficient
C_N	normal force coefficient
i	incidence angle
k	reduced frequency
N	engine speed (rpm)
$\overline{P}, P_{avg}$	average inlet total pressure
P_{max}	maximum inlet total pressure
P_{min}	minimum inlet total pressure
P_o	total pressure
R^2	R-SQUARE
$R(\omega)$	frequency response function
RNI	Reynolds number index, $\frac{\delta}{(\frac{\mu}{\mu_{sl}\sqrt{\theta}})}$
$N/\sqrt{\theta}$	corrected speed (where θ is ratio of fan or compressor entry total temperature to standard day temperature)
ΔPRS_N	constant speed loss in stall pressure ratio
ΔPRS_M	constant mass loss in stall pressure ratio
α	angle of attack
δ	ratio of total pressure to standard sea-level static pressure
θ	circumferential extent of distortion, or ratio of total temperature to standard sea-level static temperature
θ_{crit}	critical angle
μ	absolute viscosity

μ_{sl}	sea-level absolute viscosity
ρ	density
τ	time constant
ω	uncertainty

VII. INTRODUCTION

The flow of air through the compressor of an aircraft engine is largely steady and axisymmetric under normal operating conditions. This stable operating regime may be disrupted if rotating stall or surge occurs. Rotating stall results from flow separation on rotor blades and is characterized by localized regions of retarded through-flow moving circumferentially around the compressor annulus. It is a localized instability that frequently leads to surge, a global instability. When surging, the entire engine experiences large amplitude oscillations in mass flow rate and system pressure rise. Either of these flow instabilities can result in cyclic loading of engine components, reduced engine performance and possible turbine overtemperature.

A typical compressor characteristic such as the one shown in Fig. 1 includes a stall line which separates the region of stable operation from that of unstable operation. Because of the undesirable effects of unstable operation, it is important that the engine operating point remain beneath this limit of stable operation. Thus, the engine steady-state operating line is designed so that a surge margin or safety margin will exist between it and the stall line. Surge margin may be defined in terms of constant mass flow or constant engine speed. An illustration of both definitions of surge margin is presented in Fig. 2.

Surge margin is needed to accomodate upward shifts in the operating line due to accelerations, transient disturbances, control inaccuracies, and manufacturing tolerances. It must also accomodate downward shifts in the compressor surge line due to aging, manufacturing tolerances, and

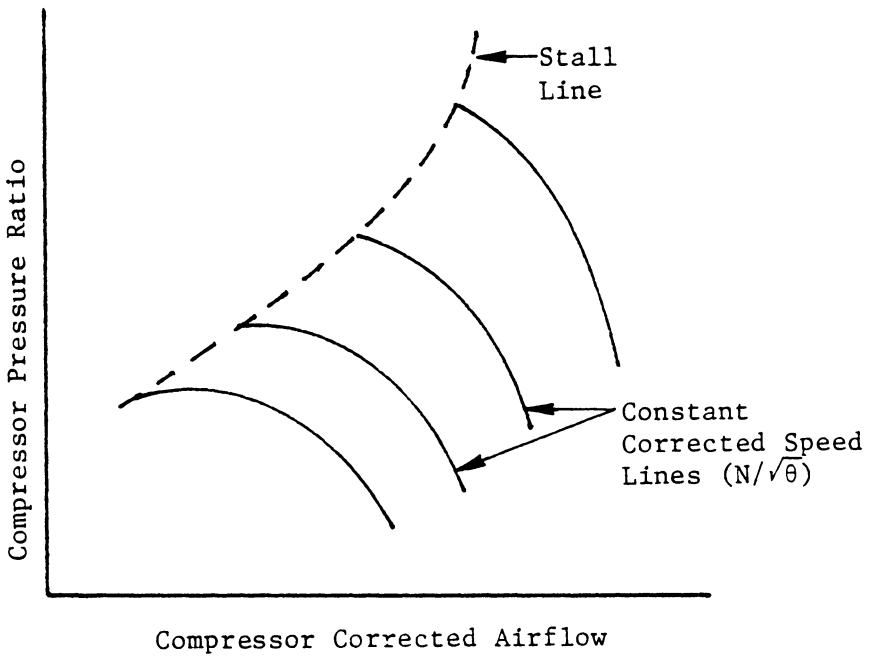

Figure 1: Typical Compressor Characteristic

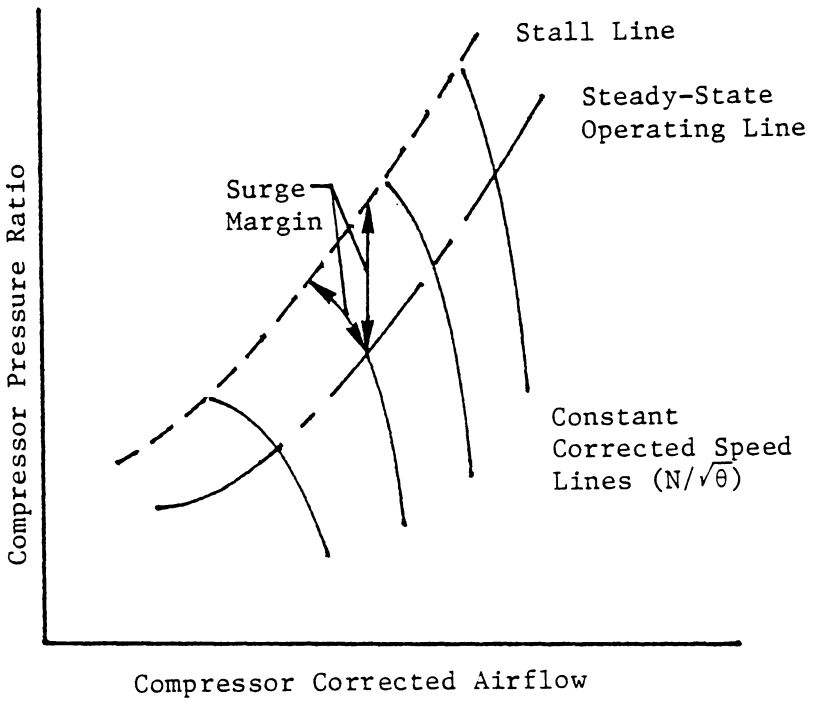

Figure 2: Compressor Characteristic With Imposed Engine Operating Line

inlet distortion. Figure 3 illustrates qualitatively how much surge margin should be allocated for each of these effects, assuming a constant speed definition of stall margin.

Excess surge margin is undesirable. A large surge margin leads to a lower compressor delivery pressure for any given corrected mass flow rate. Thus, a larger, heavier engine is required to meet performance criteria whenever surge margin is increased. Optimizing operating efficiency is also a concern when allocating surge margin and locating the steady-state operating line. Thus, surge margin allocation is a design variable that reflects the specified mission for which the engine is designed.

Inlet distortion is responsible for the single most degenerative effect on surge margin. It is defined as a nonuniform distribution of the flow properties at the engine face. These properties include total pressure, temperature, velocity, static pressure, and flow angularity. Inlet distortion may be generated by shock-boundary layer interactions, strong inlet cross-winds, armament firing, large angles of attack or yaw, afterburner transients, splitter plate stalls, etc. Whatever the source, the effect is a reduction in available surge margin to the point where surge may occur.

Engine response to inlet distortion is therefore important in any engine development program. Unfortunately, it is presently beyond state-of-the-art capability to design an engine for a desired distortion tolerance. Rather, compressor stability must be assessed during engine development and prequalification testing. Various inlet flow distor-

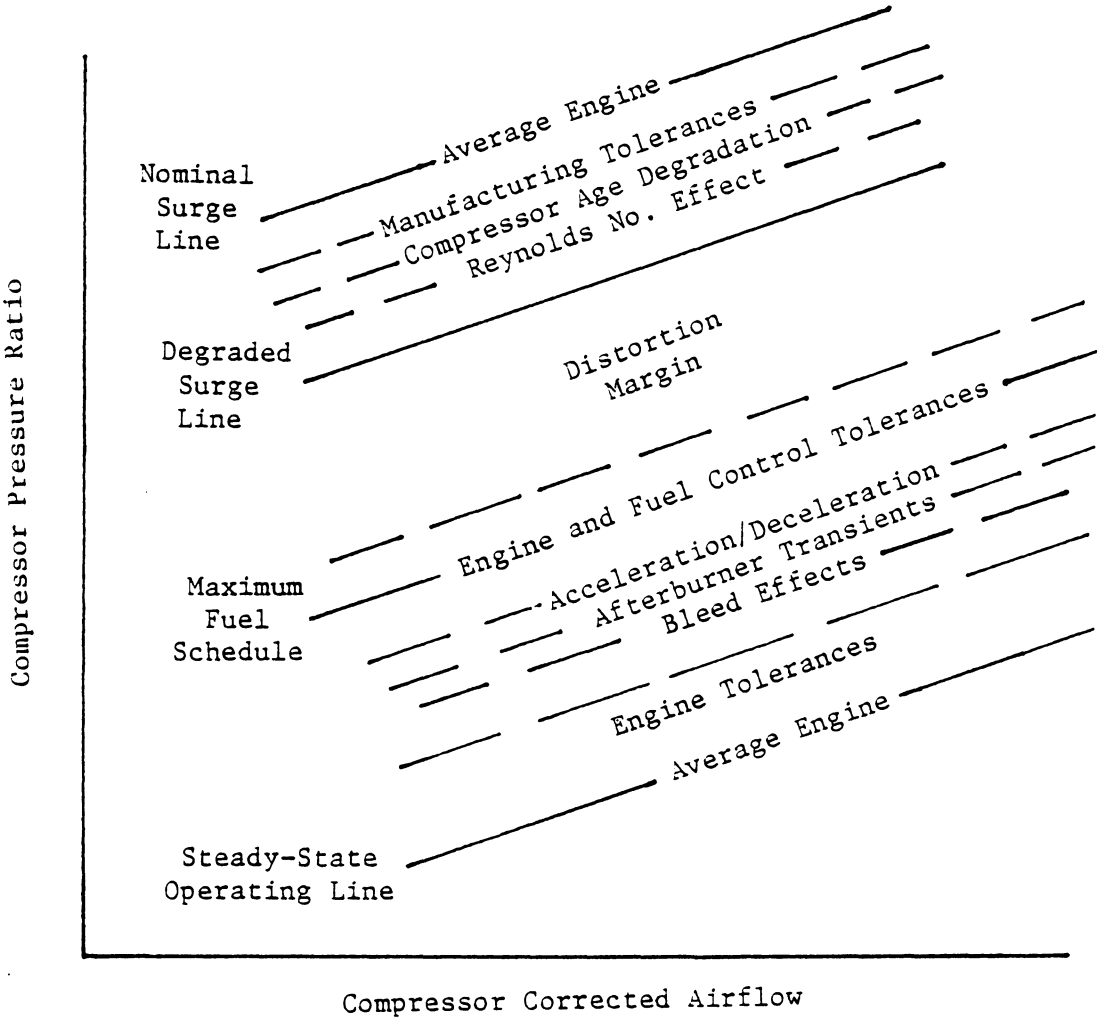

Figure 3: Cumulative Degrading Factors on a Compressor Performance Map (taken from Boytos [29])

tions are imposed via the use of screens or air jets and the resultant loss in surge margin is measured. Qualification testing must verify surge-free operation for specific operating conditions.

Distortion indices which correlate the distortion present at the engine face with resultant effect on engine stability have evolved as a natural result of this stability assessment procedure. Nearly every engine company and government propulsion research center has one or more distortion indices. Often a new or modified index is developed for each new engine program. This has led to considerable confusion when writing engine specifications and comparing engine stability test results.

The existence of so many indices merely reflects the current lack of complete understanding of compressor response to inlet distortion. Both steady-state and time-variant inlet distortions are possible, but even steady-state distortions appear as time-variant in the rotor coordinate system. The rotor does not respond instantaneously to changes in inlet flow conditions as finite time is required for airflow adjustment and boundary layer separation to occur. Clearly different compressor designs in which aspect ratio, hub-to-tip ratio, airfoil shape, etc. may vary, will strongly influence how the flow around the rotor responds to inlet distortion. Distortion indices have dealt with compressor dynamic response by including in the correlations parameters believed to affect system dynamics, such as the magnitude or intensity, shape, and extent of the distortion, compressor sensitivity, circumferential and radial distortion superposition effects, and distortion location weighting factors. The weighting given any of these

factors can vary extensively from index to index, reflecting the fact that the influence of any given factor varies with engine design.

The purpose of this investigation is to evaluate the accuracy of nine distortion index/correlation systems considering only circumferential inlet total pressure distortions and using J85-GE-13 and TF30-P-3 engine data and modified T64-GE-6B compressor test-rig data. Special attention will be given to how the indices account for the dynamic response of the particular engine for which the index was designed.

The nine indices to be evaluated are

1. $\Delta P/\overline{P}$ indices
2. Rolls Royce θ critical indices
3. NAPC Kθ index
4. AVCO Lycoming DI and DI_c indices
5. Garrett AiResearch CDI index
6. Pratt and Whitney KD_2 index
7. Pratt and Whitney Ka_2 index
8. General Electric Method D system
9. ARP 1420 correlation.

For comparison purposes, the widely-known parallel compressor model will also be evaluated. Statistical methods will be used to determine index accuracy.

In addition, a method which is believed to handle compressor rotor blade dynamic response in a more fundamental manner will be presented. This method is an outgrowth of an on-going research project dealing with

compressor blade dynamic response that is being carried out at Virginia Polytechnic Institute and State University. Sexton [1] and Sullivan [2] have developed procedures by which experimental dynamic response functions can be derived from dynamic on-rotor total pressure measurements. The ultimate goal is the development of a dynamic response function which can be used in combination with any measured inlet total pressure distribution to derive a modified or effective total pressure distribution which is related to the dynamic response of the compressor rotor blades. Using the simple distortion magnitude-descriptor indices in combination with the effective rather than the measured inlet total pressure distribution should produce a more accurate correlation because of the inclusion of dynamic response effects. Modifying the measured inlet total pressure distribution represents an alternative to adding modification factors to the distortion index. Much more experimental data is required before this experimental response function can be accurately defined. For this reason, a second order response function is used in this thesis to illustrate how the effective total pressure distribution affects the accuracy and generality of the simpler distortion indices. Calculations are carried out for parallel compressor theory and the $\Delta P/\overline{P}$ indices.

In Section VIII of the thesis, significant literature in the areas of rotor blade dynamic response and distortion index development and evaluation is reviewed. The indices to be evaluated are developed in Section IX. An explanation of how dynamic response functions can be used to improve index accuracy is presented in Section X. Section XI

describes the experimental data used in this investigation and the procedure followed in evaluating the indices. Results and a discussion of results are presented in Sections XII and XIII. Finally, conclusions and recommendations are related in Sections XIV and XV.

VIII. LITERATURE REVIEW

Distortion induced instability is of major concern to engine manufacturers and their customers. The amount of literature published on this topic reflects its importance. Only a portion of the available information on distortion induced instability is reviewed here. Specifically, the development and evaluation of distortion indices and compressor rotor blade dynamic response to steady-state inlet distortion is reviewed. The two areas will be considered separately. Distortion indices are experimental correlations and as such, dynamic response is automatically included. Thus, there has been little fundamental research in the combined area of distortion indices and dynamic response. On the other hand, analytical distortion models, whether of the global or detailed blade row-by-blade row type, have had to deal specifically with rotor blade dynamic response. Most of the current understanding of dynamic response has resulted from efforts to improve the accuracy of these analytical models. Thus, the topic of analytical distortion models is reviewed in order to relate recent advances in the understanding of compressor rotor blade dynamic response to steady-state inlet distortion. This topic is considered first, followed by a review of the development and evaluation of distortion indices.

Rotor Blade Dynamic Response

Parallel compressor theory, one of the simplest compressor models, can be used to predict loss in stall pressure ratio due to circumfer-

ential total pressure distortion. First proposed by Pearson and McKenize [3], parallel compressor theory models the distorted inflow compressor as two separate compressors operating in parallel. Each compressor operates as if experiencing undistorted flow, one with inlet conditions corresponding to the undistorted region of the original compressor and one with inlet conditions corresponding to the distorted region. Both compressors are assumed to discharge to the same exit static pressure. By modeling a distorted inflow compressor as two parallel compressors operating with uniform clean and uniform distorted inlet conditions, parallel compressor theory assumes that the original compressor responds to changes in inlet conditions in an instantaneous or quasi-steady manner.

Reid's investigation [4] of the effect of varying circumferential extent of distortion demonstrated that the assumption of quasi-steady response was grossly in error for small extent distortions. He found that as the extent of spoiling was increased from 0° to 90°, the surge delivery static pressure fell rapidly and then stabilized at a constant minimum value from 90° to 360°. He concluded that there is a critical angle of spoiling between 60° and 90°, where the critical angle is defined as the minimum angle to which the compressor responds quasi-steadily. In an investigation of the effect of distortion on a turbojet engine, Calogeras, Mehalic, and Burstadt [5] found similarly that the compressor stall pressure ratio fell rapidly as the angle of spoiling was increased from 0° to 60° and then stabilized at a nearly constant value between 90° and 180°. Reid incorporated the idea of a critical

angle of spoiling in parallel compressor theory, and thereby greatly improved the model's accuracy for small extent distortions.

Roberts, Plourde, and Smakula [6] investigated the effects of varying rotor and stator chord length on the distortion tolerance of a low-speed, multistage, axial-flow compressor. The test compressor was subjected to varying intensity, 180° extent total pressure distortions. They compared experimental values and parallel compressor theory calculations of loss in peak pressure ratio and found increasing discrepancy with increasing rotor chord length. They attributed this trend to unsteady flow effects, reasoning that the flow around long chord rotors required additional time to adjust to changes in inlet conditions. Roberts, et al. defined a reduced frequency parameter as a measure of unsteady flow effects in the following manner:

$$k = \frac{B\Omega}{V}$$

where

B = one half of the rotor chord length,

Ω = frequency of disturbance in radians per second,

V = average velocity of the air relative to the rotor.

Increasing reduced frequency indicates increasing distortion tolerance due to unsteady flow effects. Correspondingly, increasing reduced frequency means decreasing parallel compressor theory accuracy.

Mikolajczak and Pfeffer [7] expanded the reduced frequency parameter as

$$k = \frac{b}{r}\frac{360}{\theta}\frac{U}{c}$$

where

b = axial projection of rotor chord,

r = compressor radius at the blade section,

θ = distortion extent in degrees,

U = tangential blade speed,

c = axial air velocity.

Their parameter is more clearly seen as a measure of the ratio of the time a fluid particle spends in the blade passage to the time the rotor remains in the spoiled sector. Similar to Roberts et. al., Mikolajczak and Pfeffer concluded that the parallel compressor theory assumption of quasi-steady response is accurate for small values of k but becomes less accurate as k increases.

The dependence of quasi-steady response on rotor blade chord length led Mokelke [8] to relate the critical angle of spoiling for a given compressor to chord length. He concluded that the critical angle is smaller for compressors with short rotor blade chords than for those with long rotor blade chords because of the same unsteady flow effects.

Mazzawy [9] has developed a considerably more detailed multiple segment parallel compressor model. It is a non-linear, compressible flow model that uses the parallel compressor concept without assuming a constant exit static pressure or that the distorted overall compressor performance is the same as the undistorted compressor performance. The

basic model considers individual blade row performance in order to consider front to rear matching effects. Thus, the model requires the determination of blade row characteristics as a function of inlet conditions. Recognizing that the instantaneous loss and exit air angle deviate from quasi-steady values, Mazzawy assumed a first order response for both, using quasi-steady values for forcing functions. He used an empirical time constant descriptive of the boundary layer response. The first order model more nearly approximates dynamic rotor loss than it does dynamic rotor turning.

The Dynamic Digital Blade Row Compressor System Stability Model developed by General Electric Company employs a one-dimensional, pitch line, blade row-by-blade row model to solve the equations of conservation in a volume-averaged form using a time marching scheme. The original model described by Tesch and Steenken [10] assumed quasi-steady response. To improve the model's capability of handling unsteady flow effects, Tesch and Steenken [11] developed an effective incidence angle distribution derived by assuming a first order response to the instantaneous incidence angle distribution. They defined the effective incidence angle as "the incidence angle which is equivalent to the dynamic response of the blade as it passes through the distortion." They then determined blade row characteristics as functions of the effective incidence angle rather than the instantaneous angle. Various time constants were used to derive the effective incidence angle until model and test results were reasonably close in terms of loss in stall pressure ratio.

Chung, Hosney, and Steenken [12] later reported on a modified version of the GE model that simulates the unsteady aerodynamics of the NASA J85-13 planar pulse generator test installation. An analytic expression for the unsteady blade lift force was included to improve the model's capability in handling unsteady flow effects. The unsteady blade lift force was derived from an analytic expression for the lift force of a thin airfoil subjected to sinusoidal gusts. The resulting expression is quite complex, including real and imaginery parts and Hankel and Bessel functions.

Melick and Simpkin [13] analytically developed a global compressor model that relates inlet total pressure and temperature distortion to loss in stall margin. They derived an effective angle of attack which lags the instantaneous angle by assuming a first order time response using a time constant proportional to rotor blade chord length. Melick and Simpkin noted that stalling and recovery are different phenomena and should actually be characterized by different response functions; however, they did not incorporate this into their model. Melick and Simpkin assumed a uniform compressor exit pressure so that as in parallel compressor theory, the region of low inlet total pressure operates at a higher pressure ratio. They then equated normalized change in rotor work due to the distortion to the normalized change in rotor blade lift coefficient which is in turn equal to the normalized effective angle of attack. The required work increase was related to the required increase in compressor pressure ratio so that finally loss in stall margin is predicted as a function of the distortion intensity and the

reduced frequency parameter, k. Their reduced frequency parameter is identical to that of Roberts, et al.

Melick [14] later improved on the above model by assuming a second order response in deriving the effective incidence angle. The two time constants used in the second order system were determined from test results. Melick estimated them to be approximately equal and on the order of 3.5c/U.

Various models for predicting the characteristics of rotating stall have been proposed in the literature and are reviewed by Mokelke [8]. Early models used the linearized equations of motion and were therefore restricted to small perturbations. Rotor blade rows were modeled as actuator discs which are surfaces of discontinuity where energy and rotation are instantaneously added to the flow.. They also generally assumed quasi-steady rotor response or included unsteady response by using unstalled unsteady effects.

Nagano and Takata [15] and Adamczyk and Carta [16] extended these basic models by including nonlinear flow equations. Each of these two models obtains rotor characteristics from stationary cascade measurements of total pressure losses and turning angle. Unsteady effects are included in blade row characteristics by assuming a first order time response to inlet conditions.

Sexton [1], in a model similar to that of Nagano and Takata, used experimentally measured blade pressure forces to describe the dynamic blade row characteristics. He derived a "transfer function between the quasi-steady and the dynamic total pressure loss distributions ... by

considering the dynamic total pressure loss distribution to be a response function driven by the quasi-steady total pressure loss distribution as a forcing function." An experimentally-derived transfer function offers obvious advantages over an assumed first order response.

Sullivan [2], using the same experimental apparatus as Sexton, subjected an axial-flow compressor to circumferential total pressure distortion and then recorded the upstream and on-rotor dynamic pressures. She derived experimental frequency response functions by considering the relative stagnation pressure distribution to be the forcing function driving the dynamic on-rotor pressure. Transfer functions were derived separately for each of five positions along the rotor chord at 85% span (corresponding to pressure tap locations) for both the suction and pressure blade sides. She concluded that simple first or second order system response does not well-represent compressor stall behavior. Rather, the experimental response functions showed that stall and recovery should be modeled separately and as higher-than-second order systems.

Distortion Indices

The majority of the distortion index information reviewed was published by government agencies. Presumably, some of the related information held by engine manufacturers and airframe companies is considered proprietary. Detailed information concerning calculation procedures for the indices will not be presented here, but is included in Section IX of the thesis.

Reid [4] proposed the use of either of two simple circumferential indices, $\Delta P(\theta \text{ crit})/\overline{P}$ or $\Delta P(\theta \text{ crit})/\overline{q}$, where the difference between the overall average inlet pressure and the lowest average pressure of any sector equal to the critical angle is normalized by either the average inlet pressure or the mean inlet dynamic head. These are the Rolls Royce θ critical indices. Reid ignored the effects of radial distortions on the basis that they are generally less harmful than the equivalent circumferential gradients and are so much more dependent on compressor design that efforts to include their effects overshadow the benefits of improved correlation. In an experiment in which the intensity level of a fixed 90° extent distortion was varied, Reid found that the surge delivery static pressure was essentially directly proportional to the level of spoiling, P_{min}/P_{max}.

Calogeras, Mehalic, and Burstadt [5] examined the effect of radial and circumferential screen-induced distortions of varying extent and intensity on a J85-GE-13 turbojet engine. They presented graphs of each of three distortion indices versus loss in stall margin to evaluate which provided the best correlation. The indices evaluated were $(P_{min,60}/P_{max})$, $(1-P_{min,60}/\overline{P})$, and $(1-P_{min,60}/\overline{P})\cdot\sqrt{\beta/\pi}$ where $P_{min,60}$ is the lowest average inlet total pressure in any 60° segment, P_{max} is the maximum inlet pressure, $\overline{P}$ is the average inlet pressure and β is the distortion extent in radians. The second index is exactly that recommended by Reid for a critical angle of 60°. Calogeras, et al. determined 60° to be the critical angle of this J85 engine.

The first index correlated essentially all data points onto a single

curved line. The authors pointed out that this index does not in any way include the distortion extent whereas the second, because it includes an average pressure is to a limited degree affected by distortion extent. Accordingly, the second index correlated the data points of different extent distortions onto different lines. Inclusion of the normalized extent in the third index essentially collapsed these lines into one line.

Korn [17] examined the effects of circumferential and radial total pressure distortions on the low-speed spool of a TF41 turbofan engine. He used $\Delta P/\overline{P}$ as a measure of distortion intensity. When plotted versus corrected mass flow, the $\Delta P/\overline{P}$ index reduced the data to two curved lines. One line represented data from 180° circumferential distortions and the other represented both hub and tip 30% radial distortions.

Korn found that the bypass stability limit was significantly reduced by 180° circumferential distortion at all speeds and slightly reduced by tip radial distortion at high speed. In contrast, the only significant reduction in stability limit of the intermediate compressor occurred with hub radial distortion at high speed. Apparently the fan attenuated circumferential distortion so that it was no threat to primary stability.

Braithwaite, Graber, and Mehalic [18] studied the effect of temperature and pressure distortion on the performance of a J85 turbojet engine. The total pressure distortion parameter used was $((P_{ud}-P_d)/\overline{P})$ where P_d is the average of all pressure measurements behind the distortion screen, P_{ud} is the average of all those outside the

screen, and $\overline{P}$ is the overall average inlet total pressure. The authors found that for a constant corrected speed definition of loss in stall pressure ratio, ΔPRS_N, the distortion parameter was directly proportional to ΔPRS_N with a proportionality constant of 0.60. Using a constant corrected airflow definition of loss in stall pressure ratio, ΔPRS_W, resulted in considerable data scatter.

Graber and Braithwaite [19] presented results of circumferential pressure distortion tests of both a J85-GE-13 turbojet engine and a TF30-P-3 two-spool turbofan engine. They used two distortion indices, $((\overline{P} - P_{min})/\overline{P})$ and $((\overline{P} - P_{min})/\overline{q})$, to establish distortion sensitivity for each engine. The $\Delta P/\overline{P}$ index is similar to that used by Braithwaite, et al. who also investigated the distortion sensitivity of the J85 engine. Similar to their findings, Graber and Braithwaite found that the $\Delta P/\overline{P}$ index correlated reasonably well with a constant speed definition of loss in stall pressure ratio but resulted in considerable data scatter when plotted versus a constant corrected airflow definition of loss in stall pressure ratio. There was no advantage in using the $\Delta P/\overline{q}$ index for correlating J85 behavior.

Both indices were plotted versus corrected speed for the TF30 data and both indices reduced the data for different distortion extents onto approximately straight but different lines. The authors demonstrated that the inclusion of an extent function in the index would reduce the data to a single line and noted that KD_2, the index developed by Pratt and Whitney Aircraft for use with the TF30 engine, does include such an extent function.

In commenting on the multitude of indices currently in use, Graber and Braithwaite noted that the weighting of the extent of the distortion term, $\bar{\theta}$, varies significantly from index to index. They concluded that because each index was developed for and presumably best correlates the stall data of a particular engine, a fixed weighting of this term in some future universal index is not a reasonable goal.

Brunda and Boytos [20] developed and evaluated a circumferential inlet pressure distortion index, $K\theta$. Derivation of the index was based on two conditions for distortion similarity. First, the angle of attack at surge should be constant for a given engine speed. Second, the ratio of the dwell time of the blade in the low pressure region to the residence time of air in a blade passage should be constant. This second condition is equivalent to assuming a constant reduced frequency parameter. They evaluated the index using TF30-P-12 turbofan engine data. The NAPC circumferential inlet distortion index, $K\theta$, was shown to graph as an essentially straight line versus corrected engine speed. Thus, the value of the index at surge for a given corrected engine speed was independent of distortion amplitude and extent. In addition, Brunda and Boytos showed that $((\Delta P/\bar{P})(\bar{\theta}/2\pi))$ and $((\Delta P/\bar{q})(\bar{\theta}/2\pi))$, where ΔP is $P - \bar{P}$ at the compressor inlet, did not reduce the data to a single curve when plotted versus high compressor rotor speed.

Werner, Abdelwahab, and Braithwaite [21] investigated the performance of the TF30-P-3 turbofan engine when subjected to varying intensity level, 180° circumferential inlet pressure distortions. KD_2, the index developed by Pratt and Whitney Aircraft specifically for the

TF30 engine, was evaluated and found to reduce the data to a straight line when plotted versus corrected engine speed. Performance of the fan tip, fan hub, low pressure compressor and high pressure compressor were considered separately. Werner, et al. found the high pressure compressor performance to be unaffected by the inlet flow distortions. Apparently the pressure distortion was attenuated and no resulting temperature distortions were detected. The stall limits of the fan, both hub and tip regions, were lowered with increasing levels of distortion. The inlet flow distortion lowered the stall line of the low pressure compressor enough to intersect the operating line. Thus, the low pressure compressor was the limiting stability component for this TF30 engine.

Moore [22] and Moore and Leuke [23] reported on the development of a similarity parameter which facilitates prediction of full scale instantaneous pressure distortion levels from scale model inlet dynamic data when used in conjunction with the General Electric Method D distortion methodology. Two other distortion indices, $((P_{max} - P_{min})/\bar{P})$ and $((\bar{P} - P_{min})/\bar{P})$, did not produce consistent trends.

Stevens, Spong, and Hammock [24] conducted a distortion methodologies study of the F-15 aircraft using the Pratt and Whitney Aircraft (PWA) Ka_2 distortion descriptor. They verified the capability of the PWA stability audit system to predict engine stalls for both stall and nonstall flight test conditions. Farr [25] also used the PWA Ka_2 and Kc_2, fan and high pressure compressor indices respectively, in evaluating F-15 inlet dynamic distortion.

Walter and Shaw [26] used the Ka_2 and Kc_2 fan and compressor indices as a standard by which to judge some of the results of Mazzawy's multiple segment parallel compressor model in a distortion analysis of the F100 turbofan engine. They explain that separate indices are used for the fan and compressor because high pressure compressor stability for the F100 engine is affected by bypass ratio. The high pressure compressor index, Kc_2, takes this functional dependence into account.

An overview of the effects of distortion on engine stability is presented by Hercock and Williams [27]. They observed that circumferential distortion is generally destabilizing while radial distortion can stabilise or destabilise a compressor depending on the intensity and location of the distorted region. Because of the high resistance to cross flow, circumferential distortion generally exists in attenuated form even at the compressor exit and thus causes greater losses in stall margin at intermediate to high speeds when the rear stages are more highly loaded. Radial distortion is attenuated rapidly and is more detrimental at low speeds when front stages are highly loaded. They reported that the effects of multi-lobed patterns are less than or equal to those of single-lobed patterns of the same total blockage.

Hercock and Williams also reviewed some of the more common indices, namely the Rolls Royce θ critical indices, the Pratt and Whitney KD_2 and Ka_2 indices, and the General Electric Method D system. They graphically compared KD_2 to $\Delta P(120)$, $K\theta$ to DC(120), and Ka_2 to DC(120) and found that each pair agreed within experimental scatter for the subsonic-inlet steady-state data used. Calculated and experimental loss in stall

pressure ratio, based on Method D, were compared graphically using J85 radial, circumferential and mixed distortion stability data. There was some disagreement. Hercock and Williams also reported the successful use of separate DC(θ critical) parameters for core and bypass flows where appropriate mean total pressures were used.

The need to standardize industry methods of measuring distortion effects on engine performance has led to the development of the SAE S-16 Committee on Gas Turbine Engine Flow Distortion. The committee, composed of industry and government representatives, has published Aerospace Recommended Practice 1420 (ARP 1420) [28]. The publication sets guidelines for experimental test procedures and recommends certain descriptor elements as well as a method of correlating the descriptors with loss in stall margin. The ARP 1420 correlation is the most recently-developed correlation and reflects achievements made by earlier indices as well as improvements based on increased experience. The correlation is, in general, said to be accurate to within $\pm$2%.

Boytos [29] prepared an extensive review of distortion indices as part of an effort to supply NAVAIR with background information for use when evaluating propulsion systems. The review presents the indices currently in use by engine manufacturers and government agencies. Boytos compiled and presents in graphical form the results of earlier investigations of distortion indices.

Based on investigations carried out by General Dynamics in conjunction with NASA Lewis Research Center and by N. H. Cotter, Boytos concluded that DI and DC(60) do not follow any trends related to loss in

stall margin. Boytos also presented the results of studies presented to the SAE S-16 Committee by NASA Lewis Research Center using data from a J85-GE-13 turbojet engine and a TF30-P-3 turbofan engine. He concluded that the indices $((\overline{P} - P_{min})/\overline{P})$ and $K\theta$ produce better correlations for a constant speed definition than for a constant mass flow definition of loss in stall pressure ratio when used with J85 data. The indices KD_2, $((\overline{P} - P_{min})/\overline{P})$, $K\theta$, and NAPC $K\theta$ all produced "good correlations" for the TF30 data. Boytos also presented results of NASA calculations of the ARP 1420 distortion correlation using data from a J85-GE-13 engine, a F100 fan, and a research fan. The correlation was shown to be generally accurate to within $\pm 2\%$.

IX. DEVELOPMENT OF DISTORTION INDICES

Distortion indices have arisen from the need to relate levels of distortion at the engine face to resultant loss in surge margin. The compressor or engine being tested is subjected to total pressure distortion generated by wire screens of varying porosity and extent, or air jets discharging high velocity air against the incoming flow. Typically, the spatial variation in inlet total pressure is measured using total pressure probe rakes consisting of five or more probes per rake spaced around the compressor annulus. Thus, circumferential and radial variations are recorded at fixed locations. The circumferential static pressure distribution is typically measured using static pressure taps located on the outer casing of the compressor. A typical engine inlet instrumented for distortion measurements is shown in Fig. 4.

A distortion index will employ one or more of the following parameters to describe the distortion present and evaluate its resultant impact on performance:

magnitude or intensity
shape factor
spatial extent factor
multiple-per-revolution factor
sensitivity factors
superposition factors
weighting factors.

The first four factors are pattern descriptors and are evaluated from

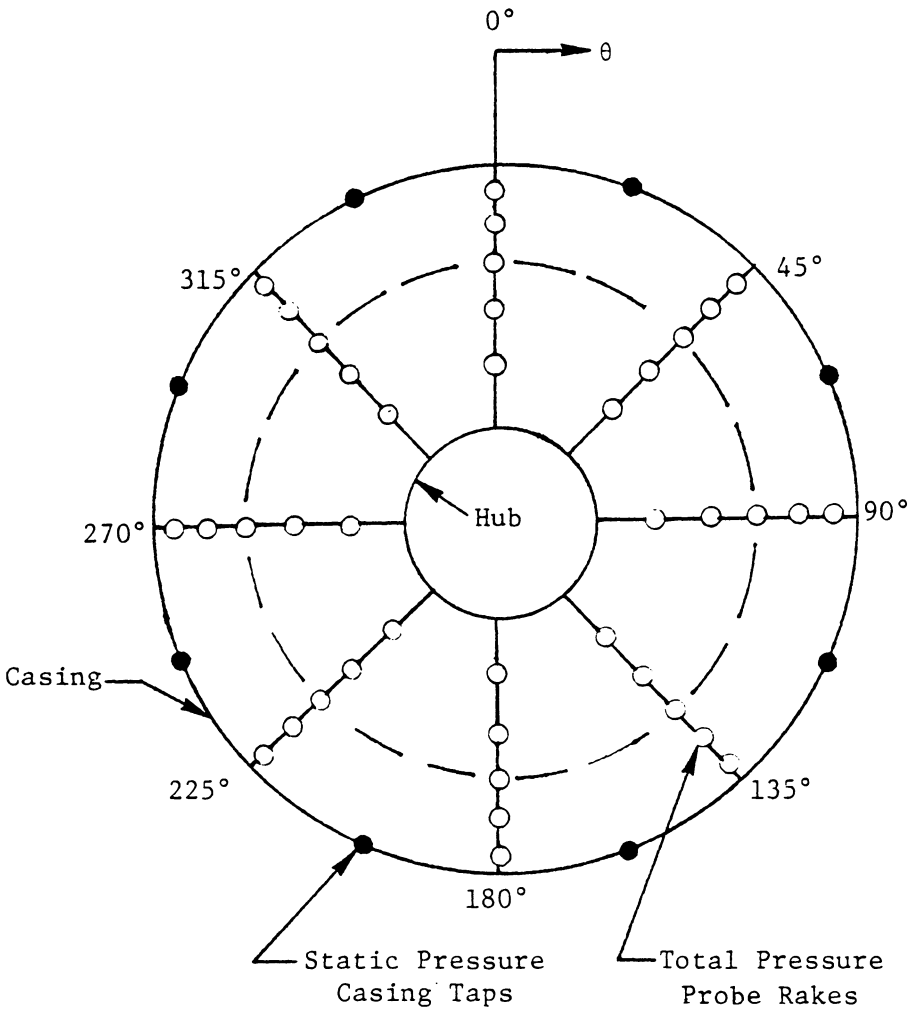

Figure 4: Typical Engine Inlet Instrumented for Distortion Measurements

the measured inlet total pressure profile. The remaining three parameters are measures of how the distortion pattern, defined in terms of the above distortion descriptors, affects the particular engine being tested. The most general distortion correlations will include all of the above factors with each parameter being evaluated from experimental data for the engine in question.

The distortion indices reviewed generally fall into three categories. The first category includes those indices designed to correlate loss in stall pressure ratio for any engine but which are not complex enough to incorporate all factors affecting dynamic response. Examples are the early $\Delta P/\overline{P}$ indices, the Rolls Royce θ critical indices, and the NAPC $K\theta$ index. The correlation derived from the parallel compressor model can also be included here. The second category includes those indices designed to correlate distortion effects for a particular engine and which do in general handle unsteady flow effects for the particular engine adequately. An example is the PWA KD_2 index. The AVCO Lycoming and Garrett AiResearch indices are included here as they contain specific weighting factors based on tests of only one or two compressor designs. In the third category are those general indices which should predict accurate results for any engine design, but which require extensive experimental data to define sensitivity coefficients and other parameters. Examples are the GE Method D and ARP 1420 correlations.

Calculation procedures for the correlation derived from the parallel compressor model and the nine total pressure distortion indices to be evaluated in this report are presented in the following paragraphs.

Similarities and differences between the indices are noted where applicable.

Parallel Compressor Model*

Parallel compressor theory, the simplest of the compressor models, divides the distorted inflow compressor into two or more compressors operating in parallel, each with uniform inlet conditions corresponding to those of the distorted and undistorted regions of the original compressor. The following three assumptions are made:

1. All compressors discharge to the same exit static pressure.
2. There is no connection between the parallel compressors.
3. Each compressor operates on the undistorted characteristic.

Parallel compressor theory may be used to predict loss in stall pressure ratio due to total pressure inlet distortion.

Two definitions of loss in stall pressure ratio exist, as it may be defined for constant mass flow or for constant engine speed. A pictoral definition of each is presented in Fig. 5. In equation form, the definitions are

$$\Delta PRS_M = \frac{PRS_b - PRS_d}{PRS_b}$$

$$\Delta PRS_N = \frac{PRS_c - PRS_d}{PRS_c}$$

* This analysis follows that of Mokelke [8].

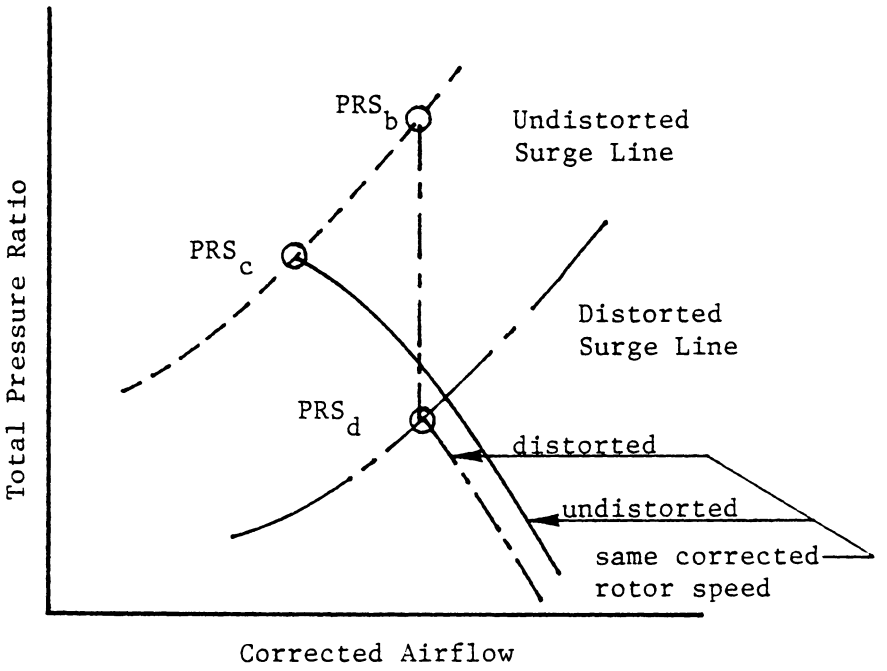

Figure 5: Compressor Characteristic Illustrating Loss in Stall Pressure Ratio Due to a Distorted Inlet

where

PRS_d = stall pressure ratio of the distorted compressor,

PRS_b = stall pressure ratio of the undistorted compressor at the same corrected mass flow rate,

PRS_c = stall pressure ratio of the undistorted compressor at the same corrected rotor speed.

The constant corrected speed definition of loss in stall pressure ratio is used in this development.

Assumption (3) of parallel compressor theory dictates that the distorted-inflow compressor will stall if one of the parallel compressors operates on the clean inlet stall line. If the additional assumption of constant exit total pressure is made, a simple relationship between loss in stall pressure ratio and the distortion index $((\overline{P} - P_{min})/\overline{P})$ can be derived.

Figure 6 illustrates a typical square wave inlet total pressure distortion. Parallel compressor theory models this distorted inflow compressor as two compressors, one with inlet conditions corresponding to the low pressure region and one with inlet conditions corresponding to the high pressure region. The parallel compressor having the low total pressure inlet condition will operate closest to the stall line. Using the operating conditions of this compressor in the definition of loss in stall pressure ratio results in the following expression:

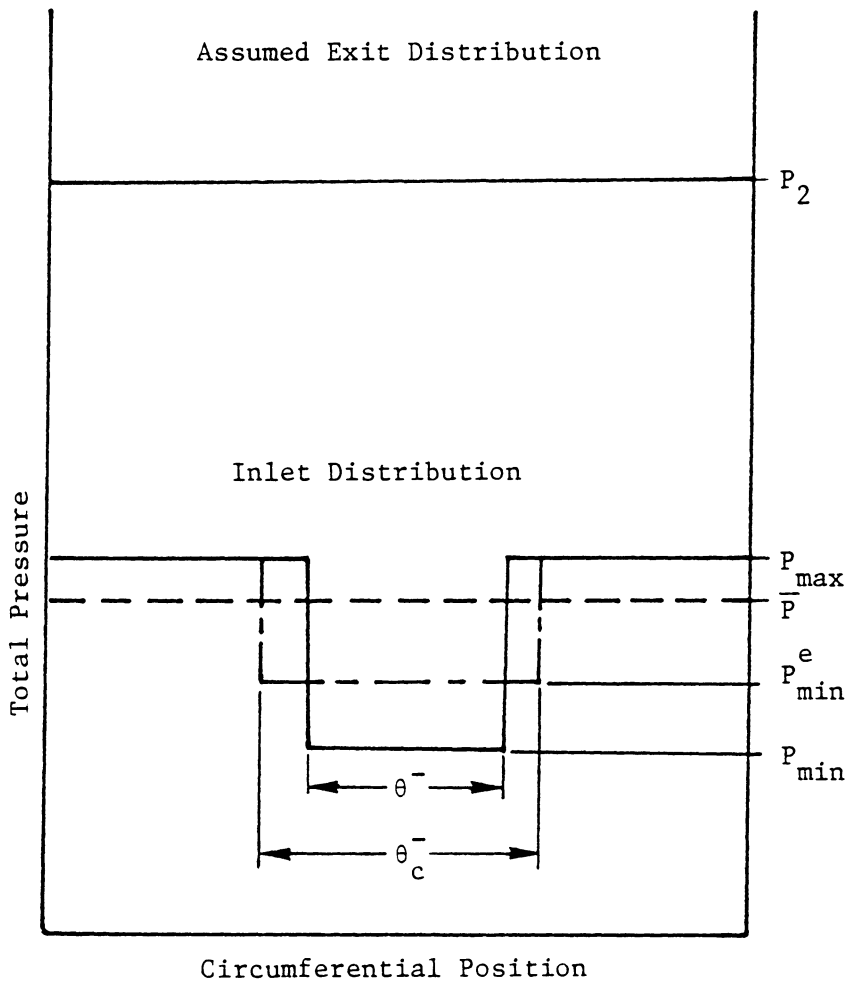

Figure 6: Total Pressure Distributions at Compressor Inlet and Exit

$$\Delta PRS_N = \frac{\frac{P_2}{P_{min}} - \frac{P_2}{\bar{P}}}{\frac{P_2}{P_{min}}} = 1 - \frac{P_{min}}{\bar{P}} \tag{1}$$

The area-averaged inlet total pressure in the above equation is calculated as follows:

$$2\pi\bar{P} = (2\pi - \bar{\theta}) P_{max} + \bar{\theta} P_{min} \tag{2}$$

Substituting this expression into equation 1 yields:

$$\Delta PRS_N = 1 - \frac{\frac{P_{min}}{P_{max}}}{1 - \frac{\bar{\theta}}{2\pi}\left(1 - \frac{P_{min}}{P_{max}}\right)} \tag{3}$$

The above expression deviates considerably from experimental results for small extent distortions. This is to be expected as parallel compressor theory assumes quasi-steady response to inlet flow conditions. Reid's [3] investigation of the effect of distortion extent or blade residence time in the low pressure region proved this to be untrue. Rather, he discovered the existence of a critical angle or minimum angle for quasi-steady response. Reid proposed including the critical angle concept in parallel compressor theory predictions for loss in stall pressure ratio. This is done by creating an effective distortion having a width equal to the critical angle and a minimum effective total pressure defined from the following equation:

$$\bar{\theta}_c (P_{max} - P^e_{min}) = \bar{\theta}(P_{max} - P_{min}) \tag{4}$$

Solving the equation for an effective distortion magnitude yields:

$$\frac{P^{e}_{min}}{P_{max}} = 1 - \frac{\bar{\theta}}{\bar{\theta}_{c}} \left(1 - \frac{P_{min}}{P_{max}}\right) \tag{5}$$

This effective total pressure ratio is used in place of the measured pressure ratio when the distortion extent is less than the critical angle. Substituting equation 5 into equation 3 yields:

$$\Delta PRS_{N} = 1 - \frac{1 - \frac{\bar{\theta}}{\bar{\theta}_{c}} \left(1 - \frac{P_{min}}{P_{max}}\right)}{1 - \frac{(\bar{\theta})^{2}}{2\pi\bar{\theta}_{c}} \left(1 - \frac{P_{min}}{P_{max}}\right)} \qquad \text{for } \bar{\theta} < \bar{\theta}_{c} \tag{6}$$

Results of parallel compressor theory calculations with and without the critical angle concept for a constant intensity distortion are presented in Fig. 7.

$\Delta P/\bar{P}$ Indices

Two of the simple $\Delta P/\bar{P}$ indices will be evaluated. Both are based on radially averaged inlet total pressure data. The first is defined as follows:

$$\frac{\Delta P_{max - min}}{\bar{P}} = \frac{P_{max} - P_{min}}{P_{avg}}$$

where

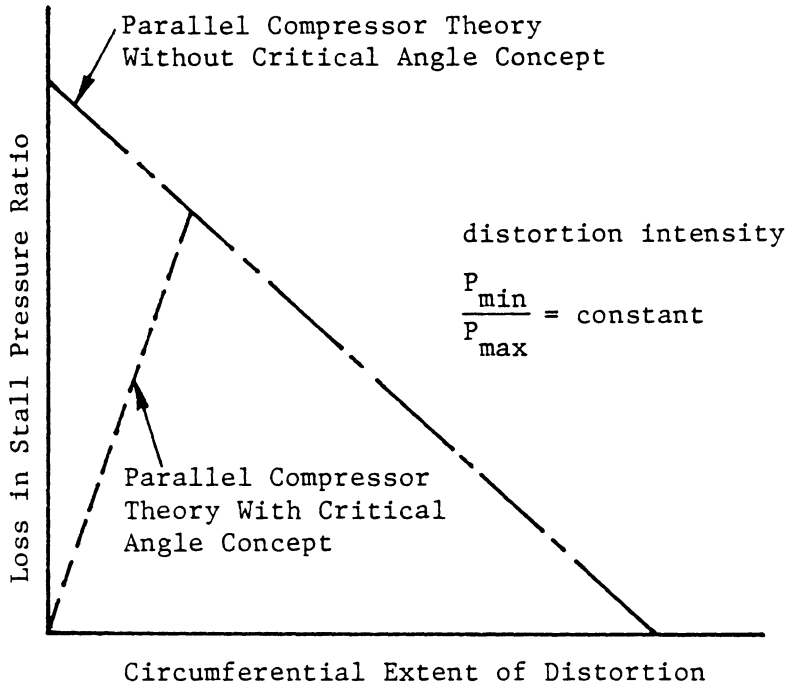

Figure 7: Parallel Compressor Theory Loss in Stall Pressure Ratio Predictions With and Without the Critical Angle Concept

P_{max} = maximum inlet total pressure,

P_{min} = minimum inlet total pressure,

P_{avg} = average inlet total pressure.

This index includes no indication of the extent of the distortion. Because of its use of maximum and minimum total pressure values, $\Delta P_{max-min}/\overline{P}$ is sensitive to single probe pressure readings.

The second $\Delta P/\overline{P}$ index incorporates circumferential extent of distortion to a small degree by including the average inlet total pressure in the numerator. It is defined as follows:

$$\frac{\Delta P_{avg\ -\ min}}{\overline{P}} = \frac{P_{avg} - P_{min}}{P_{avg}} \tag{8}$$

where the symbols are defined as before. Note the index is still sensitive to a single probe low reading because it includes minimum inlet total pressure. Both indices ignore the effects of radial distortions.

Neither of the $\Delta P/\overline{P}$ indices is capable of predicting loss in stall pressure ratio in the manner of parallel compressor theory. Rather, each index should correlate with loss in stall pressure ratio or engine/compressor rotational speed for a given set of engine/compressor stall data. Once the stalling values of the $\Delta P/\overline{P}$ indices are determined for a given data set, the indices may be used as predictive tools in the sense that values less than those at stall indicate stable operation whereas values greater than those at stall indicate unstable operation. A graph

illustrating typical results for constant extent, varying intensity circumferential distortions using the $\Delta P_{avg - min}/\overline{P}$ index is presented in Fig. 8.

Rolls Royce θ Critical Indices

References 4, 27, and 29 describe the Rolls Royce θ critical indices. The indices are defined as follows:

$$\Delta P(\theta \text{ critical})/\overline{P} = \frac{(P_{avg} - P_{min,\ \theta_c^-,\ avg})}{P_{avg}}$$

$$DC(\theta \text{ critical}) = \frac{(P_{avg} - P_{min,\ \theta_c^-,\ avg})}{q_{avg}} \qquad (9)$$

where

P_{avg} = the area-weighted mean total pressure over the engine inlet,

$P_{min,\theta_c^-,avg}$ = the minimum area-weighted mean total pressure for a sector whose circumferential extent is θ critical,

q_{avg} = the area-weighted average velocity head over the engine inlet.

The extent of the critical angle must be determined experimentally for each compressor. Reid reports that it is generally between 60° and 90° and that in the absence of experimental data, 60° is a good assumption.

The Rolls Royce indices include no allowance for effects due to

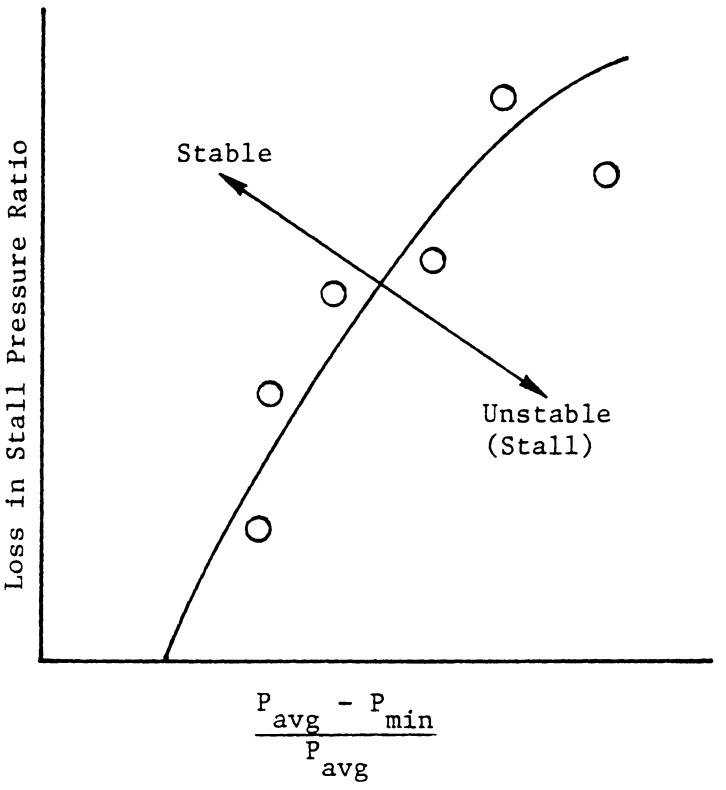

Figure 8: Gas Turbine Stalling Behavior as Correlated by the $(P_{avg} - P_{min})/P_{avg}$ Index

radial distortion. Reid explains that these effects are neglected on the following basis: (1) they are usually accompanied by circumferential distortions whose effects take precedence and (2) they are so dependent on compressor design considerations that efforts to include their effects outweigh the advantages of improved accuracy. As a compromise, for the case of high bypass ratio engines subjected to radial distortion, Reid suggests analyzing the bypass and core flows separately, neglecting radial gradients within each stream.

The Rolls Royce θ critical indices are designed to correlate with loss in stall pressure ratio in a manner similar to that of the $\Delta P/\overline{P}$ indices. Averaging of the total pressure data within a segment equal to the critical angle is a simple means of incorporating compressor dynamic response and reducing sensitivity to single probe readings.

NAPC Kθ

The Naval Air Propulsion Center (NAPC) has developed a circumferential total pressure distortion index, Kθ. The index is described by Brunda and Boytos [20] and Boytos [29]. In addition, a radial pressure distortion index, Kr, is defined by Boytos. The circumferential index is as follows:

$$K\theta = \frac{\frac{\theta}{2\pi}\left[\sqrt{q/P}\right]_{ref}}{\sqrt{q/P \;/\; \overline{q}/\overline{P}}} \qquad (10)$$

where

$\bar{\theta}$ = circumferential extent of the total pressure region less than the plane average total pressure,

P = average inlet total pressure within the low pressure region,

$\bar{P}$ = average inlet total pressure,

q = average dynamic pressure in low pressure region,

$\bar{q}$ = average inlet dynamic pressure.

The circumferential index is based on two conditions for inlet circumferential pressure distortion similarity. These conditions are (1) that the stalling rotor blade angles of attack at surge be constant for a given engine speed and (2) that the ratio of dwell time in the low pressure sector to air residence time in the blade passage be constant. Note that condition (2) requires the reduced frequency parameter defined by Mikolajczak and Pfeffer [7] to be constant for distortion similarity. Condition (1) is expressed in equation form as:

$$\frac{c_x}{\bar{c}_x} = \text{constant} \tag{11}$$

where

c_x = average axial velocity in low pressure segment,

$\bar{c}_x$ = face average axial velocity.

Condition (2) in equation form is:

$$\frac{t_{\theta^-}}{t_b} = \left(\frac{60}{N}\right) \cdot \left(\frac{\theta^-}{2\pi}\right) \cdot \left(\frac{c_x}{b}\right) = \text{constant} \qquad (12)$$

where

t_{θ^-} = dwell time in low pressure sector,

t_b = air residence time in blade passage,

N = engine speed, rpm,

b = chord length, in,

θ^- = distortion extent, radians,

c_x = average axial velocity in low pressure segment, in/sec.

The NAPC Kθ index was derived using one-dimensional, isentropic flow relations for total pressure, total temperature, and axial velocity in combination with these conditions for inlet distortion similarity.

The circumferential index can be expressed in the following form:

$$K\theta = \frac{\tau}{c_x/\bar{c}_x} \qquad (13)$$

where τ is a time constant related to the reduced frequency parameter and representative of unsteady flow effects and $c_x/\bar{c}_x$ is defined as before.

The time constant, derived from equation (12) and isentropic relations, is as follows:

$$\tau = \left[\frac{\theta^-}{2\pi} \sqrt{q/P} \right]_{ref} \qquad (14)$$

The minimum value of the above equation at the verge of stall is taken as the reference value. This reference value is the time constant used in KΘ to account for compressor rotor blade dynamic response to steady-state inlet distortion.

The axial velocity ratio may be expressed as the square root of the corresponding dynamic pressure ratio:

$$\frac{c_x}{\overline{c}_x} = \sqrt{\frac{q/P}{\overline{q/P}}}$$

Thus, the ratio is indicative of the magnitude of the distortion as well as the variation in angle of attack around the compressor circumference. If the flow is one-dimensional and isentropic, then this ratio is a function of Mach number only. In turn, for a given engine, Mach number is a function of engine speed only. Thus, if one-dimensional, isentropic flow is a reasonable assumption, the NAPC KΘ index should reduce to a function of engine speed only.

The index was evaluated using TF30 turbofan engine distortion data. Graphically, KΘ did appear to correlate well with corrected engine speed; however, variations in KΘ of up to 13% were achieved at some speeds. The KΘ index defines the maximum tolerance of an engine to steady-state circumferential pressure distortion. Because one of the similarity conditions upon which it is based applies only at the verge of surge, KΘ cannot be meaningfully evaluated for distortions that do not result in engine surge.

Boytos [29] reports the development of a NAPC radial distortion

index, Kr. The index does not reduce the data to a function of engine speed only as it is also dependent on the radial location of the distortion. Boytos reports that equally accurate results were obtained using a simple $\Delta P/\overline{P}$ index. Because the radial index did not generalize the data to a single functional dependence on engine speed, combined radial and circumferential patterns are not easily evaluated. Only circumferential inlet distortions are considered in this investigation. Consequently, the NAPC Kr index is not included here.

AVCO Lycoming DI and DI_c Indices

The calculation procedure for the AVCO Lycoming DI index is presented by Boytos [29]. The index is defined as follows:

$$DI = \left(\frac{P_{avg} - P_{low\ avg}}{P_{avg}} \right) \sqrt{M \cdot E \cdot R} \tag{16}$$

where

P_{avg} = area-weighted average total pressure,

$P_{low\ avg}$ = area-weighted total pressure in regions where P is less than P_{avg},

M = magnitude or shape factor = $6.0(P_{avg} - P_{low\ avg})/(P_{avg} - P_{low\ min})$,

$P_{low\ min}$ = minimum total pressure level,

E = extent of distorted region = $2.0(A_L)/A_{tot}$,

A_L = area over which the total pressure is less than P_{avg},

A_{tot} = total annulus area,

R = radial distortion sensitivity = maximum of $2.0(A_{L,hub}/A_L)$ or $2.0(A_{L,tip}/A_L)$,

$A_{L\ hub}$ = area extent of low pressure regions which fall in the inner 50% annulus area,

$A_{L\ tip}$ = area extent of low pressure regions which fall in the outer 50% annulus area.

Note that the extent function, E, becomes equal to 1.0 for a 180° circumferential distortion. It gives reduced weighting to shorter extent distortions and increased weighting to longer extent distortions. The radial sensitivity factor has a minimum value of 1.0 for a purely circumferential distortion and a maximum value of 2.0 for purely radial distortions. This is the only index to include a multiplicative radial distortion weighting factor.

AVCO Lycoming has also proposed the use of two indices where radial and circumferential effects are considered separately. The radial index is based on a radial profile determined by averaging probe rake data around the circumference of the compressor. Similarly, the circumferential index is based on a circumferential profile derived by radially averaging probe rake data. The resultant circumferential index is

$$DI_c = \left(\frac{P_{avg} - P_{low\ avg}}{P_{avg}} \right) \cdot Ex \cdot Sh_c \qquad (17)$$

where

$P_{low\ avg}$ = area-weighted average total pressure over the angular extent where P is less than P_{avg},

Ex = extent factor = $4.0\ \sqrt{n}\ (1.0 - \sqrt{n})$,

n = $A_L/360$,

A_L = angular extent where P is less than P_{avg},

Sh_c = circumferential shape factor = $\sqrt{A_{LL}/A_L}$,

A_{LL} = angular extent where P is less than $P_{low\ avg}$.

This index weights the common $\Delta P/\overline{P}$ descriptor with extent and shape factors. The extent factor gives maximum weight to a 60° extent distortion. (This can be determined by taking the derivative with respect to n and setting it equal to zero.) The shape factor treats a square wave distortion as the worst case with a weighting of 1.0. All other shapes are given a weighting less than 1.0.

The radial distortion index is:

$$DI_R = \left(\frac{P_{avg} - P_{low\ avg}}{P_{avg}} \right) \cdot Sh_r \qquad (18)$$

where

$P_{low\ avg}$ = area-weighted average total pressure over the channel height where P is less than P_{avg},

Sh_r = radial shape factor = $\sqrt{\frac{\text{area where P is less than } P_{low\ avg}}{\text{total area}}}$.

Recall this index is based on a circumferential average of the total pressure data. Note the radial shape factor also treats a square wave distortion as the worst case. The AVCO Lycoming DI_R index will not be evaluated as only circumferential total pressure distortions are being considered in this investigation. It was presented here for completeness.

Garrett AiResearch CDI and RDI Indices

The Garrett AiResearch indices are described by Boytos [29]. The radial and circumferential indices, RDI and CDI respectively, are computed separately. The larger of the two indices is used to correlate the effects of flow distortion on engine performance.

The two indices are calculated as follows:

$$CDI = \left(\frac{P_{R\ max} - P_{R\ min}}{P_{R\ avg}} \right) \sqrt{S \left(\frac{2A_L}{A_R} \right)}$$

$$RDI = \frac{(\bar{P}_{R\ max} - \bar{P}_{R\ min})}{P_{avg}} \qquad (19)$$

where

A_L = continuous portion of A_R where the measured total pressures are less than $P_{R\ avg}$,

A_R = annulus area of ring at distortion measurement plane,

P_{avg} = average inlet total pressure,

$P_{R\ avg}$ = average ring total pressure,

$P_{R\ max}$ = maximum ring total pressure,

$P_{R\ min}$ = minimum ring total pressure,

$P_{R\ low}$ = area-weighted average pressure in A_L of ring,

$\overline{P}_{R\ max}$ = maximum $P_{R\ avg}$ for all rings,

$\overline{P}_{R\ min}$ = minimum $P_{R\ avg}$ for all rings,

S = shape factor =

$$\frac{P_{R\ avg} - P_{R\ low}}{P_{R\ avg} - P_{R\ min}} .$$

The CDI index is very similar to the AVCO Lycoming DI index without the radial sensitivity term. Again, the extent factor is 1.0 for 180° distortions. Shorter extent distortions are derated while longer extent distortions are given added weight. The shape factor differs only by a constant from the AVCO Lycoming magnitude or shape factor. The Garrett AiResearch radial distortion index is independent of the location of the radial distortion. The radial distortion index is included here because AVCO Lycoming specifies that the maximum of CDI or RDI is used to correlate engine/compressor stall behavior; however, because only circumferential inlet total pressure data is used in this investigation, the CDI index is always larger.

Pratt and Whitney Aircraft KD_2 Index

The calculation procedure for the Pratt and Whitney Aircraft (PWA) distortion factor, KD_2, is explained by Werner, et al. [21] and Boytos [29]. The index is calculated from total pressure data measured at the

engine face using six or more total pressure rakes containing five or more probes per rake. The index is defined as follows:

$$KD_2 = \frac{\sum_{r=1}^{n} [\bar{\theta}_r \, (\frac{\Delta P}{P})_r \, \frac{OD}{D_r}]}{\sum_{r=1}^{n} [\frac{OD}{D_r}]} \tag{20}$$

where

r = particular ring of total pressure probes,

$\bar{\theta}_r$ = circumferential extent in degrees of largest single pressure depression below P_{avg} for a given ring,

$(\frac{\Delta P}{P})_r$ = $(P_{avg} - P_{min})/P_{avg}$ in percent, for a particular ring,

P_{avg} = average pressure per ring,

P_{min} = minimum pressure per ring,

OD = outer diameter of duct,

D_r = diameter of particular ring,

n = number of measurement rings.

The basic distortion magnitude-descriptor term is the $((\Delta P_{avg - min})/P_{avg})$ index. A simple extent function has been included as well as a ring weighting factor. The (OD/D_r) term is a ring weighting factor because it gives added weight to the circumferential intensity and extent functions of those instrumentation rings closest to the hub region. The KD_2 index was developed for the TF30 turbofan engine. Recall from Section VIII that Werner et. al. found the low pressure compressor to be the limiting factor in a stability analysis of the TF30

engine. Inclusion of the ring weighting factor where hub circumferential distortion is given added weight apparently reflects this characteristic of the TF30 engine.

Boytos describes a PWA KD_2 distortion index "kit". The kit describes procedures by which corrections may be made to the basic steady-state inlet distortion index to account for turbulence, Reynolds number, bleed position, and horsepower extraction effects. These corrections are not considered here. The Teledyne CAE and Williams Research Corporation indices are virtually indentical to PWA KD_2 and thus are not evaluated separately.

Pratt and Whitney Aircraft Ka_2 and Kc_2 Indices

The PWA Ka_2 and Kc_2 fan and compressor indices are described by Farr [25], Walter and Shaw [26] and Boytos [29]. The index system was designed for use with the F100/F401 turbofan engines. Each engine consists of a fan and high pressure compressor for which separate indices are defined. The fan distortion index, Ka_2, is calculated as follows:

$$Ka_2 = K\theta + b \cdot Kra_2 \tag{21}$$

where

$K\theta$ = fan circumferential distortion factor,

Kra_2 = fan radial distortion factor,

b = radial distortion weighting factor.

The inclusion of circumferential and radial distortion effects reflects the fact that the F100/F401 engine fans are sensitive to both types of inlet distortion. The radial weighting factor was found to vary from 23.42 to 0.93 with percent corrected mass flow for the F-15 distortion methodologies study. The higher value is obtained at lower mass flows when front stages are highly loaded. Because of the low resistance to radial flow, radial distortions wash out quickly and have less effect at high speeds when rear stages are more highly loaded.

The circumferential index is:

$$K\theta = \frac{\sum_{j=1}^{J} \left[\left(\frac{A_N}{N^2}\right)_{\max \text{ ring}}\right] \frac{\bar{P}_{t2}}{Q_{avg}} \left(\frac{1}{D_{ring}^{y}}\right) A_j}{\sum_{j=1}^{J} \left[\frac{1}{D_{ring}^{y}}\right] A_j} \qquad (22)$$

where

J = number of rings (probes per rake),

D = ring diameter,

y = empirical exponent,

$\bar{P}_{t2}$ = face average total pressure,

Q_{avg} = face average dynamic pressure,

A_j = ratio of ring area to total engine face area,

$A_n = \sqrt{a_n^2 + b_n^2}$, N=1,2,3,...,10,

$a_n = \frac{1}{\pi} \int_{-\pi}^{\pi} \frac{P_{t2}}{\bar{P}_{t2}} (\theta) \cos (N\theta)\, d\theta$,

$$b_n = \frac{1}{\pi} \int_{-\pi}^{\pi} \frac{P_{t2}}{\overline{P}_{t2}} (\theta) \sin (N\theta)\, d\theta,$$

$\frac{P_{t2}}{\overline{P}_{t2}} (\theta)$ = inlet total pressure distribution,

N = order of Fourier coefficient.

The Fourier coefficient terms result from approximating the circumferential pressure profile of a given instrumentation ring with a Fourier series. In general, the normalized pressure distribution is as follows:

$$\frac{P_{t2}}{\overline{P}_{t2}} = 1 + a_1 \cos\theta + a_2 \cos 2\theta + \ldots + a_N \cos N\theta + b_1 \sin\theta + b_2 \sin 2\theta + \ldots + b_N \sin N\theta$$

where a_N and b_N are defined as above. Substituting the definition of A_N results in:

$$\frac{P_{t2}}{\overline{P}_{t2}} = 1 + \sum_{N=1}^{\infty} A_N \sin (N\theta + \phi_N)$$

The maximum (A_N/N^2) term is used in calculating $K\theta$. From the above equations, it is clear that this term is a function of the distortion shape and intensity.

Similar to KD_2, this index contains a radial weighting factor reflecting the fact that hub circumferential distortion is more detrimental than tip circumferential distortion for the F100/F401 engines.

The fan radial distortion factor is calculated in the following manner:

$$Kra_2 = \frac{\sum_{j=1}^{J} \left(\frac{\Delta P_{t2}}{\overline{P}_{t2}}\right)\left(\frac{\overline{P}_{t2}}{Q_{avg}}\right)\left(\frac{1}{D^x_{ring}}\right)A_j}{\sum_{j=1}^{J} \left(\frac{1}{D^x_{ring}}\right)A_j} \tag{23}$$

where

$$\frac{\Delta P}{\overline{P}_{t2}} = \begin{cases} (\overline{P}_{t2} - \overline{P}_{t2\ ring}), \\ \text{zero if } (\Delta P_t/\overline{P}_{t2}) \text{ is less than zero based on the above equation,} \end{cases}$$

x = empirical exponent,

and all other symbols defined as before.

Both radial and circumferential components include a $\overline{P}_{t2}/Q_{avg}$ term. Some insight is achieved by considering the following two expressions:

$$\frac{\overline{P}_{t2}}{Q_{avg}} = \frac{\Delta P/Q_{avg}}{\Delta P/\overline{P}_{t2}}$$

$$\frac{\overline{P}_{t2}}{Q_{avg}} = \frac{1}{1 - \overline{P}_{s2}/\overline{P}_{t2}}$$

The first expression reveals that the term is a ratio of the two distortion indices recommended by Reid. Thus, it is a measure of the

distortion magnitude. The second expression reveals that $\overline{P}_{t2}/Q_{avg}$ is a function of Mach number (assuming one-dimensional isentropic relations apply) and therefore engine speed. Thus, the term is also a means of incorporating the functional dependence of loss in stall pressure ratio on engine speed.

The radial index is presented here for completeness in defining the PWA Ka_2 index. Because only circumferential inlet total pressure distortion data is used in the investigation, the Kra_2 index is never computed: only the PWA $K\theta$ index is evaluated.

The high compressor distortion factor, Kc_2, is calculated as follows:

$$Kc_2 = K\theta_{splitter} \left(\frac{2\theta_{crit}}{\overline{\theta}}\right) \tag{24}$$

where

$K\theta_{splitter}$ = $K\theta$ evaluated only for those rings having diameters less than or equal to the splitter diameter, $D_{splitter}$,

$\overline{\theta}$ = the greatest angular extent where $P_{t2}/\overline{P}_{t2\ ring}$ is less than 1.0 (If there are two regions of low $P_{t2}/\overline{P}_{t2\ ring}$ separated by 25° or less, they are to be treated as one low pressure region. The lower limit of $\overline{\theta}$ is θ_{crit}.),

θ_{crit} = circumferential extent of low pressure which is most detrimental to the compressor.

The splitter diameter is defined by:

$$D_{splitter} = \sqrt{\alpha_s (OD^2 - ID^2) + ID^2}$$

where

OD = outside diameter (tip),

ID = inside diameter (hub),

α_s = splitter stream tube area = ratio of engine cross-sectional area bounded by splitter streamline and compressor hub to total fan cross-sectional area.

No radial component is necessary as radial distortions are sufficiently attenuated within the fan.

Only that portion of the flow entering the engine that passes through the high pressure compressor is included in this index. The splitter stream tube area is a function of mass flow so that the percentage of flow passing through the core changes with mass flow also. This fact is incorporated into the index.

The distortion factor θ_{crit} is defined as the extent of low pressure region having the most detrimental effect on performance rather than the usual definition of minimum angle for quasi-steady response. θ_{crit} is determined to be 90° for the F100/F401 engines. The extent function of the compressor index for a 90° distortion is twice that for a 180° distortion. Walter and Shaw attribute the detrimental effects of the 90° distortion to the manner in which the circumferential distortion spreads as it passes through the F100/F401 fan.

TF30-P-3 distortion data is the only turbofan distortion data used in this investigation. All stalls occurred in the low-pressure compressor for this data set meaning that the high-pressure compressor index, Kc_2, would not be significantly tested by this data. It is therefore not computed in this investigation and was included here for completeness only.

The General Electric Method D System

The General Electric (GE) distortion methodology, Method D, is based on extensive empirical analysis of engine distortion test data but the end result, in GE's assessment, is an easy-to-implement, flexible correlation accurate to within $\pm 2\%$. Moore [22], Moore and Leuke [23], and Boytos [29] present the necessary equations for calculation of the Method D distortion system. Method D includes both radial and circumferential distortion effects and is based on data from six or more total pressure rakes of five probes per rake. The final product of the GE distortion methodology is the index, ID. ID is defined in the following manner:

$$ID = \frac{\text{stability margin loss due to distortion}}{\text{stability margin available for distortion}} . \tag{25}$$

Values of ID greater than one indicate unstable operation. The index is calculated as follows:

$$ID = B \cdot K_c \cdot IDC + KR \cdot IDR \tag{26}$$

where

IDC = larger of IDC_h and IDC_t,

IDR = larger of $K_h(IDR_h/K_r)$ and $K_t(IDR_t/K_r)$,

$IDC_h = (IDC_1 + IDC_2)/2$,

$IDC_t = (IDC_4 + IDC_5)/2$,

$IDR_h = \Delta P/PRD_1 + \alpha_h(\Delta P/PRD_2)$,

$IDR_t = \Delta P/PRD_5 + \alpha_t(\Delta P/PRD_4)$,

$IDC_r = S_r \cdot E_r \cdot M_r \cdot \Delta P/PAV_r$,

$\Delta P/PAV_r = (P_{\text{ring avg}} - P_{\text{ring min}})/P_{\text{face avg}}$ r=1,2,3,4,5,

$\Delta P/PRD_r = (P_{\text{face avg}} - P_{\text{ring avg}})P_{\text{face avg}}$ r=1,2,3,4,5.

The following terms, factors, and subscripts are used in the above formulations:

Terms

$P_{\text{face avg}}$ = face area-averaged total pressure

$P_{\text{ring avg}}$ = ring area-averaged total pressure

$P_{\text{ring min}}$ = ring minimum total pressure within largest low pressure area

Factors

B = superposition factor

K_c = circumferential sensitivity

K_r = radial sensitivity (which is either K_t or K_h depending on IDR selection)

α_h = hub radial extent factor

α_t = tip radial extent factor

S = pattern shape factor

E = circumferential extent factor

M = multiple low pressure areas factor

Subscripts

c = circumferential

r = radial

h = hub or inner region

t = tip or outer region

r = instrumentation ring where 1 is closest to hub and 5 is closest to tip

Clearly, the correlation includes many experimental coefficients. Steenken describes a simple procedure for evaluating the coefficients in a draft copy of a section of a report to be published by the SAE S-16 Committee [30]. Consider the index, ID, written as follows:

$$ID = (K_c \cdot \Delta P/PAV_r) \cdot B \cdot E \cdot S \cdot M + (K_r \cdot \Delta P/PRD_r) \tag{27}$$

For simplicity, let S = M = 1.0. Now equation 27 can be written in the following form:

$$ID = ID_{c,180} \frac{ID_{c,180,R}}{ID_{c,180}} \frac{ID_{c,\theta,R}}{ID_{c,180,R}} + ID_R \tag{28}$$

where

$ID_{c,180}$ = $K_c(\Delta P/PAV_r)$ and represents the loss of surge pressure ratio assuming the low pressure region has an extent of 180° and that no radial distortion is present,

$\frac{ID_{c,180,R}}{ID_{c,180}}$ = B and represents the ratio of the loss in pressure ratio due to a 180° 1/rev defect with radial distortion to the loss of surge pressure ratio due to a pure circumferential defect of 180°,

$\frac{ID_{c,\theta,R}}{ID_{c,180,R}}$ = E and represents the ratio of the loss in surge pressure ratio due to a circumferential defect of arbitrary angular extent with radial distortion to the loss in surge pressure ratio due to a 180° 1/rev defect with radial distortion,

ID_R = loss in surge pressure ratio due to radial distortion as if no circumferential distortion were present.

The above formulation suggests a simple method for determining K_c, K_r, B, and E. K_c is determined as a function of engine speed from test data obtained using 180° 1/rev screens. Because the test data is for purely circumferential distortions of 180° extent, B = E = 1.0 and ID_r = 0. Thus, the circumferential sensitivity may be evaluated from the following equation:

$$K_c = \frac{ID_{c,180}}{(\Delta P/PAV_r)} .$$

A graph of K_c versus engine speed may be obtained if tests are run at more than one speed.

Similarly, the radial distortion sensitivity is determined using test data from purely hub or tip radial distortions. In this case K_c = 0, so that K_R is calculated as follows:

$$K_R = \frac{ID_R}{(\Delta P/PRD_r)}.$$

Now that the circumferential and radial distortion sensitivity coefficients are known, the superposition factor, B, can be determined from test data for combined 180°, one-per-revolution, circumferential and radial distortion screens. Recognizing that E = 1.0, permits the determination of B from equation 27 in the following manner:

$$B = \frac{(ID - K_R \frac{\Delta P}{PRD})}{K_c(\frac{\Delta P}{PAV_r})}$$

Finally, the extent as a function of engine speed may be calculated from test data for varying extent distortions since K_c, K_r, and B are now all known functions of engine speed. Solving for E using equation 27 yields:

$$E = \frac{ID - K_R (\frac{\Delta P}{PRD})}{B \cdot K_c (\frac{\Delta P}{PAV_r})}$$

The above procedure requires extensive amounts of test data; however, the final result is quite general and may be used to calculate the loss in surge pressure ratio for the engine in question due to any pattern which falls within the range of the parameters tested.

In the absence of the required test data, GE proposes two alternative formulations called Phase 0 and Phase 1. Phase 0 Method D is an

extreme simplification of the original index in which the following assumptions are made:

$$S = E = M = B = K_c = K_r = 1.0$$

$$\alpha_h = \alpha_t = 0.0.$$

Thus, equation 27 is reduced to

$$ID = \frac{\Delta P}{PAV} + \frac{\Delta P}{PRD} . \tag{29}$$

Phase 0 Method D is very similar to the early indices. The circumferential intensity is the same index proposed by Reid; however, even in this simplistic form, the method does not neglect the effects of radial distortion.

Phase 1 Method D includes only the following simplifying assumptions:

$$S = E = M = 1.0$$

$$\alpha_h = \alpha_t = 0.0.$$

Thus, the radial and circumferential sensitivity coefficients and superposition factor are still determined experimentally.

Summarizing, the unmodified GE distortion methodology assumes that engine response to inlet total pressure distortion is influenced by the shape, extent, and number of low pressure regions. The effect of combined radial and circumferential distortions is not assumed to be equal to the sum of the effects of each type of distortion considered separately.

ARP 1420 Distortion Correlation

The ARP 1420 distortion correlation is the result of SAE S-16 Committee efforts to standardize procedures for describing the effects of inlet flow distortion on engine performance. The committee, formed in 1971 and comprised of representatives from engine and aircraft companies and government agencies, published their recommended procedure in 1977. The correlation scheme proposed by the committee is the most recent distortion correlation system and as such, reflects the developments and achievements of earlier indices.

Circumferential and radial distortion descriptor elements are used to quantify the distortion at the aerodynamic interface plane. These elements are correlated with percent loss in stall pressure ratio in the following manner:

$$\Delta PRS_N = \sum_{i=1}^{N} \left[KC_i \left(\frac{\Delta PC}{P}\right)_i + KR_i \left(\frac{\Delta PR}{P}\right)_i + C_i \right] \times 100. \qquad (30)$$

where

N = the number of instrumentation rings,

KC = circumferential distortion sensitivity,

$\Delta PC/P$ = circumferential distortion intensity,

KR = radial distortion sensitivity,

$\Delta PR/P$ = radial distortion intensity,

C = offset term.

The sensitivity and offset coefficients are functions of distortion

content (magnitude, extent, etc.), system design, and operating conditions. They are derived from test data and should predict loss in stall pressure ratio within $\pm$ 2%.

The circumferential intensity and extent functions are determined from linear interpolation of the pressure data for a given instrumentation ring. An example pressure profile is presented in Fig. 9. The extent and intensity functions are defined below:

$$\text{Extent} = (\bar{\theta})_i = \theta_{2i} - \theta_{1i} \quad \text{(see Fig. 9)}$$

$$\text{Intensity} = \left(\frac{\Delta PC}{P}\right) = \left(\frac{PAV_i - PAVLOW_i}{PAV_i}\right)$$

where

$$PAV_i = \frac{1}{360} \int_0^{360} P(\theta)\, d\theta = \text{ring average pressure},$$

$$PAVLOW_i = \frac{1}{\bar{\theta}_i} \int_{\bar{\theta}_i} P(\theta)_i\, d\theta.$$

If more than one low pressure area exists within a given ring pressure profile, these definitions may be altered. Figure 10 shows an example profile with two low pressure regions and consequently, two high pressure regions. If the two low pressure regions are separated by high pressure regions with extents less than θ^+_{min}, the two low regions are considered as an equivalent one-per-revolution distortion. The value of θ^+_{min} is determined from experiment but a value of 25° may be used in the absence of other information. Thus, the multiple-per-rev function, MPR, is set equal to 1.0 for this case and the extent and intensity functions

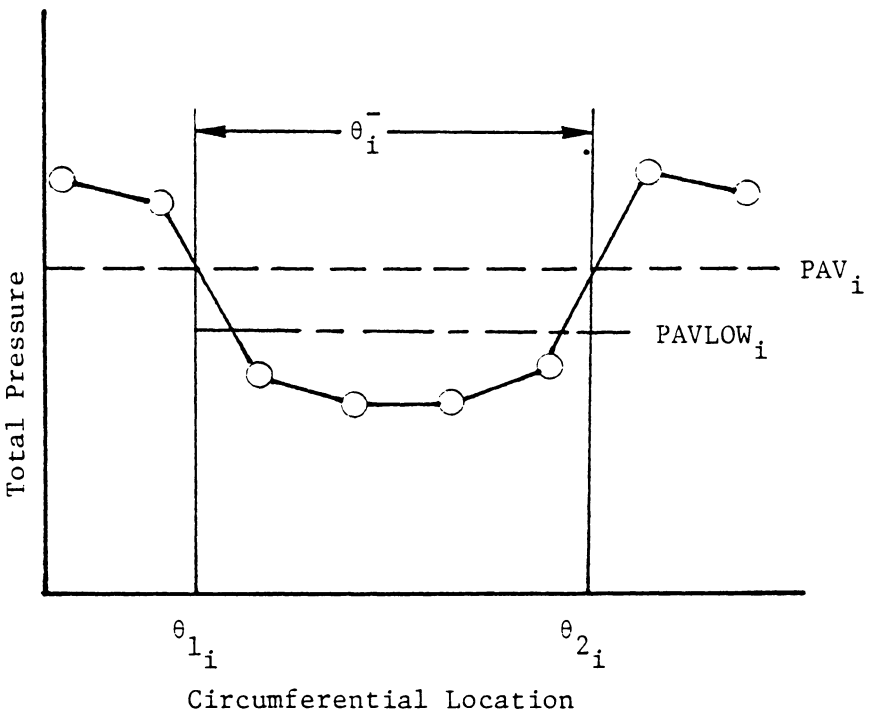

Figure 9: Ring Circumferential Distortion for a One-Per-Rev Pattern

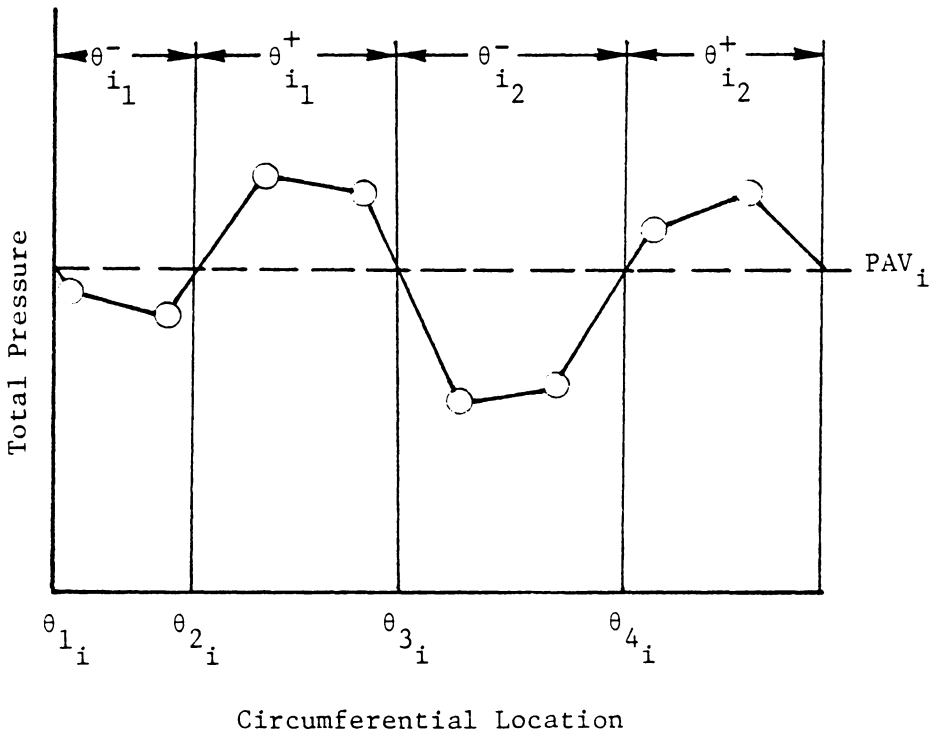

Figure 10: Ring Circumferential Distortion for a Multiple-Per-Rev Pattern

are evaluated as shown below:

$$\theta^{-} = \sum_{k=1}^{Q} [\theta^{-}_{i,k}]$$

$$(\frac{\Delta PC}{P})_i = \frac{PAV_i - PAVLOW_i}{PAV_i}$$

where $PAVLOW_i = \frac{1}{\theta^{-}_i} \sum_{k=1}^{Q} \int_{\theta^{-}_{i,k}} P(\theta)_i \, d\theta$,

or alternately,

$$(\frac{\Delta PC}{P})_i = \frac{\sum_{k=1}^{Q} [(\frac{\Delta PC}{P})_{ik} \theta^{-}_{ik}]}{\sum_{k=1}^{Q} [\theta^{-}_{i,k}]}$$

where Q = total number of low pressure regions separated by less than θ^{+}_{min}. If the extent of the high pressure region is not less than θ^{+}_{min}, then the following definitions apply:

intensity = $(\frac{\Delta PC}{P})_i$ corresponding to the maximum product, $[(\frac{\Delta PC}{P})_{ik} \theta^{-}_{ik}]$,

extent = $\theta^{-}_{i,k}$ corresponding to the maximum product, $[(\frac{\Delta PC}{P})_{ik} \theta^{-}_{i,k}]$,

$$MPR_i = \frac{\sum_{k=1}^{Q} [(\frac{\Delta PC}{P})_{ik} \theta^{-}_{i,k}]}{\max [(\frac{\Delta PC}{P})_{ik} \theta^{-}_{ik}]}$$

where the multiple-per-rev function represents the equivalent number of low pressure regions.

The radial intensity is defined as follows:

$$\left(\frac{\Delta PR}{P}\right)_i = \frac{PFAV - PAV_i}{PFAV}$$

where PFAV is the area-weighted face-average pressure. For instrumentation rings at centers of equal areas:

$$PFAV = \frac{1}{N} \sum_{i=1}^{N} (PAV)_i$$

where N is the number of instrumentation rings. Both positive and negative values of radial intensity are possible. A positive value indicates a low pressure region with corresponding detrimental effects. A negative value will increase surge pressure ratio.

The draft copy of the S-16 Committee report explains the rationale behind the descriptor definitions. Of prime importance is that the elements reflect the experimentally-established facts that engine compression component stability is a function of (1) distortion magnitude where circumferential and radial variations have different effects (accounted for by radial and circumferential intensities), (2) the time spent within the distorted sector (extent), and (3) the number of low pressure regions encountered (MPR). The form of these parameters was selected for ease of calculation and to avoid sensitivity to single low total pressure readings. The circumferential intensity was normalized by the ring average pressure rather than the face average

pressure to avoid "double bookkeeping" which sometimes occurs in complex distortion patterns. "Double bookkeeping" makes the distortion appear more severe than it actually is by contributing to both the circumferential and radial intensity elements.

As stated earlier, the sensitivity and offset coefficients are, in general, functions of distortion content, system design, and operating conditions. For clarity and ease of application, these coefficients may be expanded in a manner similar to the GE distortion methodology. For example, consider an expanded circumferential intensity:

$$KC_i = KC \cdot f(\bar{\theta}_i) \cdot f(MRP_i) \cdot \alpha_i$$

where

KC = reference sensitivity,

$f(\bar{\theta}_i)$ = extent function,

$f(MPR)$ = multiple-per-rev function,

α_i = ring weighting factor or defect location function.

The reference sensitivity is generally based on a 180°, one-per-rev, circumferential distortion and is a function of engine speed only. The extent, multiple-per-rev and distortion location functions may be determined in a manner similar to that described for the GE index, ID.

Summary

The parallel compressor model and the nine distortion index correlations evaluated in this investigation have been presented in this

section. The early indices used pattern descriptors exclusively to affect the correlation. System design influence was first incorporated via the inclusion of critical angle effects. The sensitivity and superposition factors of the more recent indices have further served to incorporate the effects of system design as well as to include the influence of operating conditions. Figure 11 is a chart illustrating index development in terms of the progressive inclusion of factors affecting correlation accuracy. Clearly the price paid for improved accuracy is increased complexity. A more fundamental and simplistic approach is described in the next section.

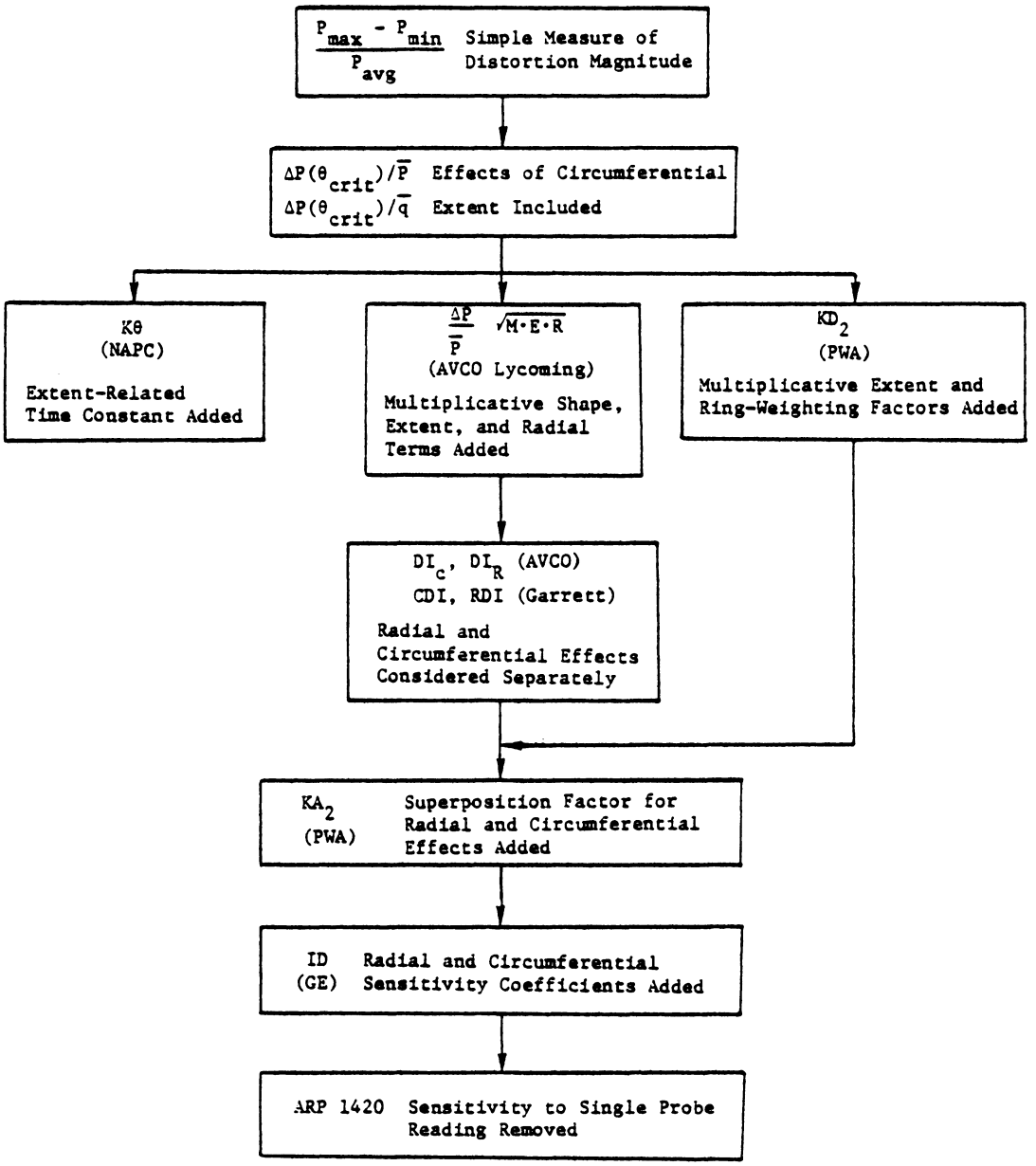

Figure 11: Relationship Between Distortion Indices

X. APPLICATION OF FREQUENCY RESPONSE FUNCTIONS TO DISTORTION INDICES

Introduction of Concept

Early distortion indices employed a simple measure of distortion magnitude or intensity to correlate the measured inlet distortion with resultant effect on engine performance. This proved inadequate in many instances so that other factors representing compressor dynamic response, e.g., distortion extent, multiples-per-revolution, distortion shape, etc., were added to the basic index. Some indices included these factors as fixed multipliers while other indices included a functional relationship evaluated for each particular engine. In the former case, general applicability of the index suffers while the latter requires extensive experimental data. An alternative approach is to modify the measured inlet total pressure distribution in such a way that the influence of dynamic response factors is contained within the modified or "effective" total pressure distribution. Thus, applying the simple distortion magnitude-descriptor indices to the "effective," rather than the measured total pressure distribution should produce a better correlation.

An illustration of how the effective total pressure distribution might modify the measured distribution for two different extent square wave distortions is presented in Fig. 12. Note that the magnitude or intensity of the small extent distortion, as defined in terms of P_{max}/P_{min}, is reduced by the effective total pressure distribution.

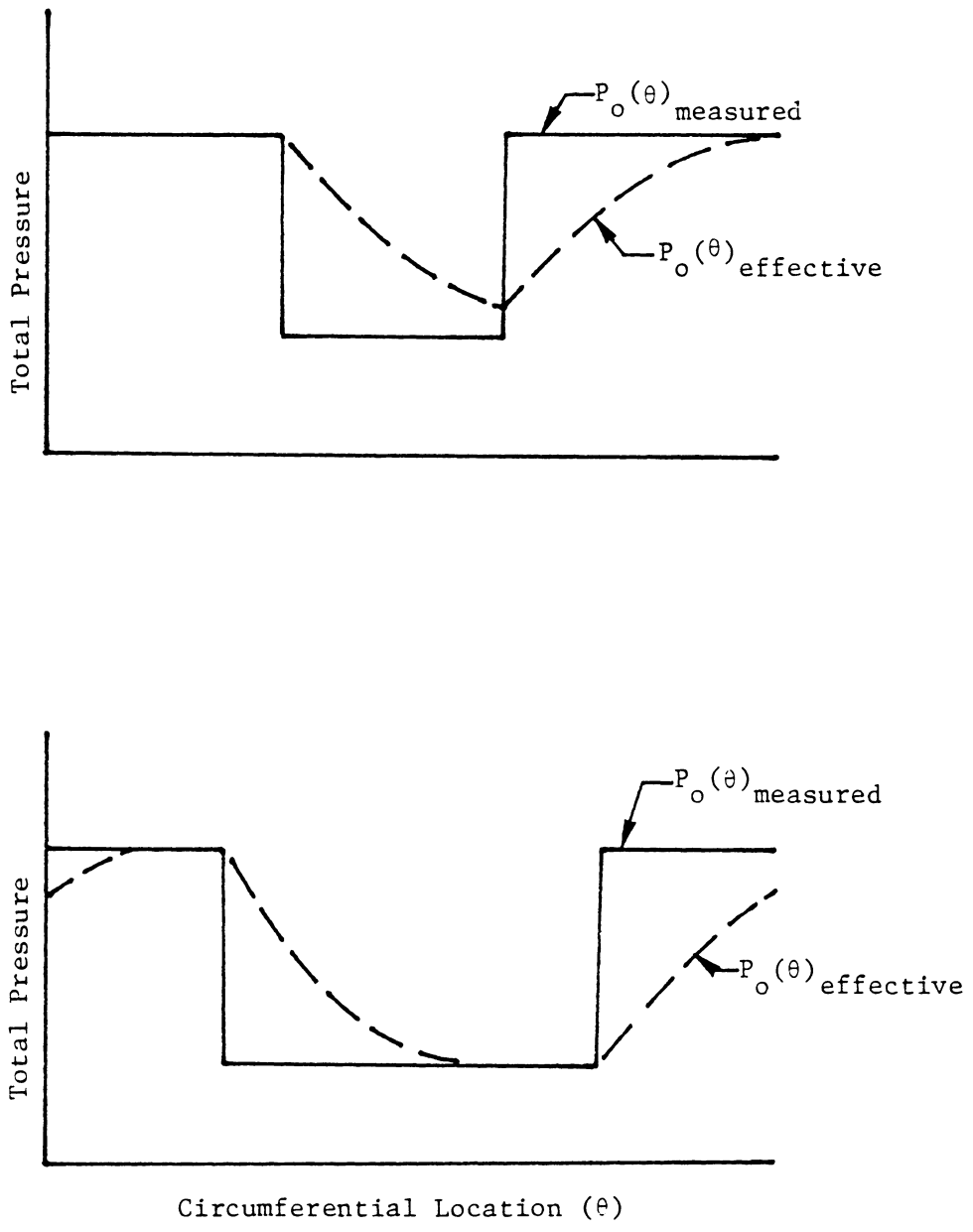

Figure 12: Effective and Measured Total Pressure Profiles for Two Different Extent Square Wave Distortions

Thus, using parallel compressor theory in combination with an effective total pressure distribution has essentially the same effect on parallel compressor theory predictions for small extent distortions as does the Reid critical angle concept [4]. This alternative approach, i.e., the concept of modifying the measured inlet total pressure distribution as a means of incorporating compressor dynamic response in a distortion index, is explored in this section.

Background Concerning Solution Technique

A method for deriving the effective total pressure distribution has been made possible by recent developments in data aquisition methods which have served to facilitate the measurement of on-rotor pressure fluctuations. It is now possible to measure rotor blade dynamic response to inlet flow distortion. The ability to measure dynamic response makes possible the use of the powerful frequency response method as a means of defining the dynamics of the compressor flow system.

The frequency response method works within the frequency domain, relating system response to the applied forcing function via a frequency response function. The frequency response function is a special case of the transfer function. The frequency response method represents an alternative to the classical method in which a linear differential equation is used to relate input and output functions. The major difficulty in using the classical approach is obtaining the appropriate differential equation. Simple experimental methods for identifying the proper response equation are not available. The frequency response

function, on the other hand, can be determined relatively simply from experimental dynamic response data.

The frequency response function is defined as the Fourier transform of the response function divided by the Fourier transform of the forcing function. Hence, all that is required to develop a frequency response function is a time domain representation of the appropriate forcing and response functions. Identifying the frequency response function for all frequencies completely defines the dynamic characteristics of a system. Thus, once the frequency response function is identified, any forcing function in the time domain can be transformed to the frequency domain, multiplied by the frequency response function and then returned to the time domain as the desired system response function, if the system being modeled is linear. For more detailed information concerning the frequency response method see Newland [31].

The frequency response method is used in this investigation as a means of deriving the effective total pressure distribution from the measured distribution. Specifically, a transfer function in the form of a frequency response function is used to transform the measured total pressure distribution to the effective total pressure distribution. The frequency response function completely defines the dynamic characteristics of the compressor. These characteristics are thus reflected in the derived effective total pressure distribution. The following equation describes the computational procedure:

$$P_o(\theta)_{eff} = F^{-1} [F(P_o(\theta)_{meas}) \times R(\omega)]$$

where

F = Fourier transform,

F^{-1} = inverse Fourier transform,

$P_o(\theta)_{meas}$ = measured inlet total pressure profile,

$P_o(\theta)_{eff}$ = effective inlet total pressure profile,

$R(\omega)$ = frequency response function.

The use of a transfer function, whether of the frequency response function type or otherwise, is appropriate only if the system is linear. Hence, employing this technique requires the assumption that non-linear dynamic departures in the flow system are small.

Clearly, determination of the effective total pressure distribution depends upon identification of the frequency response function. The initial goal is thus the development of a generally applicable frequency response function. Recall that the frequency response function is defined as the ratio of the Fourier transforms of the response and forcing functions. For this application of the frequency response method, the forcing function is the measured inlet total pressure distribution and the response function is the effective total pressure distribution. Thus, it is only necessary to identify the time domain measured and effective total pressure distributions, compute the Fourier transforms, and form the ratio to produce a frequency response function that is at least applicable for the case in point.

The frequency response method is only useful if a generalized frequency response function can be identified. There is no advantage in

utilizing a frequency response function that is able only to recreate the effective total pressure distribution from which it was derived. Verification of the general applicability or identification of necessary modification parameters, such as compressor speed, airfoil shape, number of stages, etc., will require extensive experimental investigation.

The following section describes the method by which the effective total pressure distribution is derived from on-rotor pressure measurements. This is a necessary first step in the derivation of the frequency response function. Following a general discussion of the proposed technique, actual frequency response functions are computed using experimental data from a low-speed, axial-flow compressor.

Solution Technique

The frequency response function is determined from the ratio of the Fourier transforms of the time domain representations of the effective and measured total pressure distributions. It is at present not known what influence compressor design, operating conditions, and distortion content will have on the frequency response function. This will require extensive experimental investigation. The purpose of this section is simply to demonstrate how the effective total pressure distribution is derived so that a frequency response function (not necessarily a generally-applicable frequency response function) can be determined.

An effective total pressure distribution does not exist as a physical quantity and therefore cannot be measured during an experimental investigation. However, other dynamic quantities, such as normal

force coefficient, can be experimentally determined from dynamic on-rotor pressure measurements. The dynamic normal force coefficient can be used in combination with the known steady-state normal force coefficient curve to derive an effective angle of attack distribution. The effective angle of attack distribution is defined as that angle of attack distribution which yields a normal force coefficient equivalent to the dynamic (measured) coefficient but derived from the steady-state normal force coefficient curve. This effective angle of attack distribution is used in combination with the measured inlet flow angle and static pressure distributions to derive an effective total pressure distribution. The desired frequency response function is then determined by considering the measured inlet total pressure distribution to be the forcing function and the effective total pressure distribution to be the response function. The ratio of the Fourier transforms of the response and forcing functions yeilds the frequency response function.

To further explore the concepts expressed in the preceding paragraph, a frequency response function was calculated using the experimental data of Sexton [1]. The test compressor used by Sexton was a low-speed, single-stage, axial-flow compressor subjected to a screen-induced, 165° extent, inlet flow distortion. The compressor was instrumented for on-rotor pressure measurements at 85% span for five positions along the blade chord on both pressure and suction blade sides. The inlet total and static pressure and flow angle distributions were also measured.

Sexton derived a dynamic normal force coefficient distribution from

the dynamic on-rotor pressure measurements. Sexton's dynamic normal force coefficient distribution is reproduced in Fig. 13. The independent variable in this figure is circumferential location defined in terms of the center of each of the blade passages formed by the 37 inlet guide vanes of the test compressor.

Sexton also developed a steady-state normal force coefficient curve characteristic of the rotor blades in the test compressor. This steady-state or quasi-steady normal force coefficient curve is presented in Fig. 14. Clearly, the quasi-steady normal force coefficient curve is triple-valued. Hence, attempts to derive an effective angle of attack distribution using this curve and the measured dynamic normal force coefficient resulted in three possible effective angles of attack.

In order to circumvent this problem, the dependent variable (quasi-steady normal force coefficient) was normalized by the independent variable (angle of attack). This resulted in the curve of Fig. 15. This curve is double-valued so that the problem of multiple angles of attack still existed. The dependent variable was therefore again normalized by the independent variable, producing the curve of Fig. 16. This provided the desired single-valued, quasi-steady curve. It was then necessary to normalize the dynamic (measured) normal force coefficient by the measured angle of attack squared. The effective angle of attack distribution was derived by determining the angle of attack that produced a C_N/α^2 equal to the measured C_N/α^2 but determined from the quasi-steady C_N/α^2 curve. A graph of the measured angle of attack and the angle of attack developed from the above procedure is presented

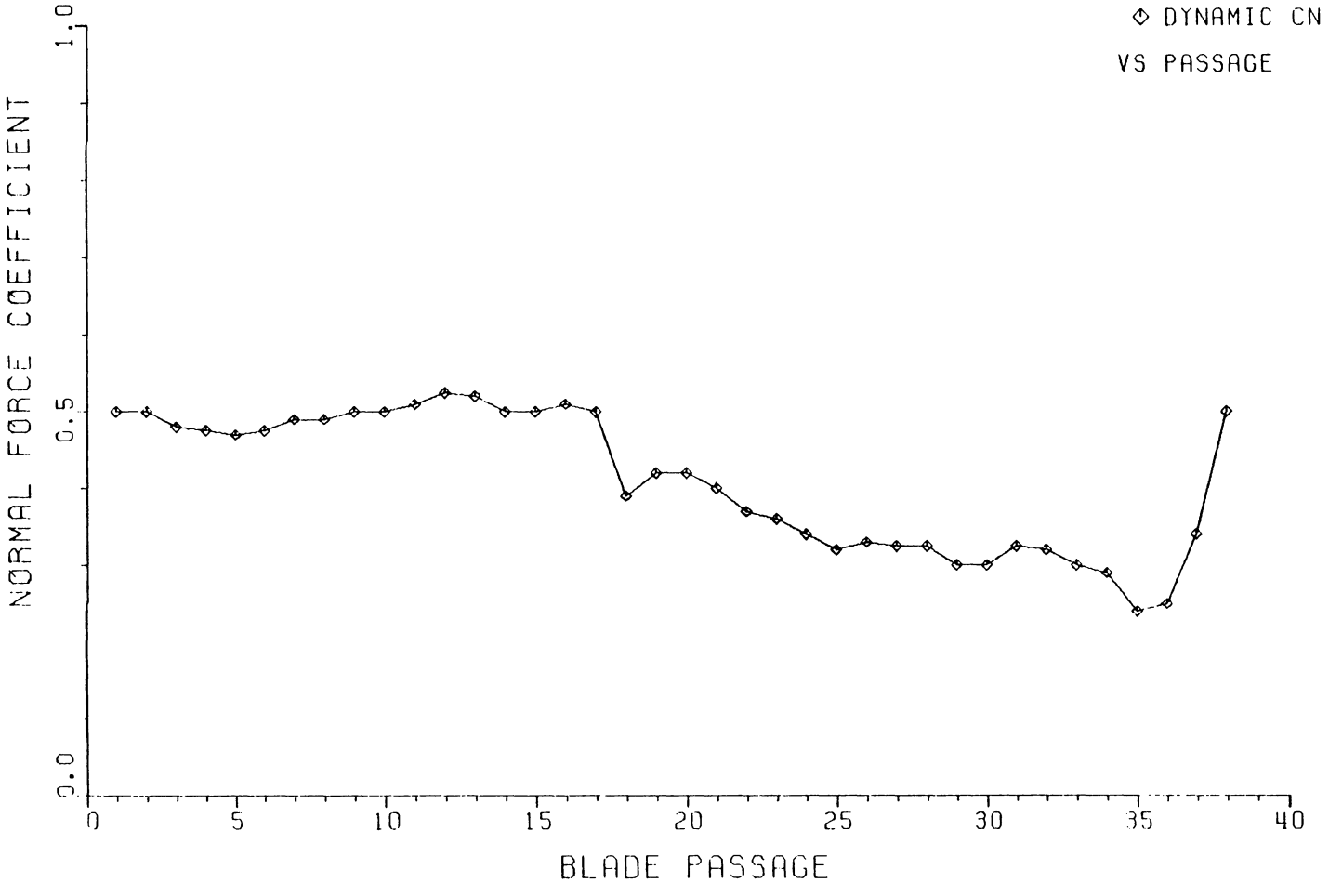

FIGURE 13: DYNAMIC NORMAL FORCE COEFFICIENT

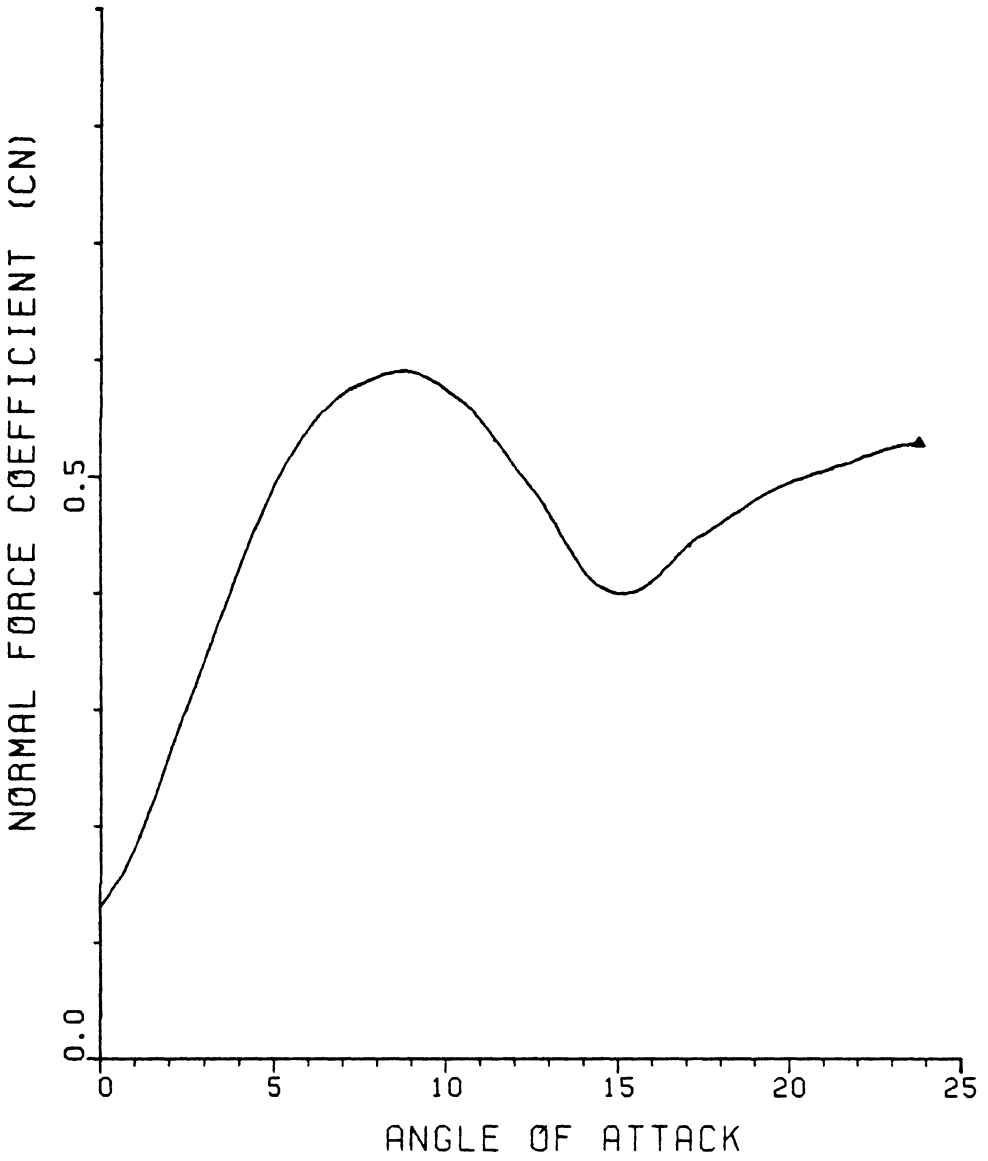

FIGURE 14: QUASI-STEADY NORMAL FORCE COEFFICIENT

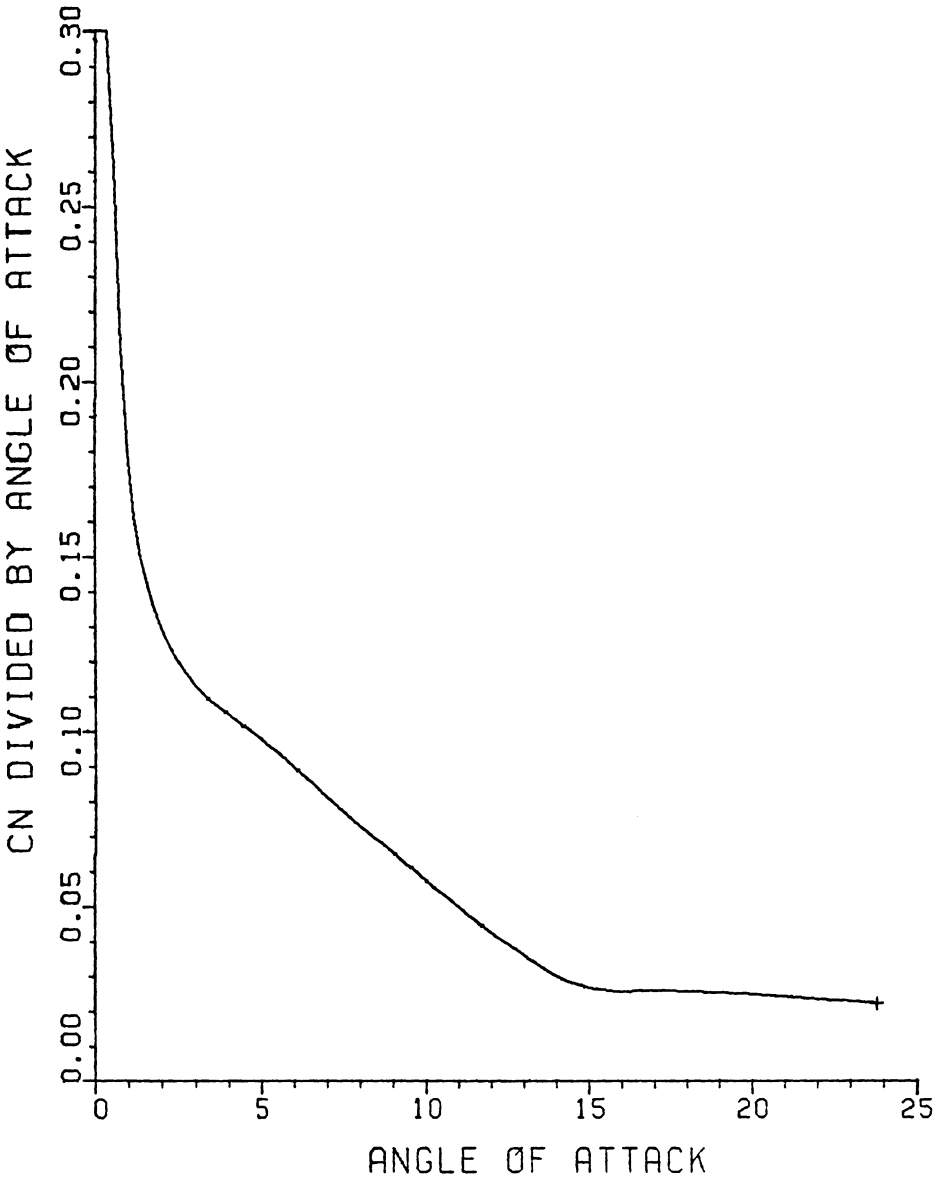

FIGURE 15: QUASI-STEADY NORMAL FORCE COEFFICIENT NORMALIZED BY ANGLE OF ATTACK

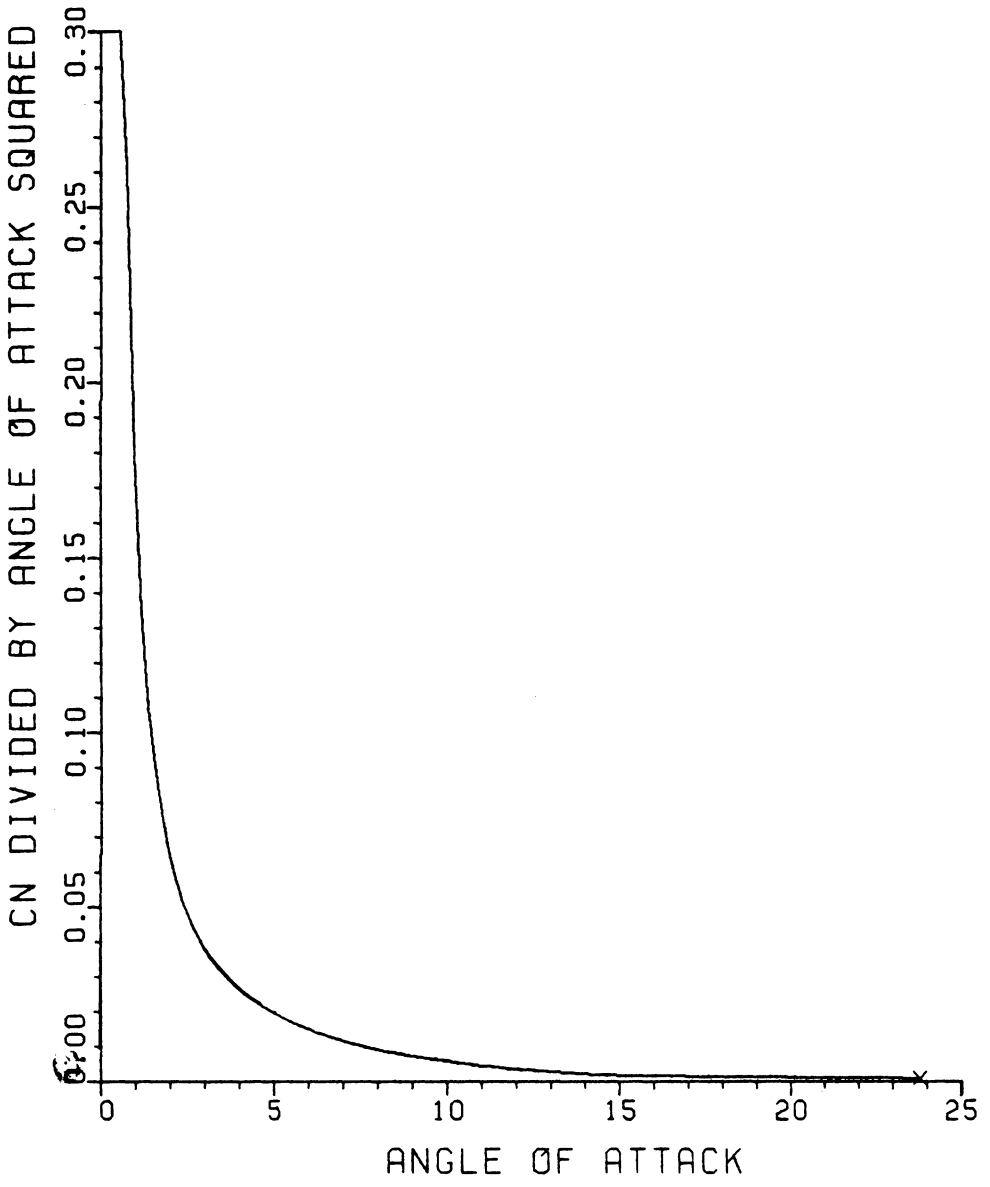

FIGURE 16: QUASI-STEADY NORMAL FORCE COEFFICIENT NORMALIZED BY ANGLE OF ATTACK SQUARED

in Fig. 17.

An effective total pressure distribution was then determined from the effective angle of attack distribution. The velocity diagram for flow into the rotor of the test compressor is presented in Fig. 18. An effective or equivalent inlet velocity was determined as follows:

$$c_{eff} = \frac{U \sin (90 - \beta - \alpha_{eff})}{\sin (\beta + \alpha_{eff} - \theta)}$$

where U is the tangential blade speed, β is the rotor blade angle, and θ is the inlet flow angle. The effective total pressure was then calculated as follows:

$$P_o(\theta)_{eff} = P_{static} + \frac{1}{2} \rho \, c_{eff}^2.$$

An overlay of the measured and effective total pressure distributions is presented in Fig. 19.

Hence, the effective total pressure profile is derived from the measured compressor dynamic response (in the form of on-rotor pressure data). It can be viewed as the input to a quasi-steady model which causes the model to produce results equivalent to the actual compressor response. A summary of the procedure followed in developing the effective total pressure profile is presented in Fig. 20. Recall the ultimate goal is the development of a generally-applicable frequency response function: the derivation of effective total pressure profiles from dynamic on-rotor data is a necessary first step in this development.

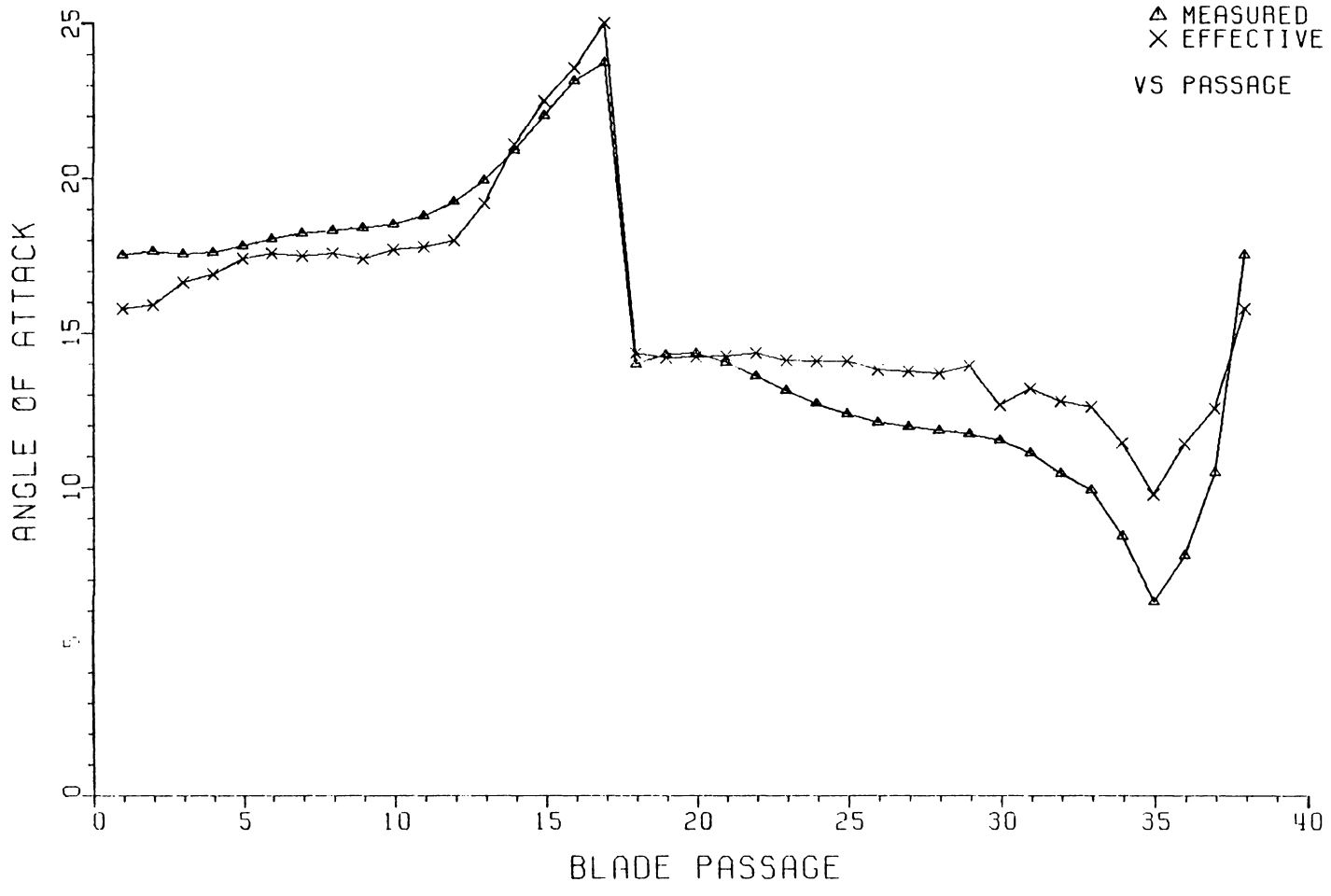

FIGURE 17: MEASURED ANGLE OF ATTACK AND EFFECTIVE ANGLE OF ATTACK DEVELOPED FROM EXPERIMENTAL DATA

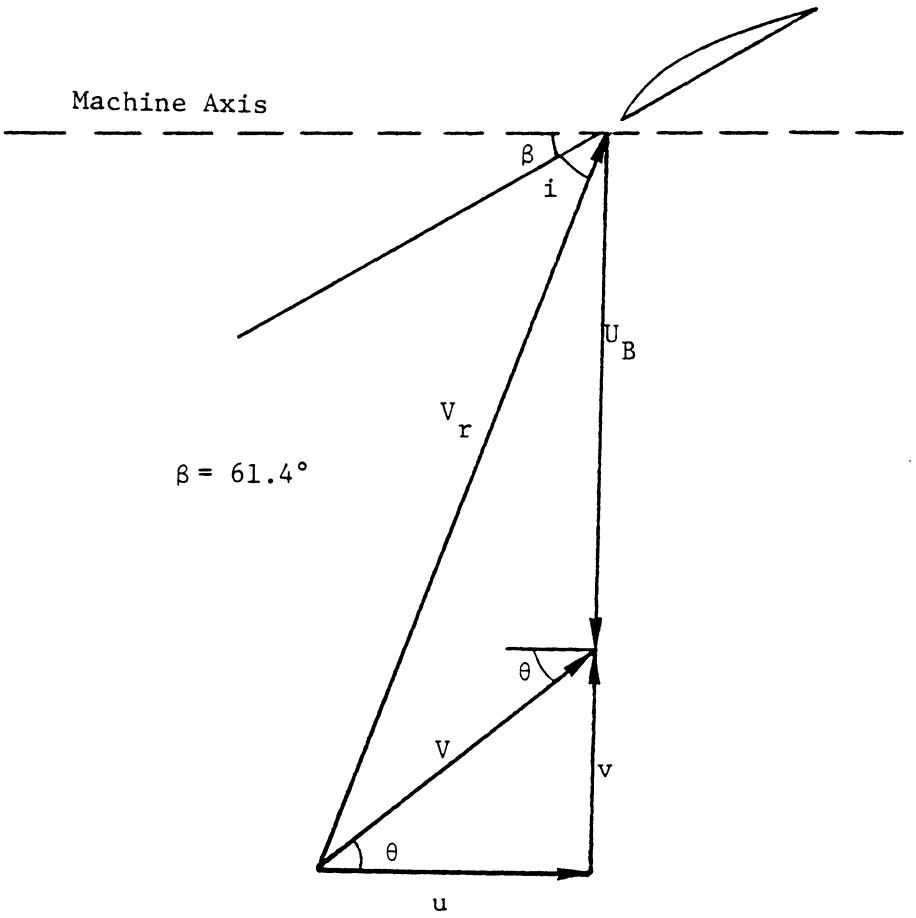

Figure 18: Rotor Velocity Diagram
(not to scale)

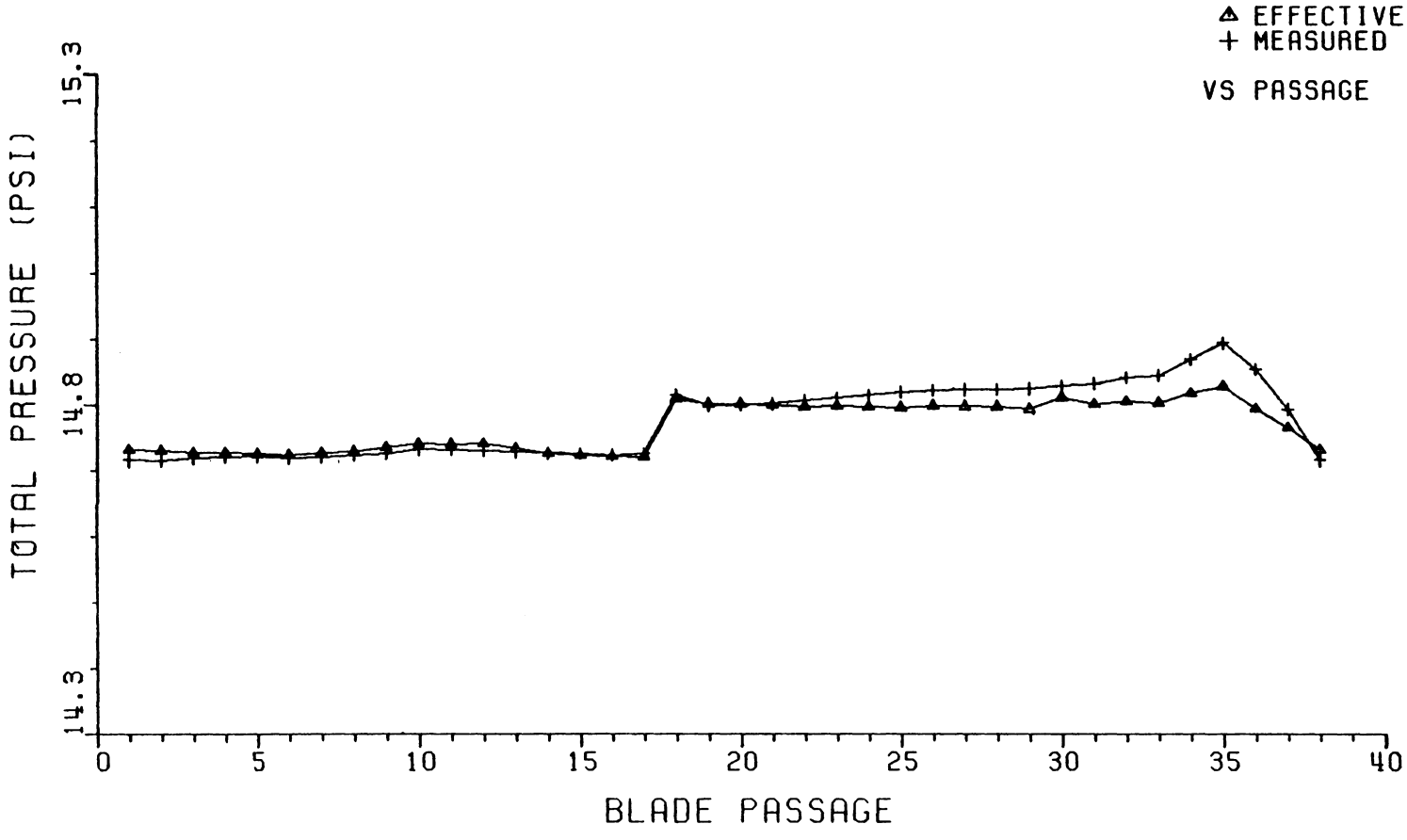

FIGURE 19: OVERLAY OF THE MEASURED TOTAL PRESSURE PROFILE AND THE EFFECTIVE TOTAL PRESSURE PROFILE DERIVED FROM THE EXPERIMENTALLY-BASED EFFECTIVE ANGLE OF ATTACK

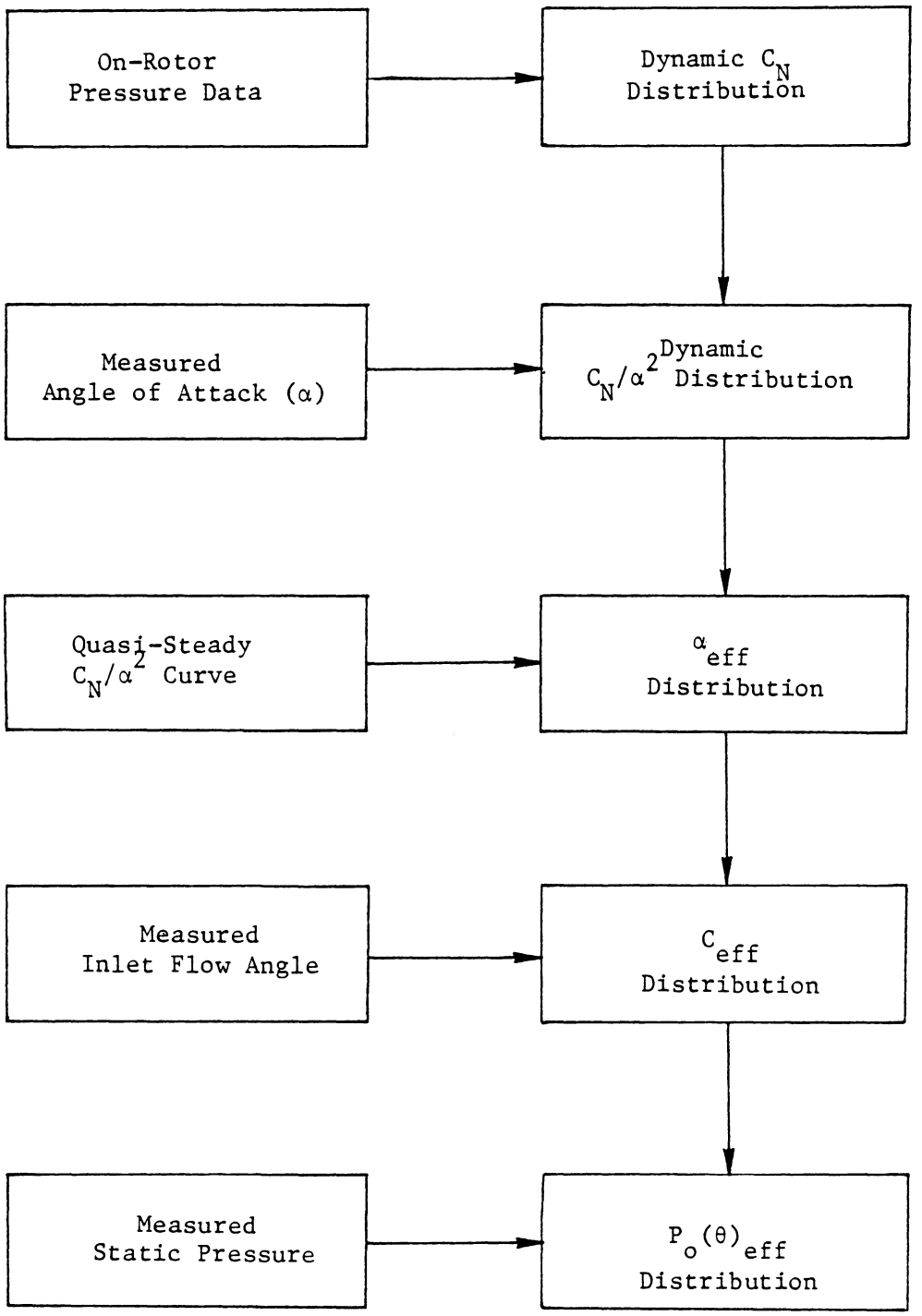

Figure 20: Flow Chart Illustrating Derivation of Effective Total Pressure Profile from Dynamic On-Rotor Pressure Data

Because of the relative novelty of the idea of the effective total pressure distribution, corroboration in the literature was sought. It was noted in Section IX that Reid [4] employed the idea of an effective distortion as a means of including the critical angle concept in parallel compressor theory. Tesch and Steenken [11], Melick and Simpkin [13], and Melick [14] have all previously worked with the concept of an effective incidence angle (or angle of attack). Tesch and Steenken employed a first order differential equation to derive an effective incidence angle. They utilized a time constant of Ac/U (a multiple of the reduced frequency parameter) where A is some constant, c is blade chord length, and U is blade relative velocity. The constant A was varied for different test runs of the General Electric Dynamic Digital Compression Component Model. An optimum value for A was not specified.

Melick and Simpkin also employed a first order differential equation but Melick later published a report recommending a second order differential equation for determining the effective angle of attack. This latter approach recommended by Melick was evaluated for the purpose of comparing the results of an analytical approach with the experimental approach described in the preceding paragraphs.

The second order differential equation used by Melick to derive the effective angle of attack is as follows:

$$\frac{d^2}{dt^2}\left[\alpha_{eff} - \alpha_o\right] + \left(\frac{1}{\tau_1} + \frac{1}{\tau_2}\right)\frac{d}{dt}\left[\alpha_{eff} - \alpha_o\right]$$

$$+ \left(\frac{1}{\tau_1}\frac{1}{\tau_2}\right)\left[\alpha_{eff} - \alpha_o\right] = \left(\frac{1}{\tau_1}\frac{1}{\tau_2}\right)\left[\alpha_{inst} - \alpha_o\right]$$

where

α_{inst} = instantaneous or actual angle of attack at time t,

α_{eff} = effective angle of attack,

α_{o} = angle of attack about which perturbations occur,

τ_1, τ_2 = time constants.

Melick determined the time constants to be equal and on the order of 3.5c/U where c is rotor blade chord length and U is relative velocity. For the compressor in question, this corresponds to a time constant of 2.625 msec.

A CSMP (Continuous System Modeling Program) program was used to compute Melick's effective angle of attack for the compressor tested. A graph comparing the experimentally measured angle of attack to Melick's effective angle of attack is presented in Fig. 21. An overlay graph of the experimentally-based effective angle of attack, Melick's effective angle of attack, and the measured angle of attack distributions is presented in Fig. 22. Note that Melick's effective angle of attack lags further behind the measured angle of attack than does the experimentally-based effective angle of attack.

An effective total pressure distribution was derived using Melick's effective angle of attack distribution in exactly the same manner as for the experimentally-based effective angle of attack. This effective total pressure distribution is presented in Fig. 23 along with the measured total pressure distribution. Note that this effective total pressure distribution lags further behind the measured distribution than

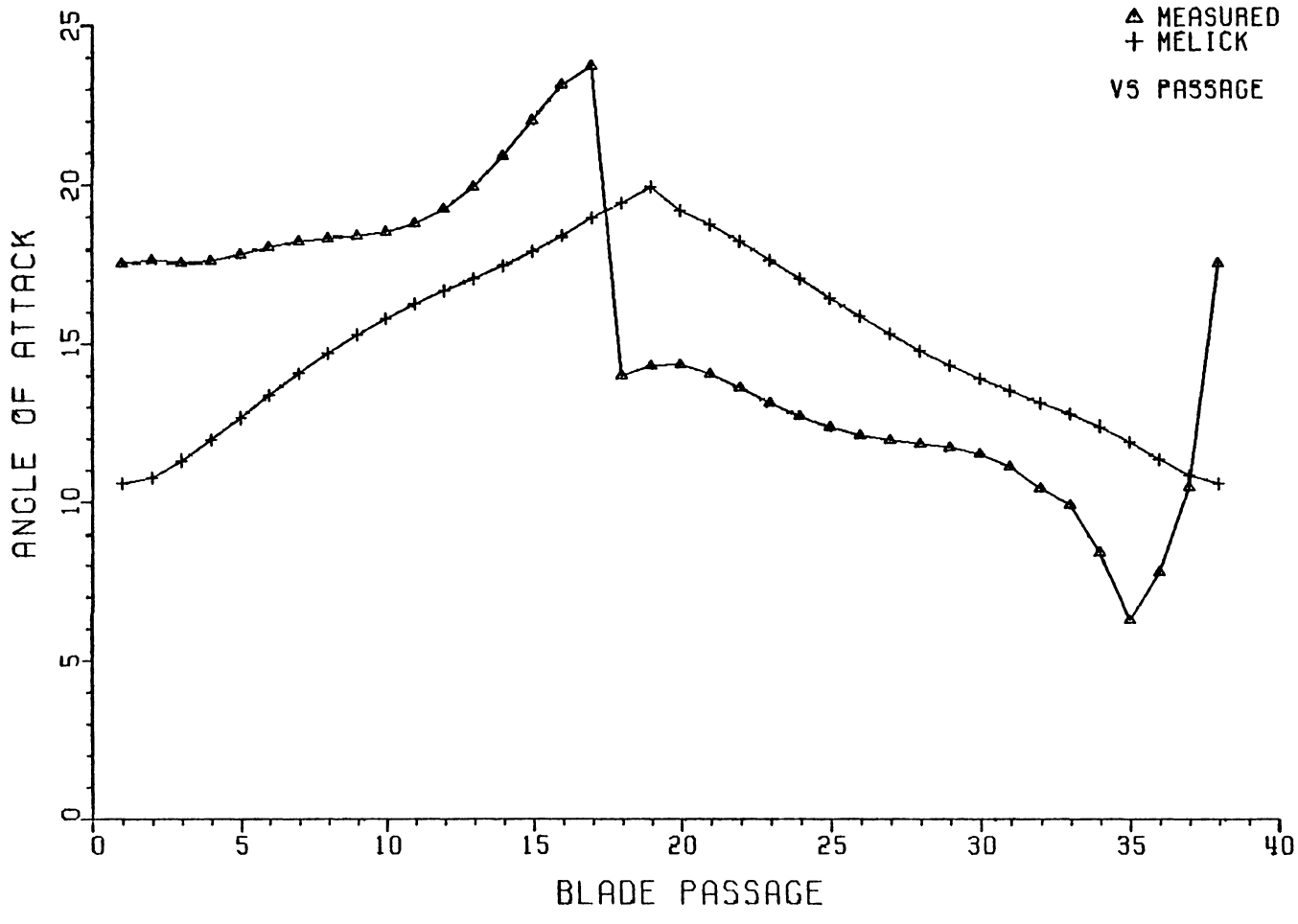

FIGURE 21: MEASURED ANGLE OF ATTACK AND MELICK (14) EFFECTIVE ANGLE OF ATTACK

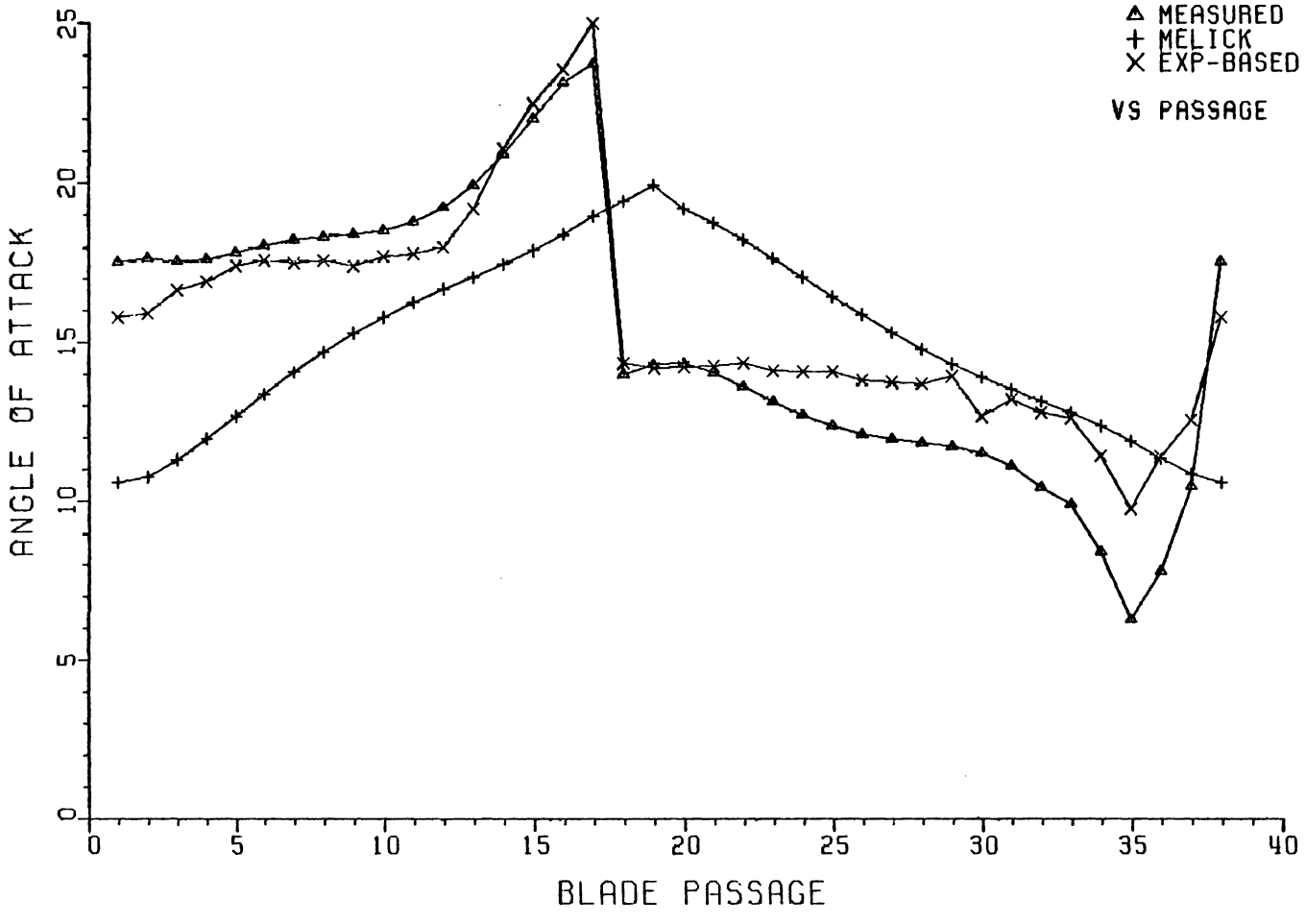

FIGURE 22: OVERLAY OF MEASURED AND EFFECTIVE ANGLE OF ATTACK DISTRIBUTIONS

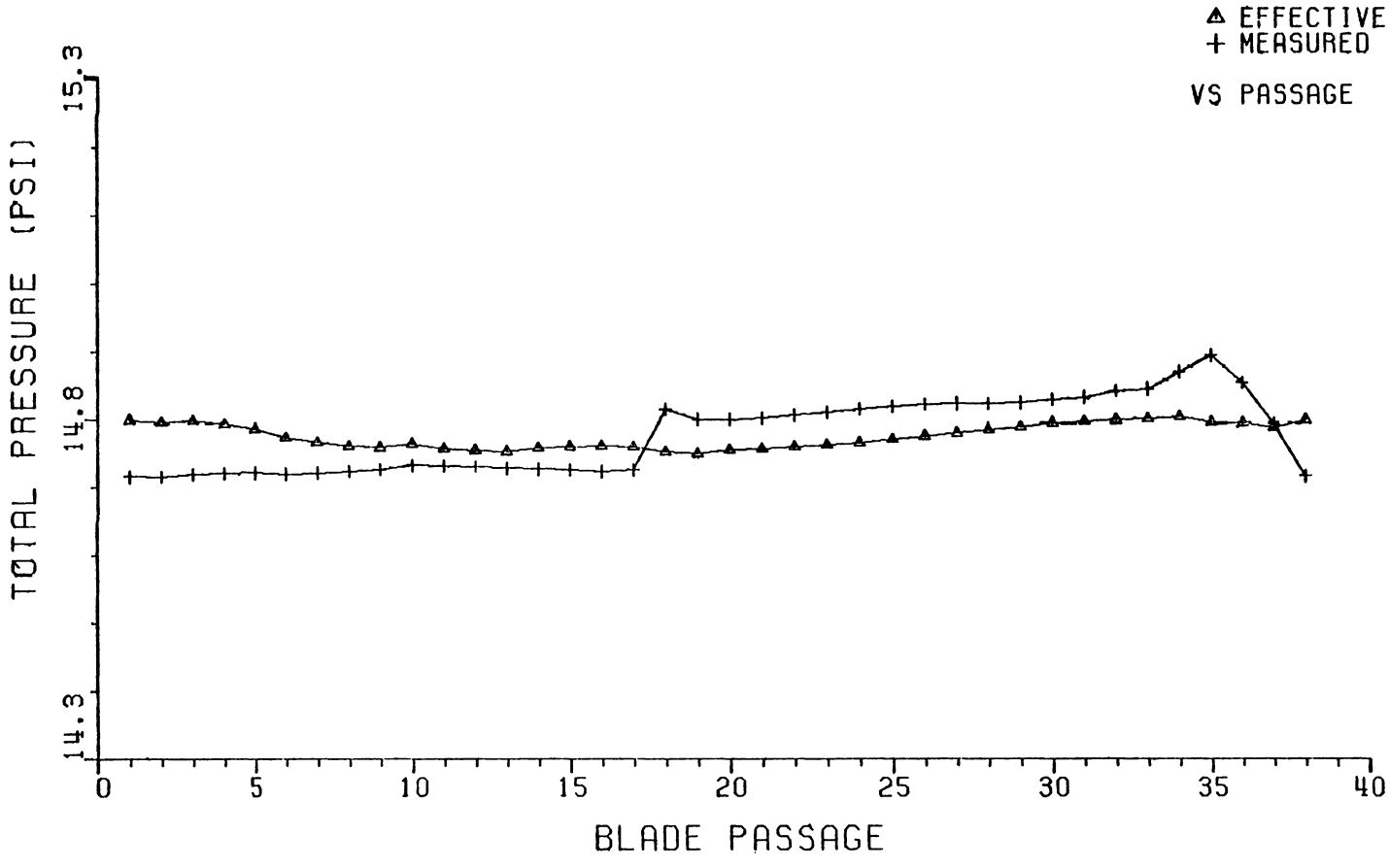

FIGURE 23: OVERLAY OF THE MEASURED TOTAL PRESSURE PROFILE AND THE EFFECTIVE TOTAL PRESSURE PROFILE DERIVED FROM THE MELICK EFFECTIVE ANGLE OF ATTACK

does the experimentally-based effective total pressure distribution (Fig. 19).

Two frequency response functions were calculated. In both cases the measured inlet total pressure distribution was considered to be the forcing function. In one case, the response function was the effective total pressure distribution derived from the experimentally-based effective angle of attack. In the other case, the response function was the effective total pressure distribution derived from Melick's effective angle of attack. The frequency response functions were calculated using an IBM 370 computer program built around an IMSL (International Mathematical and Statistical Libraries) subroutine package entitled FFTR. For further details see Sexton [1] and Sullivan [2].

The two frequency response functions are presented in Figures 24 and 25. They are presented in magnitude and phase coordinates for easier interpretation of physical meaning. The magnitude and phase of each function are plotted versus engine order which refers to the number of periods per revolution of the compressor rotor. The appropriate order of the derived frequency response functions is not identifiable.

The experimentally-based frequency response function derived from Sexton's data represents that for one compressor test-rig at one rotational speed for only one extent and intensity distortion. Clearly, the general applicability of this frequency response function is in doubt. For this reason, the frequency response function derived from the low-speed, single-stage, axial-flow compressor data was not used in analyzing the J85-GE-13 and TF30-P-3 engine data or the modified T64-GE-6B compressor test-rig data. Instead, simplifying assumptions were

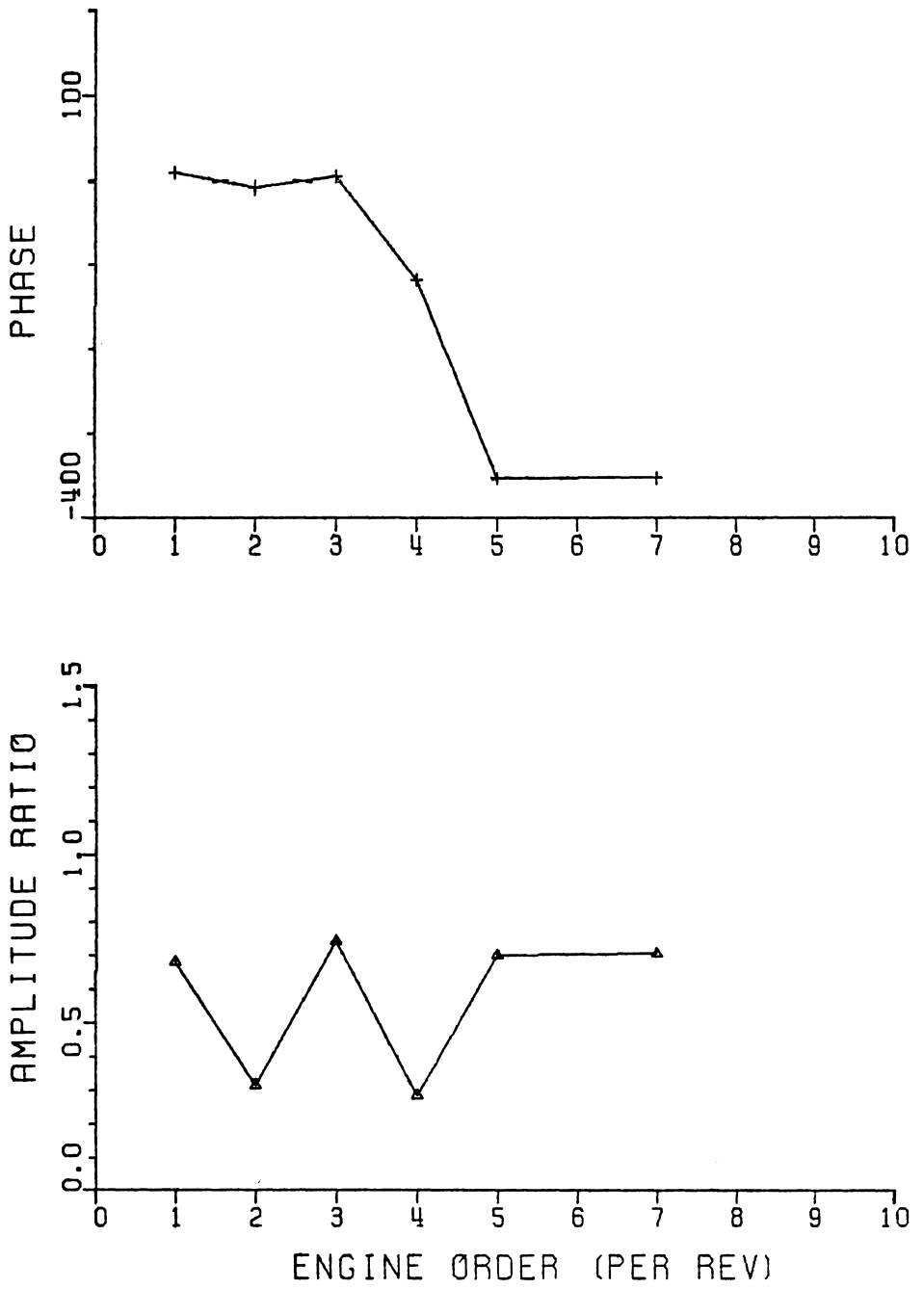

FIGURE 24: FREQUENCY RESPONSE FUNCTION DEVELOPED FROM EXPERIMENTALLY-BASED EFFECTIVE INLET TOTAL PRESSURE PROFILE

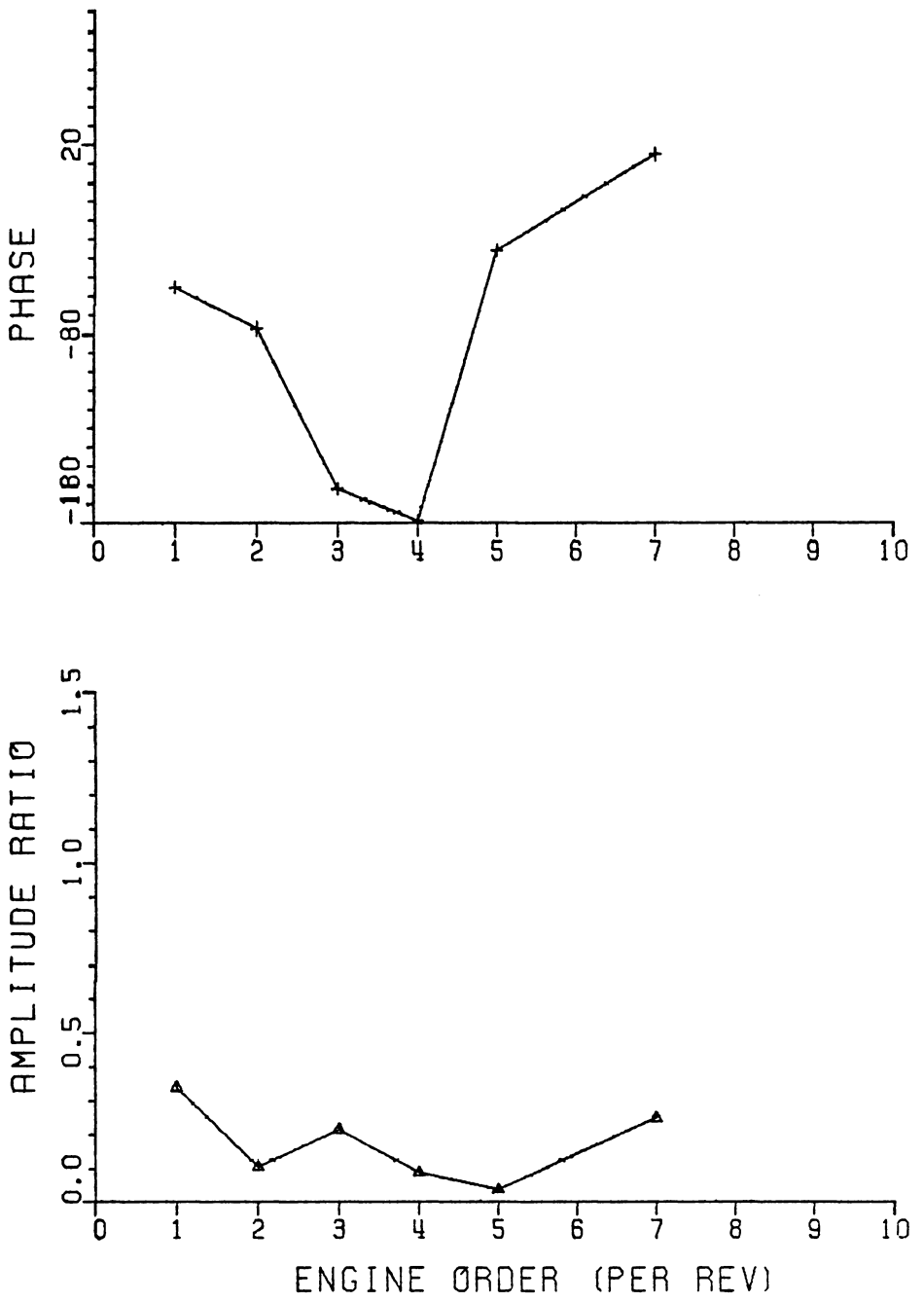

FIGURE 25: FREQUENCY RESPONSE FUNCTION DEVELOPED FROM MELICK-BASED EFFECTIVE TOTAL PRESSURE PROFILE

made concerning the frequency response function. These are described in the following section where the experimental stall data and index evaluation procedures are explained.

In summary, the frequency response method can be employed to develop an effective total pressure distribution that is representative of the dynamic response of the compressor rotor blades. Because of the inclusion of dynamic effects, simple distortion indices used in conjunction with the effective total pressure distribution should prove to be more accurate than when used in conjunction with the measured distribution. Due to the need for further experimentation to verify the generality of the frequency response function, simplifying assumptions are made in this investigation regarding the frequency response function.

XI. DESCRIPTION OF STALL DATA AND INDEX EVALUATION PROCEDURE

Stall data from a J85-GE-13 turbojet engine, a TF30-P-3 twin-spool turbofan engine, and a modified T64-GE-6B compressor test-rig were used in this investigation of distortion index accuracy. Relevant information concerning each of these data sets is presented in this section. Assumptions made in calculating the distortion indices are presented. The criteria used for measuring index accuracy is explained. Finally, assumptions made concerning the frequency response function and the procedure for evaluating how the effective total pressure distribution affected index accuracy are presented.

The J85-GE-13 is an afterburning turbojet engine consisting of an eight stage, axial-flow compressor directly coupled to a two stage turbine. For further descriptions, see Calogeras, et al. [5].

To obtain the J85 data used herein, the test engine was installed in an altitude chamber. Atmospheric air was supplied to the inlet duct and throttled to a total pressure of 61 Pa. This resulted in a Reynolds number index (RNI) of approximately 0.70 at the compressor face. The altitude chamber was maintained at approximately 31 Pa to ensure a choked exhaust nozzle.

The engine inlet was instrumented with an array of 60 probes located 3.7 cm upstream of the compressor face. The array consisted of 12 rakes of 5 probes each. Compressor discharge instrumentation was installed through four customer bleed ports at the rear of the compres-

sor. At each port, three total pressure, one static pressure, and three total temperature probes were used. For more details concerning the instrumentation, see Wenzel [32].

The effects of screen-induced, one-per-revolution, 180°, circumferential total pressure distortions were measured at 80%, 87%, 94%, and 100% corrected speeds. Three different distortion screen porosities were tested at each speed. The three distortion screens were designated 4M, 7.5M, and 9M where the mesh numbers indicate the number of wires in each linear inch of a square grid. The percent open areas of the screens were 74.0, 57.8, and 50.7 respectively.

Each compressor stall point was approached at constant corrected engine speed. The exhaust nozzle area was incrementally reduced, forcing the compressor to operate at higher pressure ratios. Engine rotor speed was maintained by manually adjusting the throttle. It was not possible to stall the engine at 80% corrected speed with the 7.5M screen in place. The total pressure probe-array data and loss in stall pressure ratio data are presented in Appendix A.

The TF30-P-3 is a two-spool, afterburning turbofan engine. The low speed spool consists of a three stage, axial-flow fan mounted on the same shaft with a six stage, axial-flow, low-pressure compressor. This unit is driven by a three stage, low-pressure turbine. The high speed spool consists of a seven stage compressor driven by a single stage, air-cooled turbine. For further details see Braithwaite, et al. [33].

The engine was installed in an altitude test chamber. Conditioned air was delivered to the inlet duct so as to yield a Reynolds number

index of 0.50. Ram-pressure ratio across the engine was held at greater than 3:1 to ensure a choked exhaust nozzle at all operating conditions. The exhaust nozzle was usually not varied and all interstage compressor bleeds were closed.

The engine inlet was instrumented with an array of total pressure probes consisting of 8 rakes with 5 probes each. Static pressures were recorded at 8 circumferential locations on the compressor casing approximately midway between each of the total pressure rakes. Hub static pressures were recorded at 4 equally spaced circumferential locations.

An air jet system developed by NASA Lewis Research Center was used to generate 180°, one-per-revolution inlet total pressure distortions at seven different corrected fan speeds. Stall was induced by slowly opening the air jet valves so as to increase the level of distortion. Low-rotor speed was held constant and 12th stage bleeds were closed. When stall occurred, the air jet valve setting was noted, the distortion reduced, and the 12th stage bleeds opened. The distortion was then increased to its stall level and data were recorded with 12th stage bleeds open.

Inlet total and static pressure data are presented in Appendix A. Exit total pressure was available only at the exit of the low speed compressor. This was deemed adequate for distortion index evaluation as all of the stalls were observed to occur in the low-speed spool. This data is also presented in Appendix A.

Stall data from a modified, three stage, axial-flow compressor originally designed with 14 stages for use as an integral component of

the T64-GE-6B turboshaft engine were also available. The test compressor was driven by a T64-GE-6B engine. A bellmouth and inlet duct were fitted to the compressor inlet in accordance with ARP 1420 specifications. The compressor discharged into a plenum which exhausted to the outside via a group of butterfly valves. For further details see Gridley [34].

Inlet total pressure circumferential and radial variations were measured using 6 rakes of 5 probes each. Inlet static pressures were recorded at six circumferential locations (aligned with the total presure rakes) on the duct casing. Plenum static pressure was recorded and assumed equal to compressor exit total pressure.

The compressor was tested at speeds of 7360 and 8160 rpm (43% and 48% of rated design speed respectively) while operating with screen-induced total pressure distortions of 45, 90, 135, and 180 degree extent. Data taken at 7360 rpm with the 135° screen in place were judged to be in error and therefore were not included in this investigation. The distortion screens were all 40 mesh.

Stall was induced by closing the plenum discharge valve with the screens in place. Throttle adjustments were made to maintain constant speed. The onset of stall was determined by the magnitude of pressure fluctuations recorded by two high response probes located directly behind the first stage. Resulting data are presented in Appendix A.

The following distortion indices were evaluated using the above data:

1) $P_{max-min}/P_{avg}$, $P_{avg-min}/P_{avg}$

2) Rolls Royce DC(θ critical) and $\Delta P(\theta \text{ critical})/\bar{P}$

3) NAPC Kθ

4) AVCO Lycoming DI and DI_c

5) Garrett AiResearch CDI

6) Pratt and Whitney Aircraft KD_2

7) Pratt and Whitney Aircraft Kθ

8) General Electric Method D

9) ARP 1420

In addition, the correlation derived from the parallel compressor model was evaluated. A Fortran program was written to compute the indices and distortion descriptor elements.

Recall that static pressure data for the J85-GE-13 engine was not available. This prevented calculation of the Rolls Royce DC(θ critical), PWA Kθ, and NAPC Kθ indices for the J85 data set.

Recall from Section IX that the NAPC circumferential index, Kθ, is calculated as follows:

$$K\theta = \frac{\left[\frac{\bar{\theta}}{2\pi} \quad \frac{q}{P}\right]_{ref}}{\sqrt{\frac{q}{P} \Big/ \frac{\bar{q}}{\bar{P}}}}.$$

The numerator is the so-called time constant, τ, associated with rotor blade response. It is defined as the minimum value of $[(\bar{\theta}/2\pi)\sqrt{q/P}]$ for a given engine rotative speed at the onset of surge. Generally this minimum value will occur for small extent distortions (45° or less).

Thus, the minimum value was not available for the TF30-P-3 engine as this data set contains only 180° extent distortion data. This precluded evaluation of the NAPC $K\theta$ index for the TF30-P-3 engine; therefore, this index was evaluated using only the modified T64 compressor test-rig data. For this data set, the minimum value of τ was assumed to occur for the 45° extent distortion.

The GE Method D correlation is designed to predict the value of ID which is defined as follows:

$$ID = \frac{\text{stability margin loss due to distortion}}{\text{stability margin available for distortion}} .$$

ID does not exist for a compressor as stability margin is defined for an engine only. The GE Method D index was therefore not evaluated for the modified T64 compressor test-rig stall data.

The Rolls Royce θ critical indices were calculated based on a critical angle of 60° for each of the three data sets. Calogeras et. al. [5] determined experimentally that 60° is the critical angle of spoiling for the J85-GE-13 engine. This information was not available for the TF30-P-3 engine or the modified T64-GE-6B compressor test-rig; however, Reid [4] has estimated the critical angle to be between 60° and 90° and suggests a value of 60° in the absence of other information.

The GE Method D and ARP 1420 correlations include radial and circumferential distortion descriptor elements. As stated earlier, only circumferential inlet total pressure distortion data was used in this investigation. Consequently, computation of the GE IDR and ARP 1420 $\Delta PR/P$ radial distortion descriptor elements resulted in values generally

one or more orders of magnitude less than the corresponding circumferential distortion descriptor elements. This was considered justification for neglecting the radial distortion components of these indices when determining sensitivity coefficients.

Neglecting radial distortion elements reduced the GE Method D index, ID, to the following:

$$ID = K_c \cdot IDC.$$

Recall IDC is defined in the following manner:

$$IDC = \text{maximum of} \left\{ \begin{array}{l} \dfrac{(IDC_1 + IDC_2)}{2} \\ \dfrac{(IDC_4 + IDC_5)}{2} \end{array} \right.$$

where

$$IDC_r = S_r \cdot E_r \cdot M_r \cdot \left(\frac{\Delta P}{PAV}\right)_r .$$

The above multiple-per-revolution, shape, and extent factors, M_r, S_r, and E_r respectively, were assumed equal to 1.0 for both the J85 and TF30 engine data as only one-per-revolution, square-wave distortions of 180° extent are included in these data sets. ID then reduced to

$$ID = K_c \cdot \text{maximum of} \left\{ \begin{array}{l} \dfrac{\left[\left(\frac{\Delta P}{P}\right)_1 + \left(\frac{\Delta P}{P}\right)_2\right]}{2} \\ \dfrac{\left[\left(\frac{\Delta P}{P}\right)_4 + \left(\frac{\Delta P}{P}\right)_5\right]}{2} \end{array} \right. .$$

K_c is a function of engine speed only and was determined from a simple linear regression analysis. Note that evaluation of ID for the TF30 engine data holds little meaning as data for only one distortion was available at each of the seven engine speeds tested. For this case, the K_c coefficient becomes

$$K_c = \frac{ID}{IDC}$$

and the GE ID index appears to produce perfect results.

Neglecting radial distortion effects reduced the ARP 1420 correlation to the following:

$$\Delta PRS_N = \sum_{i=1}^{N} \left[KC_i \left(\frac{\Delta PC}{P} \right)_i + C_i \right] \times 100.$$

For this investigation, the circumferential sensitivity coefficient was expanded as suggested by Steenken [30] in the following manner:

$$KC_i = KC \cdot f(\bar{\theta}_i) \cdot f(MPR_i) \cdot \alpha_i.$$

The multiple-per-revolution function, $f(MPR_i)$, was assumed equal to 1.0 in all cases. The extent function was assumed equal to 1.0 for 180° extent distortions. The ring weighting factor was set equal to 1.0 due to insufficient data for any other conclusion. With these assumptions, the ARP 1420 correlation reduced to the following form for 180° extent distortions:

$$\Delta PRS_N = N \cdot KC \sum_{i=1}^{N} \left[\left(\frac{\Delta PC}{P} \right)_i + \frac{C_i}{KC_i} \right] \times 100.$$

Because $N \cdot KC$ and $\Sigma(\frac{C_i}{KC_i})$ are also constants, the correlation can be reduced to the following:

$$\Delta PRS_N = KC \sum_{i=1}^{N} [(\frac{\Delta PC}{P})_i] + C.$$

KC and C are functions of engine speed only and were determined from a simple linear regression analysis. Note that, as in the case of the GE ID index, evaluation of the ARP 1420 correlation using TF30 data holds little meaning. That is, because the data set consists of only one distortion at each speed tested, the KC coefficient becomes

$$KC = \frac{\Delta PRS_n}{\sum_{i=1}^{N} [(\frac{\Delta PC}{P})_i]}$$

and the ARP 1420 correlation appears to produce perfect results.

For the T64 compressor test-rig data, the extent function, $f(\bar{\theta}_i)$, could not be assumed always equal to 1.0; however, it was assumed that $f(\bar{\theta}_i)$ did not vary with instrumentation ring. The ARP 1420 correlation then reduced to

$$\Delta PRS_N = [KC \cdot f(\bar{\theta}) \sum_{i=1}^{N} [(\frac{\Delta PC}{P})_i] + C] \, 100.$$

The extent function was set equal to 1.0 for the 180° extent distortion data, KC was determined for each engine speed, and $f(\bar{\theta})$ was then calculated for the other extent distortion data using the predetermined value of KC.

The distortion indices were evaluated in terms of their ability to correlate with ΔPRS_N, ΔPRS_M, and engine speed. The NAPC Kθ index was evaluated for its ability to correlate with engine speed only as it was specifically designed for this capability. Parallel compressor theory, GE Method D, and ARP 1420 are predictive tools rather than correlations, and therefore were not tested for correlation capability with ΔPRS_N, ΔPRS_M, and engine speed as were the other distortion indices. Rather, each was evaluated separately by comparing experimental results to index/model predictions.

ΔPRS_M data was not available for the TF30-P-3 or the compressor test-rig, making it impossible to test correlation capability with ΔPRS_M for these data sets. As a secondary means of evaluating the indices, a regression analysis was performed against ΔPRS_N, ΔPRS_M (where appropriate), and engine speed for each index. This provided a measure of the index's ability to predict stall, i.e., the ability of the index to define a "line" separating regions of stable and unstable operation. The sensitivity coefficients and extent functions of Method D and ARP 1420 were also evaluated from a simple regression analysis.

Correlation coefficients and regression models were computed using a SAS (Statistical Analysis System) program. SAS is a computer package that provides accurate, up-to-date statistical techniques. For more information concerning SAS, see reference 35. Pearson product-moment correlation coefficients were determined using the SAS CORR procedure. The SAS GLM procedure, which employs the principle of least squares, was used to produce linear models for the distortion indices in terms of

ΔPRS_N, ΔPRS_M, and/or engine speed. Sensitivity coefficients and extent functions where appropriate were also evaluated using the GLM procedure.

Correlation capability was measured directly in terms of the Pearson product-moment correlation coefficient. A coefficient of one indicates a perfect correlation and a coefficient of zero indicates no correlation between the variables being tested. A negative coefficient indicates an inverse relationship. The ability of the indices to predict stall (or, in other words, to provide a "line" separating stable and unstable operating regions) was evaluated with R-SQUARE values. R-SQUARE measures how much variation in the dependent variable can be accounted for by the regression model. The R-SQUARE value can range from zero to one; the larger the value of R-SQUARE, the better the model's fit. R-SQUARE was also used to evaluate Method D and ARP 1420. For further details regarding Pearson correlation coefficients and R-SQUARE values see Appendix B.

The concept of including compressor dynamic response effects in an effective total pressure distribution was evaluated by comparing the results of calculations of parallel compressor theory and the $\Delta P/\overline{P}$ indices from both measured and effective total pressure distributions. Effective total pressure distributions were derived assuming a second order response. A simple second order response was assumed because the general applicability of the frequency response function derived in Section X was in doubt. The experimentally-based frequency response function did indicate that compressor dynamic repsonse is of higher than second order; however, D'Azzo and Houpis [36] have reported

that the transient response of a complex system can often be considered the result of an equivalent second order system.

The assumption of an equivalent second order response required additional assumptions for the associated values of effective damping ratio and effective natural frequency. An effective damping ratio of 1.0 was assumed based on the work presented in Section X of this thesis and the work of Sexton and Sullivan, all of which indicates that compressor dynamic response is not oscillatory. An appropriate value for the effective natural frequency was not immediately obvious. It was therefore decided to test various values of effective natural frequency and to evaluate the effect of each of the resultant effective total pressure profiles on parallel compressor model and $\Delta P/\overline{P}$ index accuracy. The various effective natural frequencies were selected so as to provide settling times corresponding to 1/8, 3/16, 1/4, 3/8, and 1/2 of the time required for one revolution of the rotor. Here settling time is defined as the time required for the output or response function to reach 98% of its steady-state value. With this objective in mind, the natural frequencies were calculated as follows:

$$\omega_n = \frac{4.0}{t_s \cdot \zeta}$$

where t_s is the desired settling time and ζ is the system damping ratio.

Any improvements resulting from the use of effective total pressure distributions were measured in terms of correlation coefficients and R-SQUARE values for the $\Delta P/\overline{P}$ indices. Effects on parallel compressor theory results were measured in terms of the sum of the square of the

deviations between parallel compressor theory predictions and experimental results. The latter was necessary because parallel compressor theory is a purely predictive tool that does not lend itself to regression analysis. The smaller the sum of square of deviations, the better the predictive capability of parallel compressor theory.

The assumption of an equivalent second order response alleviated the necessity of using the Fast Fourier Transform program mentioned in Section X. It is emphasized that the equivalent second order response used in this investigation to derive effective total pressure distributions is a simplifying assumption employed because a generally-applicable frequency response function has not as yet been identified. The frequency response method as explained in Section X provides a means of experimentally deriving frequency response functions and thus offers an obvious advantage over the trial and error method employed here. The assumption of varying second order responses, however, permits a preliminary investigation of the concept of including compressor dynamic response effects in a distortion index by modifying the measured inlet total pressure profile. More dynamic on-rotor pressure data is required before the experimental approach described in Section X can be employed.

A CSMP (Continuous System Modeling Program) program was developed to calculate the effective total pressure distributions. CSMP is a special-purpose language written specifically for simulating continuous systems and is ideally suited for determining effective total pressure distributions from measured distributions for varying second order systems.

In summary, distortion indices and descriptor elements were computed for each data set containing the required information for the particular index or descriptor element in question. The indices were tested for correlation capability with ΔPRS_N, ΔPRS_M, and engine speed where appropriate. Accuracy was measured in terms of correlation coefficients and R-SQUARE values. Second order response systems based on five different natural frequencies were used to derive five different effective total pressure distributions for each distortion test of each data set. The accuracy of the parallel compressor model and the two $\Delta P/\overline{P}$ indices was evaluated for the measured and each of the five effective total pressure distributions. Accuracy was judged in terms of correlation coefficients, R-SQUARE values, and sums of square of deviations.

XII. RESULTS

Results of distortion index calculations for each of the three data sets are presented in this section. Statistical analysis results for each distortion index are also presented. In addition, the ability of effective total pressure distributions to improve the accuracy of parallel compressor theory and the two $\Delta P/\overline{P}$ indices is evaluated.

The distortion indices are evaluated in terms of Pearson product-moment correlation coefficients and R-SQUARE values. The R-SQUARE value results from a simple regression analysis in which only the index in question is used to describe variations in ΔPRS_N, ΔPRS_M, or engine speed. When only one variable is included in a regression model, the R-SQUARE value is exactly equal to the square of the Pearson product-moment correlation coefficient. Although this fact is recognized, both values are presented in this analysis for ease of interpretation by those more familiar with one or the other.

Results Employing Measured Total Pressure Data

Distortion indices and descriptor elements were calculated for each data set using a Fortran program. Results of the calculations are presented graphically. Figures 26 through 35 are plots of the individual indices versus compressor speed, using modified T64 compressor test-rig data. Parallel compressor theory, ARP 1420, and GE Method D are presented in a different format because they are predictive indices rather than correlations. Parallel compressor theory predicted

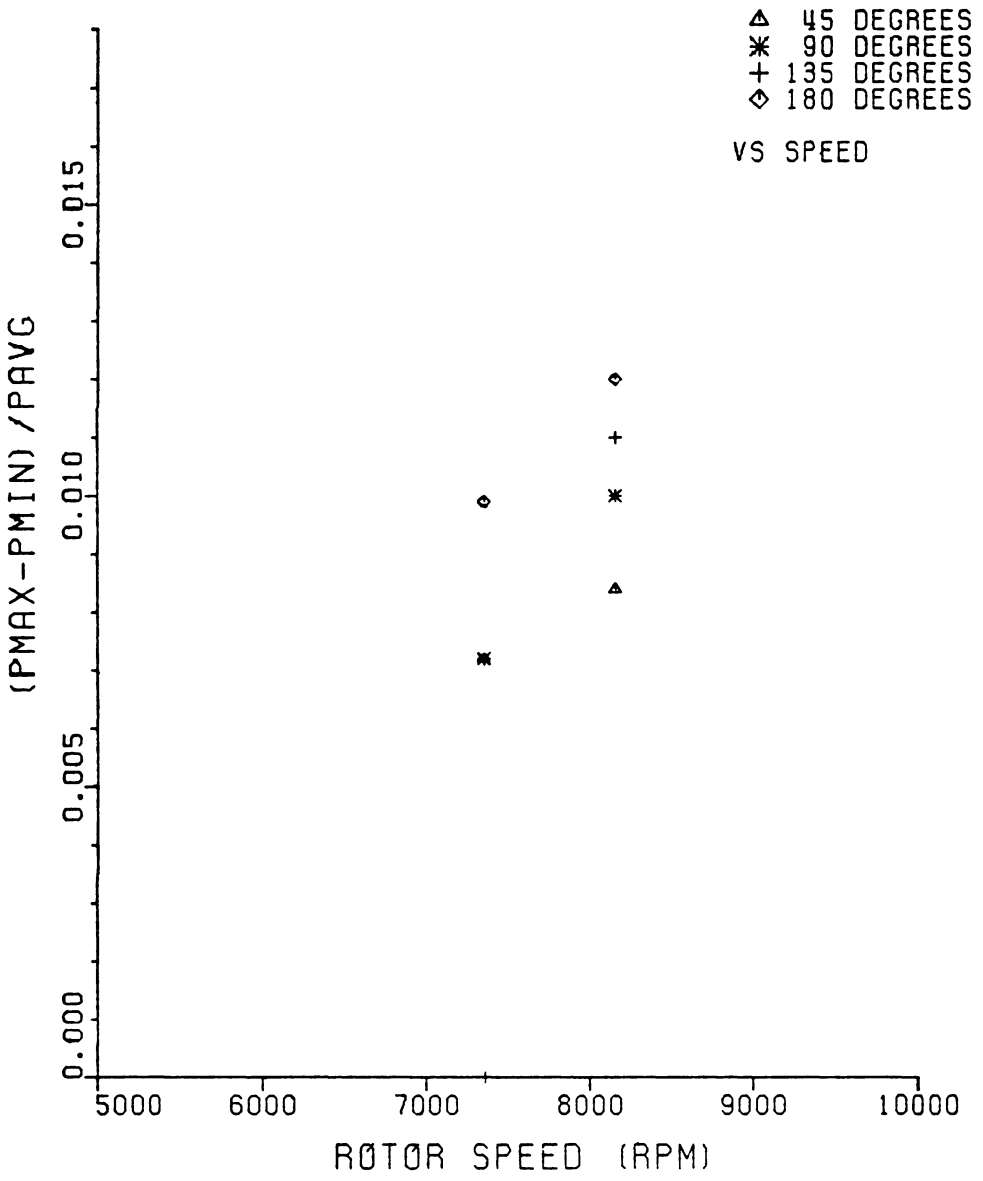

FIGURE 26: CIRCUMFERENTIAL DISTORTION-INDUCED STALL DATA FOR THE COMPRESSOR TEST-RIG, (PMAX-PMIN)/PAVG INDEX

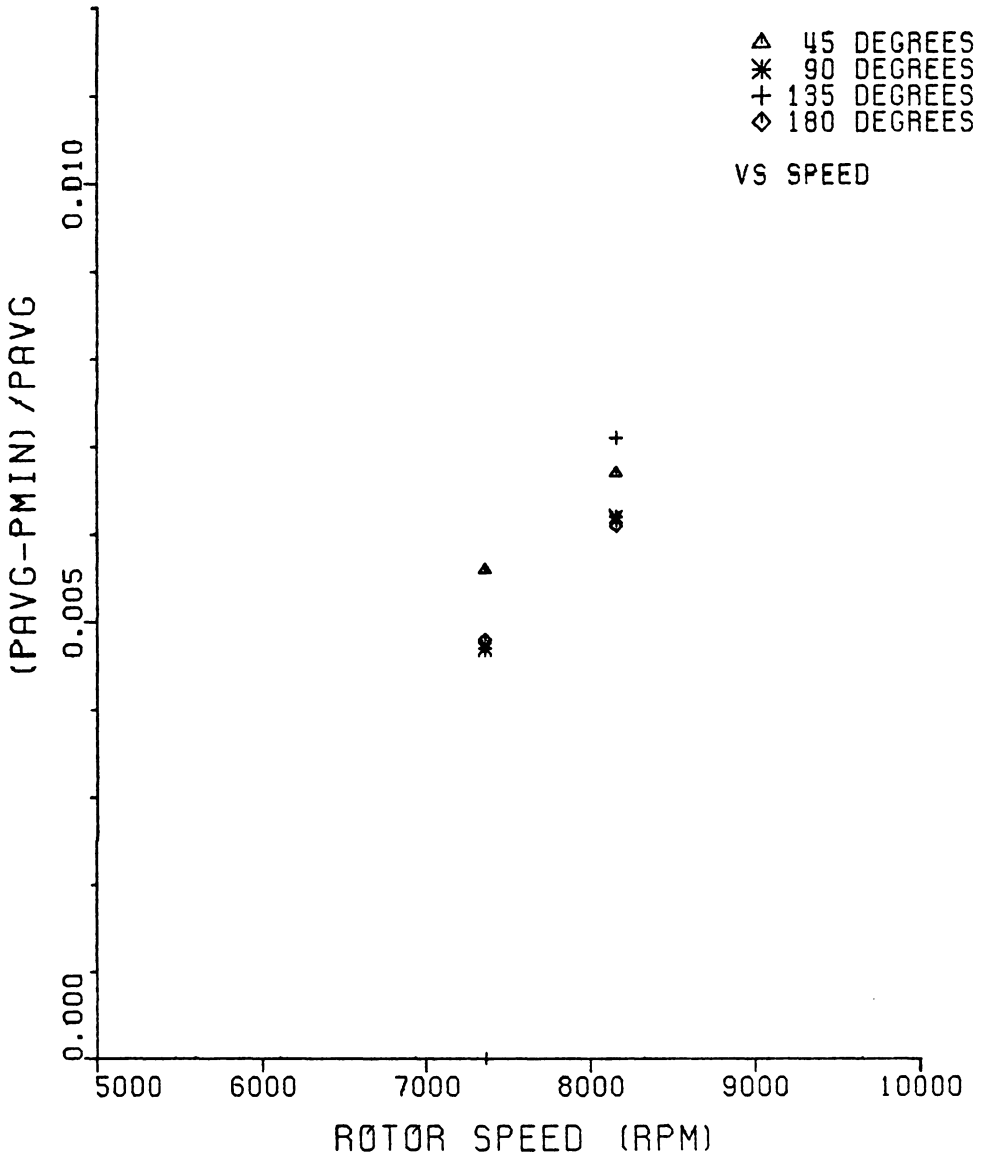

FIGURE 27: CIRCUMFERENTIAL DISTORTION-INDUCED STALL DATA FOR THE COMPRESSOR TEST-RIG, (PAVG-PMIN)/PAVG INDEX

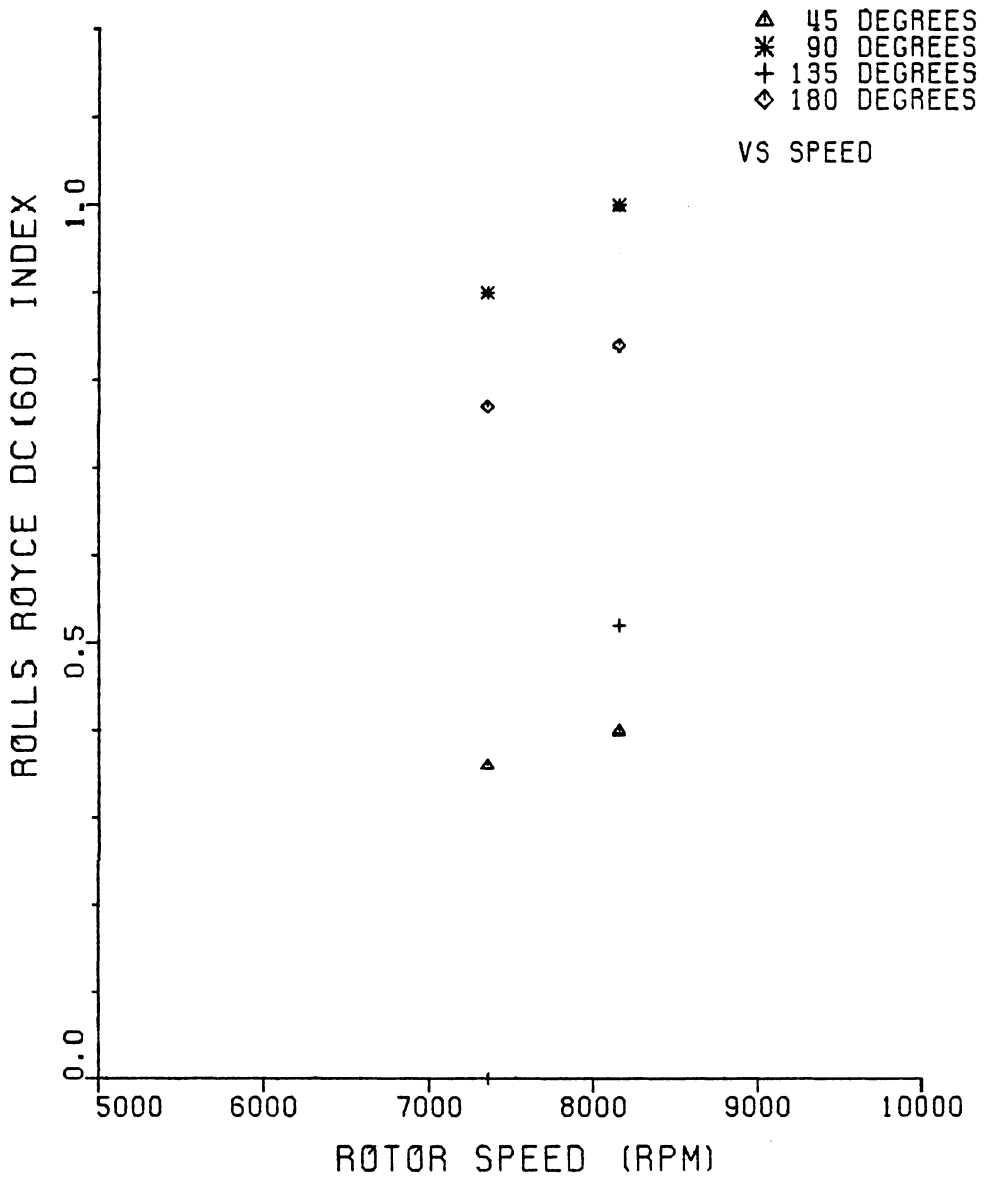

FIGURE 28: CIRCUMFERENTIAL DISTORTION-INDUCED STALL DATA FOR THE COMPRESSOR TEST-RIG, ROLLS ROYCE DC(60) INDEX

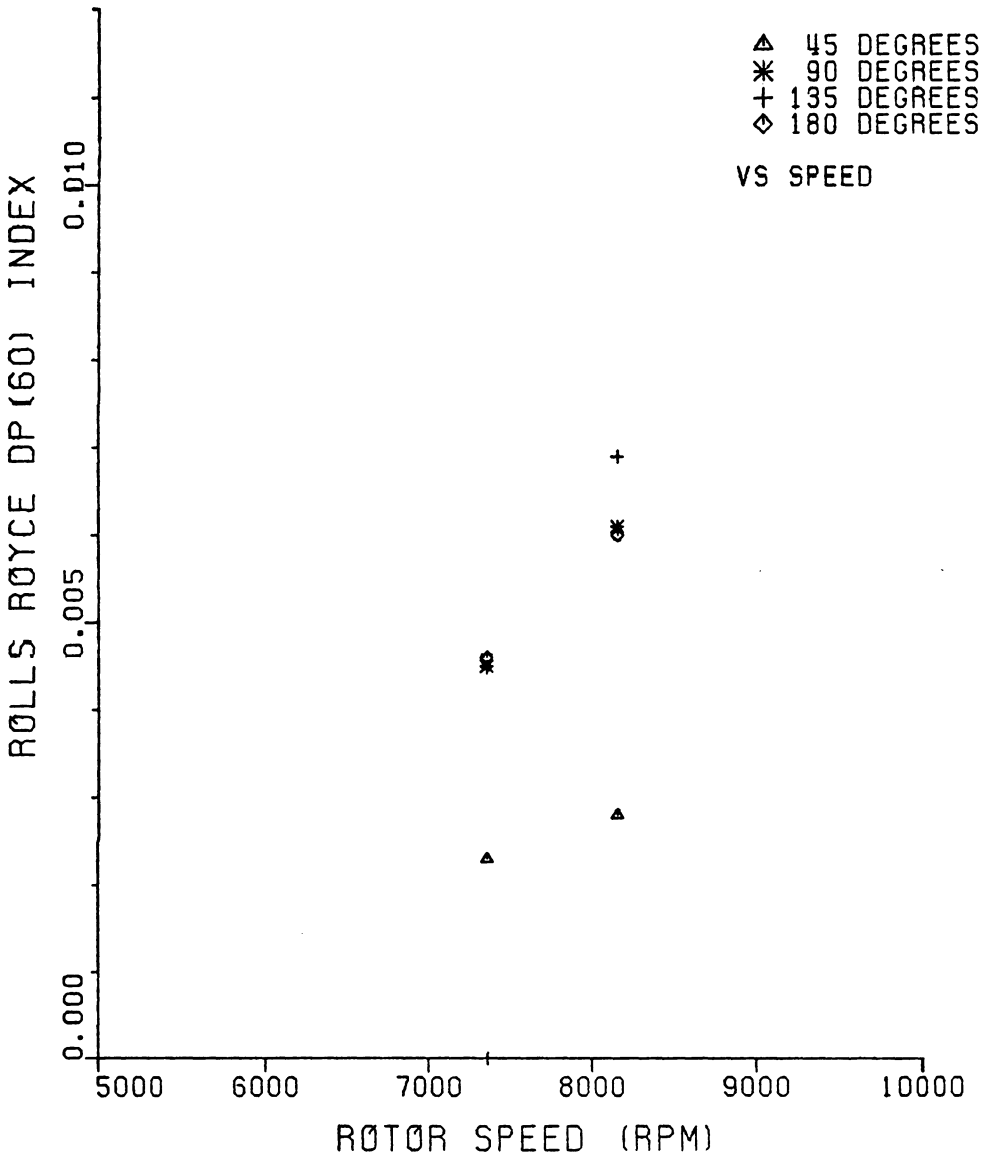

FIGURE 29: CIRCUMFERENTIAL DISTORTION-INDUCED STALL DATA FOR THE COMPRESSOR TEST-RIG, ROLLS ROYCE DP(60) INDEX

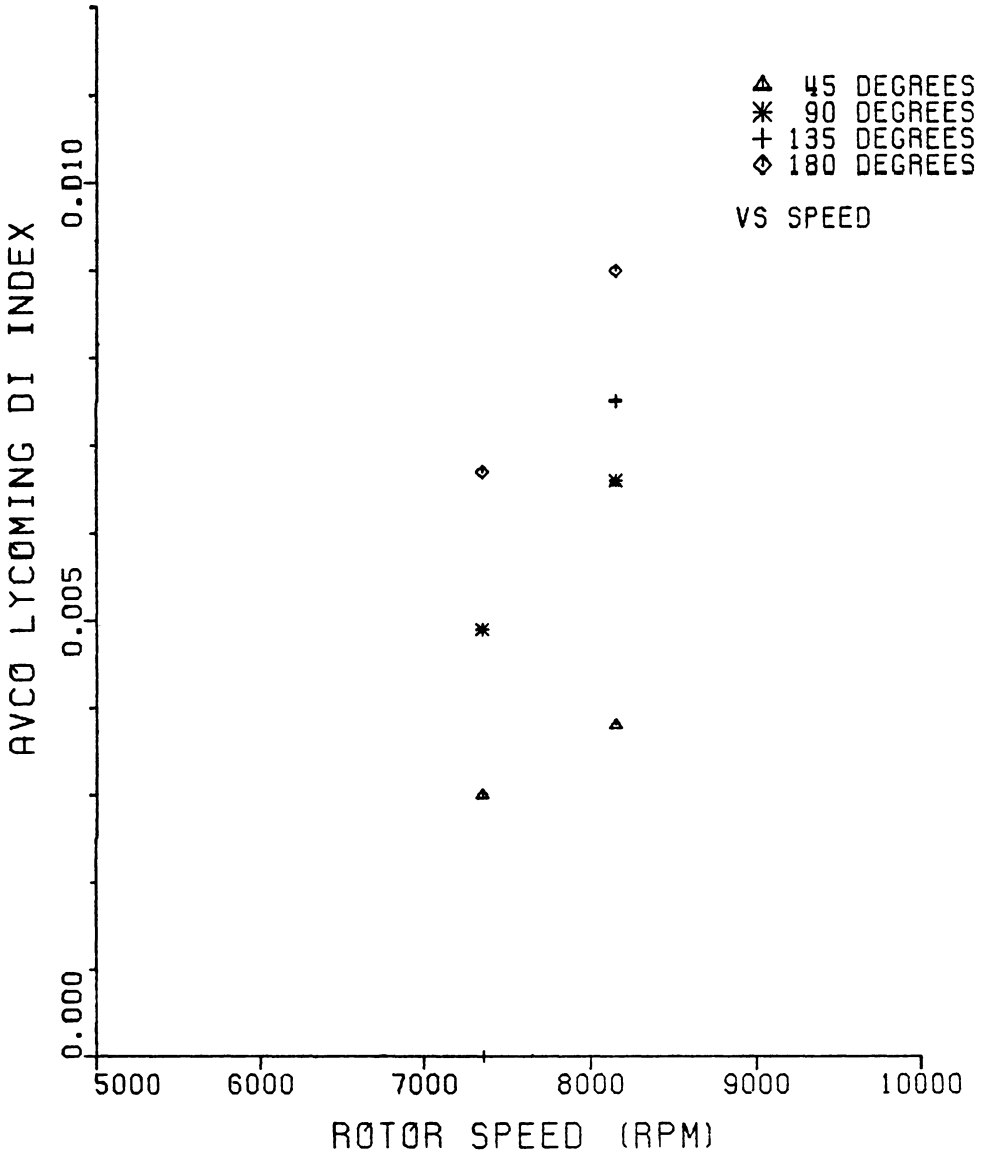

FIGURE 30: CIRCUMFERENTIAL DISTORTION-INDUCED STALL DATA FOR THE COMPRESSOR TEST-RIG, AVCO LYCOMING DI INDEX

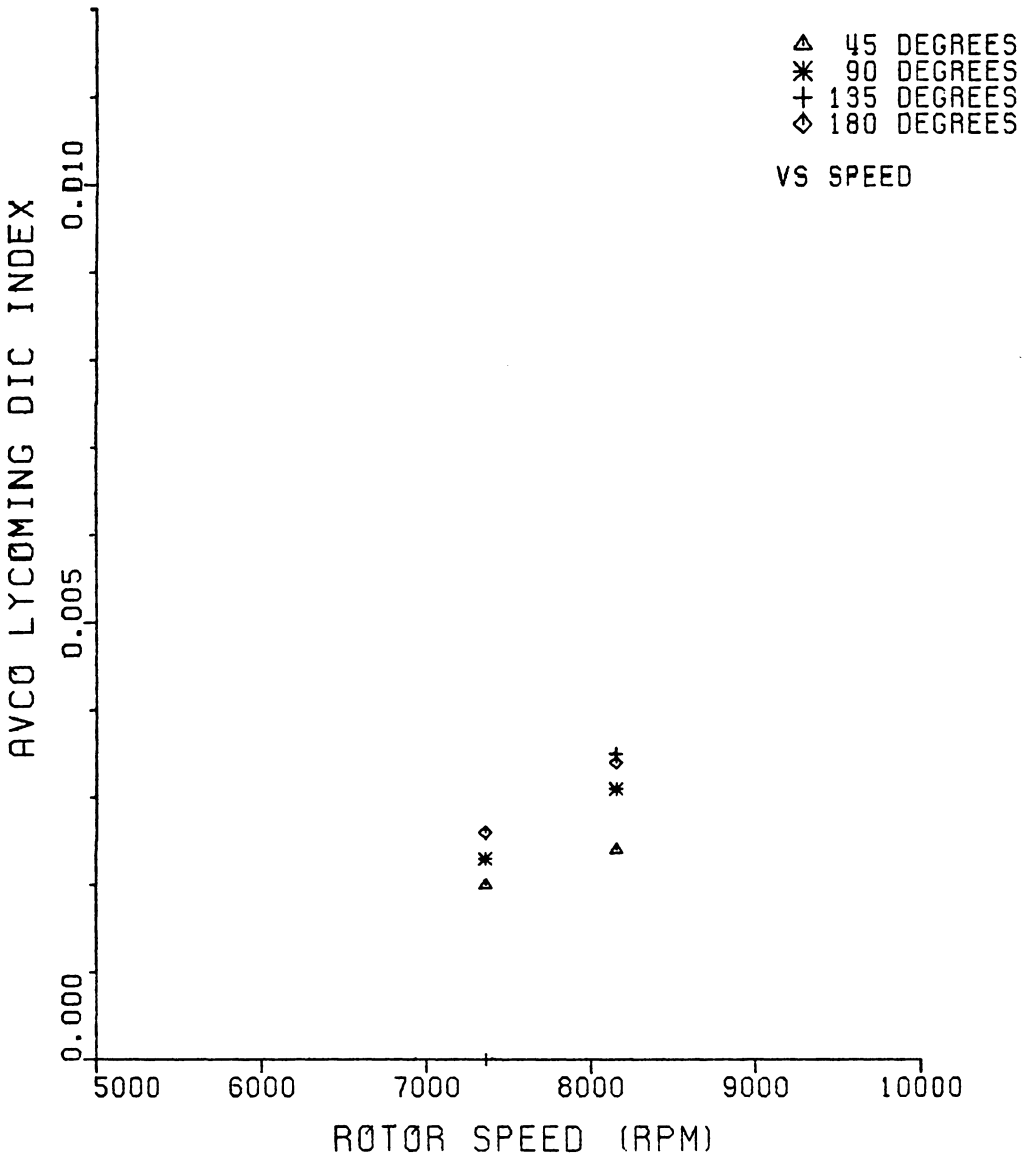

FIGURE 31: CIRCUMFERENTIAL DISTORTION-INDUCED STALL DATA FOR THE COMPRESSOR TEST-RIG, AVCO LYCOMING DIC INDEX

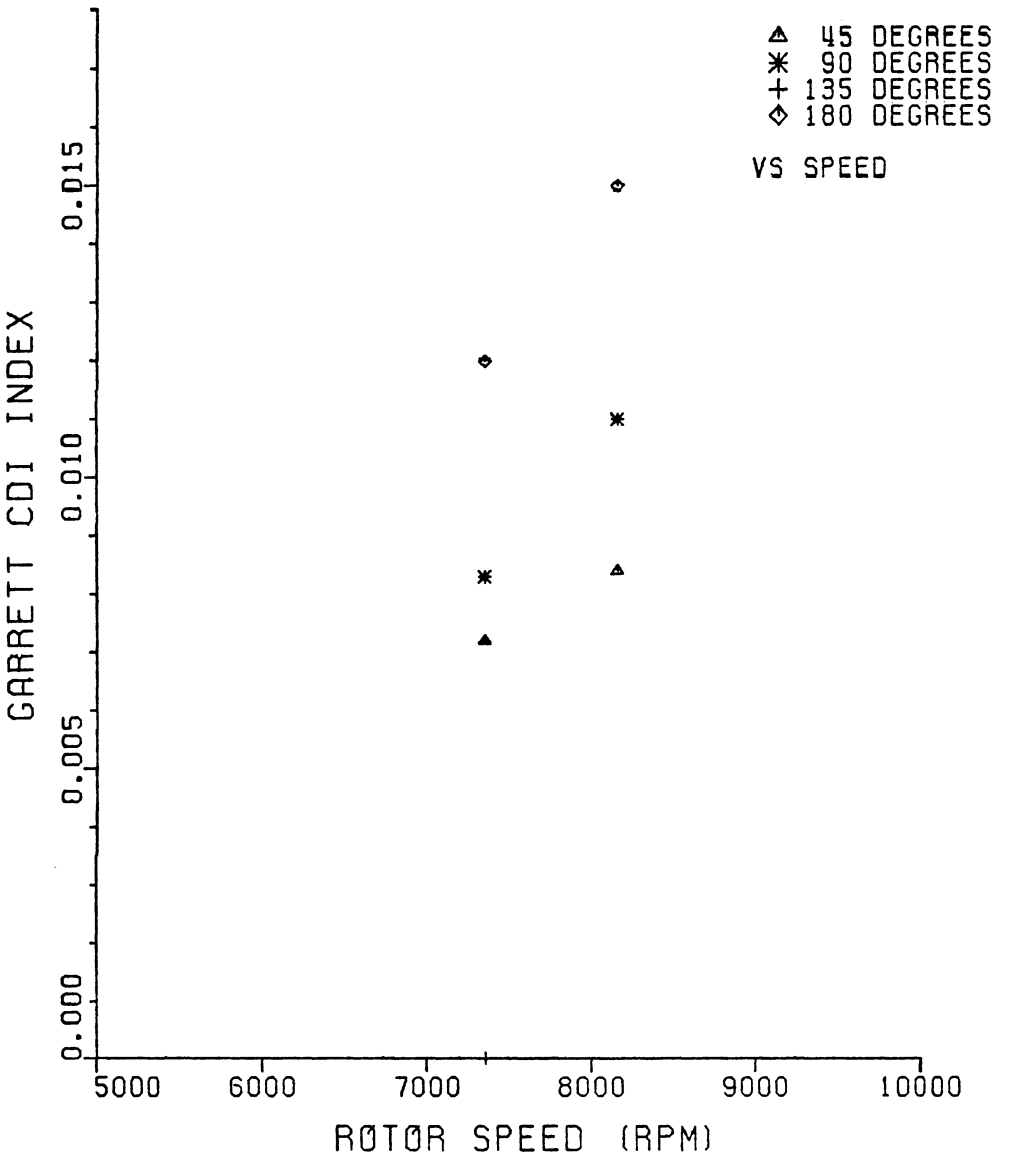

FIGURE 32: CIRCUMFERENTIAL DISTORTION-INDUCED STALL DATA FOR THE COMPRESSOR TEST-RIG, GARRETT AIRESEARCH CDI INDEX

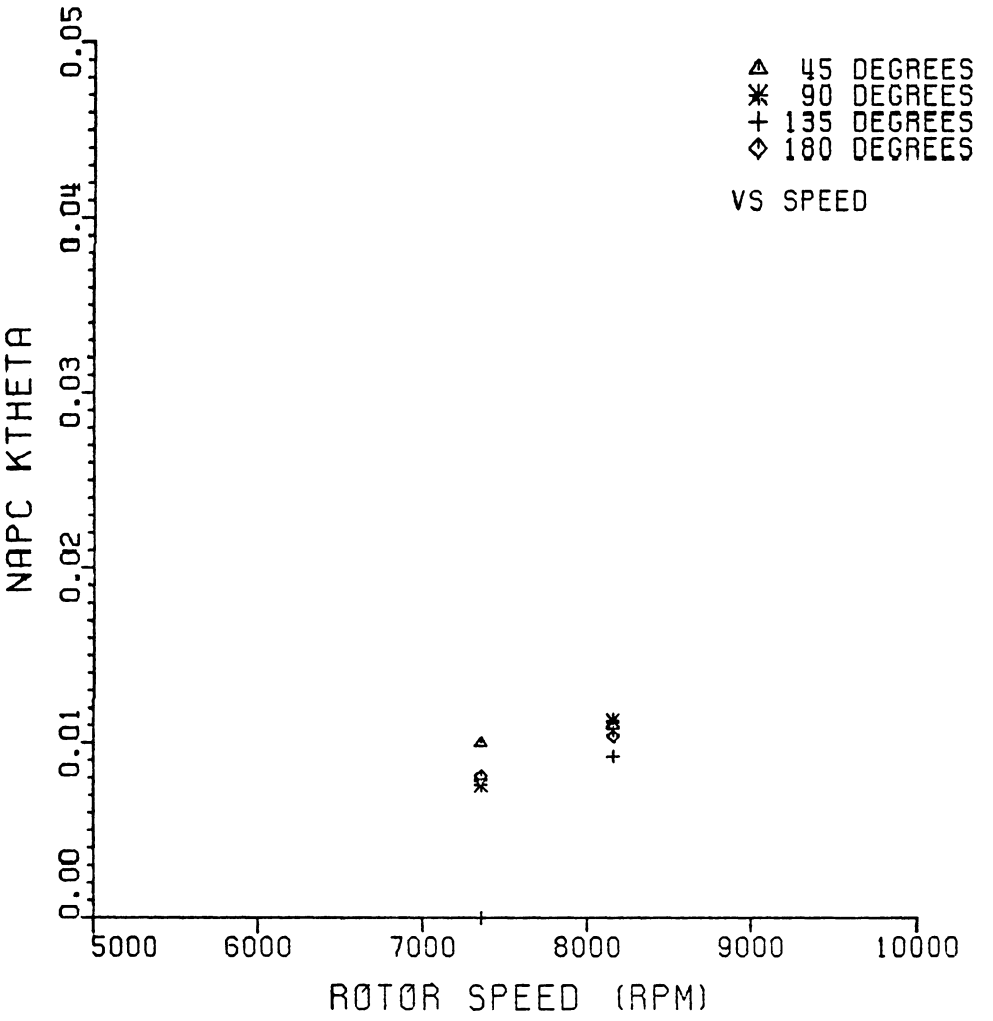

FIGURE 33: CIRCUMFERENTIAL DISTORTION-INDUCED STALL DATA FOR THE COMPRESSOR TEST-RIG, NAPC KTHETA INDEX

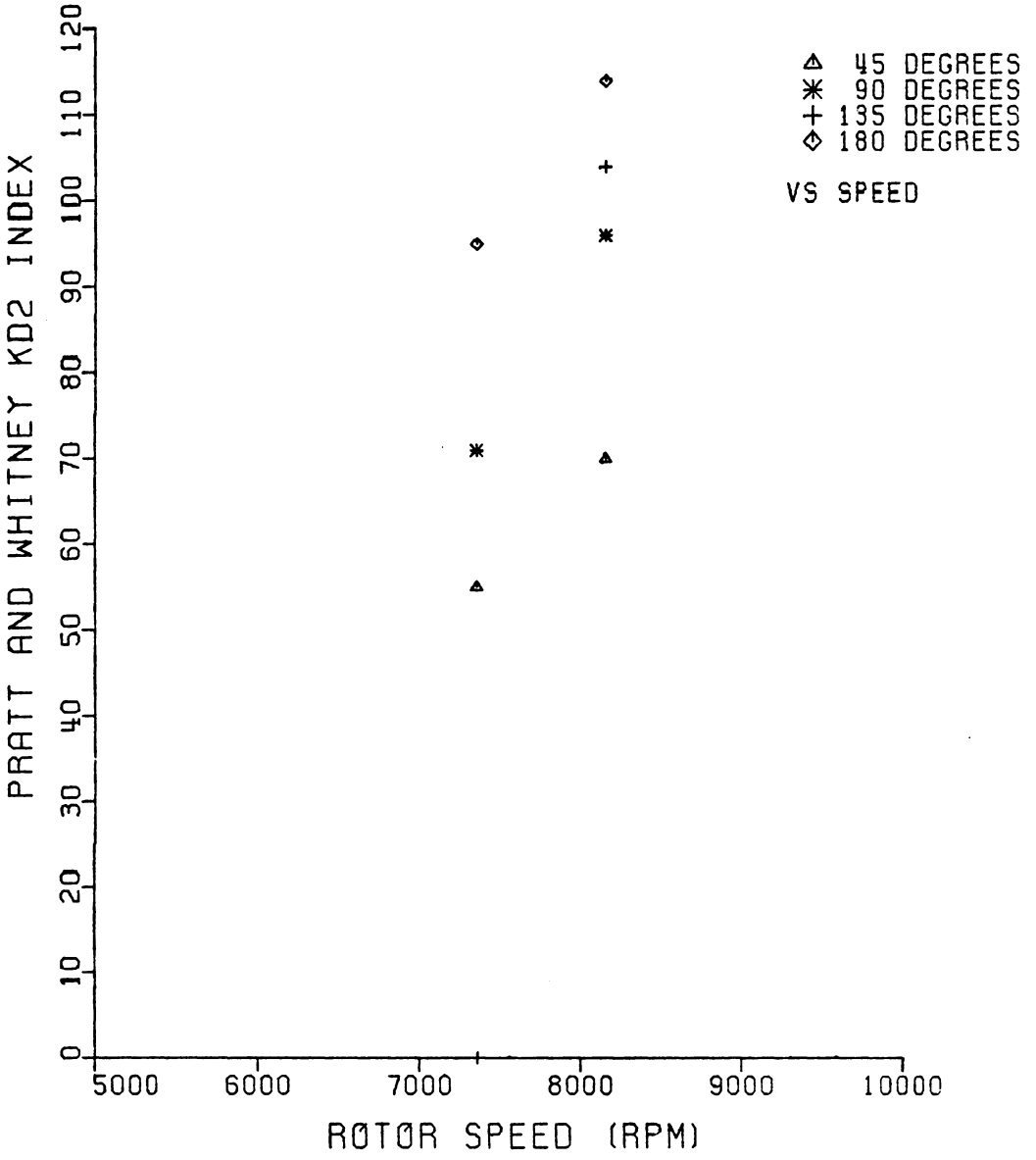

FIGURE 34: CIRCUMFERENTIAL DISTORTION-INDUCED STALL DATA FOR THE COMPRESSOR TEST-RIG, PRATT AND WHITNEY KD2 INDEX

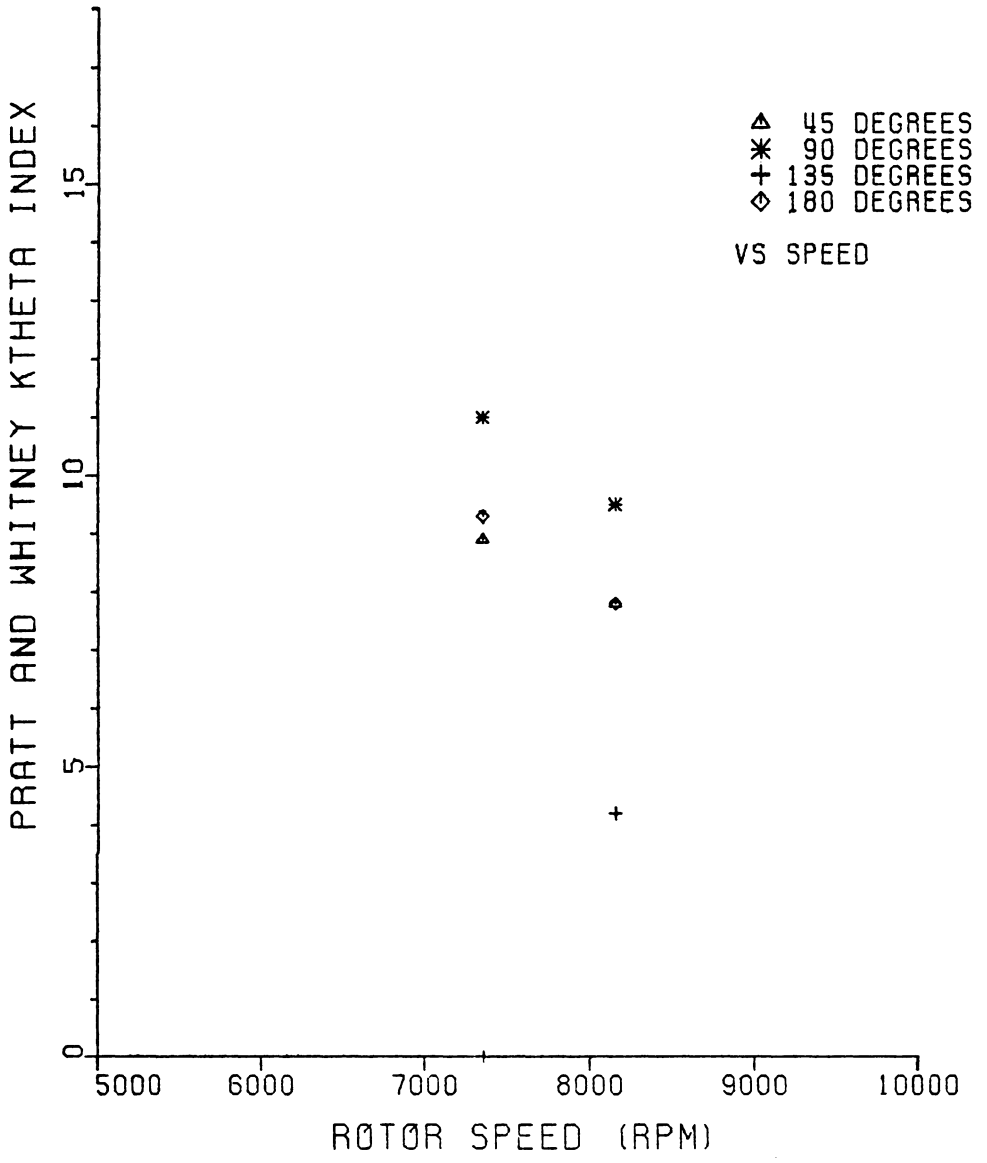

FIGURE 35: CIRCUMFERENTIAL DISTORTION-INDUCED STALL DATA FOR THE COMPRESSOR TEST-RIG, PRATT AND WHITNEY KTHETA INDEX

ΔPRS_N and experimental ΔPRS_N are compared using J85 data in Fig. 36. Figure 37 compares ARP 1420 predicted ΔPRS_N to experimental ΔPRS_N using J85 data. Figure 38 is a graphical comparison of GE Method D predicted ID and experimental ID using J85 data. Plots of the distortion indices versus ΔPRS_N and ΔPRS_M (where appropriate) for all three data sets as well as plots of the indices versus engine speed for the remaining two data sets are presented in Appendix C. Graphical comparisons of experimental results with ARP 1420, GE Method D, and parallel compressor theory predictions for the TF30 and compressor test-rig data are also contained in Appendix C.

In Figures 26 through 35, separate symbols are used for the different extent distortions tested on the compressor test-rig. Note that, with the possible exception of NAPC $K\theta$, none of the indices reduces the data of different extent distortions to a single line. Some indices, e.g., PWA KD_2 and $P_{max-min}/P_{avg}$, appear to follow a pattern of increasing magnitude with increasing distortion extent. Similarly, distortion intensity (in terms of distortion screen porosity) is plotted as a parameter in Figures C16 through C22, where each index is plotted versus percent engine speed for the J85 data. Again, none of the indices reduces the data to a single line and some appear to follow a pattern of increasing magnitude with increasing screen porosity (or distortion intensity). Engine speed is plotted as a parameter for the loss in stall pressure ratio plots of the J85 engine and compressor test-rig data, Figures C1 through C14 and Figures C44 through C52 respectively. In general, increasing speed corresponds with increasing loss in stall

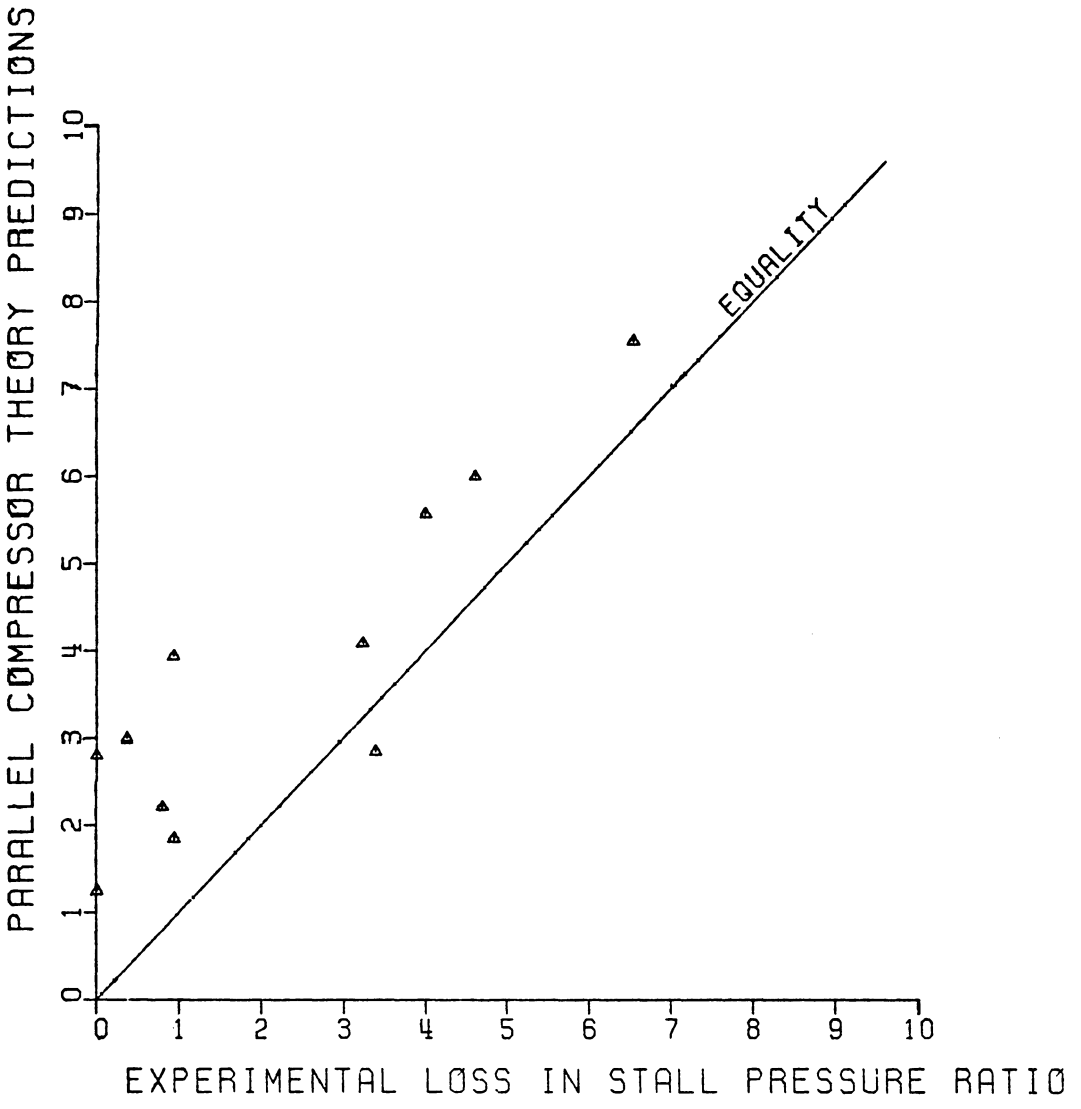

FIGURE 36: CIRCUMFERENTIAL DISTORTION-INDUCED STALL DATA FOR THE J85-GE-13 ENGINE AND PARALLEL COMPRESSOR THEORY PREDICTIONS

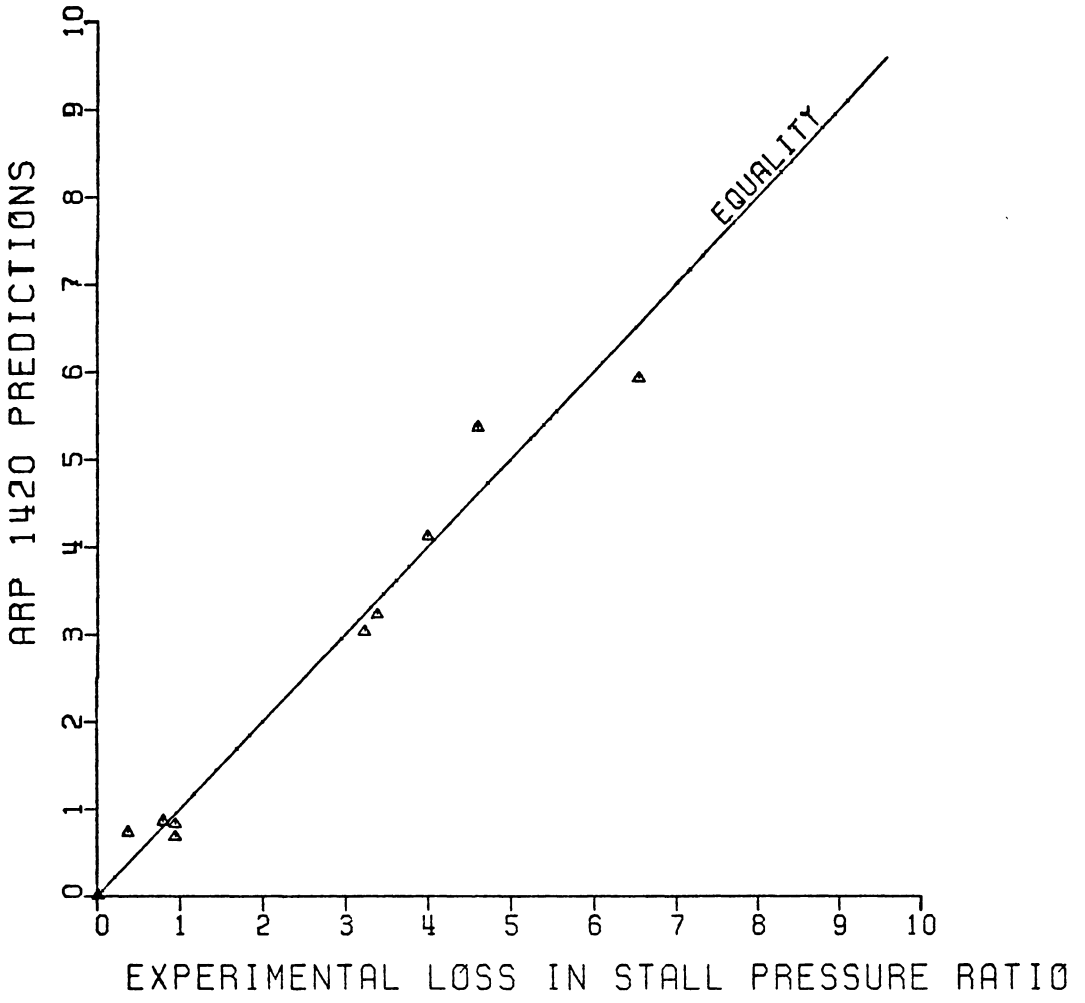

FIGURE 37: CIRCUMFERENTIAL DISTORTION-INDUCED STALL DATA FOR THE J85-GE-13 ENGINE AND ARP 1420 PREDICTIONS

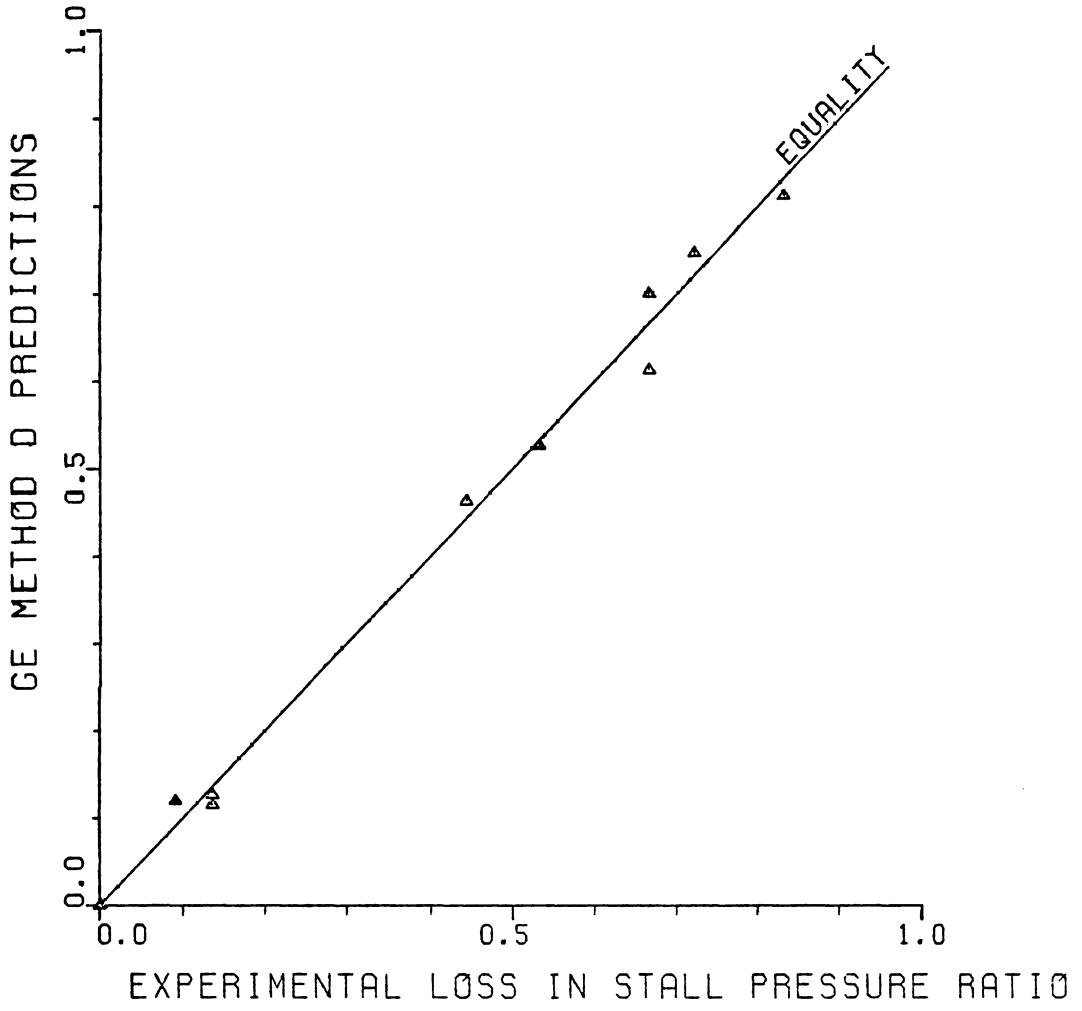

FIGURE 38: CIRCUMFERENTIAL DISTORTION-INDUCED STALL DATA FOR THE J85-GE-13 ENGINE AND GE METHOD D PREDICTIONS

pressure ratio.

Results of the statistical analyses are presented in Tables 1 through 6. Table 1 reveals that each of the indices evaluated produced a better correlation with ΔPRS_N than with ΔPRS_M or engine speed for the J85 data. The Garrett AiResearch CDI index produced the best correlation. The AVCO Lycoming DI_c and Rolls Royce $\Delta P(60)/\overline{P}$ indices produced the poorest results in all three cases; neither of these indices was able to account for even 10% of the variations in ΔPRS_N, ΔPRS_M, or engine speed.

Results of the ARP 1420 and GE Method D indices are presented separately as these are predictive indices with sensitivity coefficients that are functions of engine speed. They are evaluated in terms of R-SQUARE values. Table 2 contains these results. The apparent perfect results (R-SQUARE equal to 1.0000) at 80% corrected speed are a result of there being only two data points at this speed. This allowed the regression model to fit a straight line through the data, thereby producing a sensitivity coefficient capable of exactly reproducing experimental results. The poor results achieved at 87% corrected speed are due to the unusual experimental results which indicate that the 7.5M screen has less effect on engine performance than does the 4M screen. This unusual circumstance occurs for ΔPRS_N, ΔPRS_M, and ID. Thus, because the GE Method D and ARP 1420 distortion descriptors increase in magnitude with screen porosity (or distortion intensity), the regression model produced poor results.

Table 3 illustrates that each index calculated from TF30 data

Table 1: Results of Statistical Analyses of Distortion Indices Using J85-GE-13 Engine Data

INDEX	ΔPRS_N		ΔPRS_M		$\%N/\sqrt{\theta}$	
	CC*	R^{2**}	CC	R^2	CC	R^2
$\frac{P_{max} - P_{min}}{P_{avg}}$	0.9012	0.8121	0.8375	0.7014	0.6620	0.4382
$\frac{P_{avg} - P_{min}}{P_{avg}}$	0.9108	0.8296	0.8322	0.6925	0.6970	0.4858
Rolls Royce $\Delta P(60)/P$	0.2388	0.0570	0.2216	0.0491	-0.0870	0.0076
AVCO Lycoming DI	0.9198	0.8460	0.8405	0.7064	0.7076	0.5008
AVCO Lycoming DI_c	0.2585	0.0668	0.2367	0.0560	-0.0767	0.0059
Garrett AiResearch CDI	0.9221	0.8503	0.8268	0.6835	0.7055	0.4977
PWA KD_2	0.9206	0.8475	0.8566	0.7338	0.7084	0.5018

* Pearson correlation coefficient

** R-SQUARE

Table 2: Results of Statistical Analyses of ARP 1420 and GE Method D Using J85-GE-13 Engine Data

$\%N/\sqrt{\theta}$	ARP 1420 ($\%\Delta PRS_N$) R^{2*}	ARP 1420 ($\%\Delta PRS_M$) R^2	Method D (ID) R^2
80	1.0000	1.0000	1.0000
87	0.0463	0.0463	0.0452
94	0.9904	0.9317	0.8687
100	0.8068	0.9683	0.9752

* R-SQUARE

Table 3: Results of Statistical Analyses of Distortion Indices Using TF30-P-3 Engine Data

INDEX	$\%\Delta PRS_N$		Corrected Fan Speed	
	CC*	R^{2**}	CC	R^2
$\frac{P_{max} - P_{min}}{P_{avg}}$	0.6155	0.3788	0.9645	0.9302
$\frac{P_{avg} - P_{min}}{P_{avg}}$	0.6207	0.3853	0.9190	0.8445
Rolls Royce DC(60)	-0.6572	0.4320	-0.8992	0.8085
Rolls Royce $\Delta P(60)/\overline{P}$	0.5271	0.2778	0.9515	0.9054
AVCO Lycoming DI	0.4896	0.2397	0.9479	0.8986
AVCO Lycoming DI_c	0.5937	0.3525	0.9307	0.8662
Garrett AiResearch CDI	0.5615	0.3153	0.9632	0.9277
PWA KD_2	0.5731	0.3284	0.9062	0.8211
PWA $K\theta$	-0.6442	0.4149	-0.8732	0.7624

* Pearson correlation coefficient

** R-SQUARE

produced a better correlation with corrected fan speed than with ΔPRS_N. The simple $P_{max-min}/\overline{P}$ index produced the best correlation. The AVCO Lycoming DI_c and Rolls Royce $\Delta P(60)/\overline{P}$ indices produced significantly better results for the TF30 data than for the J85 data. ARP 1420 and GE Method D are presented in Table 4. The apparent perfect results (R-SQUARE equal to 1.0000) occur because the TF30 data set contains tests of only one distortion at each speed. Thus, the sensitivity coefficients, which are functions of speed, are simply the desired result (either ΔPRS_N or ID) divided by the value of the index at that speed. The predicted values are therefore exactly equal to the experimental values.

Table 5 contains statistical analysis results for the distortion indices calculated from the compressor test-rig data. In general, results are poorer for this data set than for the other two. All of the indices, except the Rolls Royce DC(60) index, produced better correlations with compressor speed than with ΔPRS_N. Best results were achieved by the $P_{avg-min}/\overline{P}$ index. The Rolls Royce DC(60) index produced the poorest correlations; it could not account for even 10% of the variations in ΔPRS_N or compressor speed.

Results of ARP 1420 predictions for the compressor test-rig are presented in Table 6. Apparently perfect results occur because of insufficient test cases. The circumferential sensitivity was first evaluated for the 180° extent distortions. Because only two speeds were tested, the coefficient was able to exactly reproduce experimental results. The extent function was then computed for the other extent

Table 4: Results of Statistical Analyses of ARP 1420 and GE Method D Using TF30-P-3 Engine Data

Corrected Fan Speed	ARP 1420 ($\%\Delta PRS_N$) R^{2*}	Method D (ID) R^2
6717	1.0000	1.0000
7341	1.0000	1.0000
7840	1.0000	1.0000
8190	1.0000	1.0000
8965	1.0000	1.0000
8629	1.0000	1.0000
9031	1.0000	1.0000

* R-SQUARE

Table 5: Results of Statistical Analyses of Distortion Indices Using Compressor Test-Rig Data

INDEX	$\%\Delta PRS_N$		Corrected Fan Speed	
	CC*	R^{2**}	CC	R^2
$\frac{P_{max} - P_{min}}{P_{avg}}$	0.3408	0.1161	0.6577	0.4326
$\frac{P_{avg} - P_{min}}{P_{avg}}$	0.6972	0.4861	0.8833	0.7801
Rolls Royce DC(60)	0.1550	0.0240	0.0552	0.0030
Rolls Royce $\Delta P(60)/\overline{P}$	0.3768	0.1420	0.5144	0.2646
AVCO Lycoming DI	0.2445	0.0598	0.4628	0.2142
AVCO Lycoming DI_c	0.4888	0.2389	0.7127	0.5080
Garrett AiResearch CDI	0.2423	0.0587	0.4925	0.2425
NAPC $K\theta$	--	--	0.7161	0.5129
PWA KD_2	0.3209	0.1030	0.5644	0.3185
PWA $K\theta$	-0.3080	0.0948	-0.5923	0.3508

* Pearson correlation coefficient

** R-SQUARE

Table 6: Results of Statistical Analysis of ARP 1420 Using Compressor Test-Rig Data

Speed (rpm)	Extent (degrees)	ARP 1420 ($\%\Delta PRS_N$) R^{2*}
7360	45	1.0000
7360	90	1.0000
7360	180	1.0000
8160	45	1.0000
8160	90	1.0000
8160	135	1.0000
8160	180	1.0000

* R-SQUARE

distortions. Again, because only two test cases were available for each extent distortion, the extent function was able to exactly reproduce experimental results.

Results Employing Effective Total Pressure Distributions

The results of calculating the simple $\Delta P/\overline{P}$ indices from effective rather than measured inlet total pressure distributions were also evaluated in terms of correlation coefficients and R-SQUARE values. The effect on parallel compressor theory accuracy was measured in terms of the sum of the square of the deviations of predicted ΔPRS_N from experimental ΔPRS_N. It was not possible to use R-SQUARE values for this evaluation as parallel compressor theory is a purely predictive tool that does not require regression analysis.

Table 7 contains the statistical results pertaining to $\Delta P/\overline{P}$ index calculations for the measured and effective total pressure distributions of the J85 data. Best results for the $P_{max-min}/\overline{P}$ index were achieved with the effective total pressure distribution derived from a natural frequency that produces a settling time equal to the time required to complete 1/2 of a revolution. This corresponds to the slowest response system tested in deriving the effective total pressure distributions. No one total pressure distribution produced best results for the $P_{avg-min}/\overline{P}$ index. The single best correlation was achieved with ΔPRS_N using the effective total pressure distribution derived from a natural frequency that produces a settling time equal to the time required for 1/8

Table 7: Statistical Analysis Results for the $\Delta P/\overline{P}$ Indices Using the Effective Total Pressure Profiles Derived from J85-GE-13 Engine Data

γ*	$(P_{max} - P_{min})/P_{avg}$ INDEX						$(P_{avg} - P_{min})/P_{avg}$ INDEX					
	$\%\Delta PRS_N$		$\%\Delta PRS_M$		$\%N/\sqrt{\theta}$		$\%\Delta PRS_N$		$\%\Delta PRS_M$		$\%N/\sqrt{\theta}$	
	CC**	R^{2}***	CC	R^2	CC	R^2	CC	R^2	CC	R^2	CC	R^2
0	0.9012	0.8121	0.8375	0.7014	0.6620	0.4832	0.9108	0.8296	0.8322	0.6925	0.6970	0.4858
$\frac{1}{8}$	0.9103	0.8286	0.8029	0.6446	0.6760	0.4570	0.9184	0.8434	0.7977	0.6363	0.6979	0.4870
$\frac{3}{16}$	0.9066	0.8219	0.8010	0.6415	0.6706	0.4497	0.9163	0.8396	0.8000	0.6401	0.6878	0.4730
$\frac{1}{4}$	0.9074	0.8234	0.8340	0.6956	0.6704	0.4495	0.9152	0.8377	0.8336	0.6949	0.6853	0.4697
$\frac{3}{8}$	0.9083	0.8250	0.8358	0.6986	0.6719	0.4514	0.9152	0.8376	0.8374	0.7013	0.8671	0.4721
$\frac{1}{2}$	0.9124	0.8324	0.8439	0.7121	0.6807	0.4633	0.9161	0.8393	0.8418	0.7086	0.8675	0.4726

* Number of revolutions completed before settling time (0 corresponds with measured profile)

** Pearson correlation coefficient

*** R-SQUARE

of a revolution. This corresponds to the fastest response system tested.

Parallel compressor theory results for the measured and effective total pressure distributions of the J85 engine data are presented in Table 8. Best results were achieved for the effective total pressure distribution corresponding to a settling time of 1/2 of a revolution.

Table 9 contains the statistical results pertaining to $\Delta P/\overline{P}$ index calculations for the measured and effective total pressure distributions of the TF30 data. None of the effective total pressure distributions improved the correlation capability of either of the $\Delta P/\overline{P}$ indices with ΔPRS_N. However, significant improvement was achieved with the effective total pressure distribution corresponding to a settling time of 1/4 of a revolution for both indices correlated with corrected fan speed.

Parallel compressor theory results are presented in Table 10. No improvement was achieved for any of the effective total pressure distributions; however, even parallel compressor theory predictions based on the measured distribution are very much lower than experimental ΔPRS_N. Errors range from 45 to 68% for predictions based on the measured profile.

Statistical analysis results pertaining to $\Delta P/\overline{P}$ index calculations for the measured and effective total pressure distributions of the compressor test-rig data are contained in Table 11. No improvement was provided by any of the effective total pressure distributions for the $P_{max-min}/\overline{P}$ index; however, the $P_{avg-min}/\overline{P}$ index was improved. The most significant improvement occurred for the correlation with compressor

Table 8: Statistical Analysis Results for Parallel Compressor Theory Using the Effective Total Pressure Profiles Derived from J85-GE-13 Engine Data

			Parallel Compressor Theory Predictions, $\%\Delta PRS_N$					
$\%N/\sqrt{\theta}$	Screen	Experimental $\%\Delta PRS_N$	t_s from 0 rev	t_s from $\frac{1}{8}$ rev	t_s from $\frac{3}{16}$ rev	t_s from $\frac{1}{4}$ rev	t_s from $\frac{3}{8}$ rev	t_s from $\frac{1}{2}$ rev
80	4M	0.01	1.25	1.25	1.20	1.20	1.15	1.10
80	9M	0.01	2.80	2.65	2.60	2.60	2.60	2.55
87	4M	0.94	1.85	1.85	1.81	1.81	1.81	1.81
87	7.5M	0.38	3.00	2.95	2.90	2.90	2.85	2.80
87	9M	0.94	3.94	3.73	3.73	3.69	3.69	3.59
94	4M	0.80	2.21	2.21	2.16	2.16	2.16	2.10
94	7.5M	3.23	4.09	3.99	3.94	3.90	3.90	3.90
94	9M	4.00	5.57	5.36	5.31	5.31	5.31	5.26
100	4M	3.39	2.85	2.81	2.71	2.71	2.71	2.71
100	7.5M	4.61	6.00	5.95	5.90	5.85	5.80	5.80
100	9M	6.54	7.55	7.55	7.51	7.51	7.46	7.30
Sum of Square of Deviations	--	--	34.5	31.3	30.2	29.7	29.2	27.5

Table 9: Statistical Analysis Results for the $\Delta P/\overline{P}$ Indices Using the Effective Total Pressure Profiles Derived from TF30-P-3 Engine Data

γ*	$(P_{max}-P_{min})/P_{avg}$				$(P_{avg}-P_{min})/P_{avg}$			
	ΔPRS_N		Corrected Fan Speed		ΔPRS_N		Corrected Fan Speed	
	CC**	R^{2***}	CC	R^2	CC	R^2	CC	R^2
0	0.61550	0.3788	0.9645	0.9302	0.6207	0.3853	0.9190	0.8445
$\frac{1}{8}$	0.6011	0.3613	0.9718	0.9443	0.6158	0.3792	0.9616	0.9246
$\frac{3}{16}$	0.5942	0.3531	0.9747	0.9500	0.6090	0.3709	0.9749	0.9504
$\frac{1}{4}$	0.5858	0.3431	0.9753	0.9512	0.6016	0.3620	0.9801	0.9607
$\frac{3}{8}$	0.5728	0.3281	0.9723	0.9453	0.5869	0.3444	0.9776	0.9558
$\frac{1}{2}$	0.5584	0.3118	0.9680	0.9370	0.5714	0.3264	0.9731	0.9469

* Number of revolutions completed before settling time (0 corresponds to measured profile)
** Pearson correlation coefficient
*** R-SQUARE

Table 10: Statistical Analysis Results for Parallel Compressor Theory Using the Effective Total Pressure Profiles Derived from TF30-P-3 Engine Data

		Parallel Compressor Theory Predictions, $\%\Delta PRS_N$					
Corrected Fan Speed	Experimental $\%\Delta PRS_N$	t_s from 0 rev	t_s from $\frac{1}{8}$ rev	t_s from $\frac{3}{16}$ rev	t_s from $\frac{1}{4}$ rev	t_s from $\frac{3}{8}$ rev	t_s from $\frac{1}{2}$ rev
6717	12.73	4.09	4.07	4.07	4.06	4.05	4.04
7341	12.89	5.49	5.20	5.06	4.94	4.98	5.02
7840	10.51	5.45	5.42	5.42	5.40	5.40	5.39
8190	14.08	6.19	6.09	6.07	6.06	6.02	5.98
8965	16.77	7.26	7.16	7.11	7.07	6.98	6.89
8629	12.63	6.91	6.87	6.85	6.83	6.79	6.75
9031	15.76	6.74	6.66	6.61	6.58	6.50	6.42
Sum of Square of Deviations	--	422	432	437	441	445	449

Table 11: Statistical Analysis Results for the $\Delta P/\overline{P}$ Indices Using the Effective Total Pressure Profiles Derived from Compressor Test-Rig Data

γ*	$(P_{max}-P_{min})/P_{avg}$				$(P_{avg}-P_{min})/P_{avg}$			
	ΔPRS_N		Corrected Fan Speed		ΔPRS_N		Corrected Fan Speed	
	CC**	R^{2***}	CC	R^2	CC	R^2	CC	R^2
0	0.3408	0.1161	0.6577	0.4326	0.6972	0.4861	0.8832	0.7801
$\frac{1}{8}$	0.3254	0.1059	0.6244	0.3899	0.7054	0.4976	0.9373	0.8785
$\frac{3}{16}$	0.3102	0.0962	0.6014	0.3617	0.7046	0.4965	0.9405	0.8845
$\frac{1}{4}$	0.2974	0.0884	0.5817	0.3384	0.6855	0.4699	0.9258	0.8571
$\frac{3}{8}$	0.2858	0.0817	0.5540	0.3069	0.6396	0.4091	0.8668	0.7513
$\frac{1}{2}$	0.2634	0.0694	0.5204	0.2708	0.5669	0.3214	0.7778	0.6050

* Number of revolutions completed before settling time (0 corresponds to measured profile)
** Pearson correlation coefficient
*** R-SQUARE

speed using the effective distribution corresponding to a settling time of 3/16 of a revolution. Parallel compressor theory results are presented in Table 12. Significant improvement was achieved when parallel compressor theory was evaluated using the effective total pressure distributions. Best results were achieved for those distributions producing settling times of 3/8 and 1/2 of a revolution.

In summary, each of the distortion indices produced a better correlation with ΔPRS_N than ΔPRS_M or engine speed for the J85 engine data. Best results were achieved by correlation with corrected fan speed for the TF30 engine data. In general, the indices produced poorer results using the compressor test-rig data than for the other two data sets. A better correlation was achieved with compressor speed than with ΔPRS_N for this data set. Significant tests of the accuracy of the ARP 1420 and GE Method D indices occurred only with the J85 data set. Good results were achieved at 80%, 94%, and 100% corrected speed but very poor results were achieved at 87% corrected speed.

The effective total pressure distributions tested produced mixed results. In some cases, (most notably for parallel compressor theory predictions using compressor test-rig data) significant improvement resulted.

In the following section, limitations in the available experimental data are discussed. Uncertainties associated with the data and resultant uncertainties in index calculations are presented.

Table 12: Statistical Analysis Results for Parallel Compressor Theory Using the Effective Total Pressure Profiles Derived from Compressor Test-Rig Data

			Parallel Compressor Theory Predictions, $\%\Delta PRS_N$					
Speed (rpm)	Extent (degrees)	Experimental $\%\Delta PRS_N$	t_s from 0 rev	t_s from $\frac{1}{8}$ rev	t_s from $\frac{1}{16}$ rev	t_s from $\frac{1}{4}$ rev	t_s from $\frac{3}{8}$ rev	t_s from $\frac{1}{2}$ rev
7360	45	0.23	0.74	0.57	0.55	0.53	0.50	0.47
7360	90	0.48	0.75	0.52	0.52	0.52	0.52	0.52
7360	180	0.19	0.60	0.49	0.49	0.49	0.48	0.48
8160	45	0.72	0.63	0.69	0.66	0.64	0.60	0.55
8160	90	0.64	0.54	0.74	0.74	0.74	0.74	0.73
8160	135	0.58	0.54	0.67	0.67	0.67	0.67	0.67
8160	180	0.61	0.49	0.60	0.60	0.60	0.60	0.60
Sum of Square of deviations	--	--	0.54	0.23	0.22	0.21	0.19	0.19

XIII. DISCUSSION OF RESULTS

Limitations concerning the experimental stall data used in this investigation of distortion index accuracy are discussed. In addition, uncertainties associated with the stall data are presented. Resultant uncertainties in distortion index calculations are determined.

The J85-GE-13 and TF30-P-3 data sets contained distortion tests of 180° extent only. This made it impossible to evaluate the indices' ability to correlate varying extent distortion data for these data sets. As a result of this limitation in the data, the simple $P_{max-min}/P_{avg}$ index (which has no means of accounting for distortion extent) produced the best correlation for the TF30 data, even better than the Pratt and Whitney KD_2 index which was specifically designed to correlate TF30 stall behavior. Recall that the KD_2 index does contain a multiplicative extent function and presumably would have produced better results than the $P_{max-min}/P_{avg}$ index for a more varied data set.

Different distortion extent data was available for the compressor test-rig, but each extent distortion was tested at only two speeds. This made it difficult to generalize results, i.e., the two data points for each extent distortion always produced a straight line. At least three data points for each extent distortion are required to generalize results.

Some of the stall data for the J85-GE-13 and TF30-P-3 engines were obtained from graphs and performance maps. The uncertainties associated with reading the graphs and maps are presented in Appendix A. Resultant uncertainties in loss in stall pressure ratio and ID were determined

using the method of Kline and McClintock (37). These uncertainties are presented in Tables A2 and A5 for the J85 and TF30 data respectively. The uncertainties associated with the experimental process were available for the compressor test-rig data. This is also contained in Appendix A. Resultant uncertainties in ΔPRS_N as determined using the method of Kline and McClintock are presented in Table A8.

The uncertainties associated with the inlet total pressure profiles create uncertainties in the distortion indices. Uncertainties in the simple $\Delta P/\overline{P}$ indices were calculated using the method of Kline and McClintock for the J85 and compressor test-rig data sets. TF30 index uncertainties were not computed because inlet total pressure data was provided in tabular form (meaning that there was no uncertainty associated with reading these values from graphs) and experimental uncertainties were not available.

Computed $\Delta P/\overline{P}$ index values and their associated uncertainties are presented in Tables 13 and 14 for the J85 and compressor test-rig data sets respectively. Uncertainties in compressor test-rig indices are an order of magnitude smaller than the index values; however, uncertainites in J85 $\Delta P/\overline{P}$ indices are on the same order of magnitude as the index values. Uncertainies for the more complex indices were not computed as these indices are in general based on the simple $\Delta P/\overline{P}$ indices with the added complexity of extent factors, shape factors, etc.

The uncertainties associated with loss in stall pressure ratio, ID, and the distortion indices themselves could seriously affect the statistical evaluations presented in the preceding section. It is

Table 13: Uncertainties in $\Delta P/\overline{P}$ Indices Calculated from Compressor Test-Rig Data

Speed (rpm)	Extent (degrees)	$\frac{P_{max}-P_{min}}{P_{avg}}$	$\omega^*_{\frac{P_{max-min}}{P_{avg}}}$	$\frac{P_{avg}-P_{min}}{P_{avg}}$	$\omega_{\frac{P_{avg-min}}{P_{avg}}}$
7360	45	0.00725	$\pm$0.00017	0.00559	$\pm$0.00018
7360	90	0.00722	$\pm$0.00017	0.00468	$\pm$0.00018
7360	180	0.00985	$\pm$0.00017	0.00479	$\pm$0.00018
8160	45	0.00844	$\pm$0.00017	0.00668	$\pm$0.00018
8160	90	0.00997	$\pm$0.00017	0.00622	$\pm$0.00018
8160	135	0.0112	$\pm$0.00017	0.00708	$\pm$0.00018
8160	180	0.0121	$\pm$0.00017	0.00611	$\pm$0.00018

*ω = uncertainty

Table 14: Uncertainties in $\Delta P/\overline{P}$ Indices Calculated for J85-GE-13 Engine Data

$\%N/\sqrt{\theta}$	Screen	$\frac{P_{max}-P_{min}}{P_{avg}}$	$\omega^*_{\frac{P_{max-min}}{P_{avg}}}$	$\frac{P_{avg}-P_{min}}{P_{avg}}$	$\omega_{\frac{P_{avg-min}}{P_{avg}}}$
80	4M	0.0253	±0.014	0.0122	±0.014
80	9M	0.0561	±0.014	0.0263	±0.014
87	4M	0.0373	±0.014	0.0188	±0.014
87	7.5M	0.0600	±0.014	0.0284	±0.014
87	9M	0.0791	±0.014	0.0349	±0.014
94	4M	0.0441	±0.014	0.0278	±0.014
94	7.5M	0.0821	±0.014	0.0368	±0.014
94	9M	0.112	±0.014	0.0501	±0.014
100	4M	0.0571	±0.014	0.0283	±0.014
100	7.5M	0.120	±0.014	0.0572	±0.014
100	9M	0.152	±0.014	0.0678	±0.014

*ω = uncertainty

important to note, however, that in a comparative analysis where each index is computed from the same data, such as the investigation conducted here, the effect should be less significant.

XIV. CONCLUSIONS

The ability of twelve different distortion indices to predict stalling behavior in aircraft gas turbine engines was investigated using J85-GE-13 turbojet engine data, TF30-P-3 turbofan engine data, and modified T64-GE-6B compressor test-rig data. The indices investigated were

1. $P_{max-min}/P_{avg}$
2. $P_{avg-min}/P_{avg}$
3. Rolls Royce DC(60)
4. Rolls Royce $P_{avg-min,\ \theta\ crit}/P_{avg}$
5. AVCO Lycoming DI
6. AVCO Lycoming DI_c
7. Garrett AiResearch CDI
8. NAPC $K\theta$
9. Pratt and Whitney KD_2
10. Pratt and Whitney $K\theta$
11. General Electric Method D
12. ARP 1420.

The indices were tested for correlation capability with constant speed loss in stall pressure ratio (ΔPRS_N), constant mass loss in stall pressure ratio (ΔPRS_M), and engine speed if appropriate. In addition, the concept of including the effects of compressor dynamic response by modifying the inlet total pressure profile rather than the index was

investigated. This was done by evaluating the accuracy of parallel compressor theory and the two $\Delta P/\overline{P}$ indices first with measured and then with modified or effective inlet total pressure distributions.

As a group, the indices produced better correlations with ΔPRS_N than with ΔPRS_M or engine speed for J85-GE-13 engine data. Better correlations were achieved with corrected fan speed than with ΔPRS_N for TF30-P-3 engine data. In general, poorer correlations resulted for the compressor test-rig than for the other two data sets. Better correlations were achieved with compressor speed than with ΔPRS_N when using the compressor test-rig data.

No single index produced best results for all three data sets; however, the simple $P_{avg-min}/P_{avg}$ index did provide consistently good correlations. All indices provided good correlations, i.e., produced correlation coefficients of 0.8 or better, for at least one correlation test of at least one data set. However, the Rolls Royce $\Delta P(60)/\overline{P}$ index and the AVCO Lycoming DI_c index produced poor results for all other test cases.

Application of parallel compressor theory and the $\Delta P/\overline{P}$ indices to effective rather than measured inlet total pressure profiles provided significant improvements in accuracy for most cases. Parallel compressor theory predictions were particularly improved for the small extent distortion data of the compressor test-rig data set. Because of the manner in which the effective total pressure profile is derived, the effective profile is most significantly different from the measured profile for small extent distortions. The effective total pressure

profile affects parallel compressor theory in a manner similar to the Reid critical angle concept [4]. The largely positive results of this investigation indicate that the effective total pressure profile is a viable option for improving the accuracy of parallel compressor theory and the simple $\Delta P/\overline{P}$ indices.

XV. RECOMMENDATIONS FOR FUTURE RESEARCH

The investigation conducted in this thesis has demonstrated the need for further research and study in basically two areas. First, there is a clear need for more varied distorted inflow stall data. Two of the data sets in this investigation, the J85-GE-13 and TF30-P-3 data sets, contained data from only 180° extent distortions. Whereas the compressor test-rig data set consisted of varying extent distortion data, it contained tests at only two different compressor speeds. In addition, the compressor test-rig distortions were of such small magnitude or intensity that correspondingly low distortion index levels and loss in stall pressure ratio values were unnecessarily sensitive to experimental uncertainties. Determination of J85 and TF30 data from graphs and performance maps added unnecessary uncertainty to the results of this investigation. A more accurate representation of the data would improve the results of future investigations.

The concept of modifying the inlet total pressure profile as a means of incorporating compressor dynamic response effects in the simple distortion magnitude-descriptor indices is a second area worthy of further research. Specifically, further experimental work is required to verify the existance and identify if possible, a general frequency response function that will correctly modify any measured inlet total pressure profile to account for compressor dynamic response effects. In the absence of this experimental work, further research to identify the optimum effective total pressure profile, or equivalently, the correct

second order system for deriving the effective total pressure profile is recommended.

XVI. LIST OF REFERENCES

1. Sexton, M. R., "An Investigation of Dynamic Stalling Characteristics of Rotating Axial-Flow Compressor Blades," Ph.D. dissertation, Virginia Polytechnic Institute and State University, 1980.

2. Sullivan, A. M., "An Experimental Investigation of Stall and Recovery in an Axial-Flow Compressor Subjected to Inlet Distortion," M.S. thesis, Virginia Polytechnic Institute and State University, 1980.

3. Pearson, H. and McKenzie, A. B., "Wakes in Axial Compressors," Journal of the Royal Aeronautical Society, Vol. 63, July 1959, pp. 415-416.

4. Reid, C., "The Response of Axial Flow Compressors to Intake Flow Distortion," ASME Paper No. 69-GT-29, 1969.

5. Calogeras, J. E., Mehalic, C. M., and Burstadt, P. L., "Experimental Investigation of the Effect of Screen-Induced Total-Pressure Distortion on Turbojet Stall Margin," NASA TMX-2239, March 1971.

6. Roberts, F., Plourde, G. A., and Smakula, F., "Insights into Axial Compressor Response to Distortion," AIAA Paper No. 68-565, June 1968.

7. Mikolajczak, A. A., and Pfeffer, A. M., "Methods to Increase Engine Stability and Tolerance to Distortion," AGARD Lecture Series No. 72, Sect. 7, 1974.

8. Mokelke, H., "Prediction Techniques," AGARD Lecture Series No. 72, Sect. 5, 1974.

9. Mazzawy, R. S., "Multiple Segment Parallel Compressor Model for Circumferential Flow Distortion," Journal of Engineering for Power, Vol. 99, No. 2, April 1977, pp. 288-296.

10. Tesch, W. A., and Steenken, W. G., "Blade Row Dynamic Digital Compressor Program, Vol. I," NASA-CR-134978, 1976.

11. Tesch, W. A. and Steenken, W. G., "Blade Row Dynamic Digital Compressor Program, Vol II," NASA-CR-134958, July 1978.

12. Chung, K., Hosny, W. M., and Steenken, W. G., "Aerodynamic Stability Analysis of NASA J85-13/Planar Pressure Pulse Generator Installation," NASA-CR-165141, Nov. 1980.

13. Melick, H. C., and Simpkins, W. E., "A Unified Theory of Inlet/Engine Compatability," AIAA Paper No. 72-1115 , 1972.

14. Melick, H. C., "Analysis of Inlet Flow Distortion and Turbulence Effects on Compressor Stability," NTIS CR-114577, 1973.

15. Nagano, S., and Takata, H., "Nonlinear Analysis of Rotating Stall," Institute of Space and Aeronautical Science, University of Tokyo, Report No. 449, April 1970.

16. Adamczyk, J. J., and Carta, F. O., "Unsteady Fluid Dynamic Response of an Axial-Flow Compressor Stage with Distorted Inflow," Project Squid Technical Report UARL-2-PU, 1973.

17. Korn, J. A., "The Effects of Inlet Distortion on the Performance and Stability of the Low-Speed Spool of a Turbofan Engine," AIAA Paper No. 74-233, 1974.

18. Braithwaite, W. M., Graber, E. J., and Mehalic, C. M., "The Effect of Inlet Temperature and Pressure Distortion on Turbojet Performance," AIAA Paper No. 73-1316, 1973.

19. Graber, E. J., and Braithwaite, W. M., "Summary of Recent Investigations of Inlet Flow Distortion Effect on Engine Stability," NASA TMX-71505, Feb. 1974.

20. Brunda, D. F., and Boytos, J. F., "Evaluation of a Circumferential Inlet Pressure Distortion Index on a TF30-P-12 Turbofan Engine," NAPTC-ATD-193, July 1970.

21. Werner, R. A., Abdelwahab, M., and Braithwaite, W. M., "Performance and Stall Limits of an Afterburner Equipped Turbofan Engine With and Without Inlet Flow Distortion," NASA TMX-1947, 1970.

22. Moore, M. T., "Distortion Data Analysis," AFAPL-TR-72-111, Feb. 1973.

23. Moore, M. T., and Lueke, J. E., "A Similarity Parameter for Scaling Dynamic Inlet Distortion," Journal of Engineering for Industry, Aug. 1974, pp 795-800.

24. Stevens, C. H., Spong, E. D., and Hammock, M. S., "F15 Inlet/Engine Test Technique and Distortion Methodologies Studies," NASA-CR-144866, Jun. 1978.

25. Farr, A. P., "Evaluation of F-15 Inlet Dynamic Distortion," AIAA Paper No. 78-784, Aug. 1973.

26. Walter, W. A., and Shaw, M., "Distortion Analysis for F100(3) Engine," NASA-CR-159754, Jan. 1980.

27. Hercock, R. G., and Williams, D. D., "Aerodynamic Response," AGARD Lecture Series No. 72, Sect. 3, 1974.

28. Aerospace Recommended Practice, "Gas Turbine Engine Inlet Flow Distortion Guidelines," ARP 1420, Society of Automotive Engineers, Mar. 1978.

29. Boytos, J. F., "State-of-the-Art Review Aircraft Gas Turbine Engines -Inlet Distortion Indices," NAPTC-PE-95, Mar. 1977.

30. Steenken, W. G., "2.0 Surge Pressure Ratio Correlation," Draft copy of Section 2.0 of report to be published by SAE S-16 Committee in fall of 1981.

31. Newland, D. E., Random Vibrations and Spectral Analysis, Longman Group Limited, London, 1975.

32. Wenzel, L. M., Moss, J. E., Jr., and Mehalic, C. M., "Effect of Casing Treatment on Performance of a Multistage Compressor," NASA TMX-2990, 1974.

33. Braithwaite, W. M., Dicus, J. H., and Moss, J. E., Jr., "Evaluation With a Turbofan Engine of Air Jets as a Steady State Inlet Flow Distortion Device," NASA TMX-1955, 1970.

34. Gridley, R. B., "Performance Characteristics of an Axial-Flow Compressor Operating with Circumferential Inlet Flow Distortion," M.S. thesis, Virginia Polytechnic Institute and State University, 1980.

35. SAS User's Guide 1979 Edition, SAS Institute Inc., 1979.

36. D'Azzo, J. J., and Houpis, C. H., Linear Control System Analysis and Design, McGraw-Hill, Inc., 1975.

37. Kline, S. J., and McClintock, F. A., "Describing Uncertainties in Single-Sample Experiments," Mechanical Engineering, Jan. 1953, p. 3.

38. Edwards, A. L., Statistical Methods, 3rd ed., Holt, Rinehart and Winston, Inc., 1973.

39. Edwards, A. L., An Introduction to Linear Regression and Correlation, W. H. Freeman and Company, San Francisco, 1976.

XVII. APPENDICES

APPENDIX A

DISTORTED INLET STALL DATA

Distorted inlet stall data for the J85-GE-13 turbojet engine, the TF30-P-3 turbofan engine, and the modified T64-GE-6B compressor test-rig are presented in tabular form. Uncertainties associated with the data are also presented.

J85-GE-13 Engine Data

Stall data for the J85-GE-13 engine are presented in Tables A1 and A2. The data were taken from reference 9.

The inlet total pressure data in reference 9 were normalized by the average inlet total pressure and presented in graphical form. Considering only errors resulting from reading the graphs, the uncertainty associated with the normalized inlet total pressure data in Table A1 is $\pm$ 0.0125.

The constant mass and constant speed loss in stall pressure ratio data were obtained from performance maps presented in reference 9. For example, the constant speed loss in stall pressure ratio, ΔPRS_N, was determined as follows:

$$\Delta PRS_N = \frac{PR_{stall,clean,N} - PR_{stall,distorted,N}}{PR_{stall,clean,N}}$$

Considering only errors resulting from reading the performance maps, the uncertainty in the above pressure ratios is $\pm$ 0.125. Using this value,

Table A1: Inlet Total Pressure Data ($P_{t,2}/\bar{P}_{t,2}$) for the J85-GE-13 Engine

	Ring	15°	45°	75°	105°	135°	165°	195°	225°	255°	285°	315°	345°
4M screen 80% $N/\sqrt{\theta}$	1(tip)	1.00	0.99	1.005	1.00	0.99	1.01	0.98	0.98	0.98	0.99	0.98	0.98
	2	1.01	1.01	1.005	1.005	1.01	1.01	0.985	0.99	0.985	0.99	0.99	0.99
	3	1.01	1.015	1.02	1.01	1.015	1.01	0.985	0.99	0.985	0.99	0.995	0.99
	4	1.005	1.01	1.01	1.005	1.01	1.01	0.99	0.99	0.99	0.99	0.99	0.99
	5(hub)	1.02	1.01	--*	1.015	1.015	1.01	0.99	0.99	0.99	0.99	0.995	0.99
9M screen 80% $N/\sqrt{\theta}$	1	1.005	1.01	--	1.02	1.02	1.025	0.96	0.98	0.975	0.975	0.975	0.98
	2	1.03	1.03	--	1.025	1.03	1.025	0.975	0.975	0.975	0.975	0.98	0.98
	3	1.03	1.035	--	1.025	1.03	1.025	0.975	0.975	0.975	0.975	0.98	0.98
	4	1.025	1.03	--	1.025	1.03	1.03	0.975	0.975	0.975	0.975	0.975	0.98
	5	1.025	1.03	--	1.025	1.03	1.01	0.975	0.975	0.975	0.98	0.975	0.98

*Data point judged in error by original experimentors

Table A1 (continued)

	Ring	15°	45°	75°	105°	135°	165°	195°	225°	255°	285°	315°	345°
4M screen 87% N/$\sqrt{\theta}$	1(tip)	1.005	0.995	1.01	1.005	0.995	1.015	0.975	0.97	0.97	0.98	0.98	0.975
	2	1.02	1.015	1.015	1.015	1.02	1.02	0.98	0.98	0.98	0.985	0.98	0.98
	3	1.015	1.02	1.02	1.01	1.02	1.02	0.98	0.99	0.98	0.985	0.98	0.985
	4	1.015	1.015	1.02	1.01	1.02	1.02	0.98	0.98	0.985	0.99	0.98	0.99
	5(hub)	1.025	1.02	--	1.02	1.015	0.98	0.985	0.98	0.98	0.99	0.995	0.99
7.5M screen 87% N/$\sqrt{\theta}$	1	1.015	1.015	1.01	1.025	1.015	1.02	0.97	0.96	0.955	0.97	0.96	0.97
	2	1.03	1.035	1.025	1.03	1.035	1.03	0.97	0.975	0.975	0.97	0.98	0.975
	3	1.025	1.04	1.035	1.025	1.035	1.03	0.975	0.975	0.975	0.975	0.975	0.975
	4	1.02	1.03	--	1.035	1.03	1.03	0.975	0.975	0.975	0.975	0.97	0.97
	5	1.02	1.035	--	1.025	1.03	1.025	0.98	0.97	0.975	0.975	0.97	0.98
9 M screen 87% N/$\sqrt{\theta}$	1	0.95	0.965	0.97	0.975	0.96	0.965	1.025	1.015	--	1.04	1.03	1.025
	2	0.965	0.97	0.965	0.97	0.97	0.975	1.035	1.035	--	1.035	1.05	1.04
	3	0.965	0.97	0.975	0.965	0.97	0.97	1.035	1.04	--	1.04	1.055	1.035
	4	0.965	0.965	0.97	0.97	0.97	0.97	1.025	1.04	--	1.035	1.04	--
	5	0.975	0.97	0.97	0.975	0.96	0.99	1.05	1.04	--	1.03	1.04	1.045

Table A1 (continued)

	Ring	15°	45°	75°	105°	135°	165°	195°	225°	255°	285°	315°	345°
4M screen 94% $N/\sqrt{\theta}$	1(tip)	1.0	1.0	1.005	1.01	1.0	1.02	0.975	0.97	0.965	0.98	0.975	0.97
	2	1.025	1.025	1.015	1.02	1.025	1.025	0.975	0.98	0.975	0.98	0.98	0.975
	3	1.02	1.025	1.025	1.02	1.025	1.02	0.98	0.985	0.98	0.98	0.99	0.98
	4	1.015	1.02	1.015	1.02	1.025	1.02	0.98	0.98	0.98	0.985	0.975	0.98
	5(hub)	1.03	1.02	--	1.02	1.02	0.98	0.98	0.98	0.975	0.99	0.99	0.985
7.5M screen 94% $N/\sqrt{\theta}$	1	1.025	1.025	1.025	1.035	1.02	1.025	0.95	0.95	0.945	0.955	0.945	0.96
	2	1.04	1.045	1.04	1.04	1.05	1.04	0.965	0.965	0.97	0.96	0.975	0.965
	3	1.035	1.05	1.045	1.03	1.05	1.035	0.965	0.97	0.965	0.96	0.97	0.97
	4	1.02	1.05	--	1.05	1.045	1.04	0.965	0.965	0.97	0.97	0.96	0.96
	5	1.015	1.05	--	1.045	1.035	1.035	0.97	0.96	0.97	0.97	0.96	0.965
9M screen 94% $N/\sqrt{\theta}$	1	0.9350	0.950	0.960	0.965	0.945	0.955	1.035	1.030	--	1.055	1.045	1.040
	2	0.950	0.960	0.950	0.955	0.960	0.960	1.050	1.060	--	1.060	1.070	1.060
	3	0.950	0.955	0.960	0.955	0.955	0.960	1.050	1.060	--	1.060	1.075	1.050
	4	0.950	0.950	0.955	0.96	0.960	0.955	1.030	1.065	--	1.060	1.065	--
	5	0.965	0.960	0.960	0.96	0.945	0.980	1.070	1.060	--	1.060	1.055	1.065

Table A1 (continued)

	Ring	15°	45°	75°	105°	135°	165°	195°	225°	255°	285°	315°	345°
4M screen 100% $N/\sqrt{\theta}$	1(tip)	1.000	1.000	1.015	1.015	1.010	1.030	0.970	0.960	0.960	0.975	0.975	0.960
	2	1.030	1.035	1.025	1.030	1.035	1.035	0.970	0.975	0.970	0.975	0.975	0.970
	3	1.030	1.030	1.030	1.025	1.030	1.025	0.970	0.980	0.970	0.975	0.980	0.970
	4	1.025	1.025	1.025	1.020	1.030	1.020	0.970	0.975	0.975	0.980	0.970	0.995
	5(hub)	1.050	1.020	--	1.025	1.025	0.975	0.975	0.975	0.975	0.985	0.990	0.980
7.5M screen 100% $N/\sqrt{\theta}$	1	1.045	1.040	1.025	1.065	1.03	1.045	0.930	0.930	0.925	0.940	0.925	0.940
	2	1.060	1.070	1.060	1.060	1.075	1.070	0.940	0.945	0.945	0.940	0.960	0.940
	3	1.060	1.060	1.075	1.040	1.070	1.060	0.940	0.950	0.940	0.950	0.950	0.950
	4	1.040	1.065	--	1.075	1.060	1.040	0.950	0.940	0.950	0.950	0.935	0.935
	5	1.030	1.055	--	1.060	1.045	1.055	0.960	0.935	0.970	0.945	0.935	0.950
9M screen 100% $N/\sqrt{\theta}$	1	0.915	0.925	0.940	0.950	0.930	0.940	1.040	1.050	--	1.080	1.070	1.060
	2	0.930	0.935	0.930	0.935	0.935	0.935	1.075	1.080	--	1.080	1.090	1.080
	3	0.925	0.930	0.950	0.930	0.930	0.935	1.070	1.075	--	1.080	1.100	1.050
	4	0.930	0.930	0.935	0.935	0.930	0.925	1.060	1.085	--	1.075	1.080	--
	5	0.950	0.930	0.950	0.955	0.930	--	1.080	1.085	--	1.075	1.070	1.080

Table A2: Effect of Circumferential Total Pressure Distortion on J85-GE-13 Performance

SCREEN	SPEED	$\%\Delta PRS_N$	$\omega^*_{\Delta PRS_N}$	$\%\Delta PRS_M$	$\omega_{\Delta PRS_M}$	ID	ω_{ID}
4M screen	80%	0.0	--	0.0	--	0.0	--
	87%	0.94	$\pm$ 3.32	2.42	$\pm$ 3.25	0.136	$\pm$ 0.15
	94%	0.80	$\pm$ 2.82	1.59	$\pm$ 2.78	0.444	$\pm$ 0.17
	100%	3.39	$\pm$ 2.30	3.00	$\pm$ 2.01	0.533	$\pm$ 0.17
7.5M screen	87%	0.38	$\pm$ 3.32	1.85	$\pm$ 3.24	0.091	$\pm$ 0.15
	94%	3.23	$\pm$ 2.81	6.98	$\pm$ 2.65	0.667	$\pm$ 0.17
	100%	4.61	$\pm$ 2.27	5.60	$\pm$ 2.24	0.722	$\pm$ 0.18
9M screen	80%	0.0	--	0.0	--	0.0	--
	87%	0.94	$\pm$ 3.32	2.42	$\pm$ 3.25	0.136	$\pm$ 0.15
	94%	4.00	$\pm$ 2.77	7.41	$\pm$ 2.63	0.667	$\pm$ 0.17
	100%	6.54	$\pm$ 2.24	7.14	$\pm$ 2.22	0.833	$\pm$ 0.18

*ω = uncertainty

the uncertainty associated with ΔPRS_N, as determined from the square law (or, equivalently, the method of Kline and McClintock), was calculated as follows:

$$\omega_{\Delta PRS_n} = \left[\left(\frac{PR_{stall,distorted,N}}{PR^2_{stall,clean,N}} \times 0.125 \right)^2 + \left(\frac{1}{PR_{stall,clean,N}} \times 0.125 \right)^2 \right]^{1/2}$$

The uncertainty associated with ΔPRS_M was determined in a similar fashion.

The GE stability index, ID, was determined using the performance maps of references 4 and 9. This was necessary because the clean inlet operating line was not included in the performance maps of reference 9. ID was calculated as follows:

$$ID = \frac{PR_{clean,stall,N} - PR_{distorted,stall,N}}{PR_{clean,stall,N} - PR_{clean,operating,N}}$$

An uncertainty analysis of ID based on an uncertainty of $\pm$ 0.125 for the above pressure ratios, yielded the following:

$$\omega_{ID} = \left[\left(\frac{PR_{clean,operating,N} - PR_{distorted,stall,N}}{(PR_{clean,stall,N} - PR_{clean,operating,N})^2} \times 0.125 \right)^2 + \left(\frac{0.125}{PR_{clean,stall,N} - PR_{clean,operating,N}} \right)^2 + \left(\frac{PR_{clean,stall,N} - PR_{distorted,stall,N}}{(PR_{clean,stall,N} - PR_{clean,operating,N})^2} \times 0.125 \right)^2 \right]^{1/2}$$

Tabulated values for ΔPRS_N, ΔPRS_M, ID, and their associated uncertainties are presented in Table A2.

The tabulated uncertainties represent maximum estimated variation as predicted by the square law based on uncertainties associated with reading pressure ratios from J85-GE-13 performance maps. In some cases, the uncertainty band would permit negative ΔPRS_N and ΔPRS_M. Clearly, this is not possible as this would mean that the distorted inflow resulted in increased engine stall margin. The uncertainty bands in Table A2 are thus felt to represent maximum possible error with probable error being somewhat less.

TF30-P-3 Engine Data

The TF30-P-3 engine data used in this investigation was supplied by Peter S. Batterton of NASA Lewis Research Center. Descriptions of engine and instrumentation were obtained from reference 33.

Inlet total pressure and static pressure data were supplied in tabular form and are reproduced in Tables A3 and A4 respectively. Hence, there was no uncertainty associated with reading this data. Uncertainties associated with the experimental process were not available.

Total pressure data at the exit of the low-pressure compressor were also supplied in tabular form. The supplied exit total pressure data were determined from the TF30-P-3 characteristic and the experimentally measured mass flow rate rather than by direct measurement.

In order to calculate ΔPRS_N, it was necessary to determine the clean inlet stall pressure ratio at the speed in question. This was done using performance maps for the TF30-P-3 engine contained in references 21 and 33. It was necessary to determine fan and low-pressure compressor clean inlet stall pressure ratios from separate maps. The desired clean inlet stall pressure ratio for the low-speed spool was calculated as the product of the two individual ratios. The uncertainty associated with reading the individual pressure ratios from the performance maps was estimated to be $\pm$ 0.05. The resultant uncertainty in the clean inlet stall pressure ratio was calculated as follows:

Table A3: Inlet Total Pressure Data for the TF30-P-3 Engine

Corrected Fan Speed	Ring	0°	45°	90°	135°	180°	225°	270°	315°
6717	1(tip)	55.45	53.26	53.14	53.17	55.19	57.23	57.42	58.31
	2	55.91	53.48	53.66	53.41	55.54	57.94	58.42	59.02
	3	56.31	53.77	53.90	53.63	55.98	58.15	58.73	58.74
	4	57.27	54.42	54.19	54.13	56.63	57.90	58.39	57.74
	5(hub)	57.99	55.31	55.28	55.01	57.74	58.66	59.25	58.50
7341	1	54.57	52.06	51.92	52.08	54.32	57.17	57.08	58.27
	2	55.13	52.34	52.48	52.41	54.81	57.83	58.21	59.01
	3	55.54	52.63	52.72	52.67	55.29	58.05	58.53	58.53
	4	56.73	53.23	53.06	53.08	56.10	57.50	58.11	57.30
	5	57.56	50.74	54.21	53.99	57.35	58.53	59.07	58.21

All pressures in kPa

Table A3 (continued)

Corrected Fan Speed	Ring	0°	45°	90°	135°	180°	225°	270°	315°
7840	1(tip)	55.05	52.52	52.15	52.46	54.54	58.10	57.87	59.52
	2	55.65	52.85	52.77	52.82	55.16	58.72	59.14	60.09
	3	56.08	53.03	52.99	52.97	55.72	58.96	59.49	59.54
	4	56.10	53.49	53.28	53.32	56.55	58.26	58.94	58.05
	5(hub)	58.27	54.51	54.52	54.27	57.98	59.36	60.05	59.09
8190	1	49.54	46.99	47.94	47.99	49.45	52.67	52.15	54.14
	2	50.13	47.42	47.99	47.74	49.72	53.26	53.32	54.87
	3	50.42	47.59	47.44	47.23	49.90	53.22	53.69	54.37
	4	50.86	47.71	47.49	47.56	50.28	52.52	53.31	52.72
	5	51.90	48.29	47.49	47.82	51.61	53.53	54.33	53.32
8965	1	48.77	45.89	47.19	46.23	48.57	52.16	51.01	53.65
	2	49.47	46.14	47.35	46.17	48.77	52.67	52.34	54.21
	3	49.64	46.10	46.46	46.08	48.99	52.48	52.79	53.66
	4	50.03	46.28	45.97	46.04	49.33	51.66	52.30	51.80
	5	50.87	45.32	44.93	44.95	50.65	52.48	53.47	52.05

All pressures in kPa

Table A3 (continued)

Corrected Fan Speed	Ring	0°	45°	90°	135°	180°	225°	270°	315°
8629	1(tip)	48.62	53.40	51.54	53.39	49.50	46.71	45.98	46.32
	2	49.24	53.78	52.37	53.57	49.30	46.90	46.16	46.24
	3	49.43	52.68	52.88	53.42	49.08	46.30	46.05	45.90
	4	49.53	51.40	52.35	51.68	49.34	45.68	46.52	45.91
	5(hub)	50.52	52.41	53.35	52.68	50.53	45.37	46.24	46.14
9031	1	49.39	53.71	51.41	53.50	48.77	46.99	46.91	46.26
	2	49.79	54.17	52.32	53.71	49.26	47.31	47.48	46.37
	3	49.95	53.07	52.83	53.34	49.61	46.88	47.13	46.41
	4	50.08	51.64	52.29	51.95	49.92	46.46	46.83	46.94
	5	50.59	52.30	53.30	52.61	50.24	45.77	45.48	45.64

All pressures in kPa

Table A4: Inlet Static Pressure Data for TF30-P-3 Engine

Casing Tap Hub Tap	22.5° 22.5°	67.5	107.5° 107.5°	157.5°	205.5° 205.5°	247.5°	287.5° 287.5°	337.5°
6717 N/$\sqrt{\theta}$	51.86 51.79	51.12	51.38 51.13	51.78	52.84 53.19	53.70	BAD 53.75	53.03
7341 N/$\sqrt{\theta}$	50.21 50.13	49.33	49.70 49.39	50.10	51.48 51.81	52.41	BAD 52.50	51.57
7840 N/$\sqrt{\theta}$	49.93 49.81	48.92	49.32 48.99	49.81	51.27 51.65	52.28	BAD 52.35	51.34
8190 N/$\sqrt{\theta}$	44.26 44.29	43.39	43.59 43.46	44.19	45.46 45.65	46.53	BAD 46.18	45.60
8965 N/$\sqrt{\theta}$	41.55 41.58	40.67	40.81 40.77	41.51	42.99 43.06	43.91	BAD 43.60	43.00
8629 N/$\sqrt{\theta}$	43.68 44.06	44.56	45.15 44.79	43.89	42.11 42.09	41.44	BAD 41.46	42.29
9031 N/$\sqrt{\theta}$	43.09 43.37	43.72	44.43 44.00	43.21	41.69 41.60	40.96	BAD 41.02	41.84

All pressure in kPa

$$\omega_{\frac{P_{t3}}{P_{t2}}} = \left[\left(\frac{P_{t2.3}}{P_{t2}}\,0.05\right)^2 + \left(\frac{P_{t3}}{P_{t2.3}}\,0.05\right)^2\right]^{1/2}$$

where 2 designates engine inlet, 2.3 low-pressure compressor inlet, and 3 low-pressure compressor exit. Finally, the uncertainty in ΔPRS_N was calculated as follows:

$$\omega_{\Delta PRS_N} = \left(\frac{PR_{stall,distorted,N}}{PR^2_{stall,clean,N}}\right)\left(\omega_{\frac{P_{t3}}{P_{t2}}}\right)$$

The above equation assumes zero uncertainty in $PR_{stall,distorted,N}$ because it was provided in tabular form and experimental uncertainties were not available.

In order to calculate the GE stability index, ID, it was necessary to determine the clean inlet operating pressure ratio at the speed in question. This was also done using the performance maps of references 21 and 33. Again, the fan and low-pressure compressor pressure ratios were estimated within $\pm$ 0.05. The resultant uncertainty in the clean inlet operating pressure ratio was calculated as follows:

$$\omega_{\left(\frac{P_{t3}}{P_{t2}}\right)_{op}} = \left[\left(\left(\frac{P_{t2.3}}{P_{t2}}\right)_{op} \times 0.05\right)^2 + \left(\left(\frac{P_{t3}}{P_{t2.3}}\right)_{op} \times 0.05\right)^2\right]^{1/2}$$

Finally, uncertainty in ID was calculated as follows:

$$\omega_{ID} = \left[\left(\frac{PR_{op} - PR_{stall,distorted}}{(PR_{stall,clean} - PR_{op})^2} \times \omega_{PR_{stall,clean}} \right)^2 + \left(\frac{PR_{stall,clean} - PR_{stall,distorted}}{(PR_{stall,clean} - PR_{op})^2} \times \omega_{PR_{op}} \right)^2 \right]^{1/2}$$

Tabulated values for ΔPRS_N, ID, and their associated uncertainties are presented in Table A5. Note that these uncertainties were calculated in the same way as for the J85-GE-13 engine. It is believed that probable error is somewhat less.

Table A5: Effect of 180° Extent Circumferential Total Pressure Distortion on TF30-P-3 Performance

Corrected Fan Speed	$\%\Delta PRS_N$	$\omega^*_{\Delta PRS_N}$	ID	ω_{ID}
6717	12.73	$\pm$ 3.40	0.762	$\pm$ 0.17
7341	12.89	$\pm$ 3.12	0.778	$\pm$ 0.16
7840	10.51	$\pm$ 2.96	0.566	$\pm$ 0.12
8190	14.08	$\pm$ 2.71	0.725	$\pm$ 0.11
8965	16.77	$\pm$ 2.35	0.815	$\pm$ 0.10
8629	12.63	$\pm$ 2.60	0.665	$\pm$ 0.11
9031	15.76	$\pm$ 2.38	0.707	$\pm$ 0.09

*ω = uncertainty

Compressor Test-Rig Data

Stall data for the modified T64-GE-6B compressor test-rig are presented in Tables A6, A7, and A8. The data were obtained from Ross Gridley, a former graduate student at Virginia Polytechnic Institute and State University. The compressor is described in reference 34.

Inlet total and static pressure data were available in tabular form. The results of a statistical analysis performed by Gridley at a compressor speed of 7360 rpm for a 45° distortion revealed a standard deviation of the mean of 4.8 Pa for the undistorted sector inlet total pressures and 6.2 Pa for the distorted sector inlet total pressures. No results were available for the inlet static pressure data. Inlet total and static pressure data are reproduced in Tables A6 and A7 respectively.

Loss in stall pressure ratio was calculated assuming that the plenum static pressure was equal to the exit total pressure. A standard deviation of the mean for the plenum static pressure of 76 Pa was determined from the statistical analysis. The resultant uncertainty in ΔPRS_N was calculated as follows:

$$\omega_{\Delta PRS_N} = \left[\left(\frac{1}{PR_{clean,stall,N}} \omega_{PR_{distorted,stall,N}} \right)^2 + \left(\frac{PR_{distorted,stall,N}}{PR^2_{clean,stall,N}} \omega_{PR_{clean,stall,N}} \right)^2 \right]^{1/2}$$

Table A6: Inlet Total Pressure Data for the Modified T64-GE-6B Compressor Test-Rig

	Ring	0°	60°	120°	180°	240°	300°
	1(tip)	94.76	94.25	94.81	94.85	94.57	94.73
7360 rpm	2	94.74	94.10	94.81	94.74	94.74	94.73
45° extent	3	94.77	94.12	94.87	94.81	94.77	94.79
	4	94.77	94.10	94.85	94.78	94.74	94.79
	5(hub)	94.84	94.15	94.81	94.80	94.72	94.90
	1	94.43	93.59	93.73	94.36	94.32	94.41
7360 rpm	2	94.31	93.67	93.81	94.34	94.24	94.22
90° extent	3	94.43	93.76	93.72	94.36	94.40	94.23
	4	94.34	93.64	93.67	94.22	94.47	94.36
	5	94.29	93.74	93.61	94.26	94.32	94.38
	1	94.21	93.43	93.29	93.41	94.18	94.26
7360 rpm	2	94.19	93.47	93.37	93.34	94.26	94.23
180° extent	3	94.08	93.25	93.44	93.40	94.11	94.25
	4	94.16	93.37	93.24	93.36	94.12	94.25
	5	94.17	93.31	93.30	93.35	94.24	94.27

All pressures in kPa

Table A6 (continued)

	Ring	0°	60°	120°	180°	240°	300°
	1(tip)	94.18	93.47	94.15	94.21	94.34	94.30
8160 rpm	2	94.29	93.39	94.05	94.18	94.18	94.38
45° extent	3	94.18	93.46	94.23	94.09	94.26	94.26
	4	94.23	93.36	94.14	94.11	94.23	94.09
	5(hub)	94.26	93.54	94.27	94.08	94.18	94.07
	1	94.13	93.43	93.25	94.23	94.31	94.13
8160 rpm	2	94.11	93.32	93.27	94.14	94.19	94.37
90° extent	3	94.15	93.27	93.23	94.03	94.25	94.21
	4	94.17	93.19	93.37	94.15	94.24	94.24
	5	94.14	93.34	93.36	94.10	93.86	94.21
	1	94.28	93.32	93.37	94.16	94.16	94.37
8160 rpm	2	94.47	93.29	93.36	94.24	94.26	94.45
135° extent	3	94.19	93.23	93.39	94.28	94.39	94.30
	4	94.29	93.36	93.36	94.26	94.39	94.30
	5	94.33	93.34	93.25	94.16	94.27	94.38
	1	94.20	93.12	93.02	93.16	94.27	94.24
8160 rpm	2	94.21	92.99	93.08	93.07	94.03	94.02
180° extent	3	94.08	93.08	93.03	93.12	94.33	94.24
	4	94.12	93.05	92.96	93.00	94.05	94.00
	5	94.14	92.98	93.00	93.09	93.98	94.05

All pressures in kPa

Table A7: Inlet Static Pressure Data for the Modified T64-GE-6B Compressor Test-Rig

SPEED	EXTENT	0°	60°	120°	180°	240°	300°
7360	45°	94.14	93.91	94.02	94.06	94.11	94.24
7360	90°	93.77	93.44	93.29	93.69	93.84	93.85
7360	180°	93.32	93.00	92.99	93.08	93.36	93.54
8160	45°	93.37	93.07	93.31	93.41	93.67	93.60
8160	90°	93.36	93.02	93.02	93.45	93.50	93.67
8160	135°	92.85	92.52	92.35	92.62	92.94	93.08
8160	180°	93.15	92.69	92.72	92.60	93.13	93.27

All pressures in kPa

Table A8: Loss in Stall Pressure Ratio Due to Circumferential Total Pressure Distortion for the Compressor Test-Rig

SPEED (rpm)	EXTENT (degrees)	$\%\Delta PRS_N$	$\omega^* \Delta PRS_N$
7360	45	0.23	$\pm$ 0.21
	90	0.48	$\pm$ 0.21
	180	0.19	$\pm$ 0.21
8160	45	0.72	$\pm$ 0.21
	90	0.64	$\pm$ 0.21
	135	0.58	$\pm$ 0.21
	180	0.61	$\pm$ 0.21

*ω = uncertainty

The uncertainties in pressure ratio were calculated from the following equation:

$$\omega_{PR} = \left[\left(\frac{152}{\bar{P}_1} \right)^2 + \left(\frac{P_2}{\bar{P}_2^2} \times 11 \right)^2 \right]^{1/2}$$

where 1 indicates compressor inlet and 2 compressor exit. The above equation assumes the uncertainties in exit and inlet pressures are equal to twice the standard deviations of the mean. Loss in stall pressure ratio data and the associated uncertainties are presented in Table A8. Because the uncertainty bands are based on measurement uncertainties equal to twice the standard deviation of the mean, there is a 95.4% probability that the actual value is within the band specified.

APPENDIX B

PROCEDURES FOR CALCULATING THE PEARSON PRODUCT-MOMENT CORRELATION COEFFICIENT AND THE R-SQUARE VALUE

Mathematical expressions for the Pearson product-moment correlation coefficient and the R-SQUARE value are presented. The R-SQUARE value is proven to be equal to the square of the correlation coefficient for regression models including only one independent variable. Equations and definitions were obtained from references 38 and 39.

Assume a population such that each element in the population consists of an ordered pair (X,Y), where X represents the independent variable and Y the dependent variable. Let

y = a deviation of Y from the mean of the Y values = $Y - \overline{Y}$,

x = a deviation of X from the mean of the X values = $X - \overline{X}$,

b = the regression coefficient of Y on X.

The correlation coefficient is defined as the ratio between the covariance and the geometric mean of the variance of X and the variance of Y. The geometric mean of two numbers is the square root of their product. Thus, the correlation coefficient, r, is calculated as follows:

$$r = \frac{\frac{\Sigma(xy)}{n-1}}{\left[\left(\frac{\Sigma x^2}{n-1}\right)\left(\frac{\Sigma y^2}{n-1}\right)\right]^{\frac{1}{2}}} = \frac{\Sigma(xy)}{[\Sigma x^2\ \Sigma y^2]^{\frac{1}{2}}} \qquad \text{(A-1)}$$

Expanding the terms in the numerator and denominator yields:

$$\Sigma(xy) = \Sigma(X - \bar{X})(Y - \bar{Y}) = \Sigma(XY) - \frac{\Sigma X \Sigma Y}{n}$$

$$\Sigma x^2 = \Sigma(X - \bar{X})^2 = \Sigma X^2 - \frac{(\Sigma X)^2}{n}$$

$$\Sigma y^2 = \Sigma(Y - \bar{Y})^2 = \Sigma Y^2 - \frac{(\Sigma Y)^2}{n} .$$

Substituting into equation A-1 gives

$$r = \frac{\Sigma XY - (\Sigma X)(\Sigma Y)/n}{[(\Sigma X^2 - (\Sigma X)^2/n)(\Sigma Y^2 - (\Sigma Y)^2/n)]^{\frac{1}{2}}} \qquad \text{(A-2)}$$

Equation A-2 is the basic computational formula for the Pearson product-moment correlation coefficient. It provides a measure of the degree of accuracy with which Y values can be predicted from X values. It ranges in value from -1 to 1 with -1 indicating a perfect inverse relationship and 1 a perfect proportional relationship. A Pearson product-moment correlation coefficient of zero indicates that there is no linear relationship between X and Y.

R-SQUARE is defined as the ratio between the regression sum of squares and the total sum of squares where sum of squares means the sum of squared errors or deviations. Thus,

$$R^2 = \frac{SS_{reg}}{SS_{tot}}. \qquad \text{(A-3)}$$

The regression sum of squares is determined as follows for a multiple regression model in which there are k independent variables:

$$SS_{reg} = b_1 \Sigma(x_1 y) + b_2 \Sigma(x_2 y) + \ldots + b_k \Sigma(x_k y).$$

The total sum of squares is

$$SS_{tot} = \Sigma y^2 = \Sigma(Y - \bar{Y})^2.$$

Thus,

$$R^2 = \frac{b_1 \Sigma(x_1 y) + b_2 \Sigma(x_2 y) + \ldots + b_k \Sigma(x_k y)}{\Sigma y^2}. \qquad \text{(A-4)}$$

The above R^2 is a measure of how much variation in the dependent variable can be accounted for by the model. It can range in value from 0 to 1: the larger the value of R^2, the better the model's fit.

When only one independent variable is present, R^2 is reduced to the following:

$$R^2 = \frac{b\Sigma(xy)}{\Sigma y^2} \qquad \text{(A-5)}$$

When a least squares criteria is used to develop the regression model between two variables, the regression coefficient, b, is calculated as follows:

$$b = \frac{\Sigma(xy)}{\Sigma x^2}.$$

Substituting this expression into equation A-5 yields

$$R^2 = \frac{(\Sigma xy)^2}{\Sigma x^2 \Sigma y^2} \qquad \text{(A-6)}$$

Comparing this to equation A-1 demonstrates that for a regression model including only one independent variable, the R-SQUARE value is exactly equal to the square of the correlation coefficient.

APPENDIX C

DISTORTION INDEX PLOTS

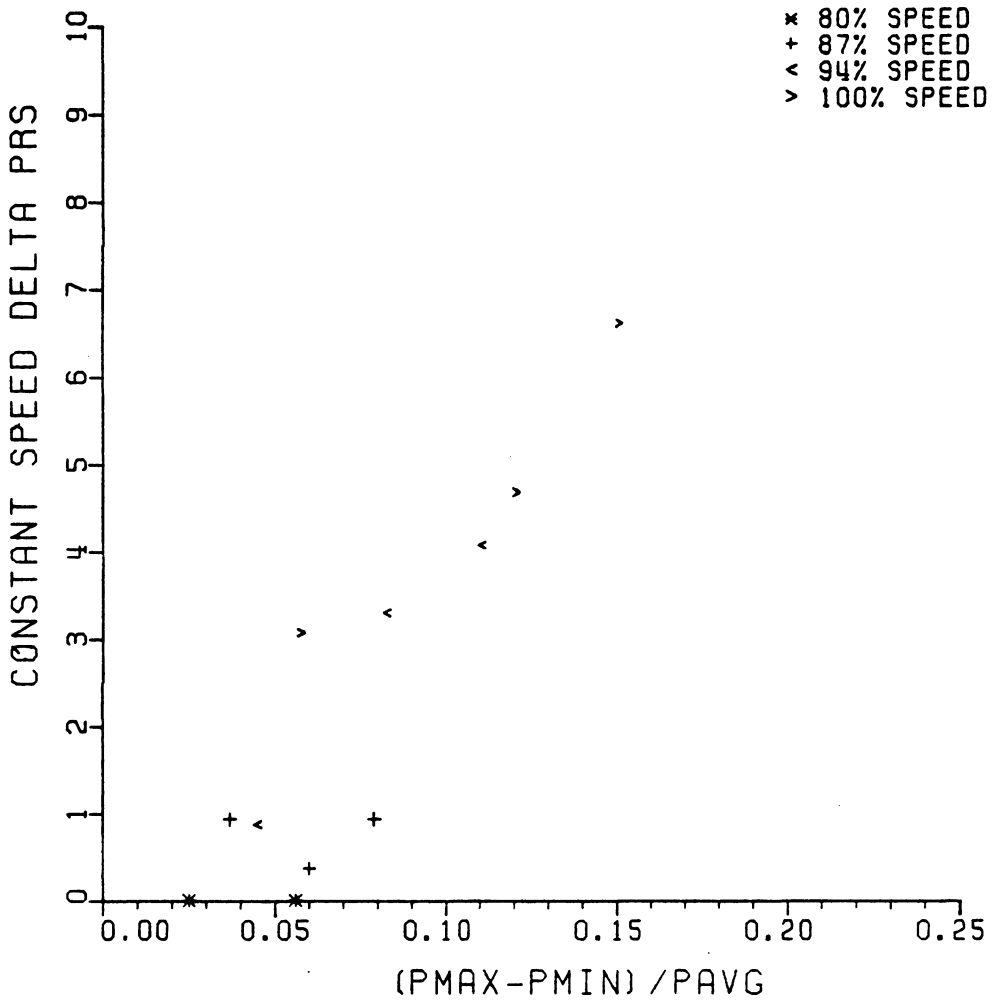

FIGURE C1: CIRCUMFERENTIAL DISTORTION-INDUCED STALL DATA FOR THE J85-GE-13 ENGINE, (PMAX-PMIN)/PAVG INDEX, DELTA PRSN

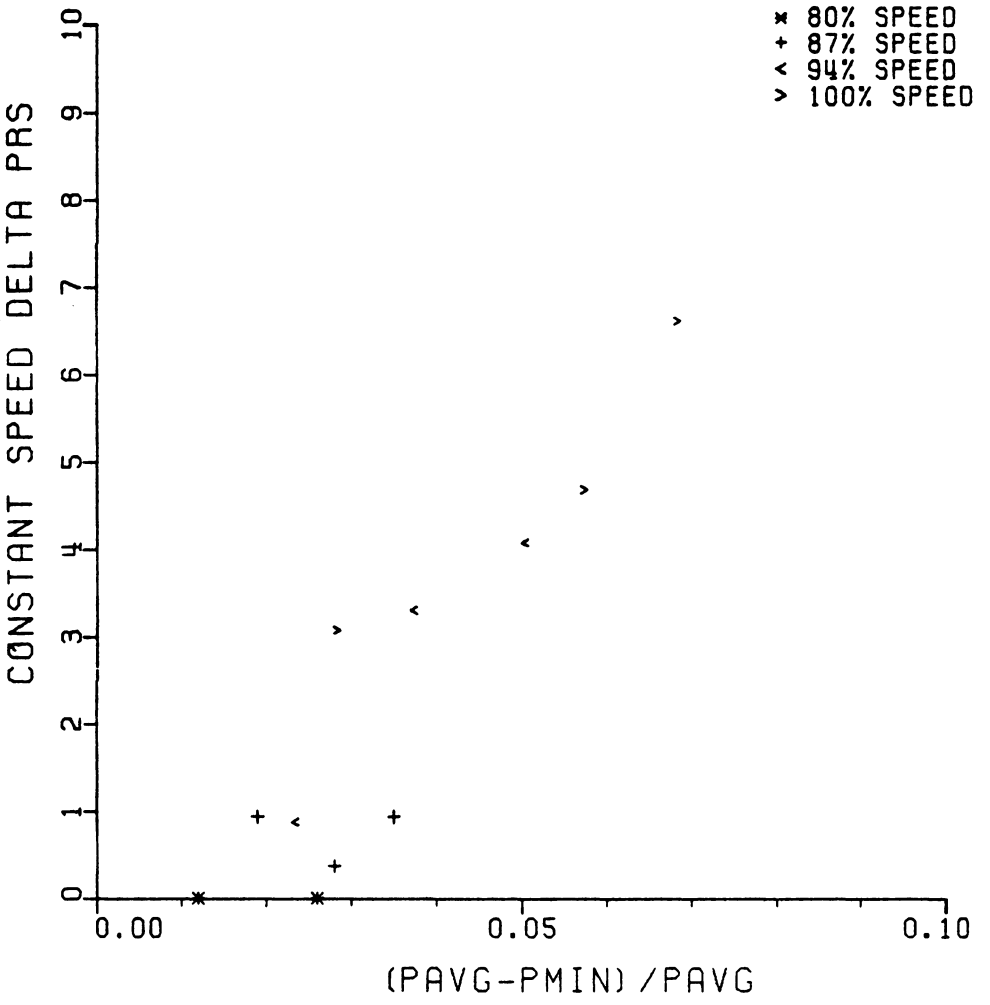

FIGURE C2: CIRCUMFERENTIAL DISTORTION-INDUCED STALL DATA FOR THE J85-GE-13 ENGINE, (PAVG-PMIN)/PAVG INDEX, DELTA PRSN

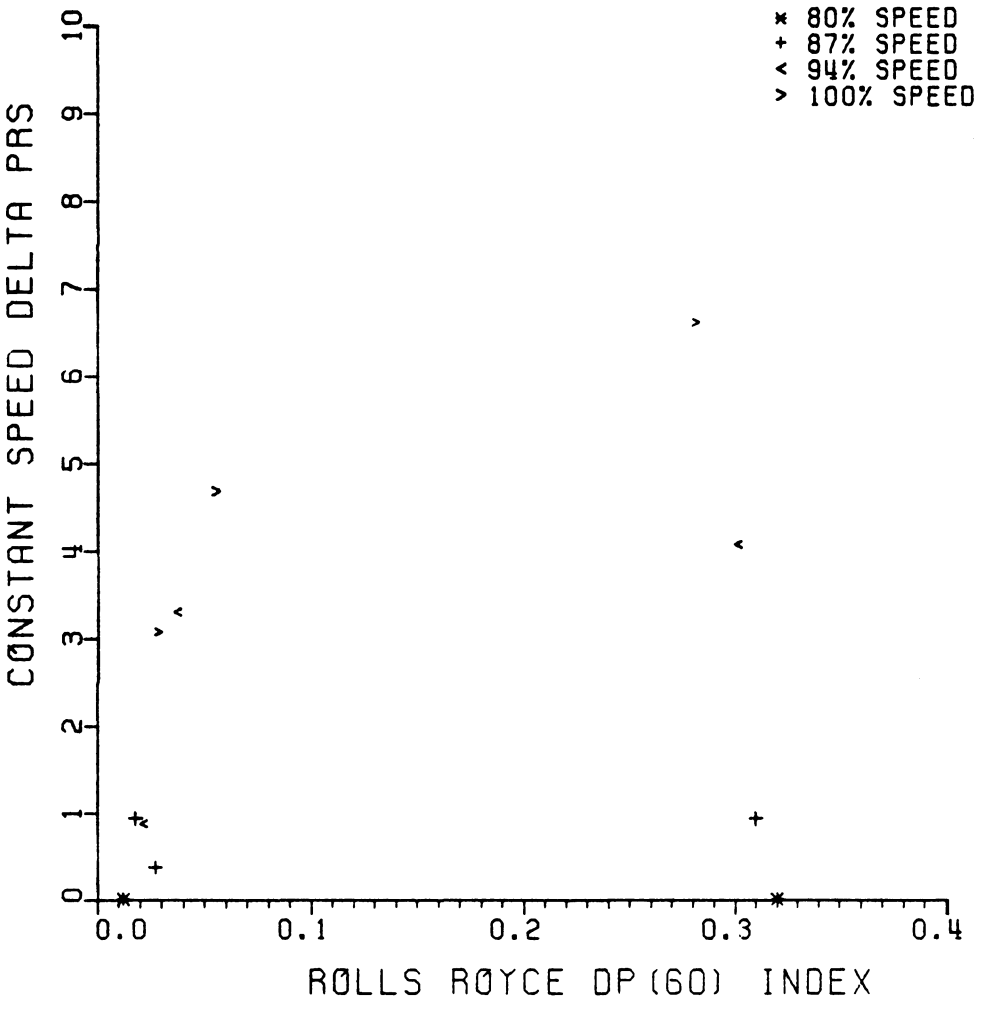

FIGURE C3: CIRCUMFERENTIAL DISTORTION-INDUCED STALL DATA FOR THE J85-GE-13 ENGINE, ROLLS ROYCE DP(60) INDEX, DELTA PRSN

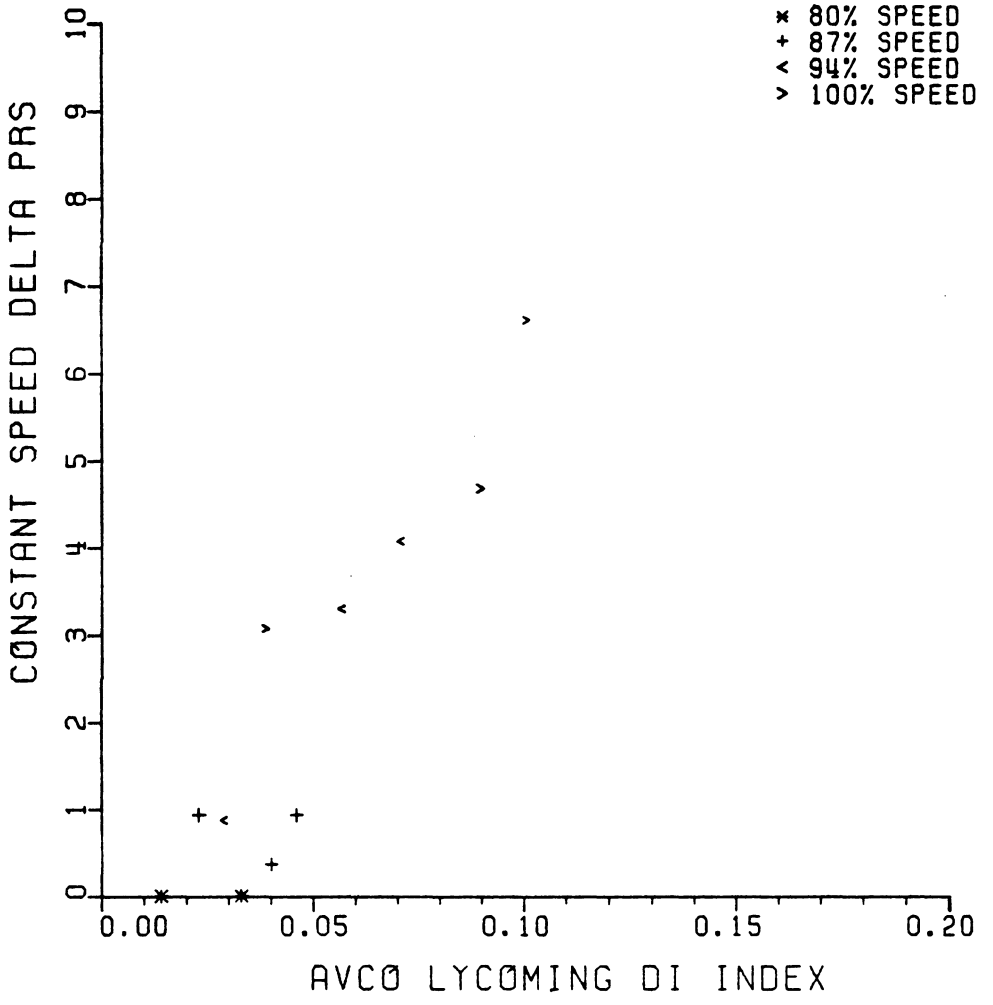

FIGURE C4: CIRCUMFERENTIAL DISTORTION-INDUCED STALL DATA FOR THE J85-GE-13 ENGINE, AVCO LYCOMING DI INDEX, DELTA PRSN

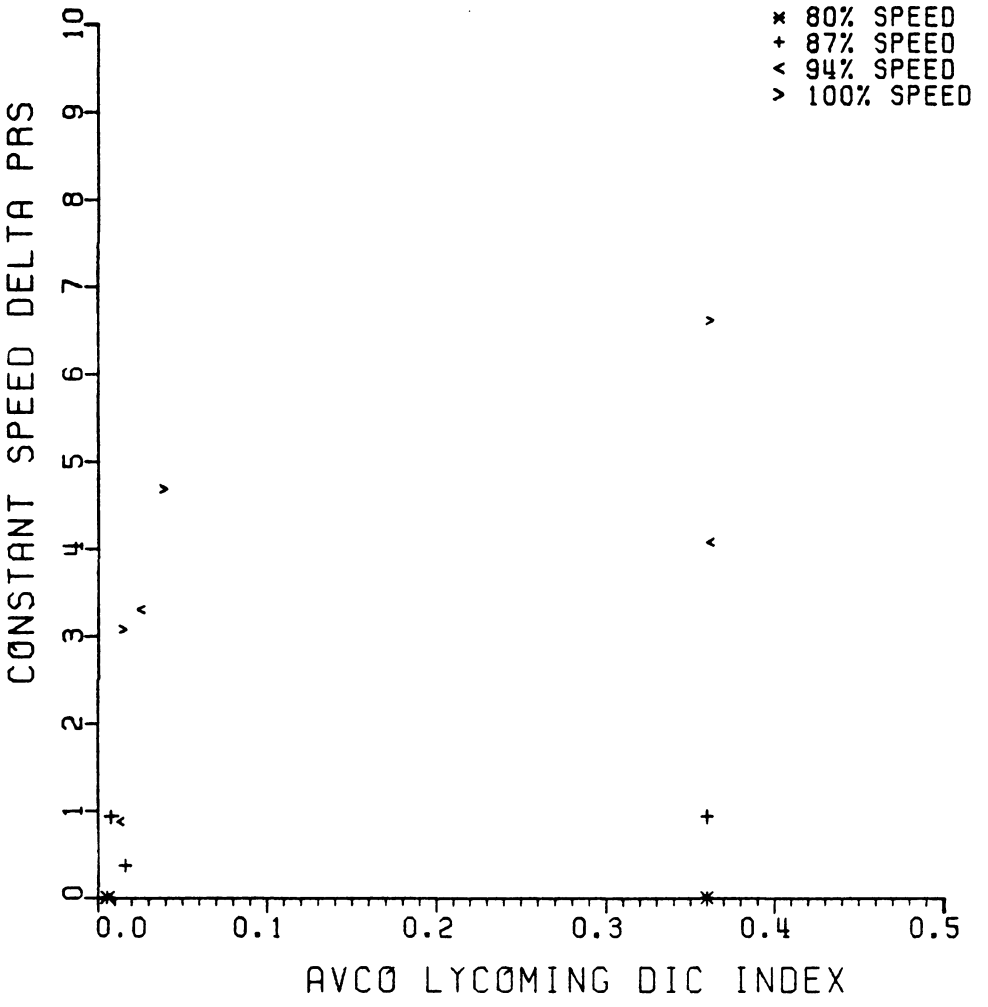

FIGURE C5: CIRCUMFERENTIAL DISTORTION-INDUCED STALL DATA FOR THE J85-GE-13 ENGINE, AVCO LYCOMING DIC INDEX, DELTA PRSN

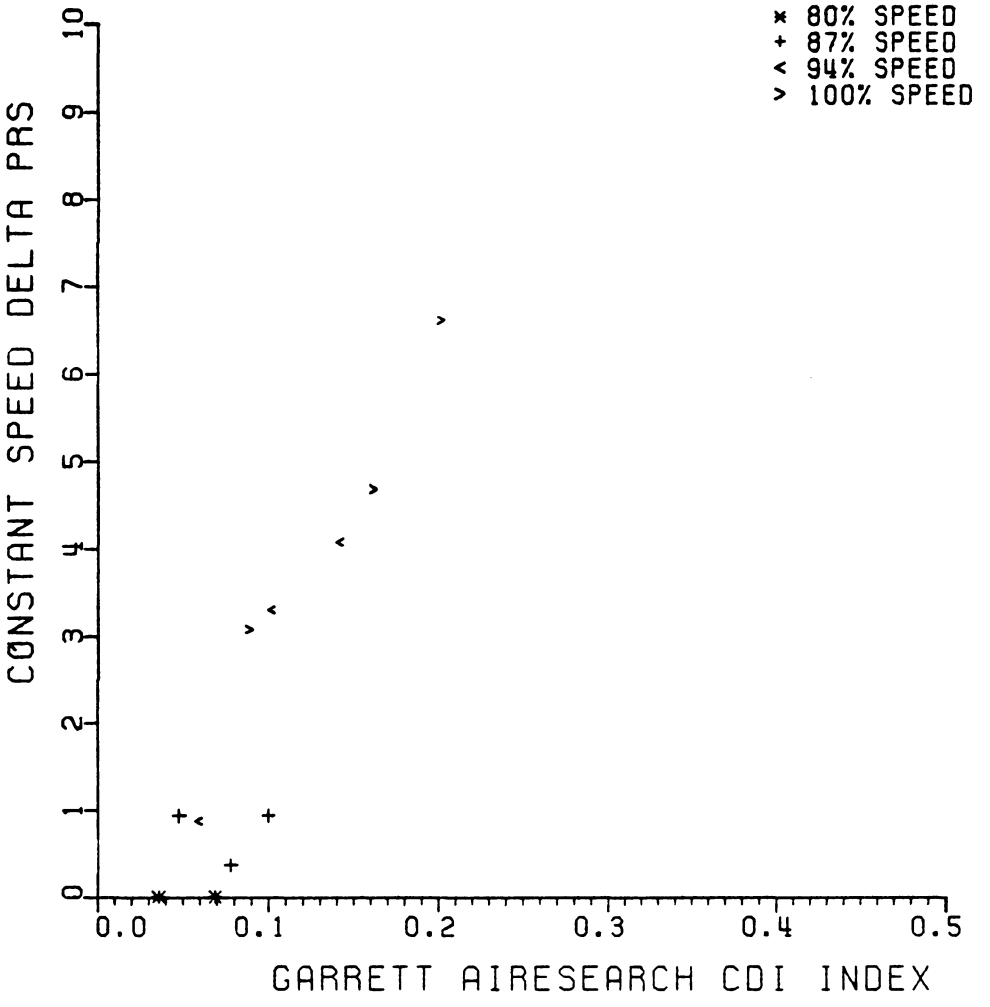

FIGURE C6: CIRCUMFERENTIAL DISTORTION-INDUCED STALL DATA FOR THE J85-GE-13 ENGINE, GARRETT AIRESEARCH CDI INDEX, DELTA PRSN

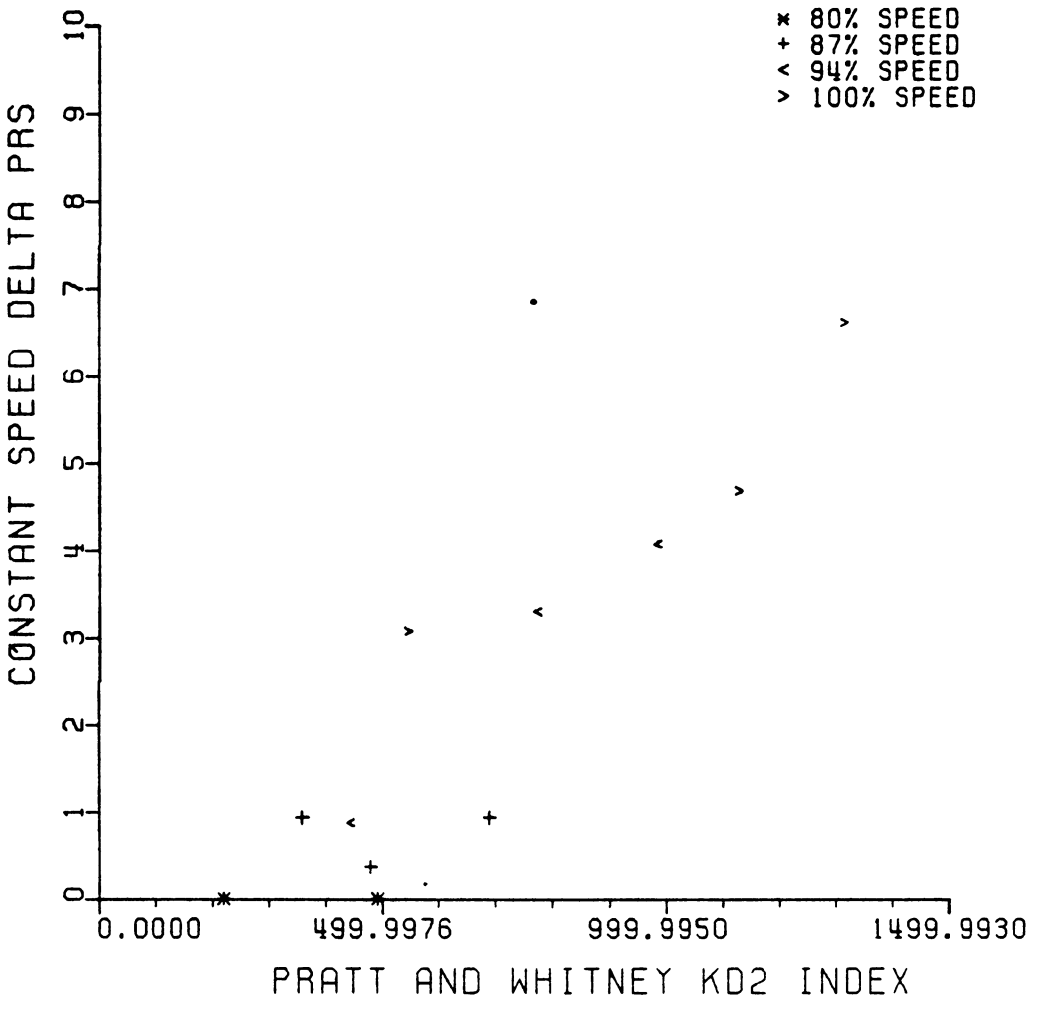

FIGURE C7: CIRCUMFERENTIAL DISTORTION-INDUCED STALL DATA FOR THE J85-GE-13 ENGINE, PRATT AND WHITNEY KD2 INDEX, DELTA PRSN

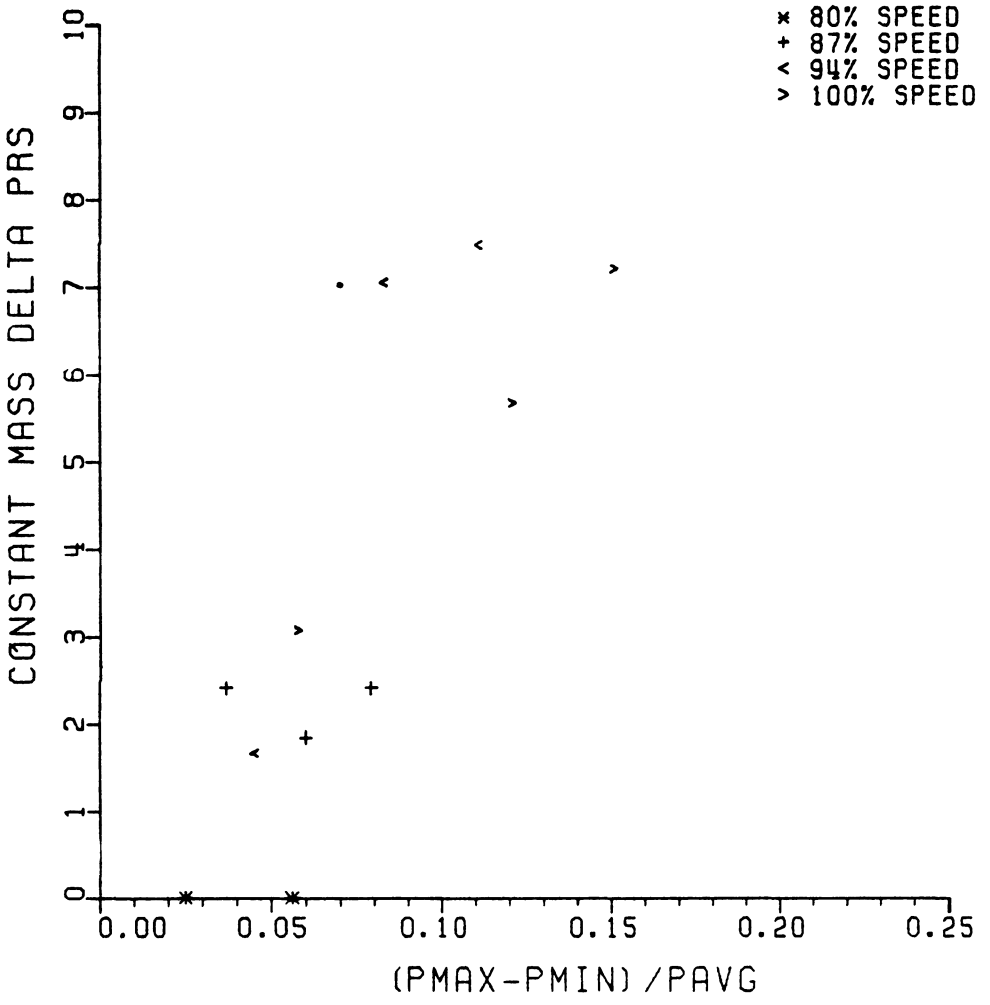

FIGURE C8: CIRCUMFERENTIAL DISTORTION-INDUCED STALL DATA FOR THE J85-GE-13 ENGINE, (PMAX-PMIN)/PAVG INDEX, DELTA PRSM

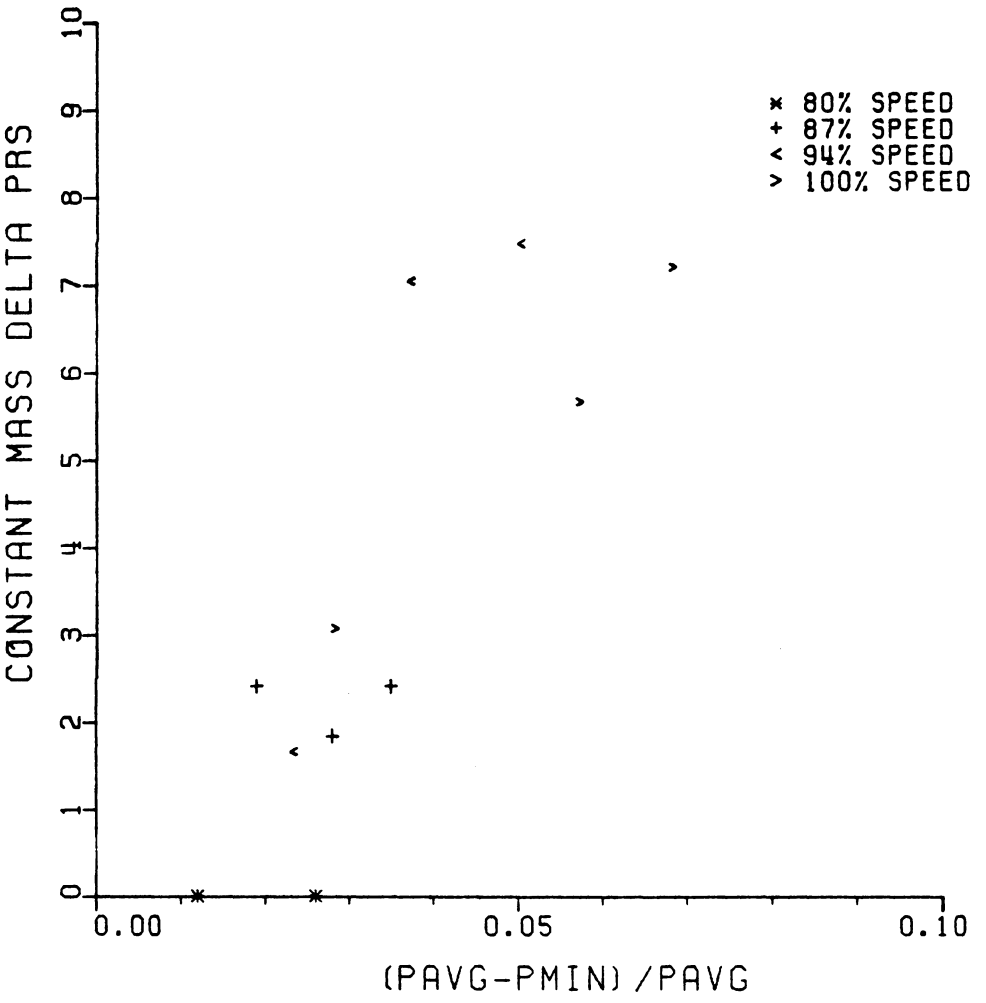

FIGURE C9: CIRCUMFERENTIAL DISTORTION-INDUCED STALL DATA FOR THE J85-GE-13 ENGINE, (PAVG-PMIN)/PAVG INDEX, DELTA PRSN

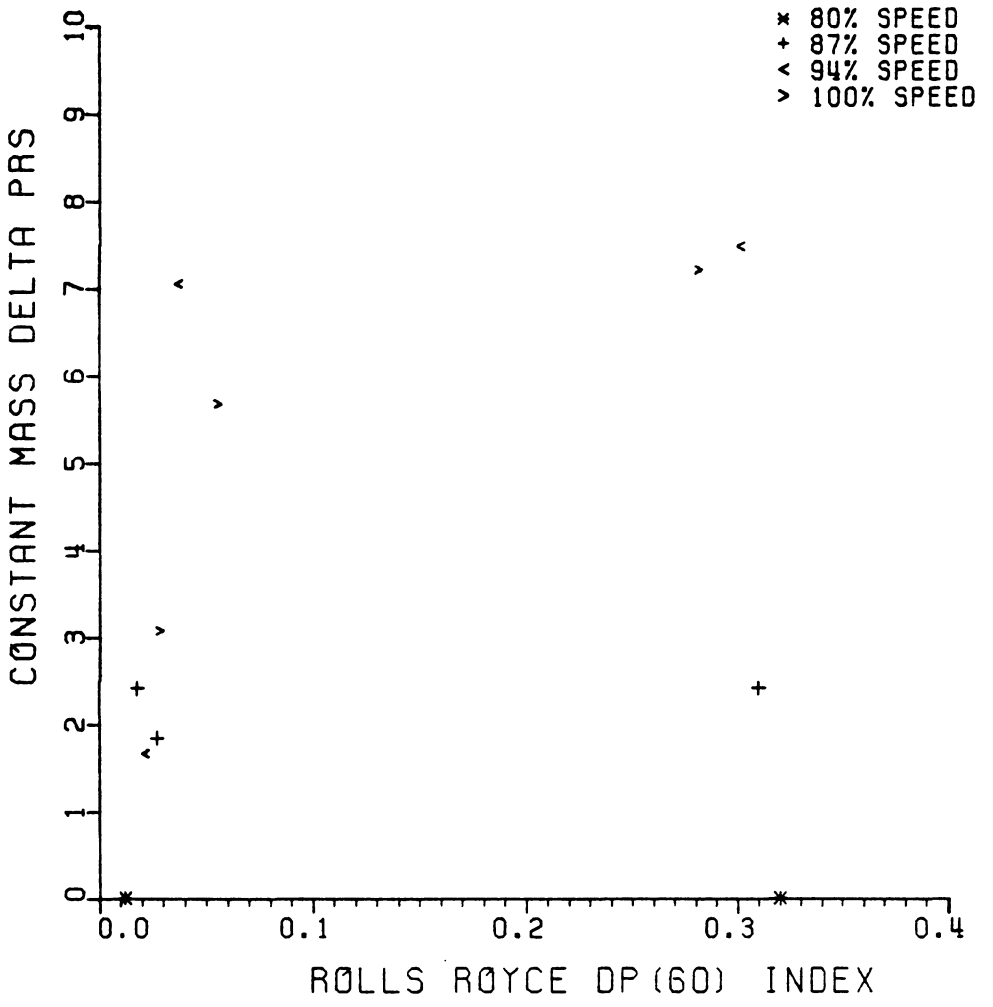

FIGURE C10: CIRCUMFERENTIAL DISTORTION-INDUCED STALL DATA FOR THE J85-GE-13 ENGINE, ROLLS ROYCE DP(60) INDEX, DELTA PRSM

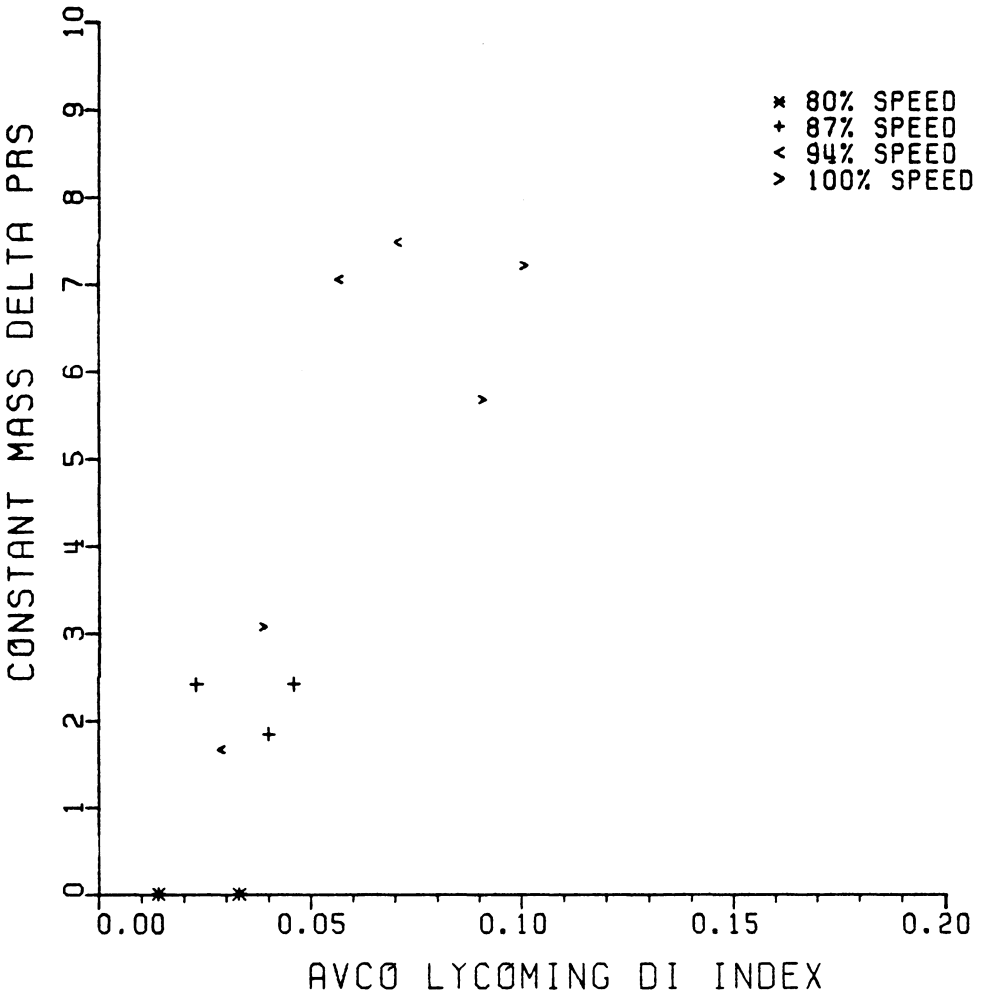

FIGURE C11: CIRCUMFERENTIAL DISTORTION-INDUCED STALL DATA FOR THE J85-GE-13 ENGINE, AVCO LYCOMING DI INDEX, DELTA PRSM

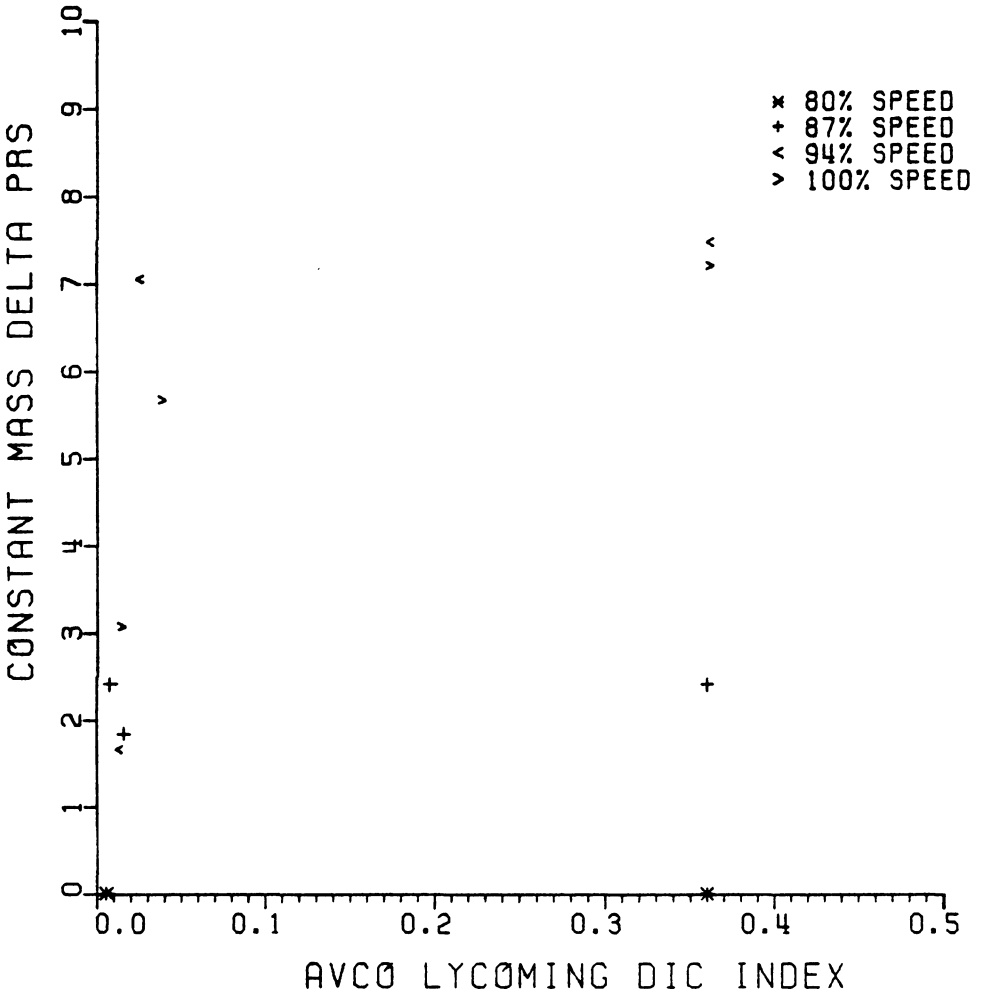

FIGURE C12: CIRCUMFERENTIAL DISTORTION-INDUCED STALL DATA FOR THE J85-GE-13 ENGINE, AVCO LYCOMING DIC INDEX, DELTA PRSM

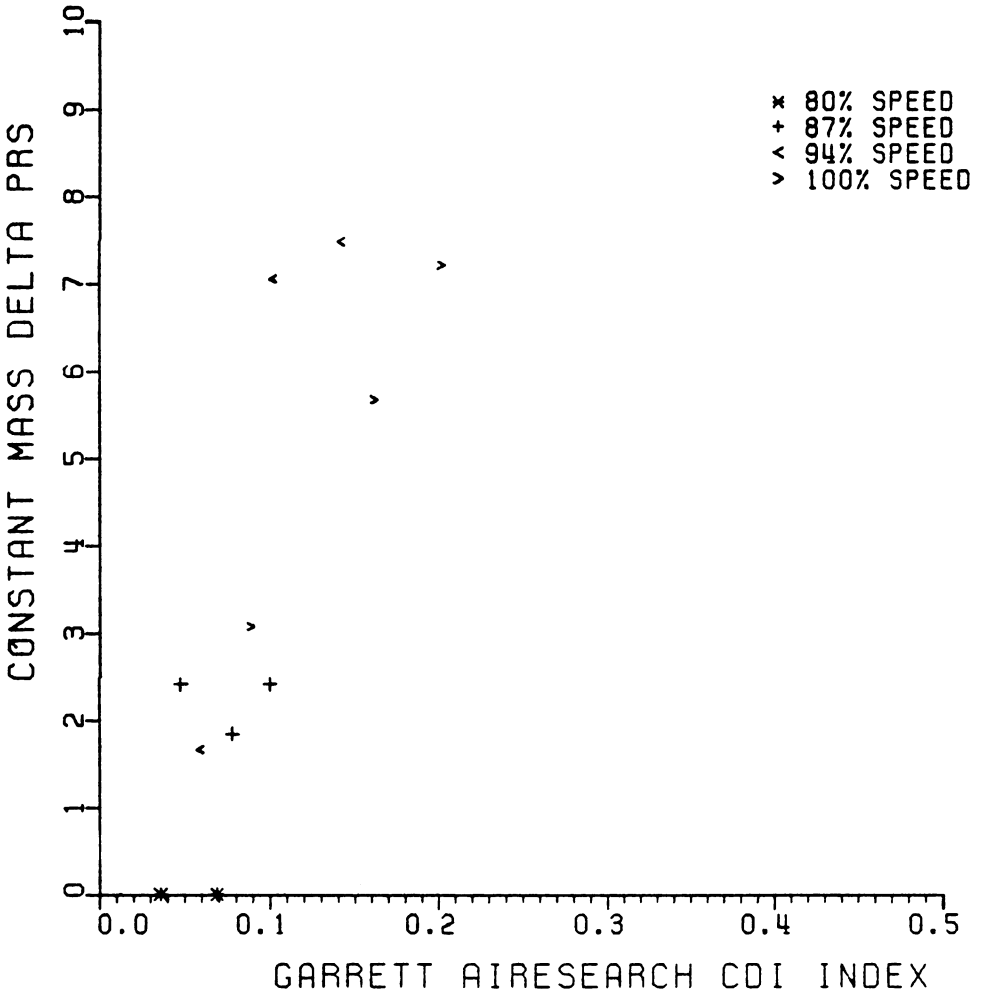

FIGURE C13: CIRCUMFERENTIAL DISTORTION-INDUCED STALL DATA FOR THE J85-GE-13 ENGINE, GARRETT AIRESEARCH CDI INDEX, DELTA PRSM

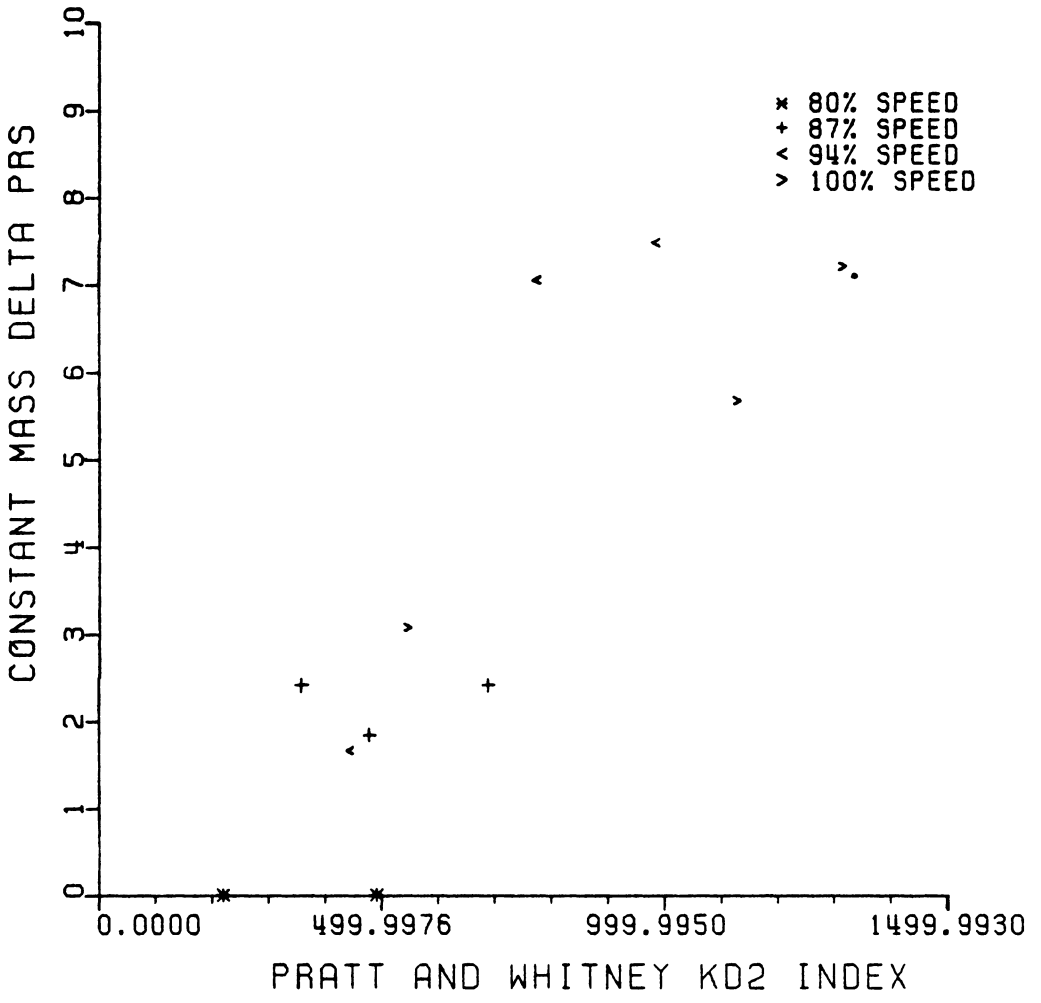

FIGURE C14: CIRCUMFERENTIAL DISTORTION-INDUCED STALL DATA FOR THE J85-GE-13 ENGINE, PRATT AND WHITNEY KD2 INDEX, DELTA PRSM

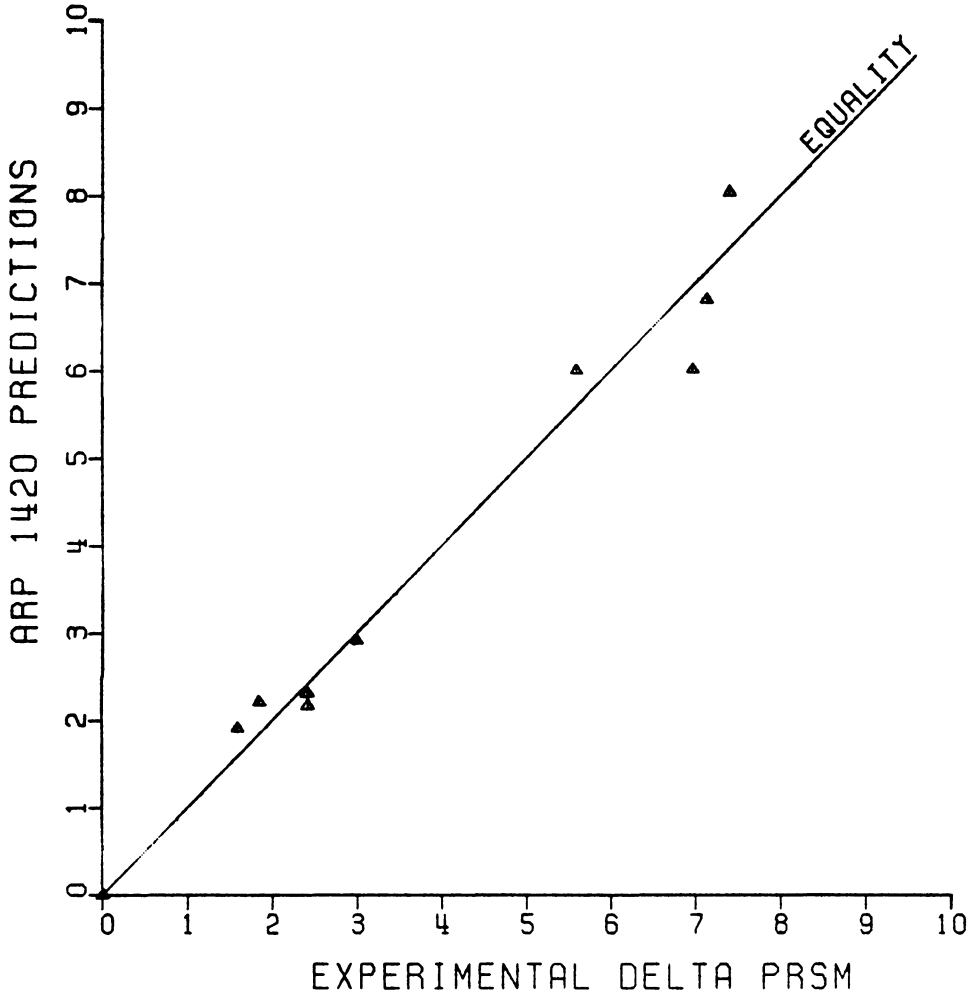

FIGURE C15: CIRCUMFERENTIAL DISTORTION-INDUCED STALL DATA FOR THE J85-GE-13 ENGINE AND ARP 1420 PREDICTIONS (DELTA PRSM)

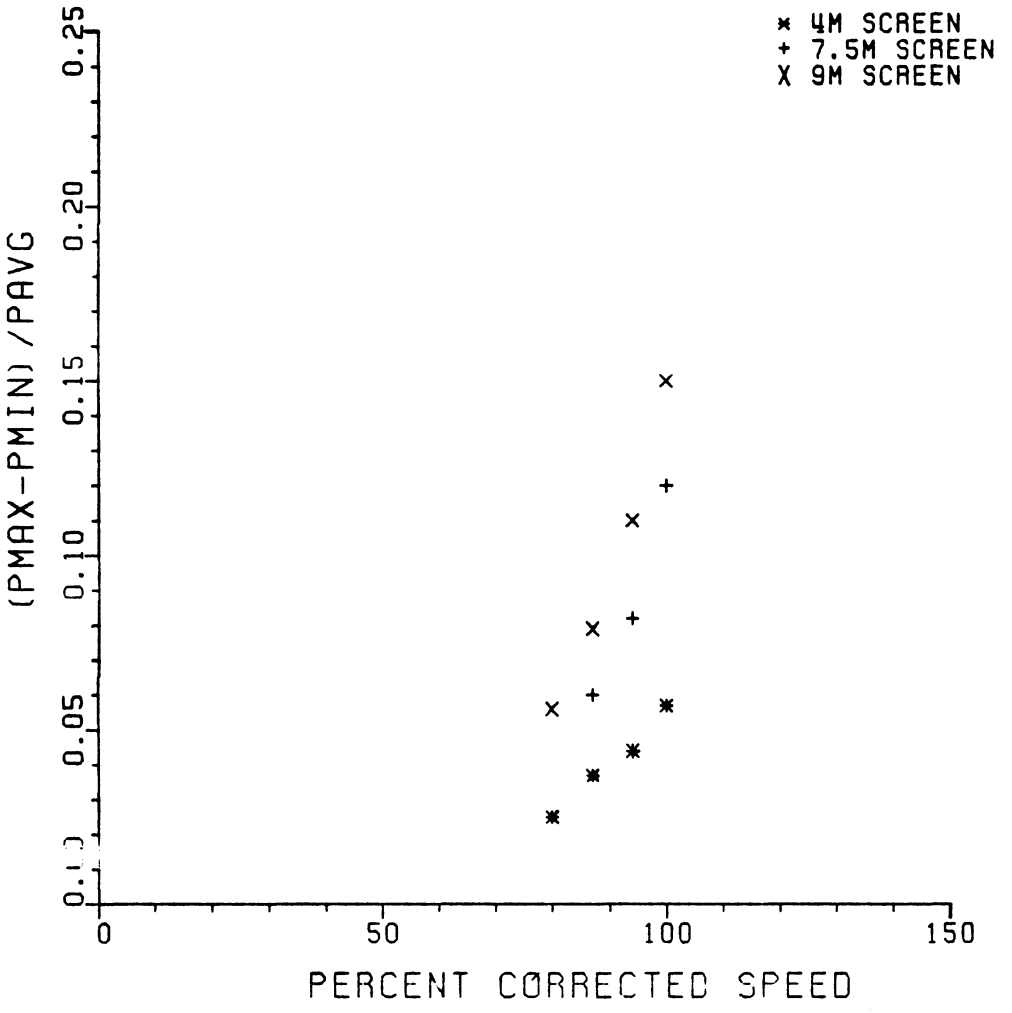

FIGURE C16: CIRCUMFERENTIAL DISTORTION-INDUCED STALL DATA FOR THE J85-GE-13 ENGINE, (PMAX-PMIN)/PAVG INDEX VS SPEED

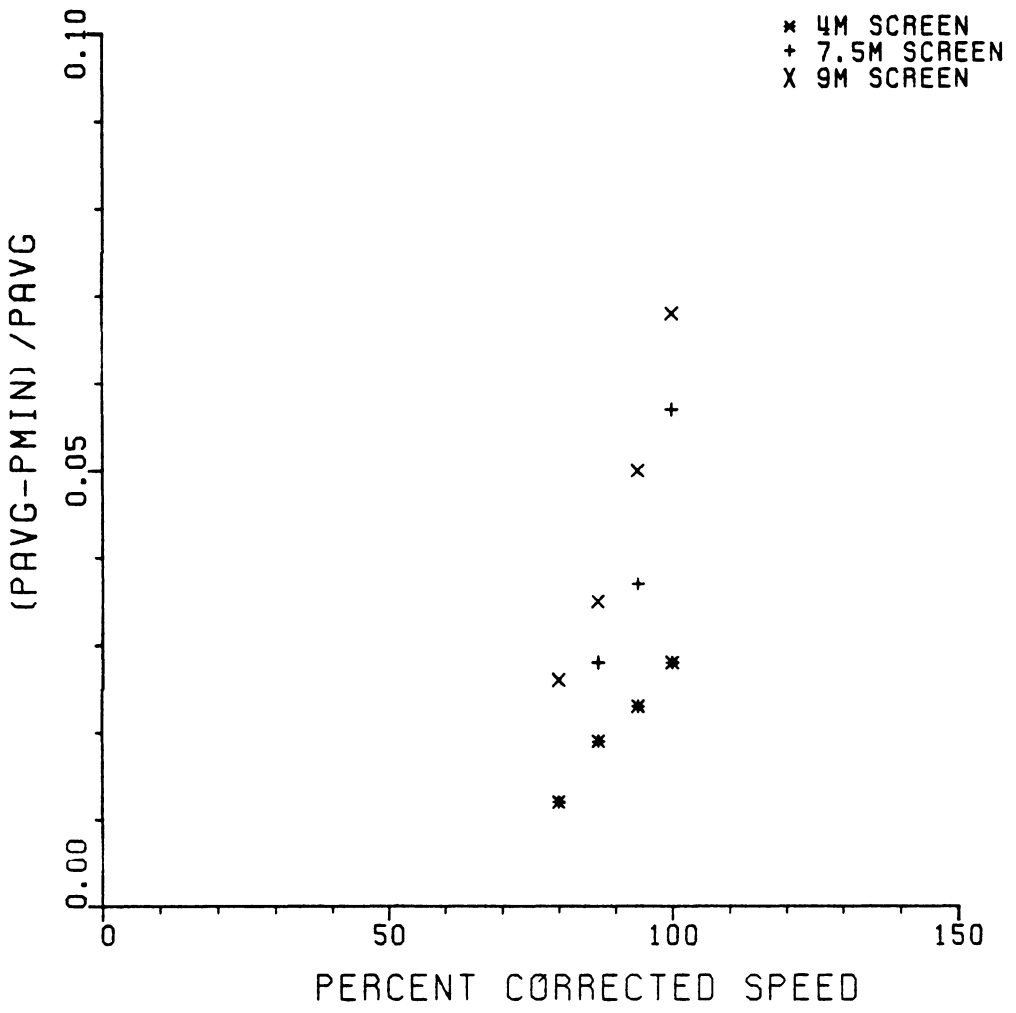

FIGURE C17: CIRCUMFERENTIAL DISTORTION-INDUCED STALL DATA FOR THE J85-GE-13 ENGINE, (PAVG-PMIN)/PAVG INDEX VS SPEED

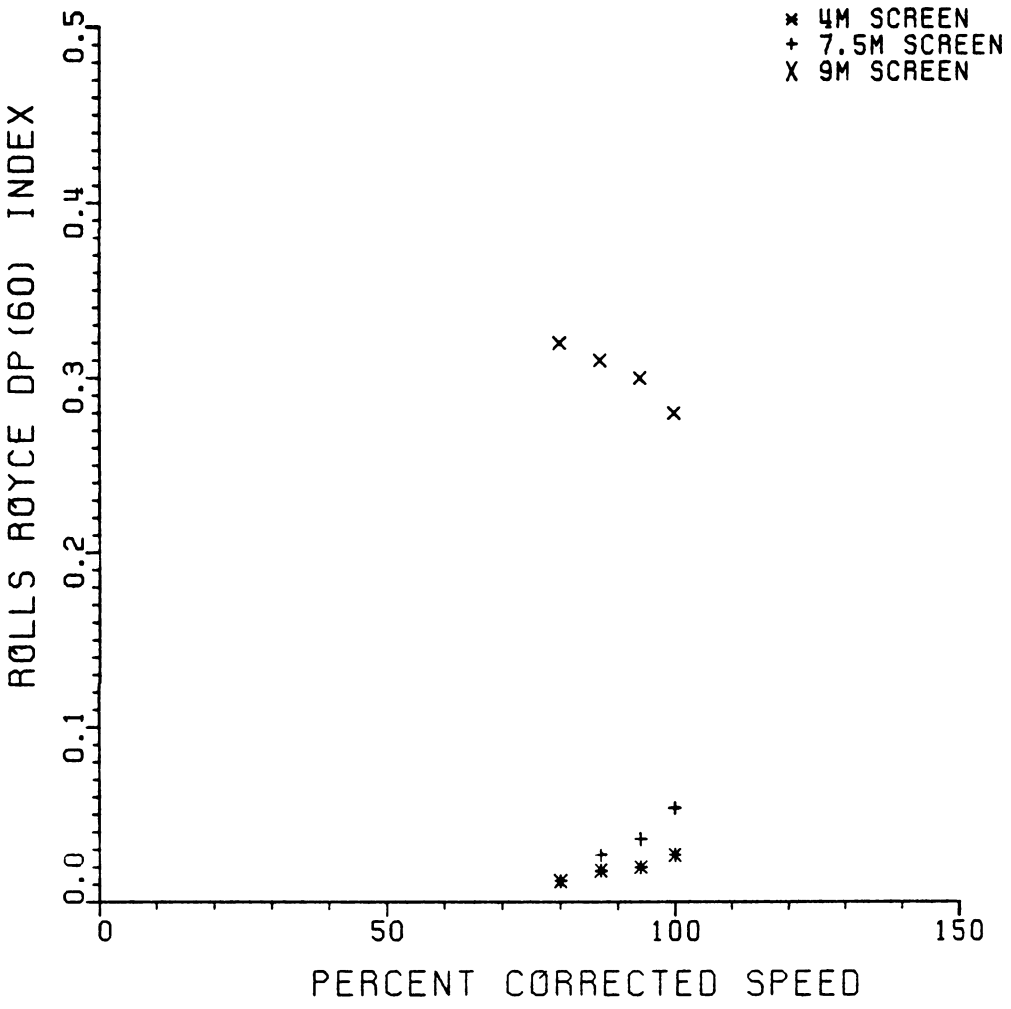

FIGURE C18: CIRCUMFERENTIAL DISTORTION-INDUCED STALL DATA FOR THE J85-GE-13 ENGINE, ROLLS ROYCE DP(60) INDEX VS SPEED

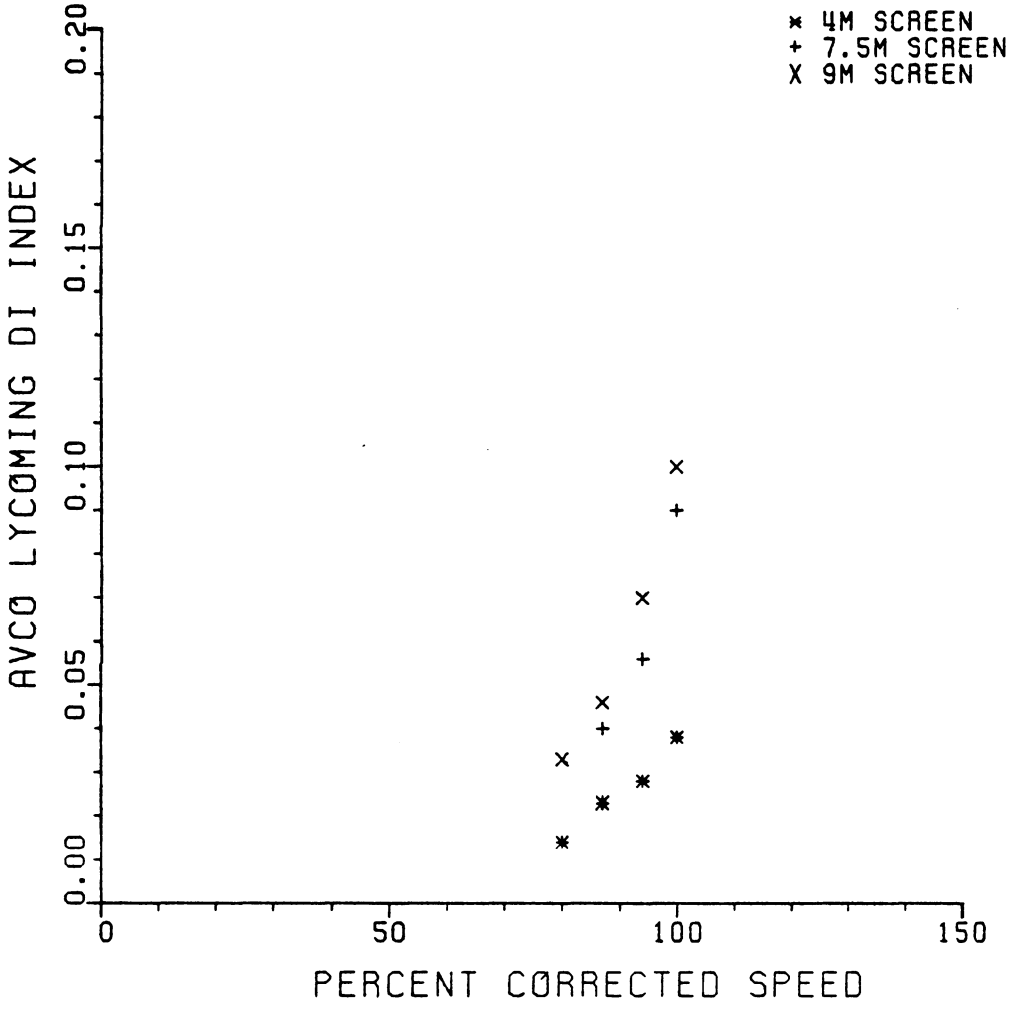

FIGURE C19: CIRCUMFERENTIAL DISTORTION-INDUCED STALL DATA FOR THE J85-GE-13 ENGINE, AVCO LYCOMING DI INDEX VS SPEED

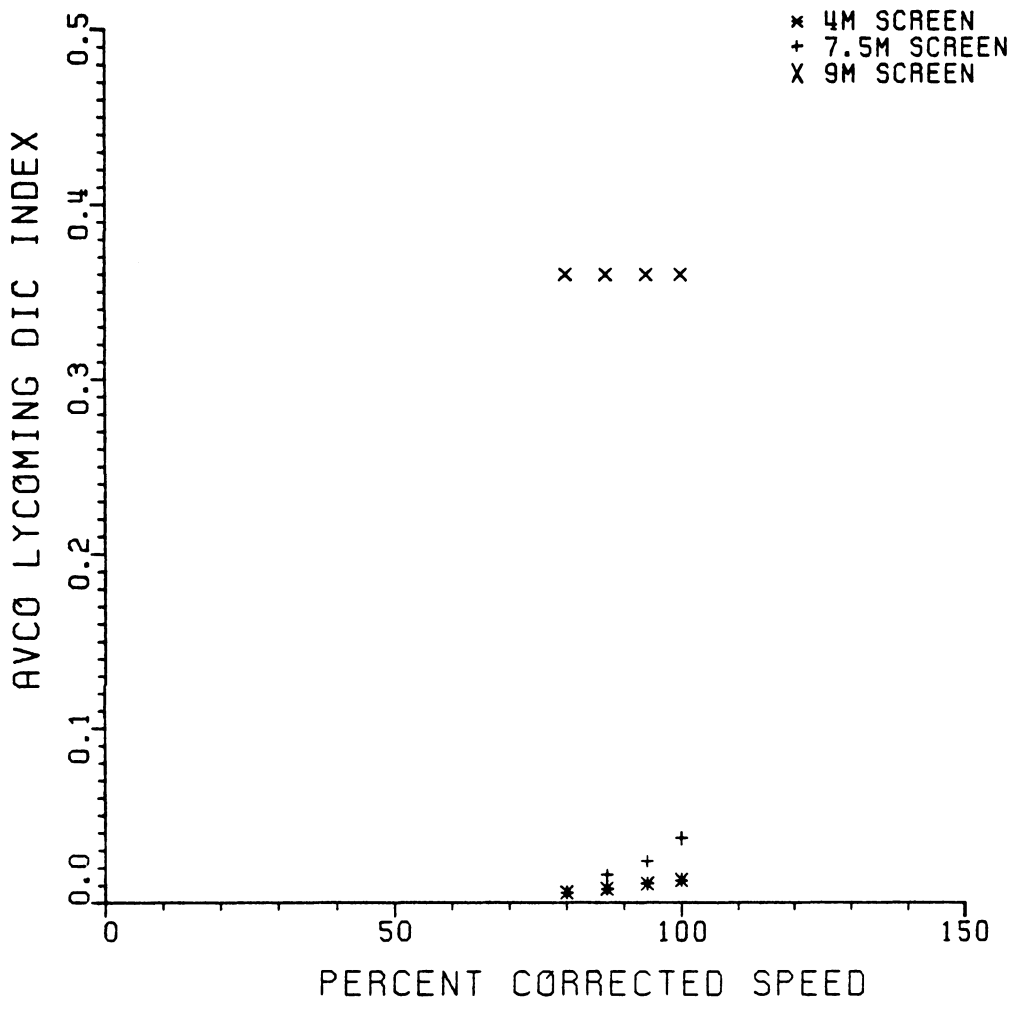

FIGURE C20: CIRCUMFERENTIAL DISTORTION-INDUCED STALL DATA FOR THE J85-GE-13 ENGINE, AVCO LYCOMING DIC INDEX VS SPEED

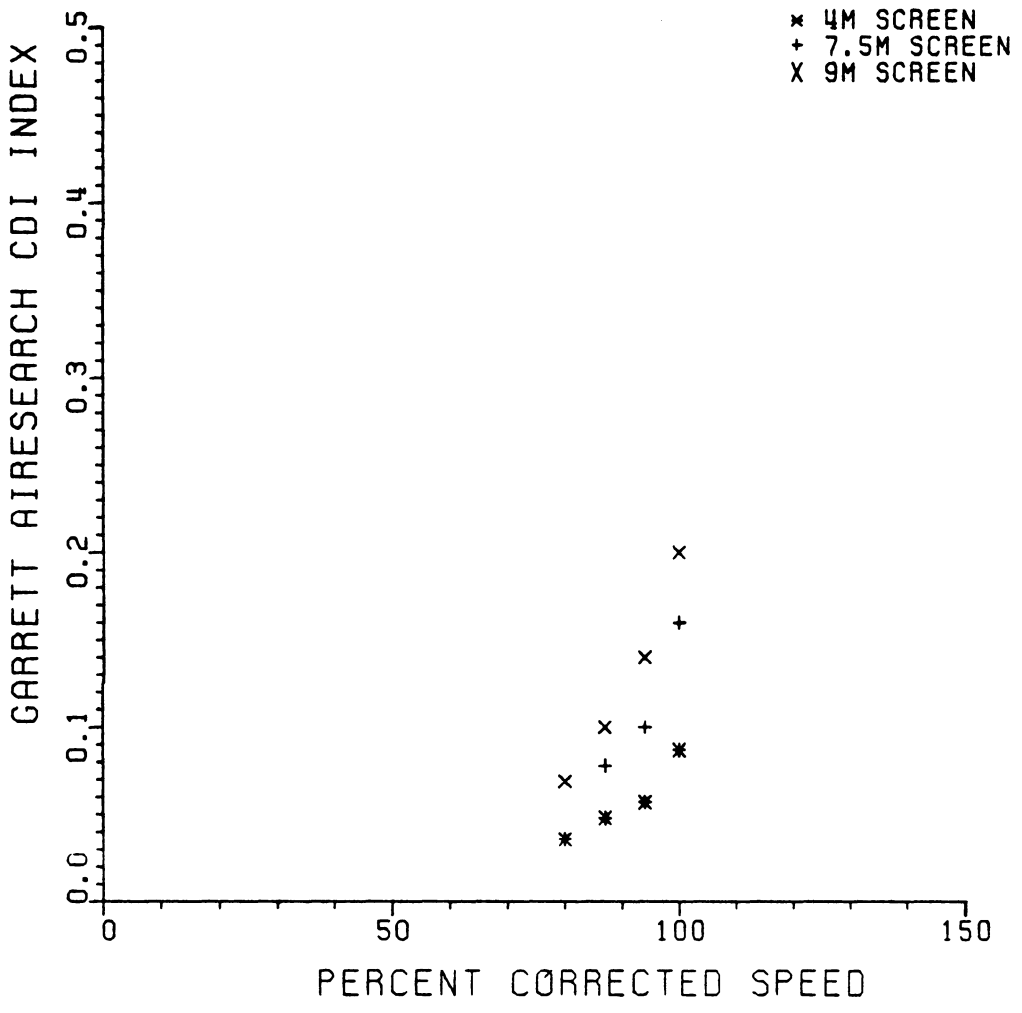

FIGURE C21: CIRCUMFERENTIAL DISTORTION-INDUCED STALL DATA FOR THE J85-GE-13 ENGINE, GARRETT AIRESEARCH CDI INDEX VS SPEED

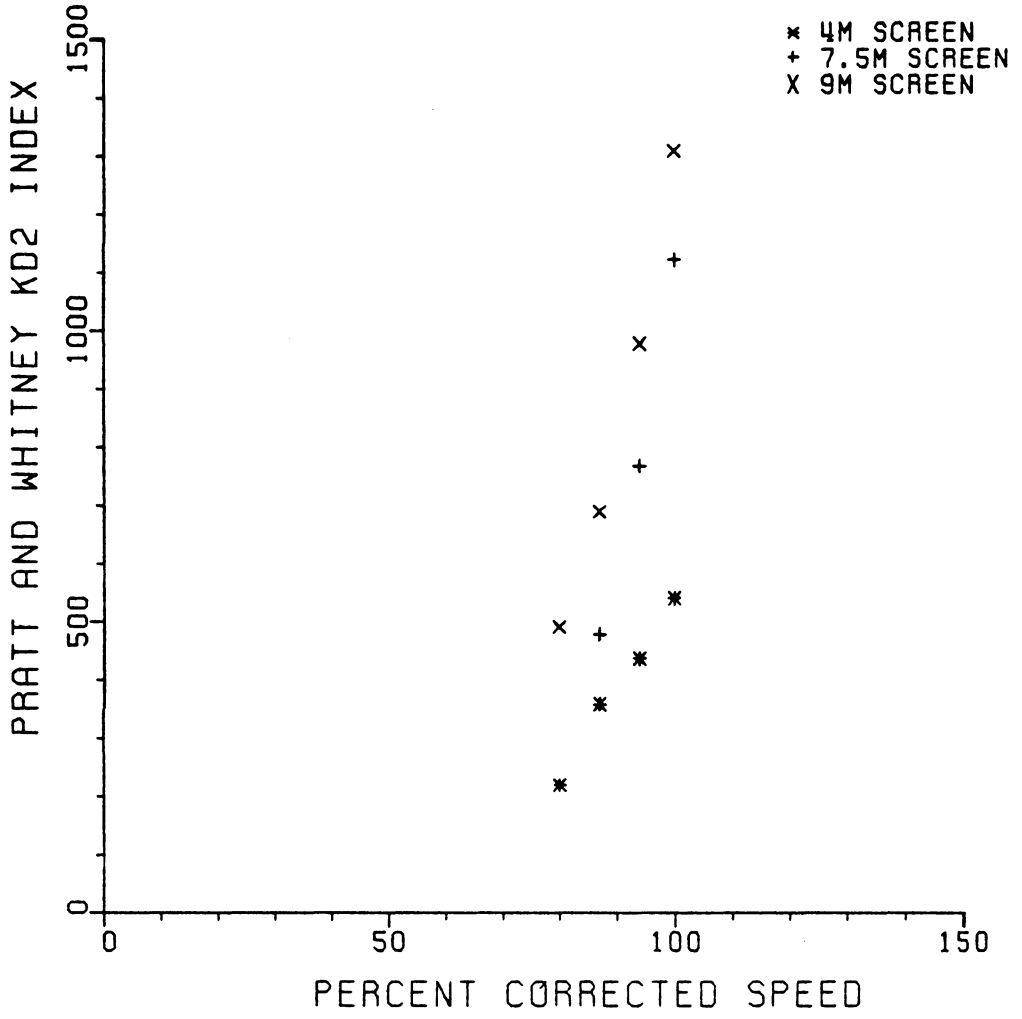

FIGURE C22: CIRCUMFERENTIAL DISTORTION-INDUCED STALL DATA FOR THE J85-GE-13 ENGINE, PRATT AND WHITNEY KD2 INDEX VS SPEED

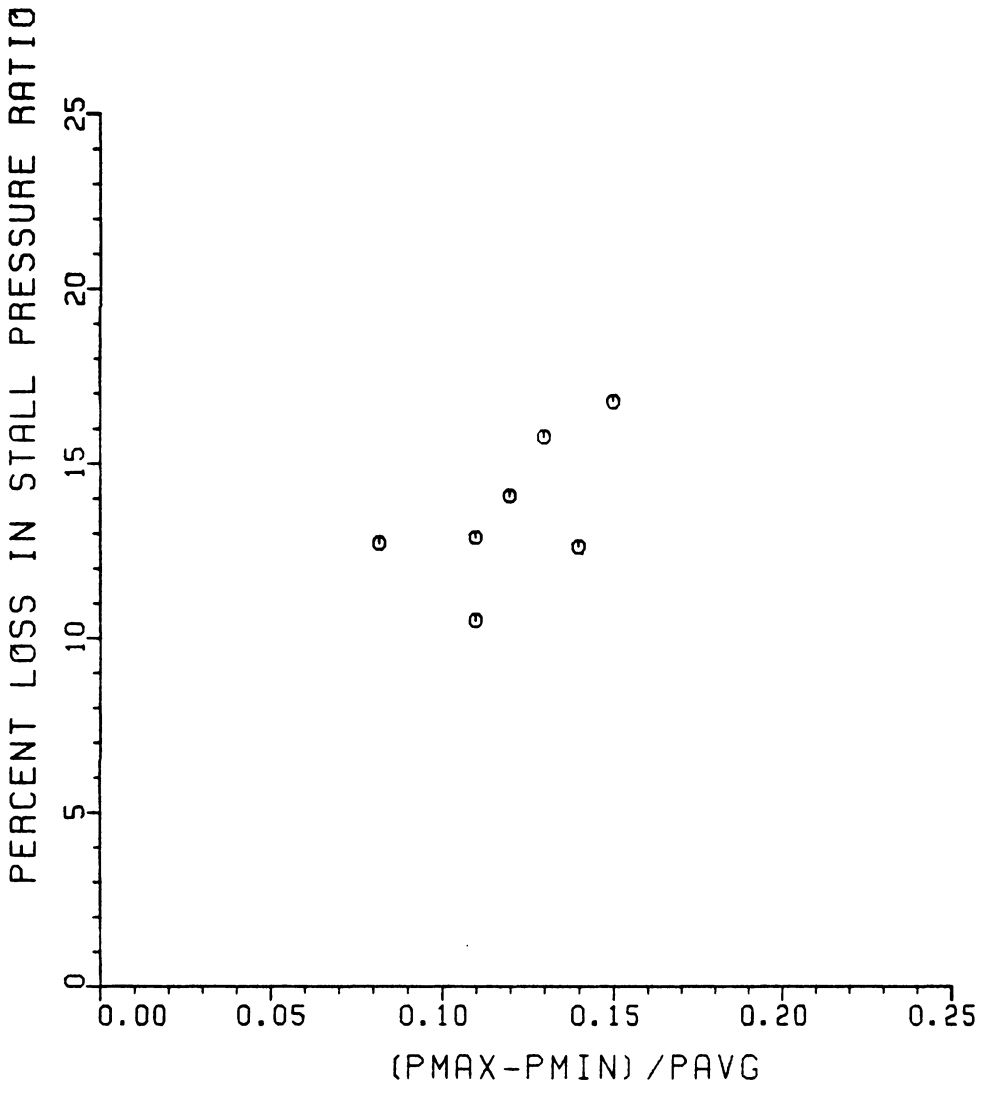

FIGURE C23: CIRCUMFERENTIAL DISTORTION-INDUCED STALL DATA FOR THE TF30-P-3 ENGINE, (PMAX-PMIN)/PAVG INDEX, DELTA PRSN

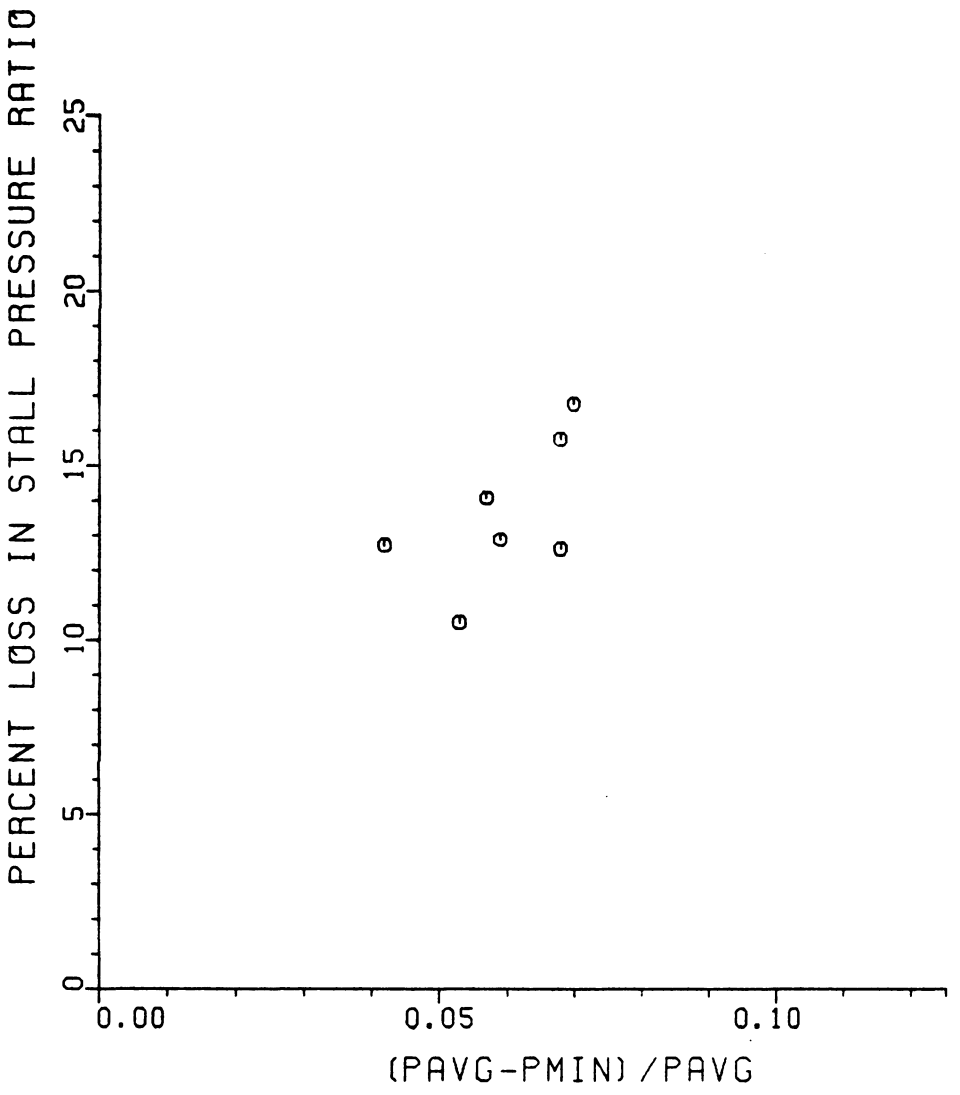

FIGURE C24: CIRCUMFERENTIAL DISTORTION-INDUCED STALL DATA FOR THE TF30-P-3 ENGINE, (PAVG-PMIN)/PAVG INDEX, DELTA PRSN

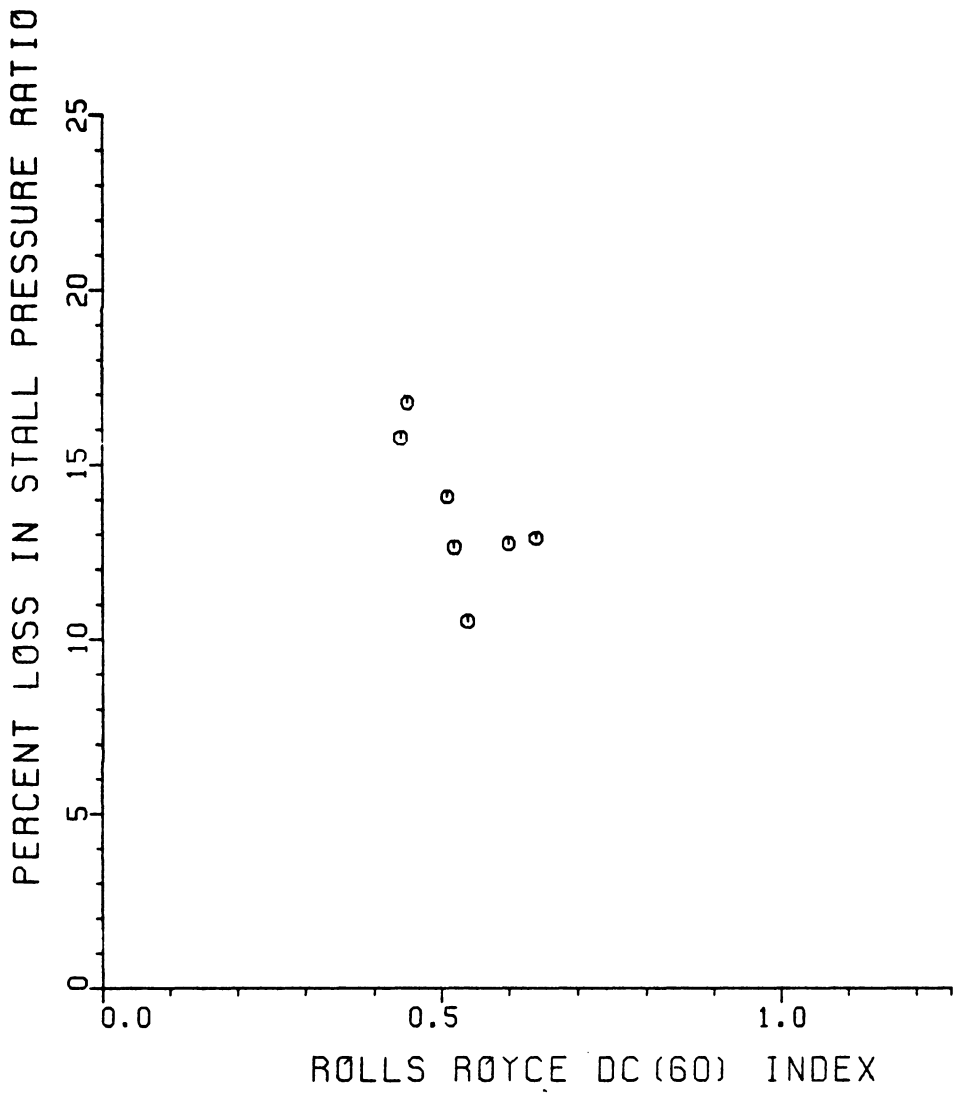

FIGURE C25: CIRCUMFERENTIAL DISTORTION-INDUCED STALL DATA FOR THE TF30-P-3 ENGINE, ROLLS ROYCE DC(60) INDEX, DELTA PRSN

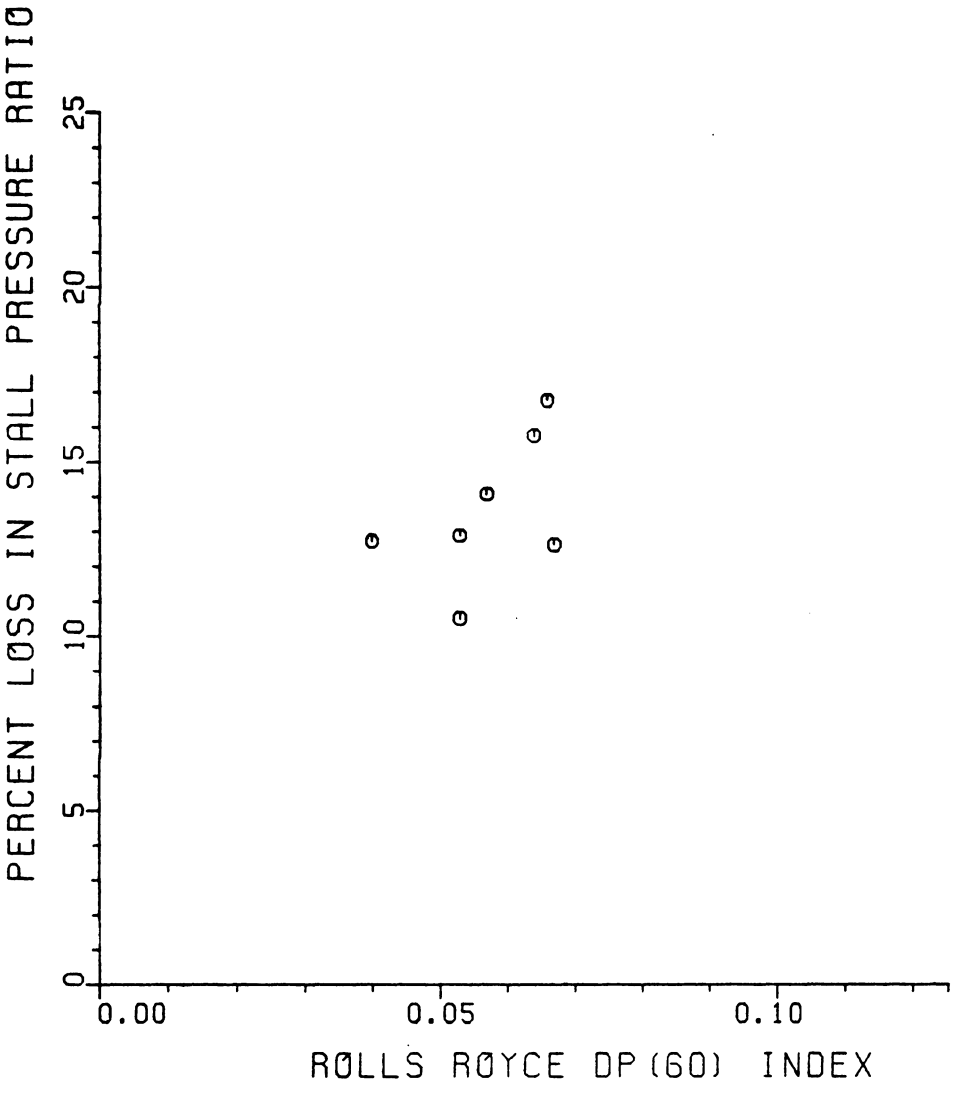

FIGURE C26: CIRCUMFERENTIAL DISTORTION-INDUCED STALL DATA FOR THE TF30-P-3 ENGINE, ROLLS ROYCE DP(60) INDEX, DELTA PRSN

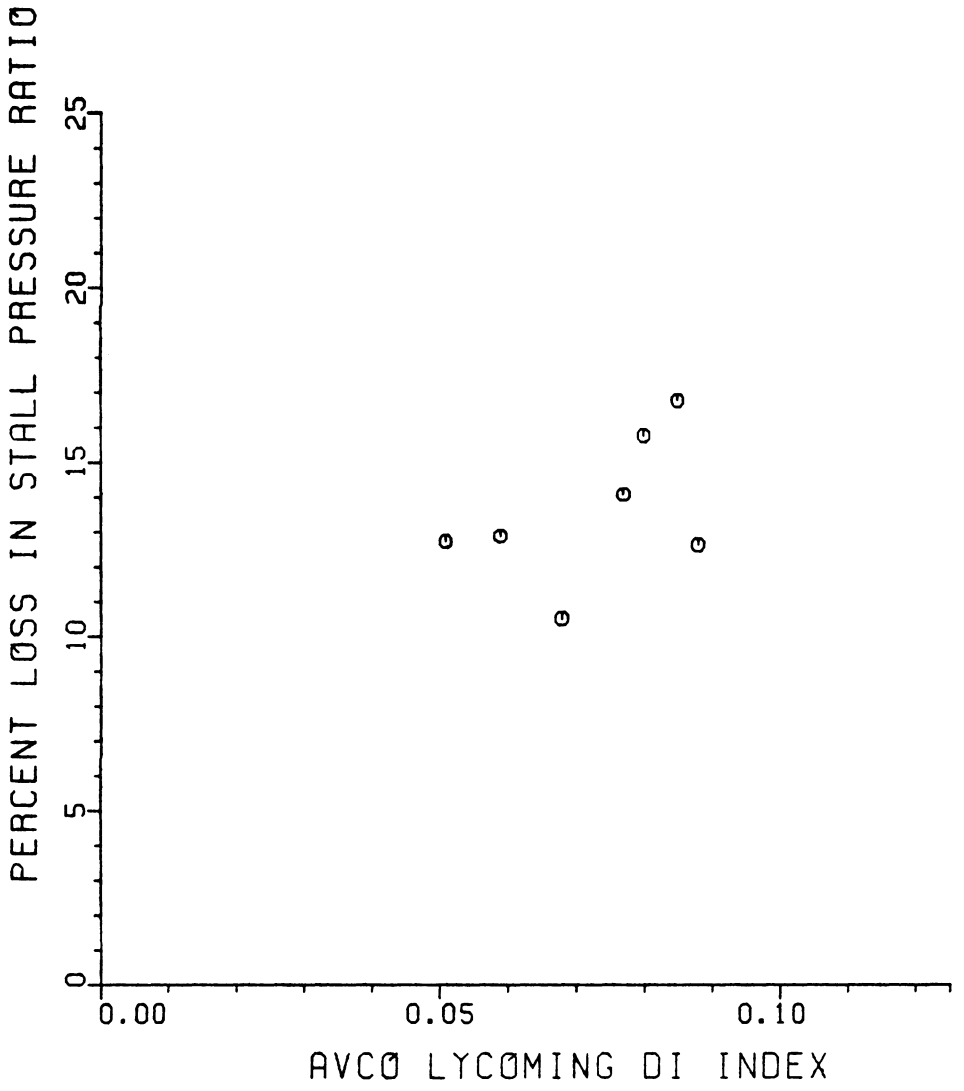

FIGURE C27: CIRCUMFERENTIAL DISTORTION-INDUCED STALL DATA FOR THE TF30-P-3 ENGINE, AVCO LYCOMING DI INDEX, DELTA PRSN

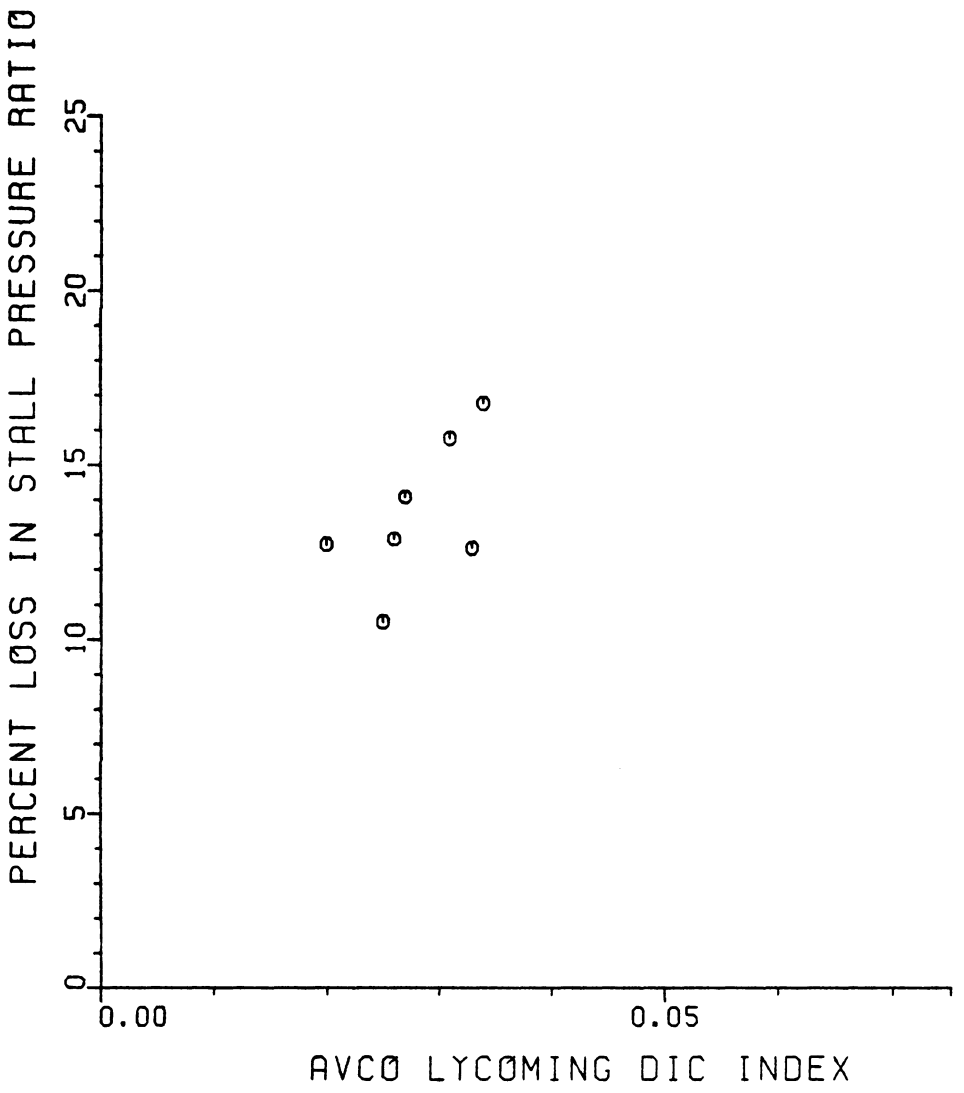

FIGURE C28: CIRCUMFERENTIAL DISTORTION-INDUCED STALL DATA FOR THE TF30-P-3 ENGINE, AVCO LYCOMING DIC INDEX, DELTA PRSN

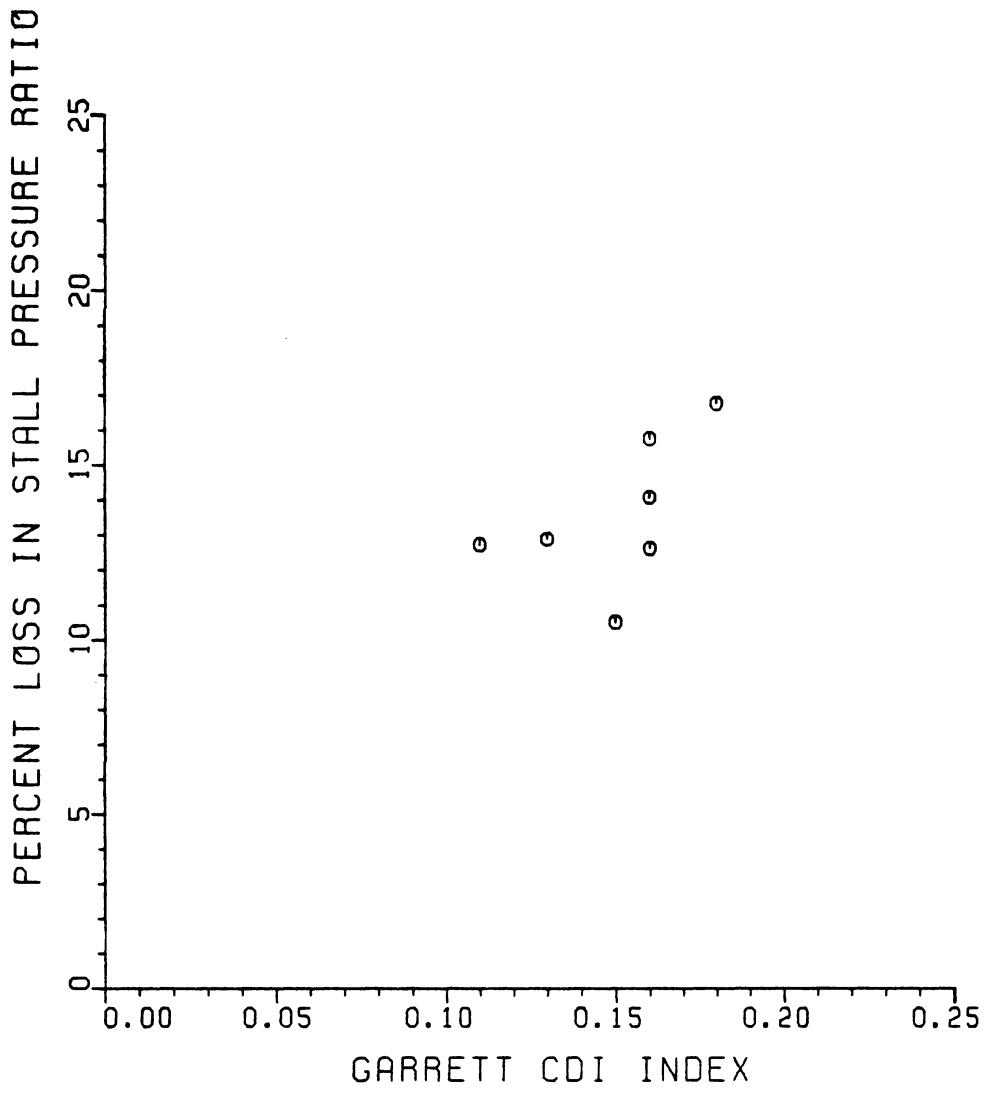

FIGURE C29: CIRCUMFERENTIAL DISTORTION-INDUCED STALL DATA FOR THE TF30-P-3 ENGINE, GARRETT AIRESEARCH CDI INDEX, DELTA PRSN

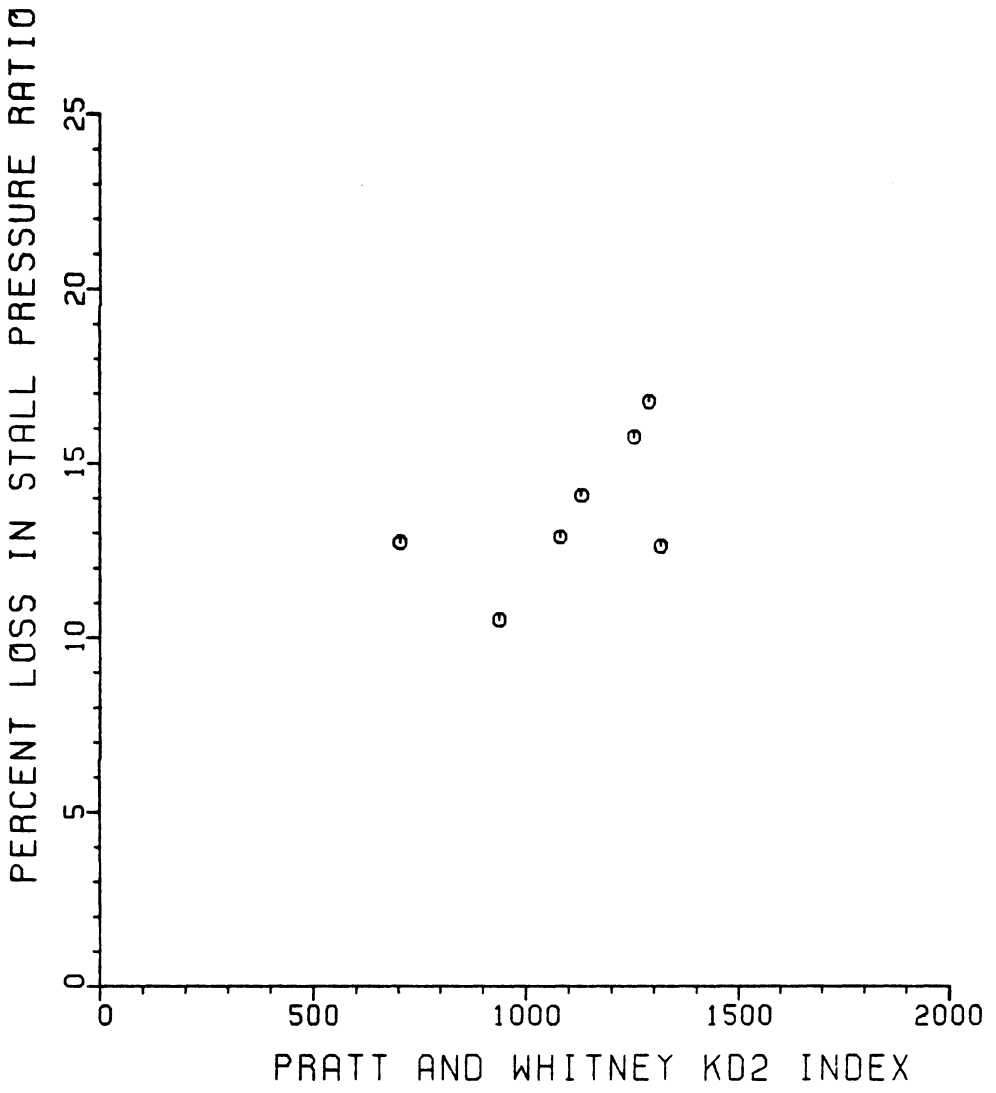

FIGURE C30: CIRCUMFERENTIAL DISTORTION-INDUCED STALL DATA FOR THE TF30-P-3 ENGINE, PRATT AND WHITNEY KD2 INDEX, DELTA PRSN

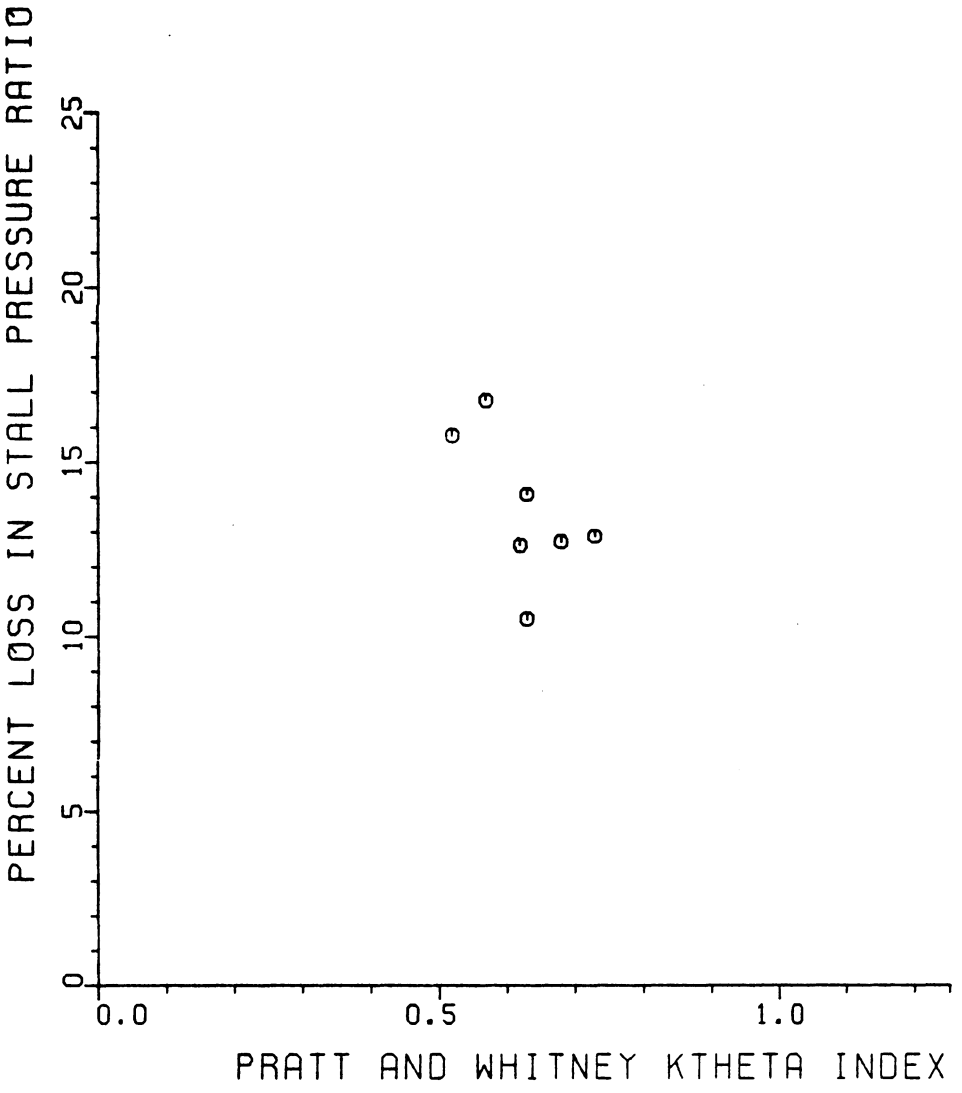

FIGURE C31: CIRCUMFERENTIAL DISTORTION-INDUCED STALL DATA FOR THE TF30-P-3 ENGINE, PRATT AND WHITNEY KTHETA INDEX, DELTA PRSN

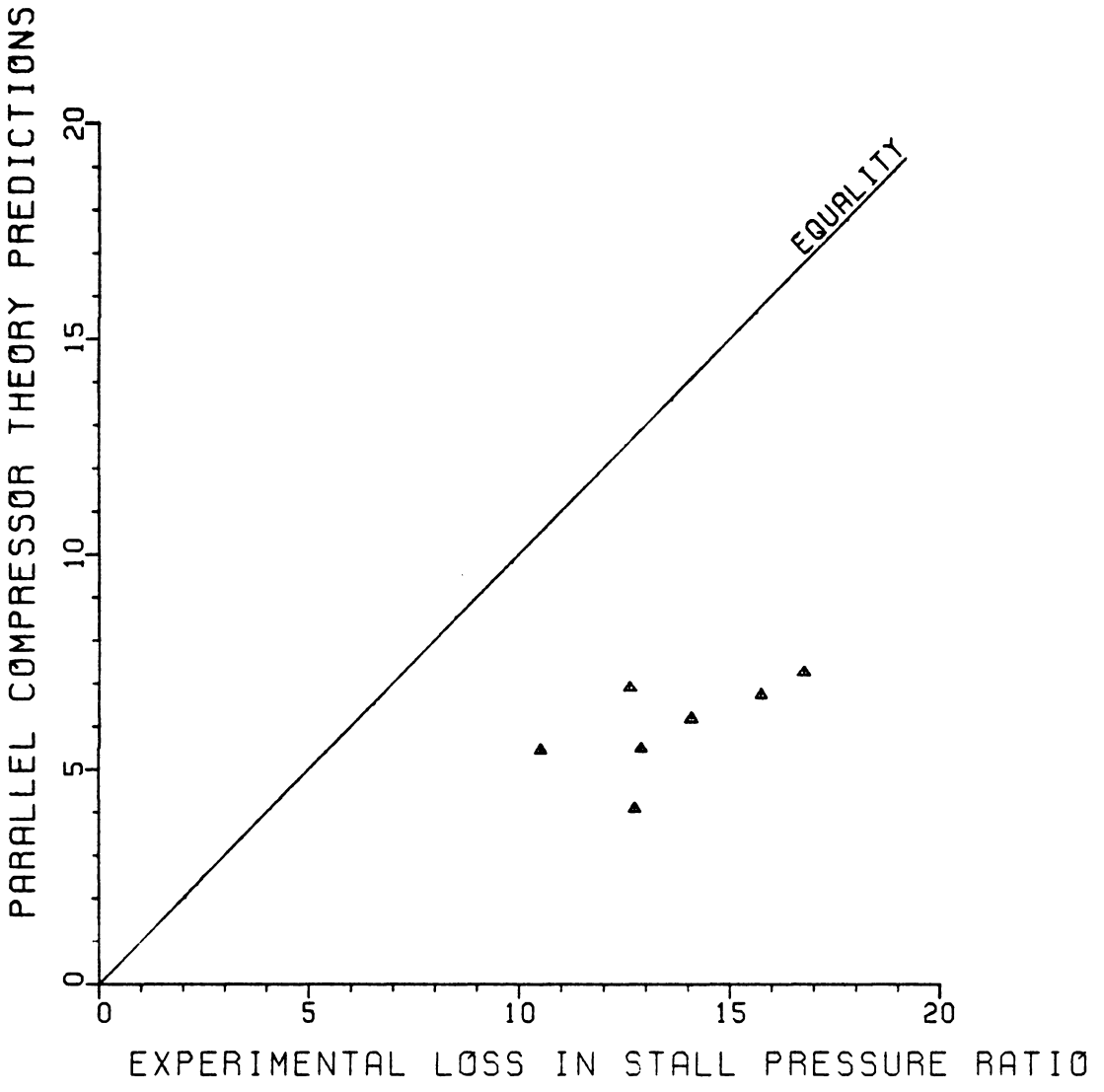

FIGURE C32: CIRCUMFERENTIAL DISTORTION-INDUCED STALL DATA FOR THE TF30-P-3 ENGINE, PARALLEL COMPRESSOR THEORY

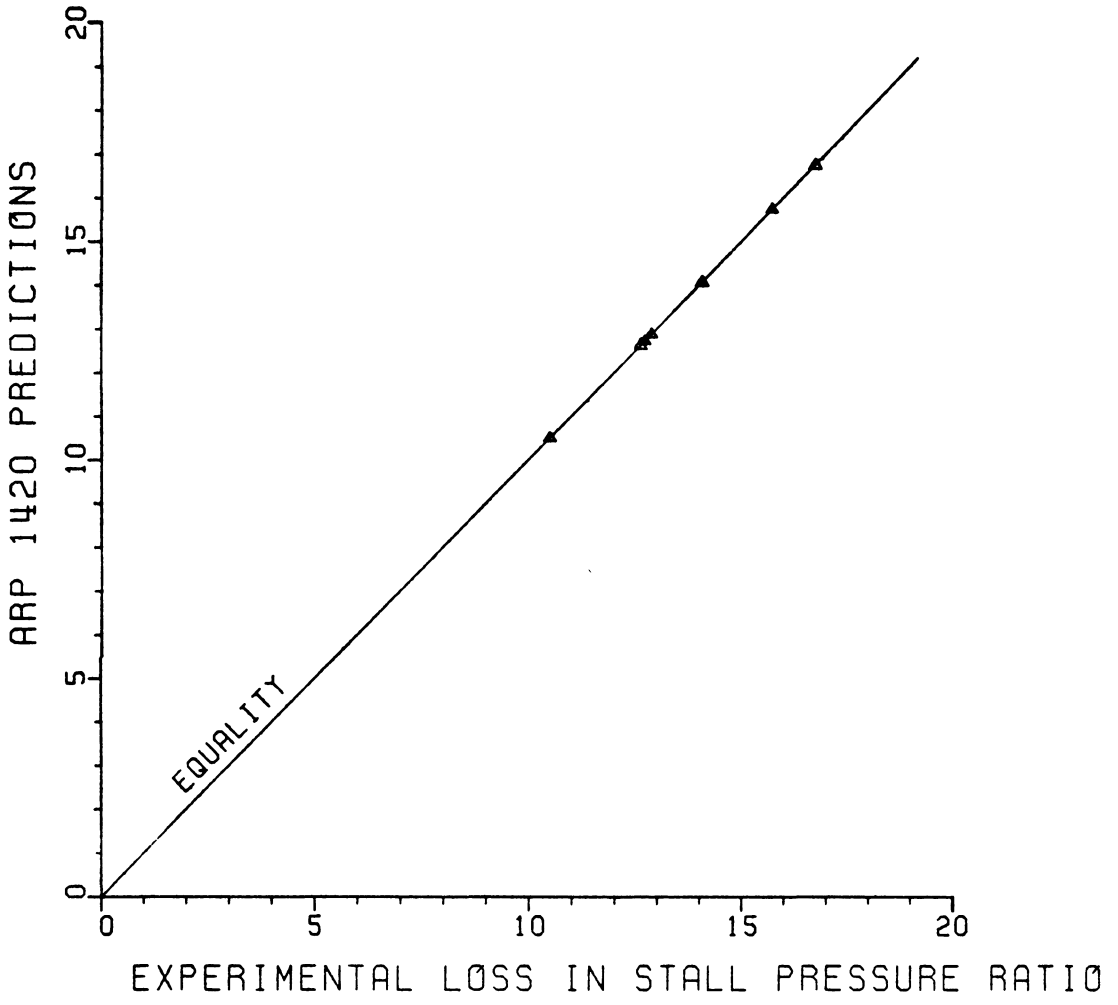

FIGURE C33: CIRCUMFERENTIAL DISTORTION-INDUCED STALL DATA FOR THE TF30-P-3 ENGINE AND ARP 1420 PREDICTIONS

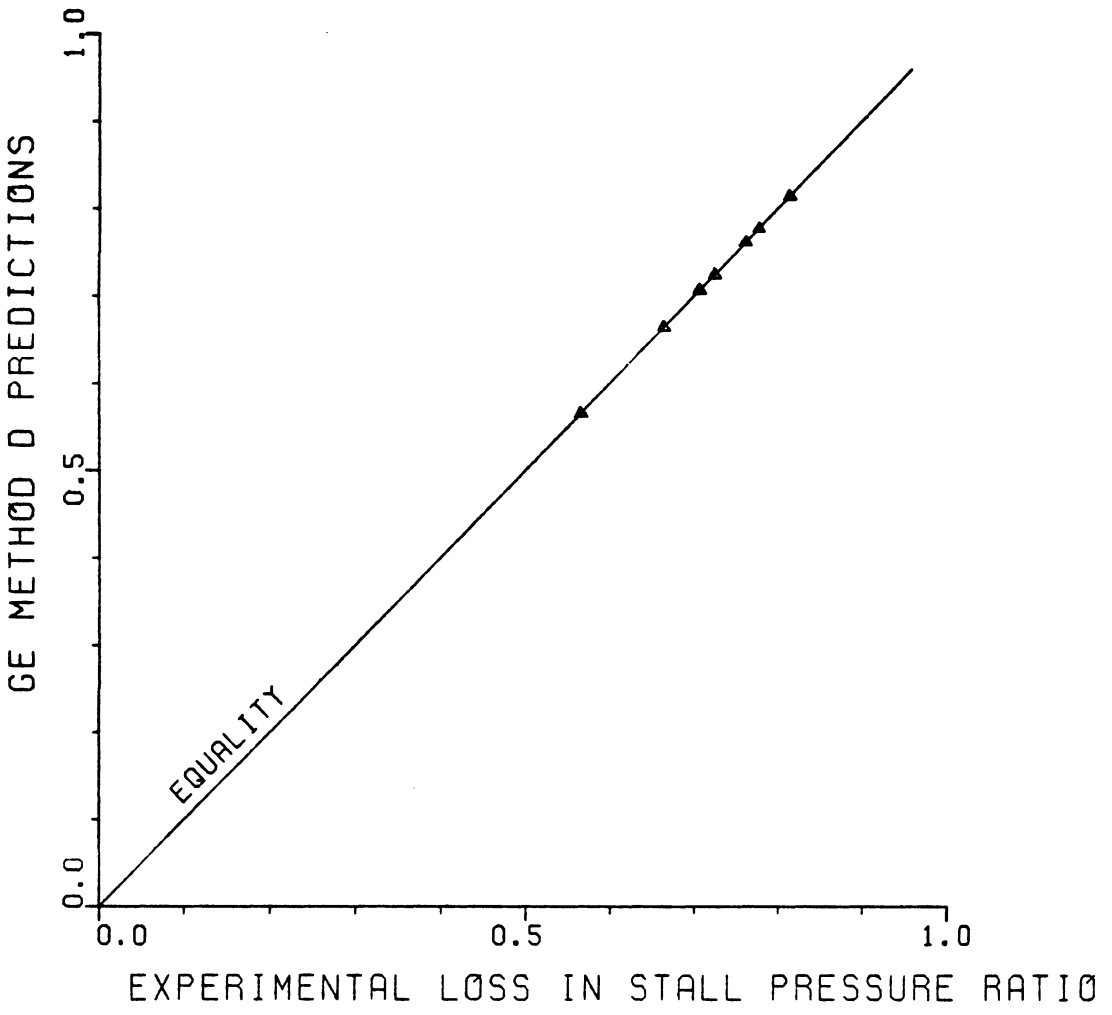

FIGURE C34: CIRCUMFERENTIAL DISTORTION-INDUCED STALL DATA FOR THE TF30-P-3 ENGINE AND GE METHOD D PREDICTIONS

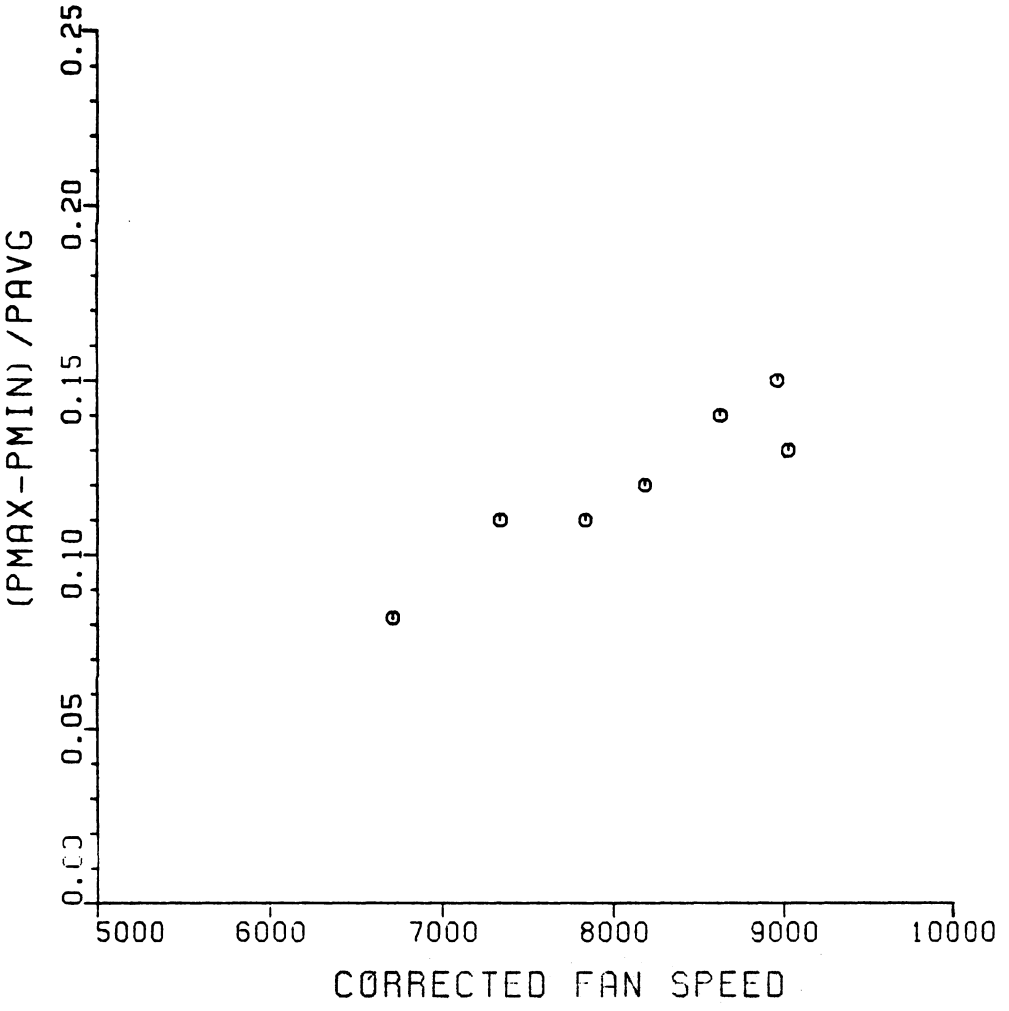

FIGURE C35: CIRCUMFERENTIAL DISTORTION-INDUCED STALL DATA FOR THE TF30-P-3 ENGINE, (PMAX-PMIN)/PAVG INDEX VS FAN SPEED

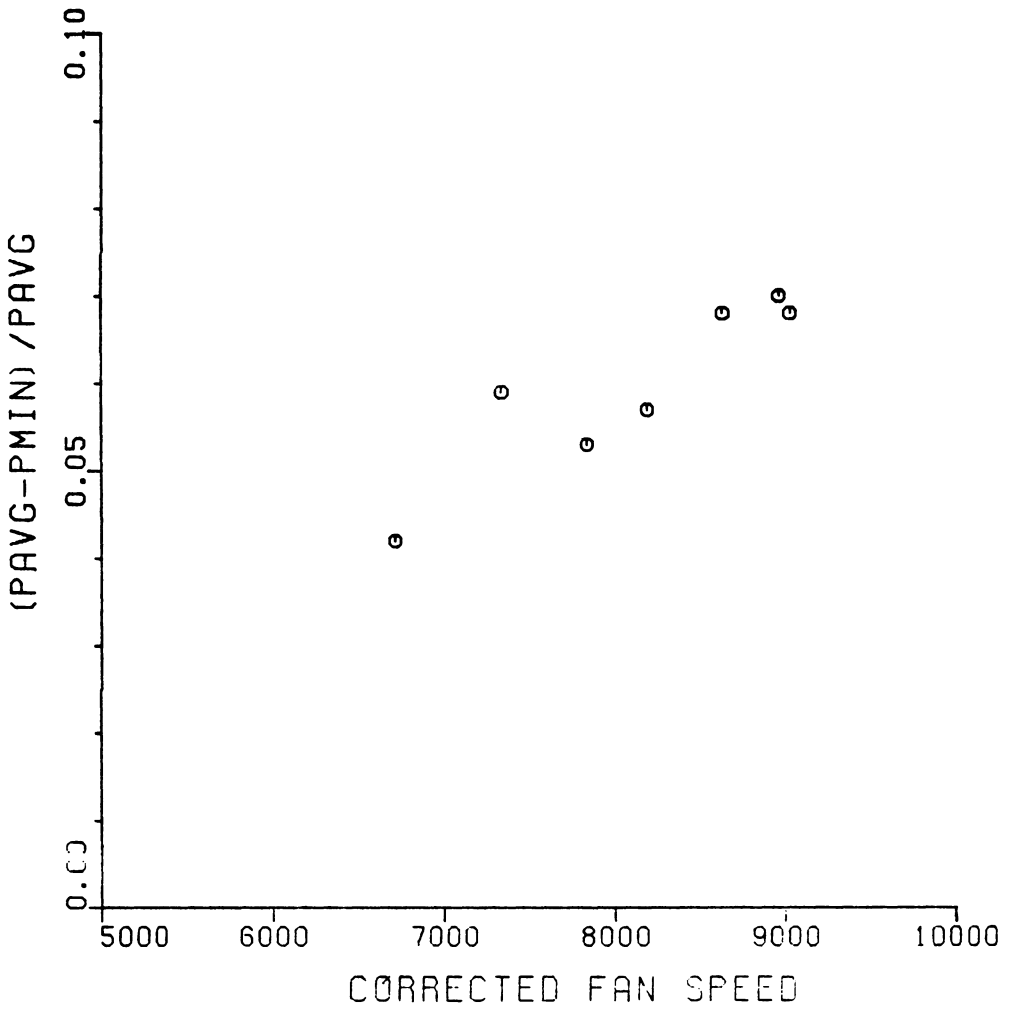

FIGURE C36: CIRCUMFERENTIAL DISTORTION-INDUCED STALL DATA FOR THE TF30-P-3 ENGINE, (PAVG-PMIN)/PAVG INDEX VS FAN SPEED

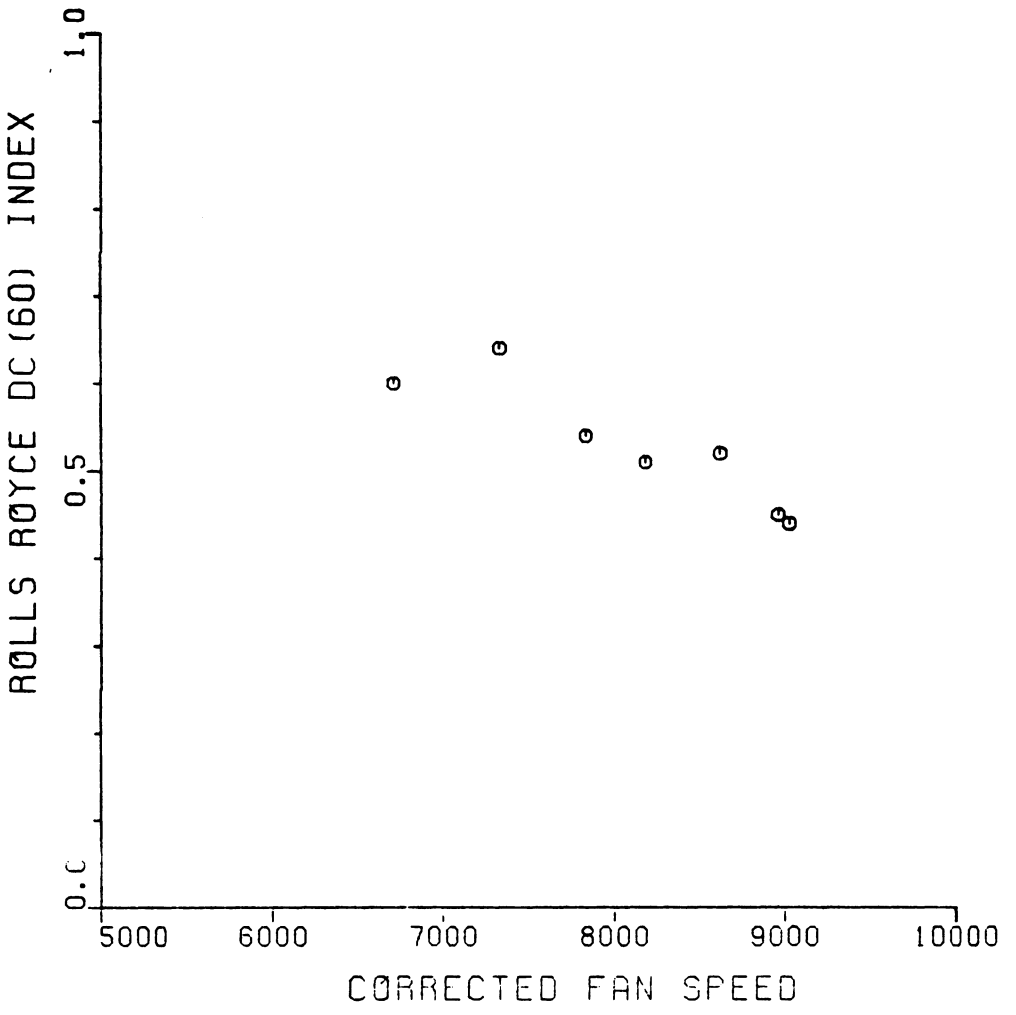

FIGURE C37: CIRCUMFERENTIAL DISTORTION—INDUCED STALL DATA FOR THE TF30-P-3 ENGINE, ROLLS ROYCE DC(60) INDEX VS FAN SPEED

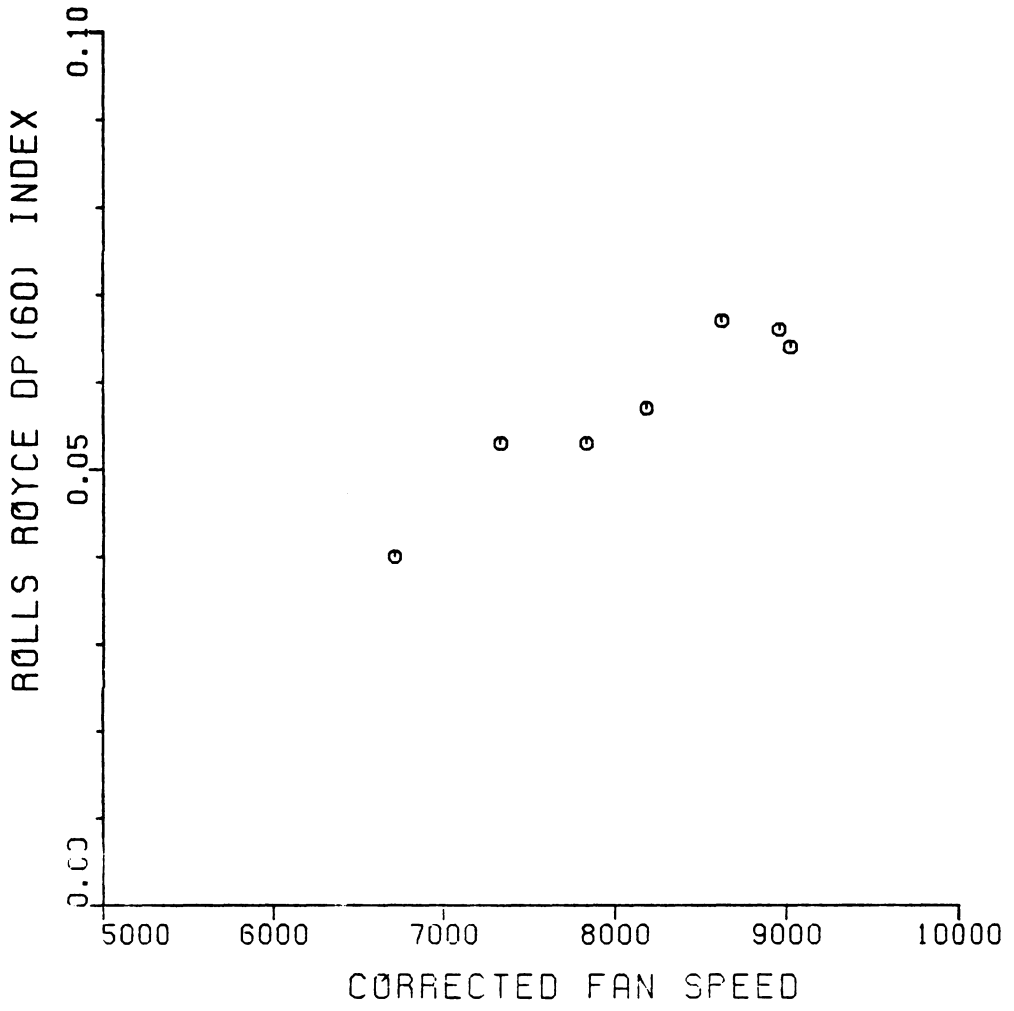

FIGURE C38: CIRCUMFERENTIAL DISTORTION-INDUCED STALL DATA FOR THE TF30-P-3 ENGINE, ROLLS ROYCE DP(60) INDEX VS FAN SPEED

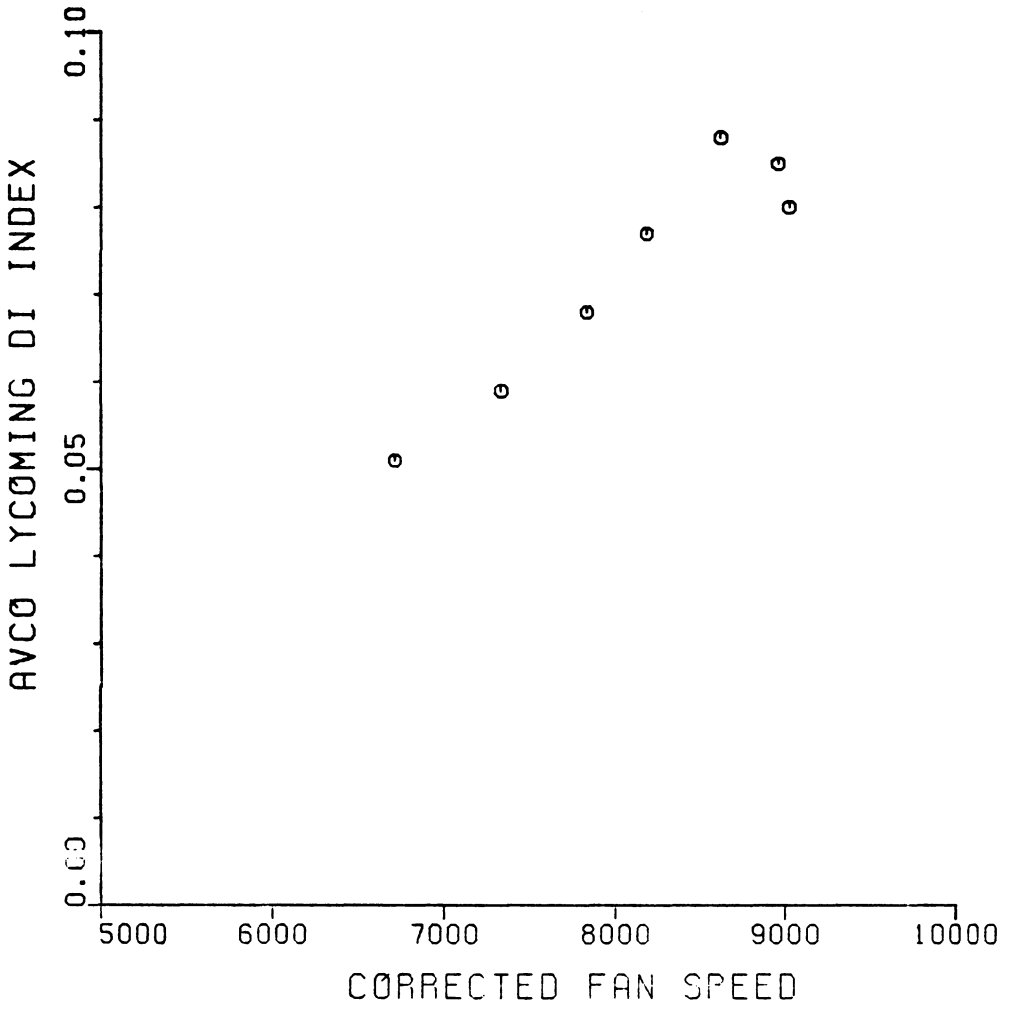

FIGURE C39: CIRCUMFERENTIAL DISTORTION-INDUCED STALL DATA FOR THE TF30-P-3 ENGINE, AVCO LYCOMING DI INDEX VS FAN SPEED

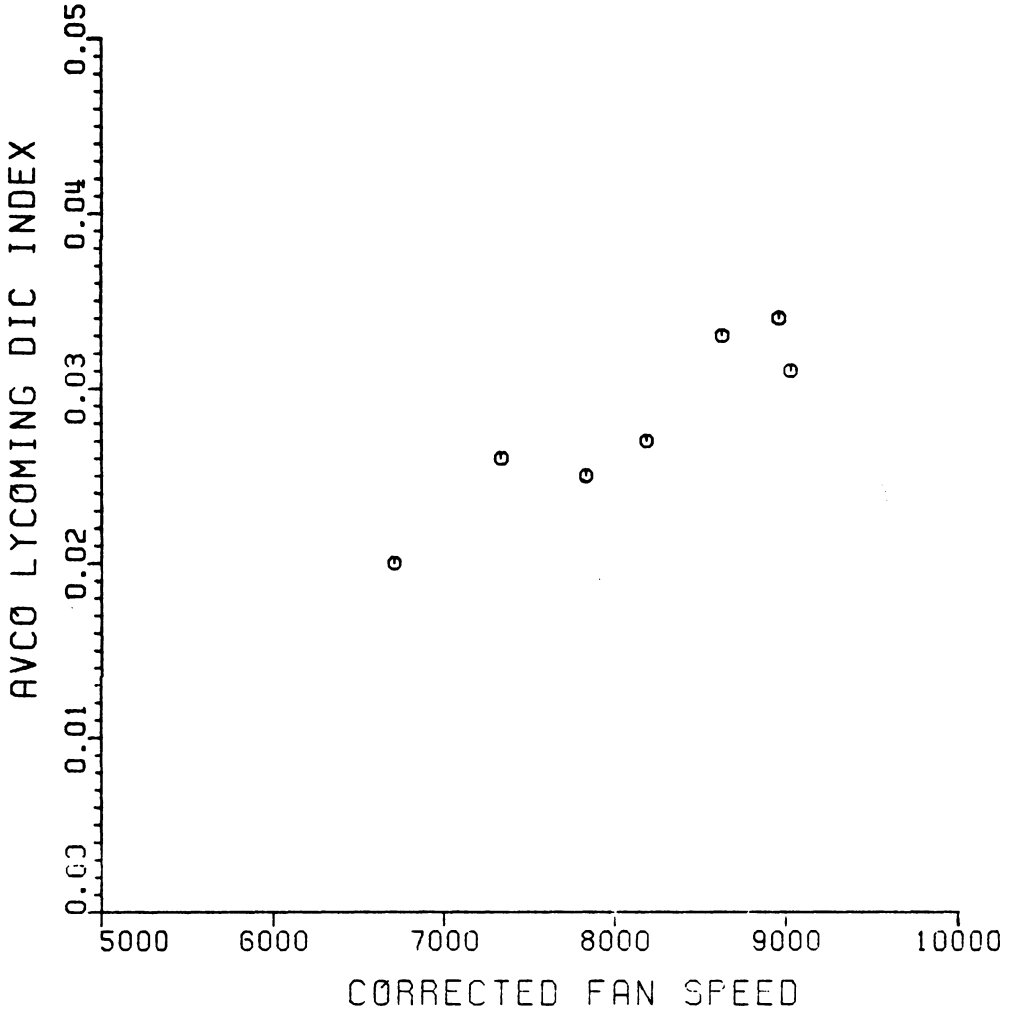

FIGURE C40: CIRCUMFERENTIAL DISTORTION-INDUCED STALL DATA FOR THE TF30-P-3 ENGINE, AVCO LYCOMING DIC INDEX VS FAN SPEED

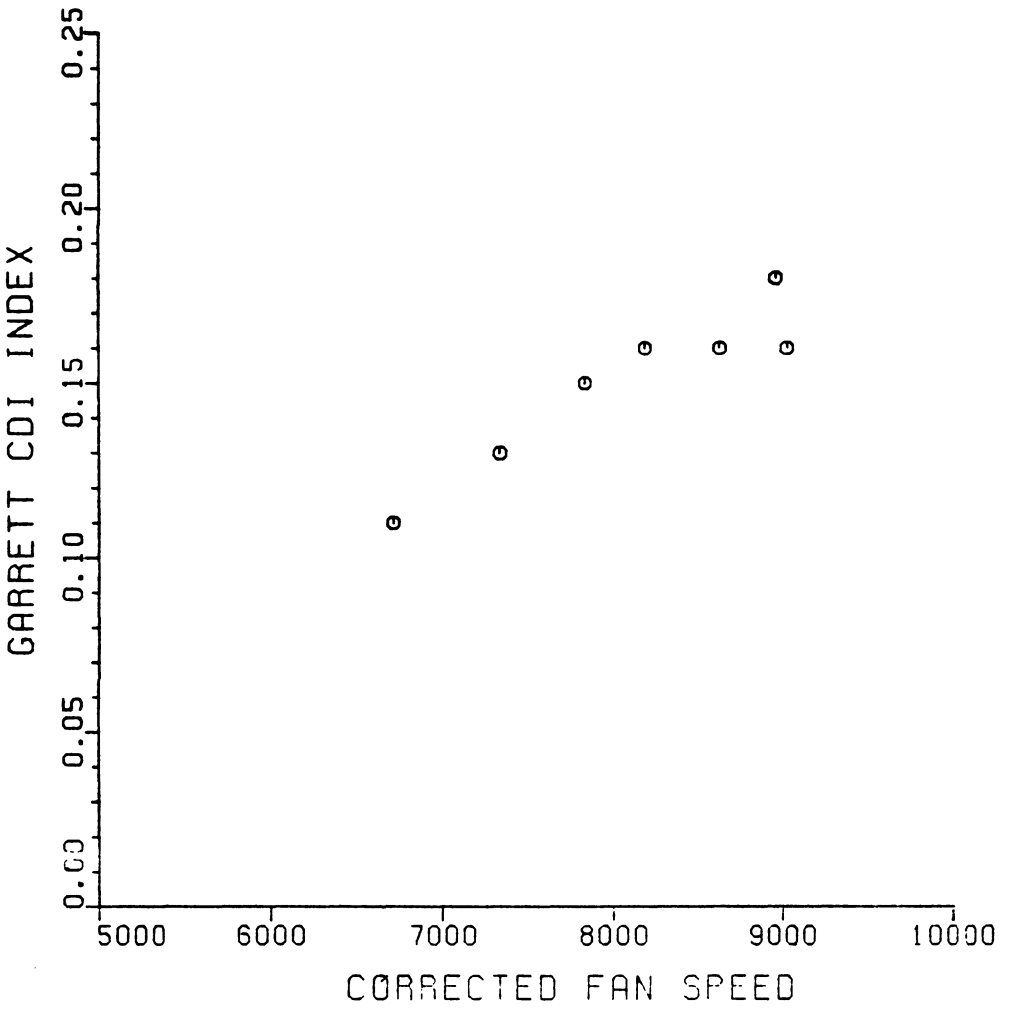

FIGURE C41: CIRCUMFERENTIAL DISTORTION-INDUCED STALL DATA FOR THE TF30-P-3 ENGINE, GARRETT AIRESEARCH CDI INDEX VS FAN SPEED

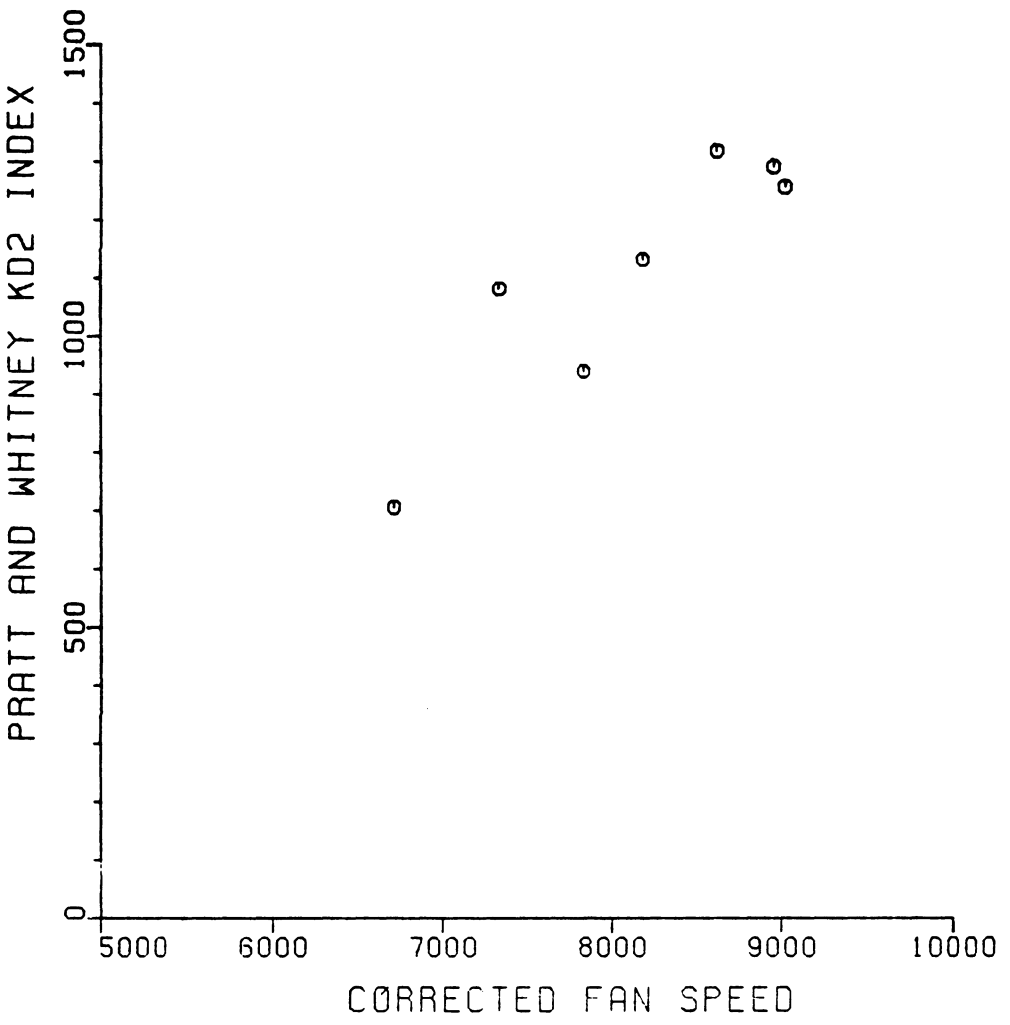

FIGURE C42: CIRCUMFERENTIAL DISTORTION-INDUCED STALL DATA FOR THE TF30-P-3 ENGINE, PRATT AND WHITNEY KD2 INDEX VS FAN SPEED

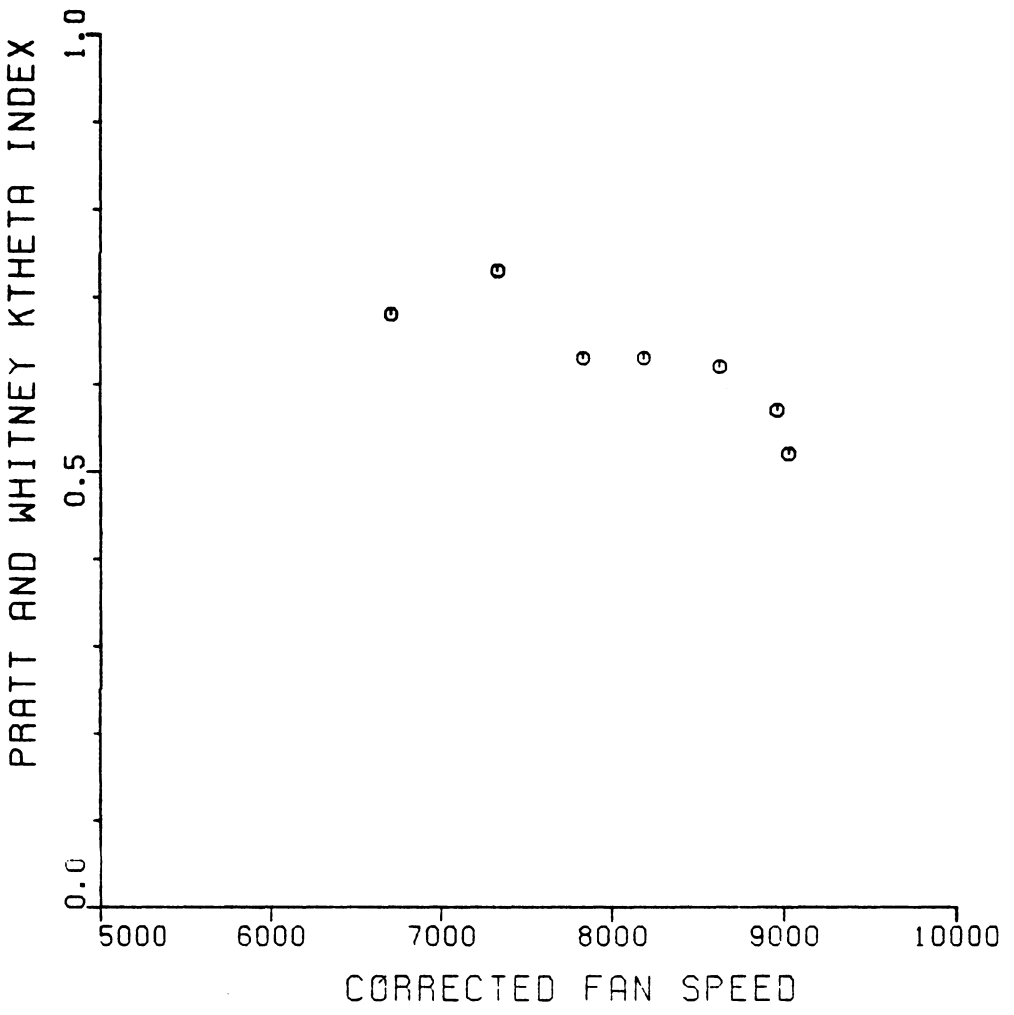

FIGURE C43: CIRCUMFERENTIAL DISTORTION-INDUCED STALL DATA FOR THE TF30-P-3 ENGINE, PRATT AND WHITNEY KTHETA INDEX VS FAN SPEED

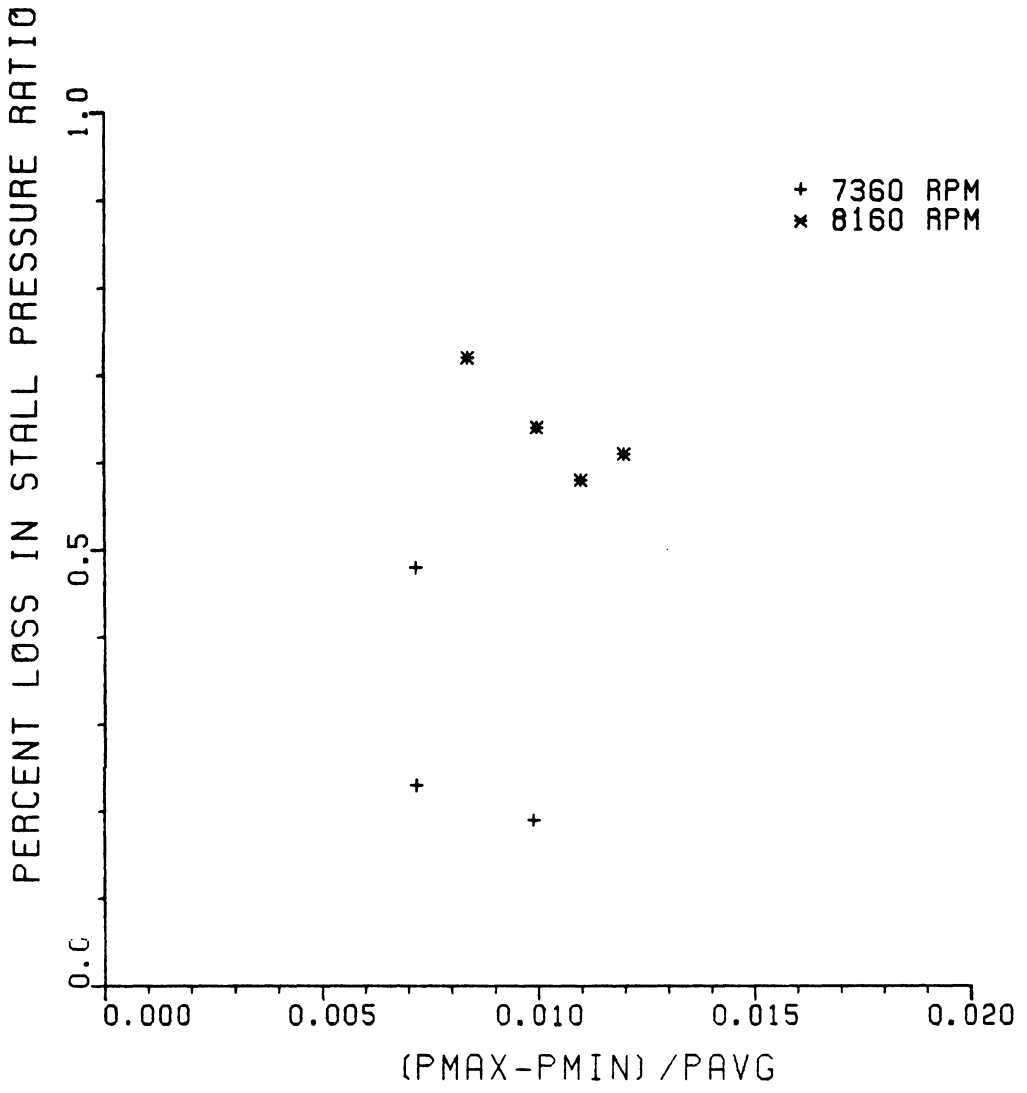

FIGURE C44: CIRCUMFERENTIAL DISTORTION-INDUCED STALL DATA FOR THE COMPRESSOR TEST-RIG, (PMAX-PMIN)/PAVG INDEX

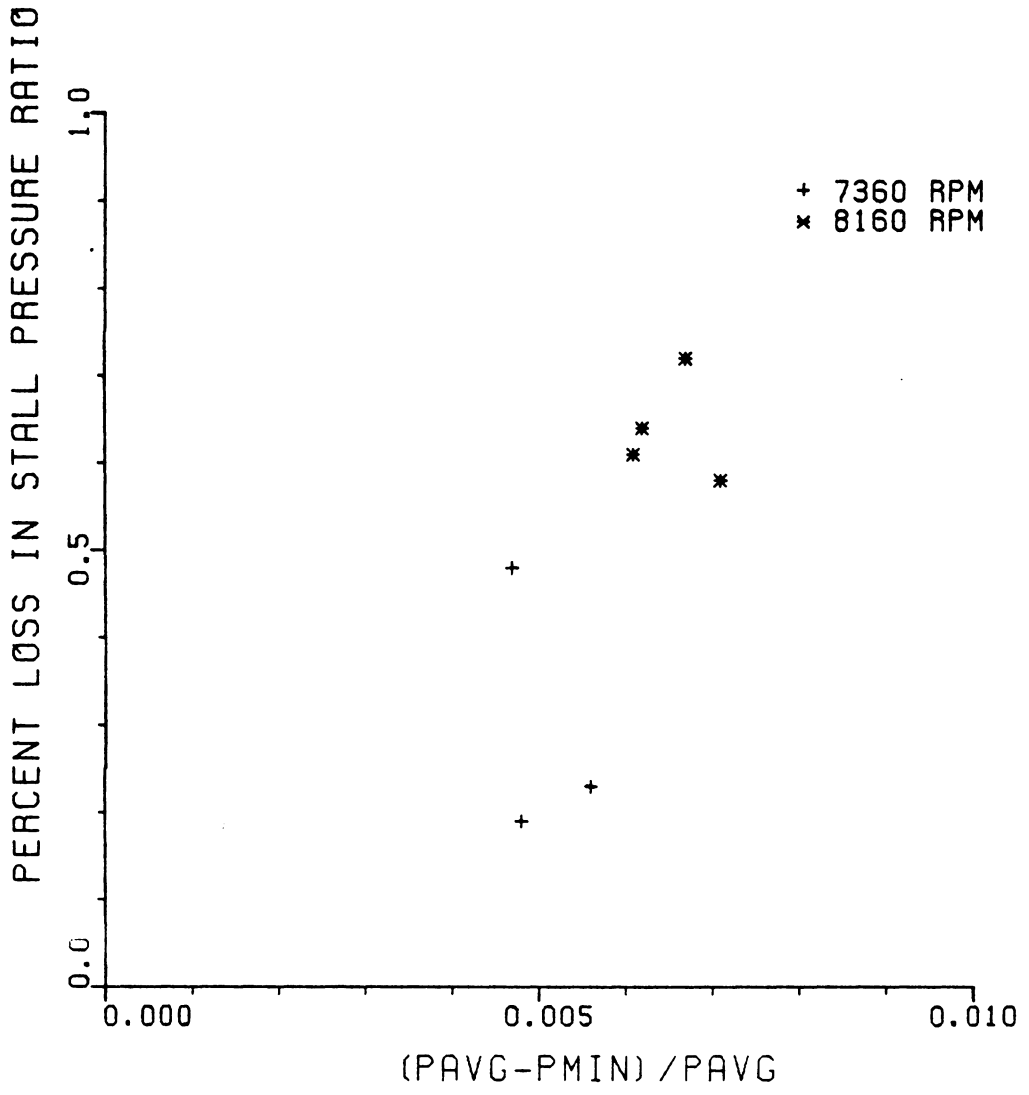

FIGURE C45: CIRCUMFERENTIAL DISTORTION-INDUCED STALL DATA FOR THE COMPRESSOR TEST-RIG, (PAVG-PMIN)/PAVG INDEX, DELTA PRSN

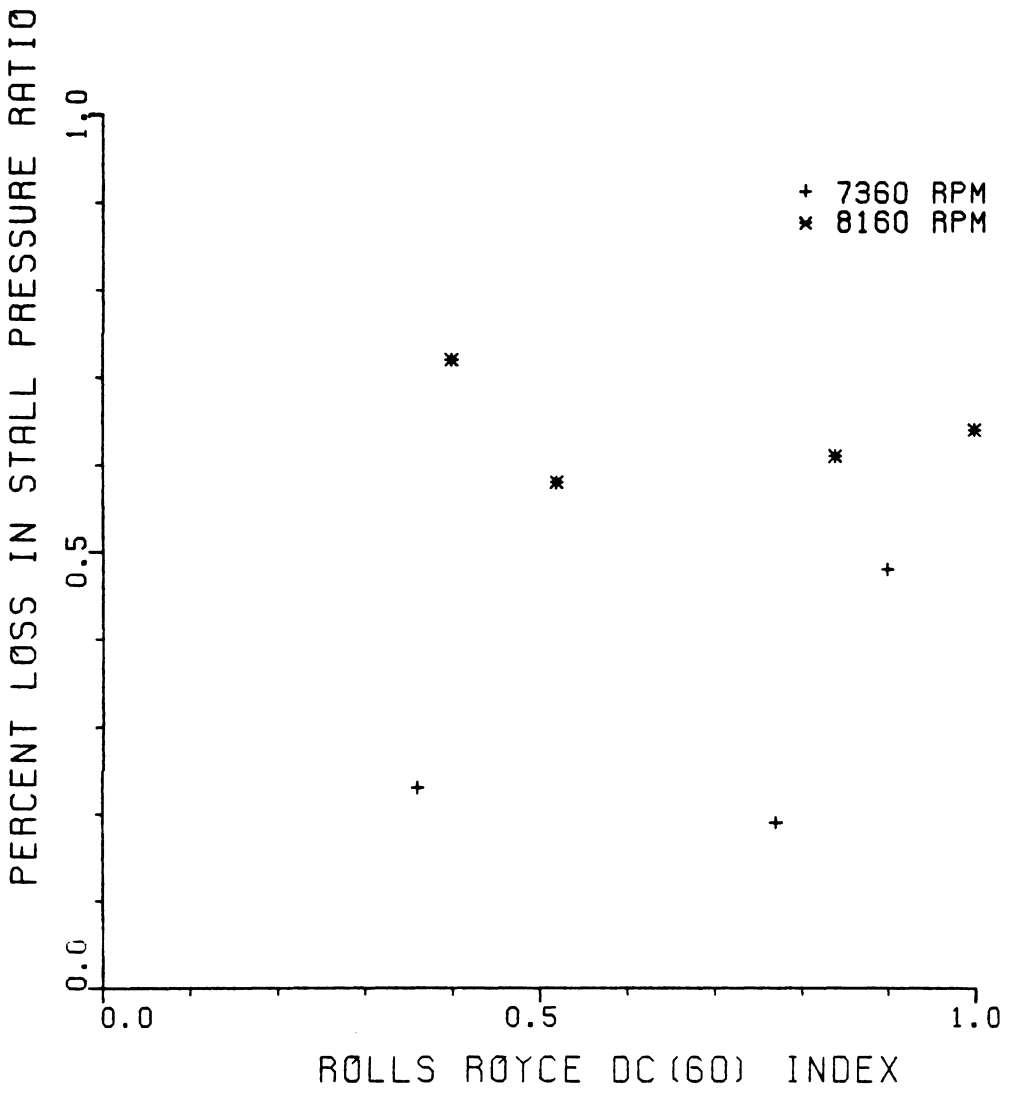

FIGURE C46: CIRCUMFERENTIAL DISTORTION-INDUCED STALL DATA FOR THE COMPRESSOR TEST-RIG, ROLLS ROYCE DC(60) INDEX, DELTA PRSN

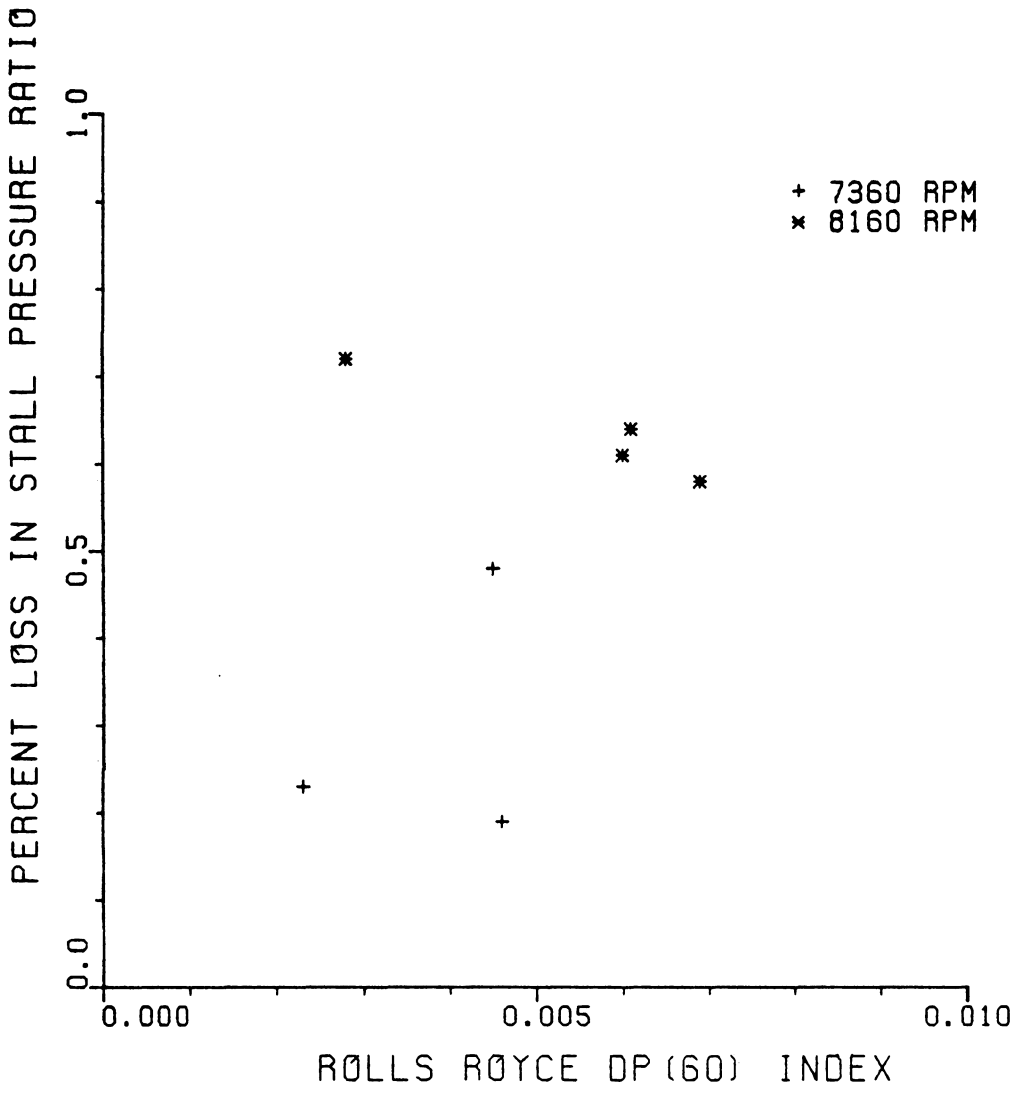

FIGURE C47: CIRCUMFERENTIAL DISTORTION-INDUCED STALL DATA FOR THE COMPRESSOR TEST-RIG, ROLLS ROYCE DP(60) INDEX, DELTA PRSN

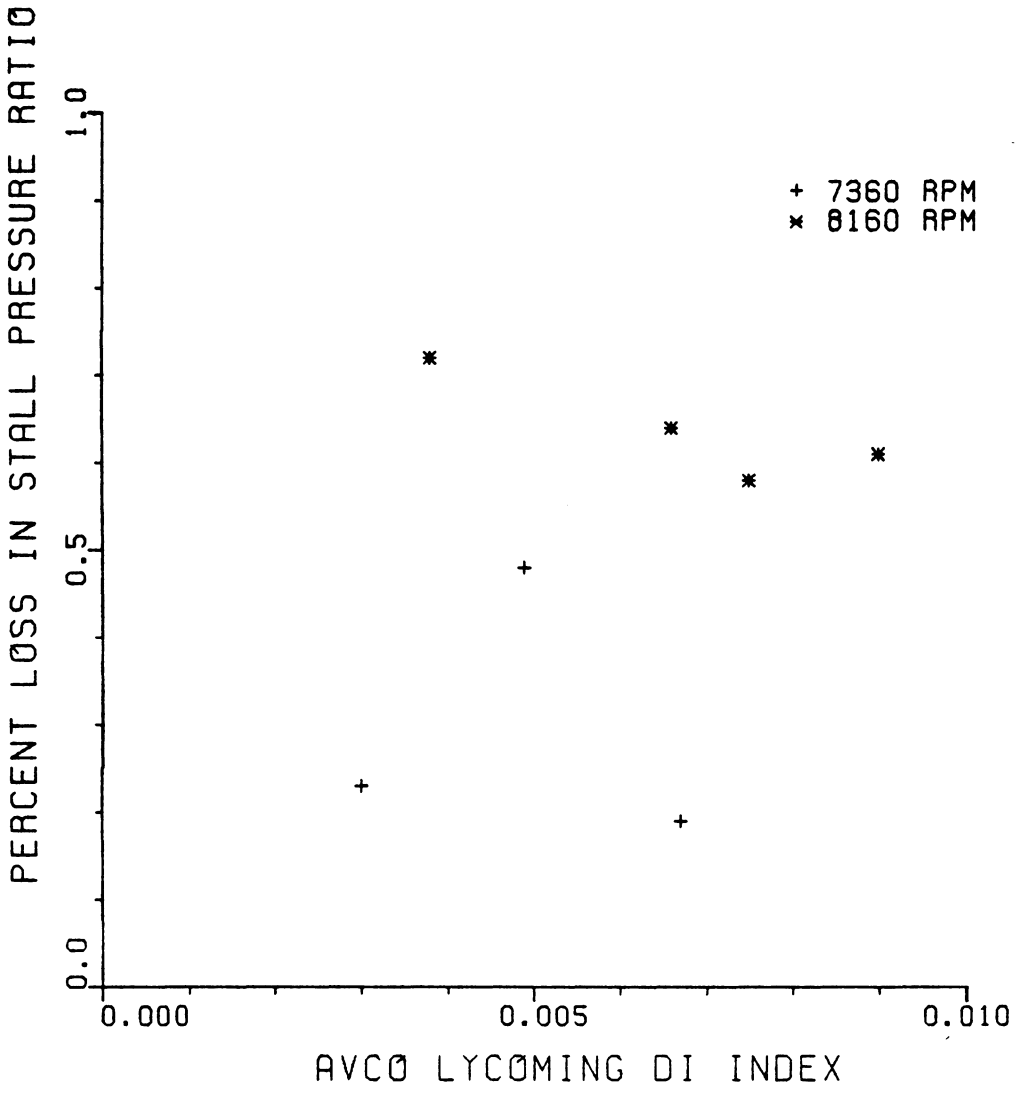

FIGURE C48: CIRCUMFERENTIAL DISTORTION-INDUCED STALL DATA FOR THE COMPRESSOR TEST-RIG, AVCO LYCOMING DI INDEX, DELTA PRSN

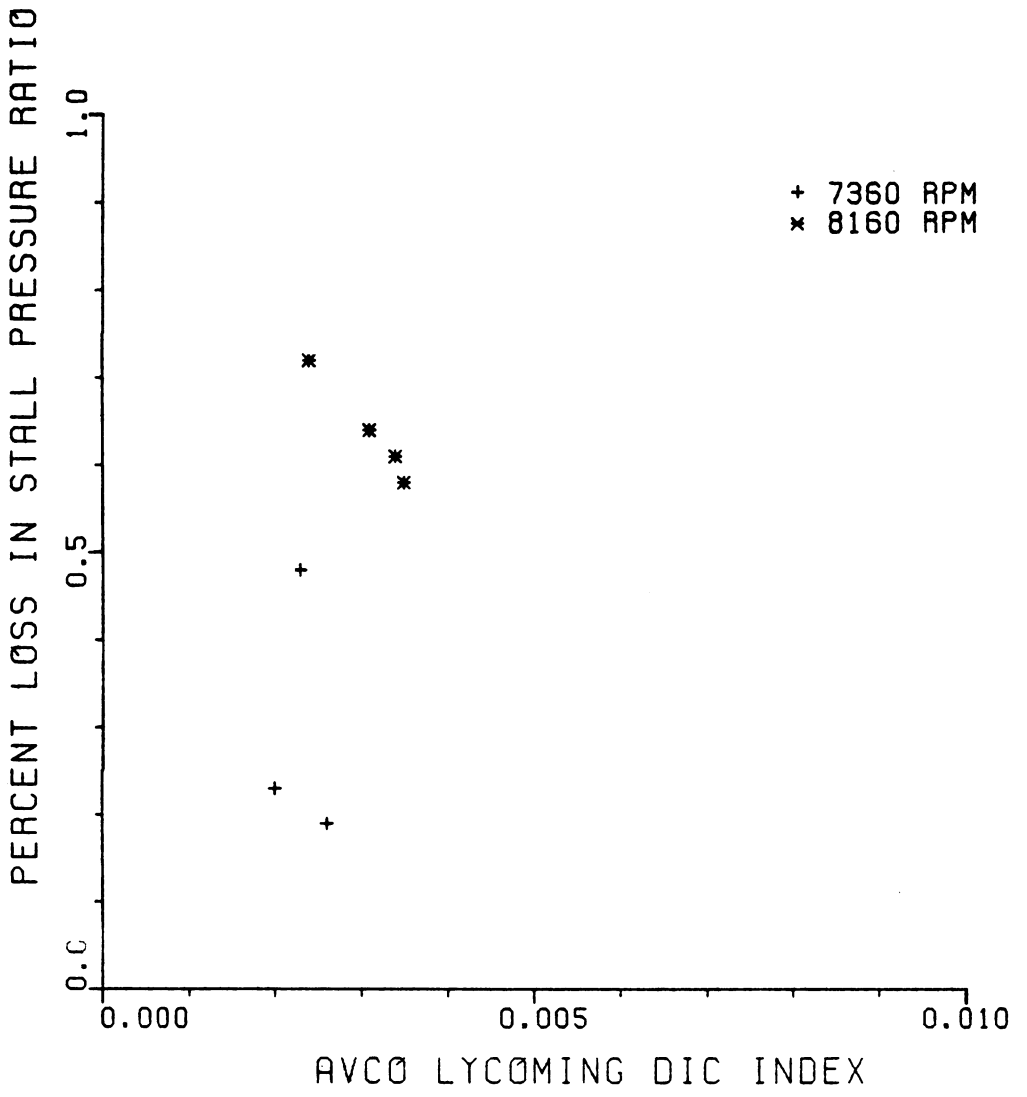

FIGURE C49: CIRCUMFERENTIAL DISTORTION-INDUCED STALL DATA FOR THE COMPRESSOR TEST-RIG, AVCO LYCOMING DIC INDEX, DELTA PRSN

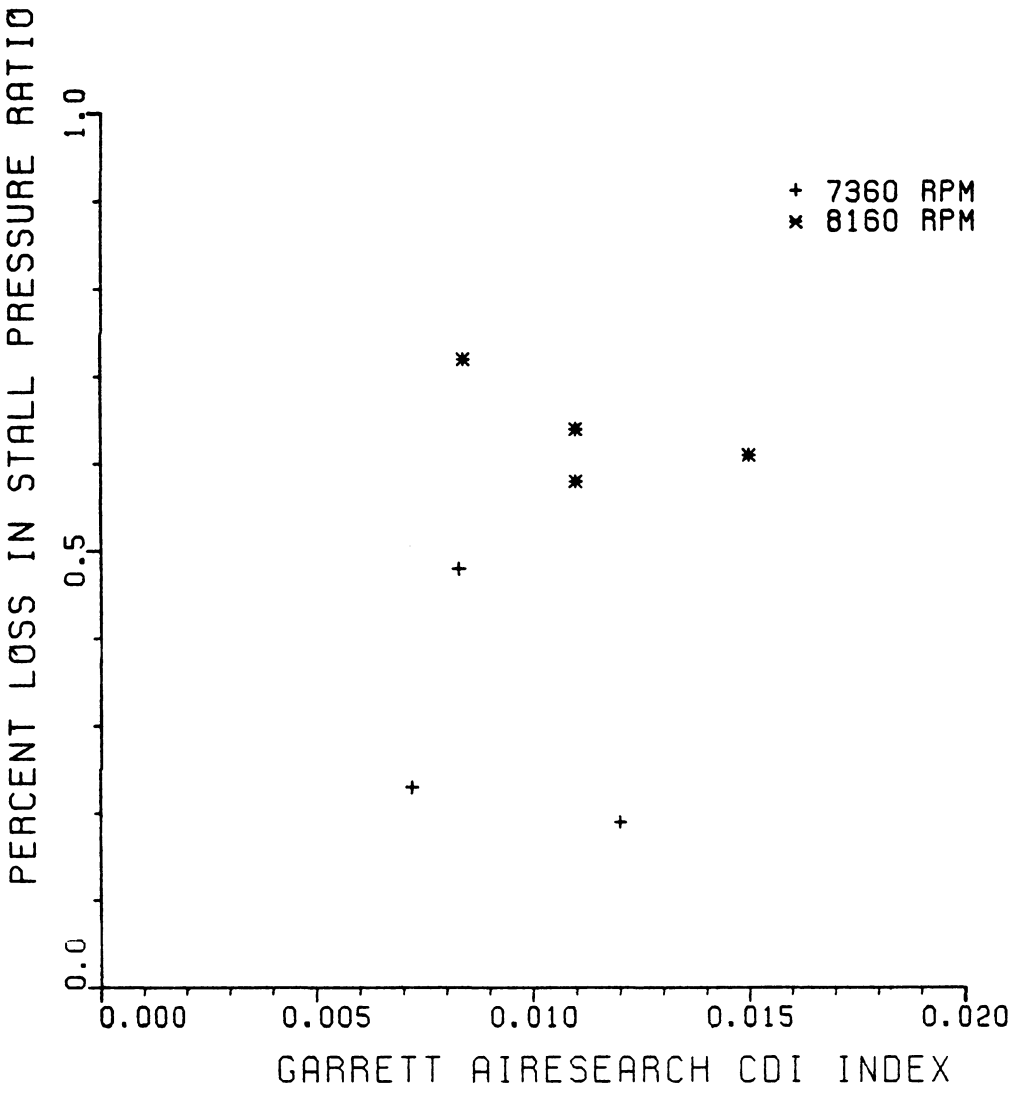

FIGURE C50: CIRCUMFERENTIAL DISTORTION-INDUCED STALL DATA FOR THE COMPRESSOR TEST-RIG, GARRETT AIRESEARCH CDI INDEX, DELTA PRSN

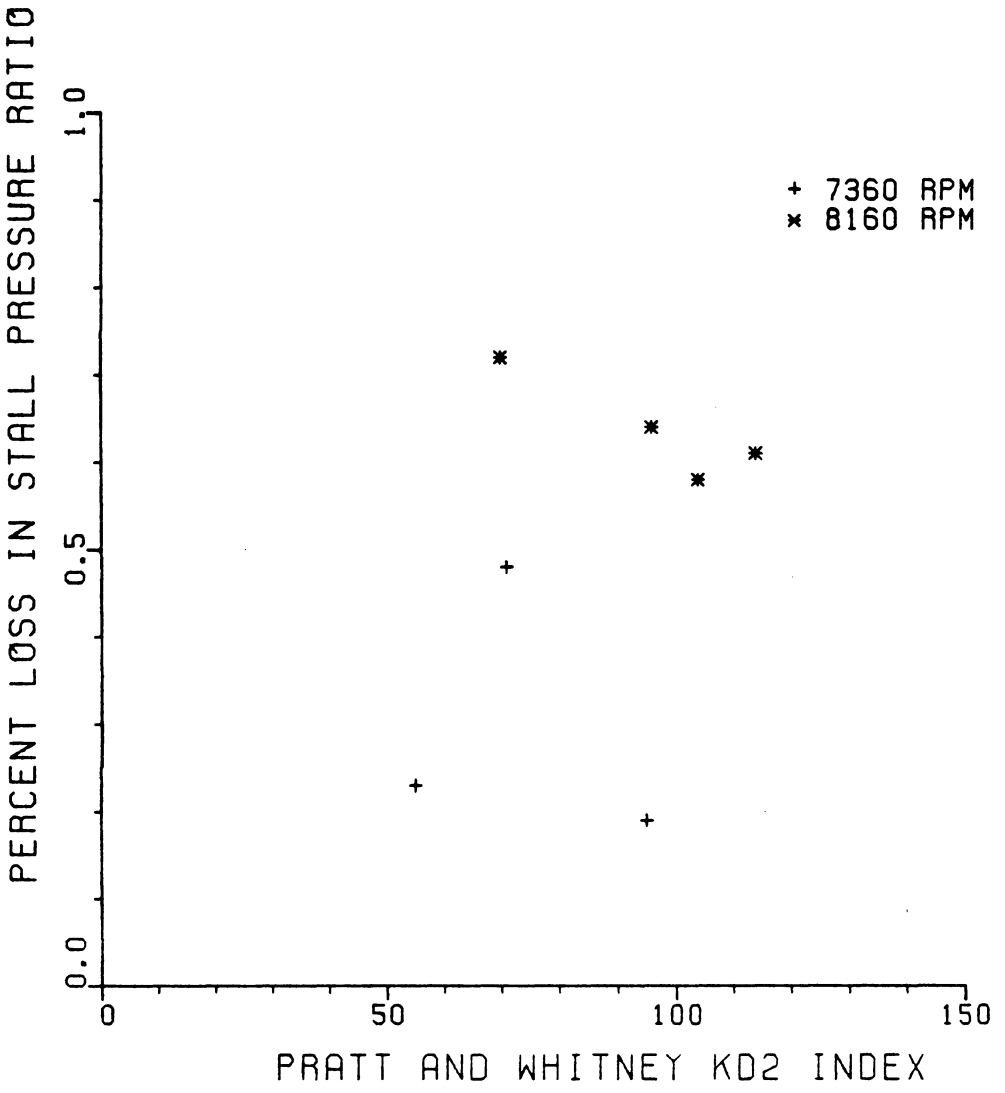

FIGURE C51: CIRCUMFERENTIAL DISTORTION-INDUCED STALL DATA FOR THE COMPRESSOR TEST-RIG, PRATT AND WHITNEY AIRCRAFT KD2 INDEX, DELTA PRSN

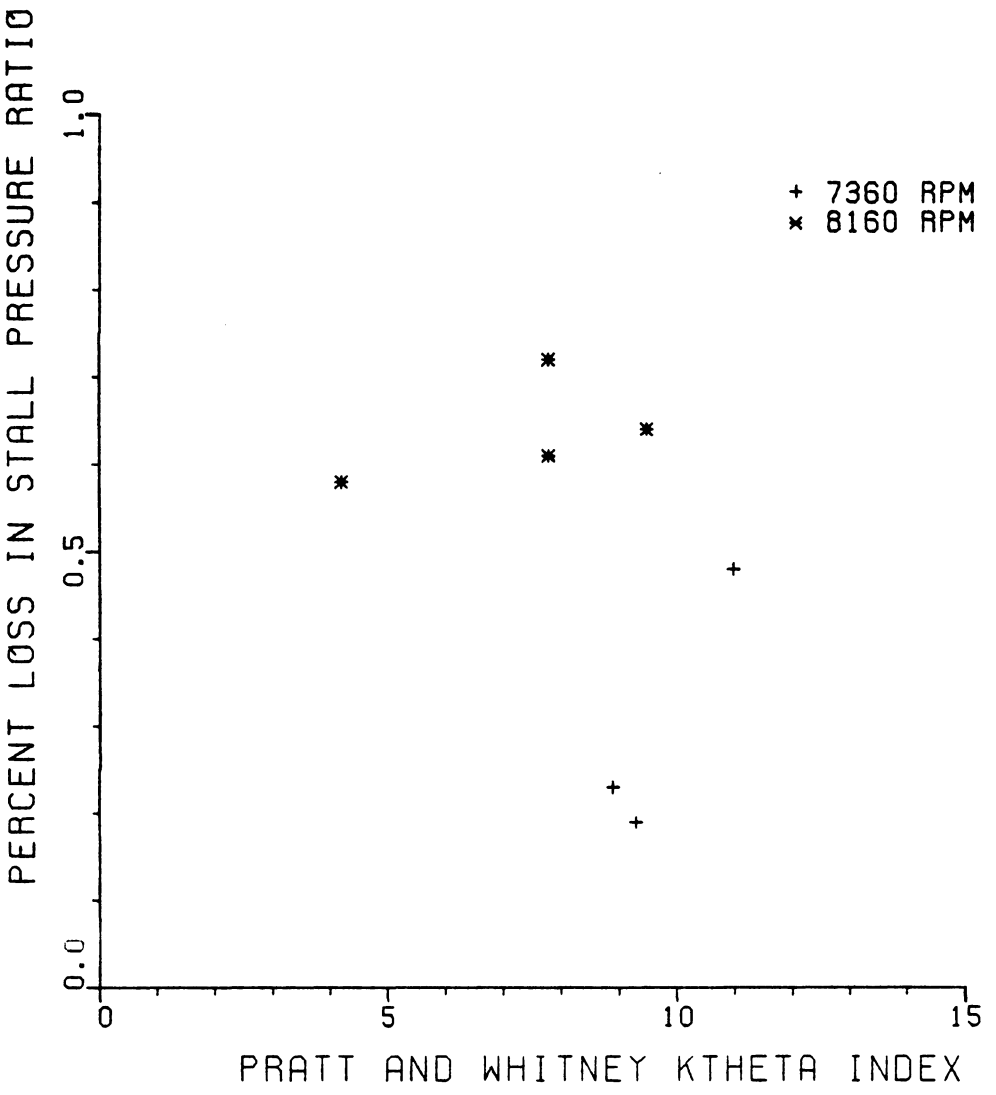

FIGURE C52: CIRCUMFERENTIAL DISTORTION-INDUCED STALL DATA FOR THE COMPRESSOR TEST-RIG, PRATT AND WHITNEY KTHETA INDEX, DELTA PRSN

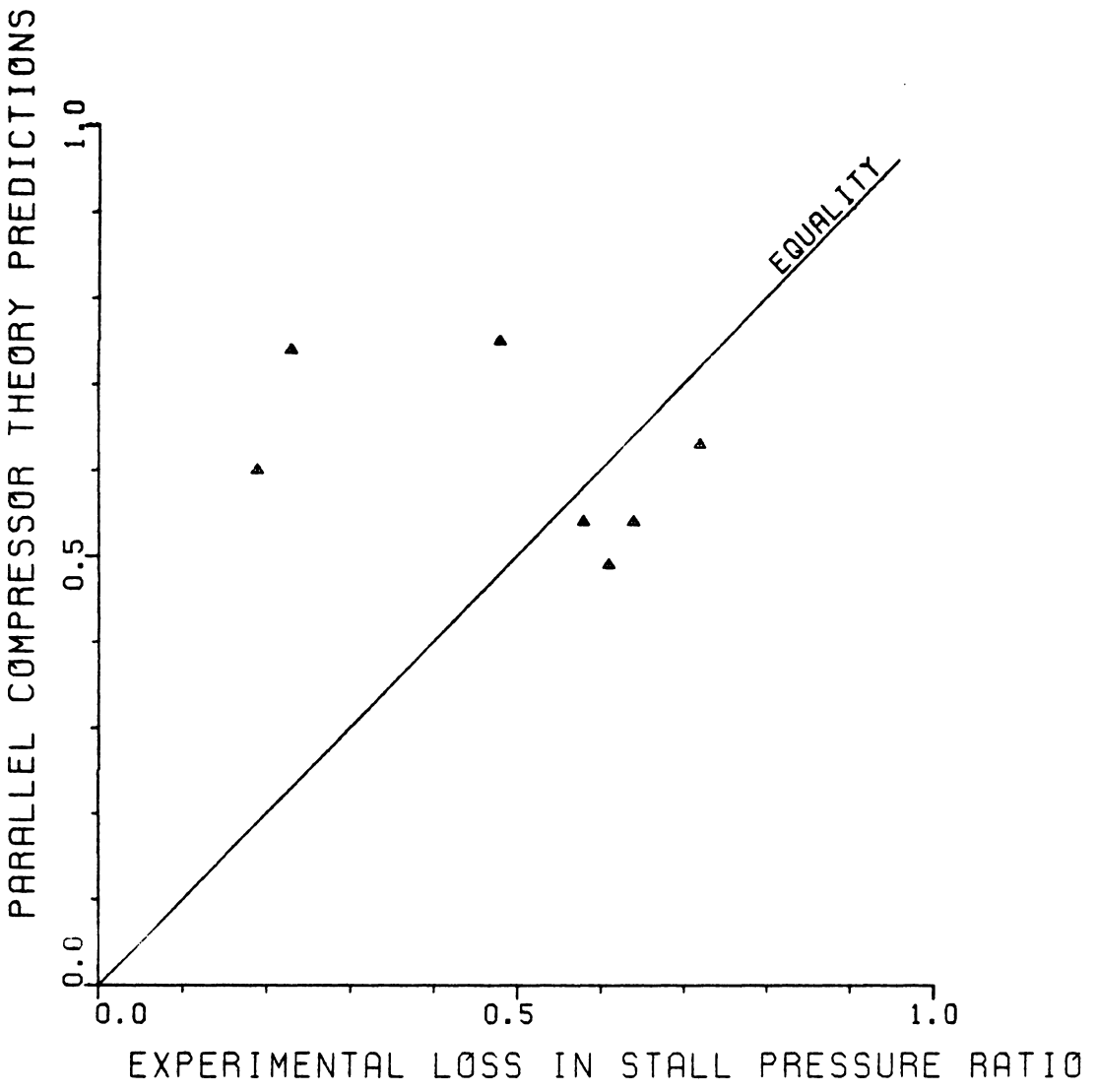

FIGURE C53: CIRCUMFERENTIAL DISTORTION-INDUCED STALL DATA FOR THE COMPRESSOR TEST-RIG AND, PARALLEL COMPRESSOR THEORY PREDICTIONS

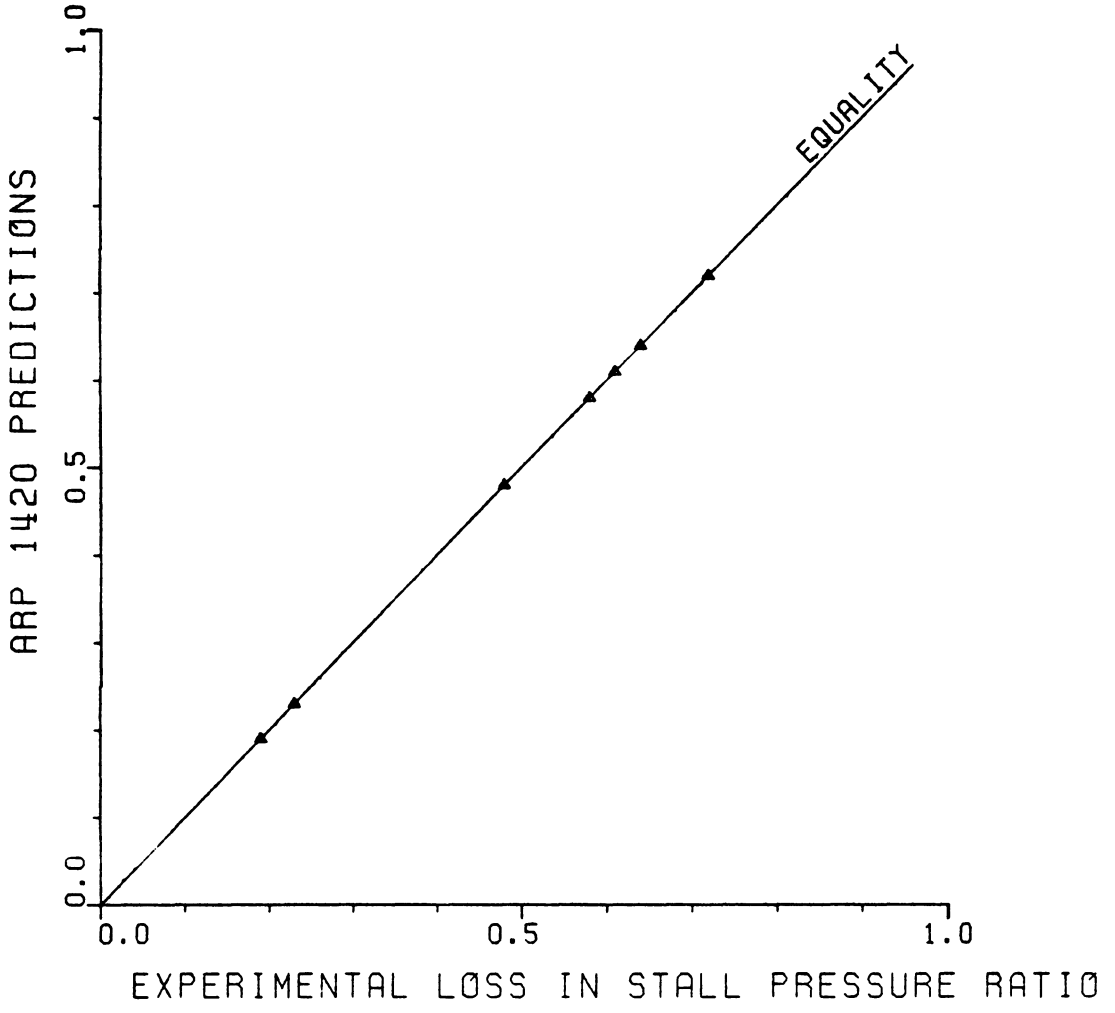

FIGURE C54: CIRCUMFERENTIAL DISTORTION-INDUCED STALL DATA FOR THE COMPRESSOR TEST-RIG AND ARP 1420 PREDICTIONS

The vita has been removed from the scanned document

AN INVESTIGATION OF DISTORTION INDICES FOR PREDICTION OF STALLING BEHAVIOR IN AIRCRAFT GAS TURBINE ENGINES

by

Annette Flanagan Campbell

(ABSTRACT)

The ability of twelve distortion indices to predict stalling behavior in aircraft gas turbine engines was investigated using J85-GE-13 turbojet engine data, TF30-P-3 turbofan engine data, and modified T64-GE-6B compressor test-rig data. The indices were tested for correlation capability with constant speed loss in stall pressure ratio, constant mass loss in stall pressure ratio, and engine speed where appropriate. Predictive indices/models were compared directly with experimental data.

In addition, the concept of including the effects of compressor dynamic response by modifying the inlet total pressure profile rather than the index was investigated. This was done by evaluating the accuracy of parallel compressor theory and two simple $\Delta P/\overline{P}$ indices first using measured inlet total pressure data and then using modified or "effective" inlet total pressure profiles. A procedure was developed for deriving the effective inlet total pressure distribution from the measured distribution.